Spring 5-2016

Addressing the Issues of Drug Delivery via Advanced Macromolecular Design

Brooks Allen Abel
University of Southern Mississippi

ADDRESSING THE ISSUES OF DRUG DELIVERY

VIA ADVANCED MACROMOLECULAR DESIGN

by

Brooks Allen Abel

A Dissertation
Submitted to the Graduate School
and the School of Polymers and High Performance Materials
at The University of Southern Mississippi
in Partial Fulfillment of the Requirements
for the Degree of Doctor of Philosophy

Approved:

_____
Dr. Charles L. McCormick, Committee Chair
Professor, School of Polymers and High Performance Materials

_____
Dr. Robson F. Storey, Committee Member
Professor, School of Polymers and High Performance Materials

_____
Dr. Daniel A. Savin, Committee Member
Associate Professor, Chemistry, University of Florida

_____
Dr. Derek L. Patton, Committee Member
Associate Professor, School of Polymers and High Performance Materials

_____
Dr. Sarah E. Morgan, Committee Member
Professor, School of Polymers and High Performance Materials

_____
Dr. Karen S. Coats
Dean of the Graduate School

May 2016

ABSTRACT

ADDRESSING THE ISSUES OF DRUG DELIVERY VIA ADVANCED MACROMOLECULAR DESIGN

by Brooks Allen Abel

May 2016

The work described in this dissertation focuses on the development of synthetic approaches toward novel polymer architectures that specifically address the issues of *in vivo* drug delivery. Successful implementation of the synthetic methodologies described herein required fundamental investigations into the underlying chemistries in ways that now provide greater insights into the nature of the these chemical reactions.

In Section I, the synthesis of tunable pH- and CO_2-responsive sulfonamide-containing polymers using reversible addition-fragmentation chain transfer (RAFT) polymerization is described. Initially, poor polymerization control of methacryloyl sulfonamide (MSA) monomers was observed using traditional RAFT polymerization conditions. Ultimately, reducing the polymerization temperature to 30 °C afforded polymers of controlled molecular weights and low dispersities. A library of sulfonamide-containing polymers was subsequently synthesized and their tunable pH-responsive and reversible CO_2-responsive aqueous solution properties investigated.

The work in Section II provides mechanistic understanding of the limited molecular weight control observed during the RAFT polymerization of MSAs at 70 °C (from Section I). This work demonstrates the unique influence of N-arylmethacrylamide substitution on trithiocarbonate chain-end degradation during RAFT polymerization at elevated temperatures. Detailed kinetic and structural analysis of RAFT polymer small

molecule analogs showed trithiocarbonate chain-end degradation occurs by N-5 nucleophilic attack on the terminal thiocarbonyl by the ultimate methacrylamide unit. On-going work regarding the development of a mechanistic and kinetic theory aimed at explaining the unique influence of N-arylsubstitution on amide nucleophilicity is further discussed in Appendix B.

In section III we investigate deleterious side reactions that occur during "one-pot" aminolysis/thiol-maleimide end group modification of RAFT polymers. Commonly employed thiol-ene Michael catalysts including amines, amidines, and phosphines were demonstrated to initiate the anionic polymerization of maleimide in a range of organic solvents, resulting in reduced RAFT polymer end group functionalization efficiency. Additionally, thiols and thiol-maleimide adducts were shown to initiate maleimide polymerization in polar solvents in the presence of triethylamine (TEA). Reaction conditions which favor rapid and quantitative end group functionalization of RAFT polymers using "one-pot" aminolysis/thiol-maleimide chemistry were ultimately identified.

Section IV details a new "grafting through" synthetic route towards molecular brushes capable of intracellular-induced disassembly. RAFT polymer-derived macromonomers were synthesized using "one-pot" aminolysis/thiol reactions with maleimide- or methanethiosulfonate-functional oxanorbornenes. Subsequent ring opening metathesis polymerization (ROMP) of the resulting macromonomers afforded molecular brushes with RAFT polymer side chains attached to a polyoxanorbornene backbone via either permanent thioether linkages or reversible disulfide linkages. Molecular brushes

comprised of disulfide linkages were shown to undergo reduction-induced disassembly and show promise as a new class of stimuli-responsive polymer therapeutics.

ACKNOWLEDGMENTS

I would like to extend my sincerest thanks to my research advisor, Dr. Charles L. McCormick, for his patience, support, and mentorship throughout my graduate career. I am particularly grateful to Dr. McCormick for granting me the intellectual freedom to pursue projects of my interest and to "dig deep" into the unknown. I would also like to thank my graduate committee, Dr. Robson F. Storey, Dr. Derek L. Patton, and Dr. Daniel A. Savin for their efforts and guidance. Dr. William J. Jarrett is gratefully acknowledged for his extensive assistance in performing many of the NMR experiments in this work.

I am thankful for all past and current McGroup members for their camaraderie. I especially thank Dr. Deedee Smith, Dr. Wenming Wan, Dr. Marco Oliveira, Dr. Christopher Holley, Keith Parsons, Phil Pickett, Michael Sims, David Siefker, and Aaron Spahr. I am forever indebted to Dana Froelich for her years of dedication and friendship.

With too many names to list, I am especially grateful for the many friends I have made throughout my graduate career. They have been the source of inumerable memories that I will cherish forever.

I would also like to acknowledge the financial support for this research provided by the National Science Foundation Graduate Research Fellowship Program (GM004636/GR04355) and National Science Foundation's EPSCoR (IIA1430364).

And lastly but not least, my most heartfelt thanks go to my best friend and wife Emily for her love, companionship, and understanding. She has made these years especially worthwhile.

DEDICATION

This work is dedicated to mom and dad for their limitless love, sacrifice, and support of any and all pursuits that I have chosen to partake in.

TABLE OF CONTENTS

ABSTRACT ii

ACKNOWLEDGMENTS v

DEDICATION vi

LIST OF TABLES ix

LIST OF ILLUSTRATIONS x

LIST OF SCHEMES xv

LIST OF ABBREVIATIONS xvii

CHAPTER

I. INTRODUCTION 1

Pharmacologically Active Polymers
Reversible Addition-Fragmentation Chain Transfer Polymerization
Stimuli-Responsive Polymers
Advanced Macromolecular Architectures

II. OBJECTIVES OF RESEARCH 32

III. EXPERIMENTAL SECTION 36

Materials
Characterization
Chapter IV Section 1 Experimental
Chapter IV Section 2 Experimental
Chapter IV Section 3 Experimental
Chapter IV Section 4 Experimental

IV. RESULTS AND DISCUSSION 72

Section 1. Tunable pH- and CO_2-Responsive Sulfonamide-Containing Polymers by RAFT Polymerization
Section 2. Mechanistic Insights into Temperature-Dependent Trithiocarbonate Chain-End Degradation during the RAFT Polymerization of N-Arylmethacrylamides
Section 3. “One-Pot” Aminolysis/Thiol-Maleimide End Group Functionalization of RAFT Polymers: Identifying and Preventing Michael Addition Side Reactions

Section 4. Growth-Then-Coupling Method of Molecular Brush Synthesis from RAFT Polymers and Thiol-Reactive Oxanorbornenes

V. CONCLUSIONS 146

Section 1. Tunable pH- and CO_2-Responsive Sulfonamide-Containing Polymers by RAFT Polymerization
Section 2. Mechanistic Insights into Temperature-Dependent Trithiocarbonate Chain-End Degradation during the RAFT Polymerization of N-Arylmethacrylamides
Section 3. "One-Pot" Aminolysis/Thiol-Maleimide End Group Functionalization of RAFT Polymers: Identifying and Preventing Michael Addition Side Reactions
Section 4. Growth-Then-Coupling Method of Molecular Brush Synthesis from RAFT Polymers and Thiol-Reactive Oxanorbornenes

APPENDIXES 149

REFERENCES 175

LIST OF TABLES

Table

4.1. Conversion, molar mass, and molecular weight distribution data for the RAFT polymerization of MSAs in DMF at 70 °C. 77

4.2. Conversion, molar mass, and molecular weight distribution data for the RAFT polymerization of MSAs in DMF at 30 °C. 83

4.3. MSA monomer and polymer titration data. 87

4.4. Conversion, Molar Mass, and Molecular Weight Distribution Data for the RAFT Polymerizations of **33** and **34** in DMF at 70 and 30 °C. 93

4.5. "One-pot" aminolysis/thiol-maleimide reactions of **45** with **46**. 129

4.6. Summary of end group functionalization of RAFT polymers **57** and **58** with thiol-reactive oxanorbornenes **52** and **56**. 139

4.7. ROMP of RAFT-derived macromonomers summary. 143

LIST OF ILLUSTRATIONS

Figure

1.1. Ringsdorf "depot" model of idealized polymer-based therapeutic. 1

1.2. Enhanced permeation and retention (EPR) effect. 3

1.3. Cellular internalization of polymer therapeutics by endocytosis. 7

1.4 Percentage of dithiobenzoate species present during the AIBN-initiated polymerization of styrene in the presence of 2-cyano-2-propyl dithiobenzoate (AD). 14

1.5. General structures of commonly used RAFT agents. 18

1.6. Guidelines for RAFT agent Z-group, R-group, and monomer selection based upon previously reported experimental results. Dashed lines indicate marginal polymerization control. 18

1.7. R/Z-group approach toward the synthesis of α,ω-telechelic polymers by RAFT. 19

1.8. Common pH-responsive monomers polymerizable by RDRP techniques. 21

1.9. Common temperature-responsive monomers polymerizable by RDRP techniques. 23

1.10. Polymer architectures accessible through the use of controlled/"living" polymerization techniques. 25

1.11. "Grafting from," "grafting onto," and "grafting through" synthetic routes toward molecular brush synthesis. 27

1.12. Ruthenium-based metathesis catalysts. 29

1.13. Norbornene-functional macromonomer synthesis by direct-growth (DG-MM) and growth-then-coupling (GC-MM) synthetic routes. 30

1.14. Drug-loaded, bivalent molecular brush polymers synthesized using "grafting through" ROMP of norbornene-functional macromonomers. 31

4.1. Kinetic plots for the **23**- and **26**-mediated RAFT polymerization of **27** at 70 °C in DMF ($[M]_0$:$[CTA]_0$:$[I]_0$ = 150:1:0.2). 76

4.2. SEC traces of **P27** macroCTA (M_n = 7300 g/mol, M_w/M_n = 1.35) and **P27**-b-**P27** after chain extension at 70 °C in DMF. 79

4.3. DMF SEC RI traces of **P27** polymerized at 30 °C and 70 °C using V-70 and V-501, respectively. 80

4.4. a) Pseudo-first-order kinetic plots for the **26**- and **23**-mediated RAFT polymerization of **27** at 30 °C in DMF ($[M]_0$:$[CTA]_0$:$[I]_0$ = 150:1:0.2). b) SEC overlay for **26**-mediated polymerization of **27** at 30 °C in DMF. c) M_w/M_n versus conversion. d) M_n versus conversion. 82

4.5. SEC traces of **P27** macroCTA (M_n= 25 100 g/mol, M_w/M_n = 1.09) and **P27**-b-**P27** (M_n = 49 600 g/mol, M_w/M_n = 1.07) after chain extension in DMF. Both polymerizations were conducted at 30 °C. 85

4.6. EP and $EP_{1/2}$ locations on the titration curve of **27** (1 mM) titrated against HCl (0.05 N) at 25 °C using a Metrohm 848 Titrino Plus autotitrator. 86

4.7. Substituent effects on pH-dependent solubility transitions of sulfonamide-containing polymers. Percent transmittance was measured using a UV-Vis spectrophotometer (λ = 500 nm). 88

4.8. Reversible solubility of **P29** in response to presence or absence of CO_2. Solutions were purged with either CO_2 for 10 s (shaded regions) or N_2 for 25 min (unshaded regions) and % transmittance measured using a UV-Vis spectrophotometer (λ = 500 nm). 89

4.9. Kinetic plot for the **37**-mediated polymerization of **33** and **34** in DMF at 70 °C ($[M]_0$ = 2.0 M, $[M]_0$:$[CTA]_0$:$[I]_0$ = 200:1:0.2). 95

4.10. SEC RI chromatogram showing the effect of temperature on molecular weight distribution for the **37**-mediated RAFT polymerization of **33** at 70 and 30 °C. ... 96

4.11. Kinetic plot for the **37**-mediated polymerization of **33** and **34** in DMF at 30 °C ($[M]_0$ = 2.0 M, $[M]_0$:$[CTA]_0$:$[I]_0$ = 200:1:0.2). 97

4.12. Individual and combined influences of solvent, initiator, and monomer on the time-dependent change in [TTC]/$[TTC]_0$ as measured by UV-Vis spectroscopy ($[M]_0$:$[CTA]_0$:$[I]_0$ = 10:1:0.2). Trithiocarbonate degradation experiments were performed using (a) **33** or (b) **34** as the monomer. 99

4.13. Trithiocarbonate degradation during the **37**-mediated polymerization of **33** ($[M]_0$:$[CTA]_0$:$[I]_0$ = 10:1:0.2) at 70 and 30 °C using V501 and V-70 as initiators respectively. 100

4.14. ^{1}H NMR (300 MHz, $CDCl_3$) spectrum of isolated N-5 cyclization/elimination product **40**. 101

4.15. ^{1}H NMR (300 MHz, $CDCl_3$) spectra of (a) **41** and (b) **42** SMUI adducts. 102

4.16. ^{1}H NMR (600 MHz, DMF-d_7) overlay following the time-dependent degradation of **41** at 70 °C. 103

4.17. ^{1}H NMR (600 MHz, DMF-d_7) overlay following the time-dependent degradation of **42** at 70 °C. 104

4.18. Time-dependent fractional change in the area of select ^{1}H chemical shifts during the degradation of (a) **41** and (b) **42** in DMF-d_7 at 70 °C. 106

4.19. Time-dependent change in [TTC]/[TTC]$_0$ at 70 °C in DMF as measured by UV-vis spectroscopy during polymerization (open circles) and as measured by *in situ* ^{1}H NMR during SMUI adduct degradation analysis (closed circles). 107

4.20. (a) Kinetic plot and (b) SEC RI chromatogram overlay for the **40**-mediated polymerization of **33** in DMF at 70 °C ([**33**]$_0$ = 2.0 M, [**33**]$_0$:[**40**]$_0$:[V501]$_0$ = 200:1.0:0.2). 110

4.21. Effect of solvent on the time-dependent fractional change in [Mal]/[Mal]$_0$ upon reaction of **65** with representative nucleophiles a) hexylamine (HexAM), b) 1,8-diazabicyclo[5.4.0]undec-7-ene (DBU), c) tributylphosphine (TBP), and d) trimethylphosphite (TMP) as measured by *in situ* ^{1}H NMR analysis. 115

4.22. Effect of solvent on the time-dependent fractional change in [Mal]/[Mal]$_0$ during the TEA-catalyzed reaction of E2MP with **65** as measured by *in situ* ^{1}H NMR analysis. 120

4.23. Effect of solvent on the time-dependent fractional change in [Mal]/[Mal]$_0$ during the TEA-catalyzed reaction of **43** with **65** as measured by *in situ* ^{1}H NMR analysis. 123

4.24. a) Time-dependent fractional change in peak area (A_t/A_0) for protons H_a, H_b, and H_c during TEA-catalyzed H-D exchange of **43** in DMSO. b) ^{1}H NMR spectral overlay of select time points during H-D exchange experiments with **43**. 124

4.25. ^{1}H NMR (300 MHz, acetone-d_6) end group analysis of **57**, **59**, and **60**. 138

4.26. ^{1}H NMR (300 MHz, D_2O) end group analysis of **58**, **61**, and **62**. 138

4.27. a) SEC RI traces of the parent RAFT polymer (**57**), **52**-functional macromonomer (**59**), and corresponding molecular brush (**P59**). b) SEC RI traces of the parent RAFT polymer (**57**), **56**-functional macromonomer (**60**), and corresponding molecular brush (**P61**). 141

4.28. a) SEC RI traces of the parent RAFT polymer (**58**), **52**-functional macromonomer (**61**), and corresponding molecular brush (**P61**). b) SEC RI traces of the parent RAFT polymer (**58**), **56**-functional macromonomer (**62**), and corresponding molecular brush (**P62**)..... 143

4.29. SEC RI trace of the disulfide-containing molecular brush after purification by dialysis (**P62**) and SEC RI trace of **P62** 5 min after the addition of DTT (5 eq.). **P62** molecular brush reduction reactions were performed in pH = 7.4 phosphate buffered saline (10 mM) at 23 °C. 145

A1. M_n versus % conversion for **37**-mediated polymerization of **33** at 70 °C. 149

A2. M_n versus % conversion for **37**-mediated polymerization of **34** at 70 °C. 149

A3. M_n versus % conversion for **37**-mediated polymerization of **33** at 30 °C. 150

A4. M_n versus % conversion for **37**-mediated polymerization of **34** at 30 °C. 150

A5. Beer-Lambert plot and molar extinction coefficients (ε) for **37**, **41**, and **42** in acetonitrile measured using a Lambda 35 UV-vis spectrometer (λ = 320 nm). . 151

A6. (a) ^{1}H NMR (600 MHz, DMF-d_7) spectrum of 1-dodecanethiol, (b) ^{1}H NMR (600 MHz, DMF-d_7) spectrum acquired at t = 491 min during the *in situ* degradation analysis of **41** at 70 °C, (c) ^{1}H NMR (600 MHz, DMF-d_7) spectrum of **40**. Peaks of interest corresponding to degradation byproducts formed during *in situ* degradation analysis (Figure A6b) are colored red and blue and correspond well with key peaks of analogous compounds 1-dodecanethiol (red) and **40** (blue) (Figures A6a and A6c respectively). 152

A7. Expanded region (3.00 - 0.5 ppm) of the ^{1}H NMR (600 MHz, DMF-d_7) spectrum acquired at t = 5 min during *in situ* degradation analysis of **41** at 70 °C..... 153

A8. Expanded region (3.00 - 0.5 ppm) of the ^{1}H NMR (600 MHz, DMF-d_7) spectrum acquired at t = 491 min during *in situ* degradation analysis of **41** at 70 °C. Overlapping peaks are colored red or blue for improved visualization..... 153

A9. a) ^{1}H NMR spectrum of E2MP in DMSO-d_6 at T = 0 min. b) ^{1}H NMR spectrum during the reaction of E2MP and **65** in DMSO-d_6 at T = 3 min. Disappearance of the thiyl (peak c) and methyne (peak d) protons of E2MP confirm quantitative thiol conversion by 3.0 min. 154

A10 a) ^{1}H NMR spectrum of E2MP in MeCN-d_3 at T = 0 min. b) ^{1}H NMR spectrum during the reaction of E2MP and **65** in MeCN-d_3 at T = 2.3 min. Disappearance of the thiyl (peak c) and methyne (peak d) protons of E2MP confirm quantitative thiol conversion by 2.3 min 154

A11. a) ^{1}H NMR spectrum of E2MP in CD_2Cl_2 at T = 0 min. b) ^{1}H NMR spectrum during the reaction of E2MP and **65** in CD_2Cl_2 at T = 2.5 min. Disappearance of the thiyl (peak c) and methyne (peak d) protons of E2MP confirm quantitative thiol conversion by 2.5 min. 155

A12. Effect of solvent on the time-dependent fractional change in $[Mal]/[Mal]_0$ during the reaction of TEA with **65** as measured by *in situ* ^{1}H NMR analysis. 156

A13. Effect of solvent on the time-dependent fractional change in $[Mal]/[Mal]_0$ during the TEA-catalyzed reaction of HexAM with **65** as measured by *in situ* ^{1}H NMR analysis. 156

A14. ^{1}H NMR (300 MHz, D_2O) spectrum of **45**. 157

A15. Representative ^{1}H NMR (300 MHz, D_2O) spectrum of **46**-functionalized **45** (Table 4.5 entry 1a). 157

A16. ^{1}H NMR spectrum (300 MHz, $CDCl_3$) of **52**. 158

A17. ^{1}H NMR spectrum (300 MHz, $CDCl_3$) of **56**. 158

A18. Proposed inverse relationship between amide pK_a and apparent amide nucleophilicity. 163

A19. ^{1}H NMR (300 MHz, DMSO-d_6) overlay following the TEA-catalyzed degradation of **41** at room temperature. 168

A20. $[TTC]^{1/2}$ vs time plots for the degradation of **41** and **42** in DMF-d_7 at 70 °C ($[TTC]_0$ = 0.0329 M). 171

LIST OF SCHEMES

Scheme

1.1. Proposed mechanism of RAFT polymerization. 11

4.1. pH-dependent solubility of pMSAs. 72

4.2. Synthetic pathway for the **23**- or **26**-mediated RAFT polymerization of MSAs in DMF. 75

4.3. Synthetic route for **37**-mediated polymerization of **33** and **34** in DMF at 70 or 30 °C. 92

4.4. Proposed trithiocarbonate degradation by O-5 or N-5 nucleophilic attack by the terminal methacrylamide unit. 99

4.5. Synthetic route for small molecule analog **40a**. 101

4.6. Synthesis of **41** and **42** by single monomer unit insertion. 102

4.7. Possible N-5 nucleophilic attack degradation pathways. 105

4.8. Proposed mechanism for radical addition to 3-phenyl-2-thioxothiazolidin-4-one chain ends during RAFT polymerization of **33** at 70 °C. 108

4.9. "One-pot" aminolysis/thiol-maleimide end group functionalization of RAFT polymers. 111

4.10. Mechanism of nucleophile-initiated thiol-maleimide Michael addition. 112

4.11. Proposed mechanisms of initiation, propagation, and termination for the nucleophile-initiated anionic polymerization of N-substituted maleimides. 118

4.12. Proposed reaction pathways for the TEA-catalyzed thiol-maleimide reaction where reversible enolate formation is operational. 126

4.13. "One-pot" aminolysis/thiol-maleimide modification of **45** with **46**. 128

4.14. "One-pot" end group functionalization of RAFT polymers with thiol-reactive oxanorbornenes **52** and **56**. 135

4.15. Synthetic route for **52**. 136

4.16. Synthetic route for **56**. 136

4.17. ROMP of ω-oxanorbornenyl-functionalized macromonomers (**59**–**62**) into the corresponding molecular brushes (**P59**–**P62**). 140

4.18. DTT reduction of **P62** in pH = 7.4 phosphate buffered saline (10 mM) at 23 °C. 144

A1. Influence of ionized (**A2**) or conjugate base (**A4**) resonance forms on amide nucleophilicity..... 159

A2. Proposed degradation of **41** by N-5 cyclization/elimination (pathway A). 161

A3. Possible N-arylamide conjugate base resonance forms. 162

LIST OF ABBREVIATIONS

Abbreviation	
AcOH	acetic acid
AIBN	azobisisobutyronitrile
*a*RAFT	aqeous reversible addition-fragmentation chain transfer
ATRP	atom transfer radical polymerization
BIC	block ionomer complex
$CDCl_3$	deuterated chloroform
CH_2Cl_2	dichloromethane
CMC	critical micelle concentration
CT	Camptothecin
CTA	chain transfer agent
d	doublet
Đ	dispersity
D_2O	deuterium oxide
DBU	1,8-diazabicyclo[5.4.0]undec-7-ene
dd	doublet of doublets
DG-MM	direct-growth macromonomer
DMA	N,N-dimethylacrylamide
DMF	N,N-dimethylformamide
DMSO	dimethylsulfoxide
DOX	Doxorubicin
E2MP	ethyl-2-mercaptopropionate

EPR	enhanced permeation and retention
ESI-MS	electrospray ionization mass spectrometry
EtOAc	ethyl acetate
EtOH	ethanol
Fab	fragment antigen binding
ΔG	Gibbs free energy
GC-MM	growth-then-coupling macromonomer
GSH	Glutathione
ΔH	change in enthalpy
H_2O	water
HCl	hydrogen chloride
HexAM	hexylamine
HSAB	hard and soft Lewis acids and bases
IPEC	interpolyelectrolyte complex
K_a	acid dissociation constant
LAM	less activated monomers
LCST	lower critical solution temperature
Mal	maleimide
MALLS	multi angle laser light scattering
MAM	more activated monomers
MeCN	acetonitrile
MeOH	methanol

MM	macromonomer
M_n	number average molecular weight
MSA	methacryloyl sulfonamide
MTS	methanethiosulfonate
M_w	weight average molecular weight
NaH	sodium hydride
NaOH	sodium hydroxide
NIPAM	N-isopropylacryalmide
NMP	nitroxide-mediated polymerization
NMR	nuclear magnetic resonance
Nu	nucleophile
PBS	phosphate buffered saline
PEG	poly(ethylene glycol)
PEI	polyethylene imine
pHPMA	poly(N-(2-hydroxypropyl)methacrylamide)
pMSA	poly(methacryloyl sulfonamide)
RAFT	reversible addition-fragmentation chain transfer
RDRP	reversible-deactivation radical polymerization
RNAi	RNA interference
ROMP	ring opening metathesis polymerization
R_p	rate of propagation
ΔS	change in entropy

SEC	size exclusion chromatography
siRNA	small interfering ribonucleic acid
SMUI	single monomer unit insertion
TBP	tributylphosphine
TEA	triethylamine
TFA	trifluoroacetic acid
THF	tetrahydrofuran
TMP	trimethylphosphite
TTC	trithiocarbonate
UCST	upper critical solution temperature
UV	ultraviolet
UV-Vis	ultraviolet-visual
V-501	azobis(4-cyanovaleric acid)
V-70	2, 2’-azobis(4-methoxy-2-4-dimethyl valeronitrile)

CHAPTER I

INTRODUCTION

Pharmacologically Active Polymers

Barriers to Polymer-Facilitated Drug/Gene Delivery

The "depot" model (Figure 1.1), first proposed by Helmut Ringsdorf in 1975, has been the basis of design for many polymer therapeutics.[1] According to this model, Ringsdorf proposed the use of a modifiable polymer scaffold that would incorporate four major components including i) a water-soluble and biocompatible polymer backbone, ii) targeting moiety/diagnostic agent, iii) therapeutic agent, and iv) a degradable spacer for reversible attachment of the therapeutic agent. Various interpretations of this approach to polymer-facilitated drug delivery have since yielded many new solutions to addressing the issues associated with drug delivery. However, successful implementation of the idealized "depot" model has proven difficult, largely due to synthetic challenges and the complex nature of *in-vivo* drug delivery.[2]

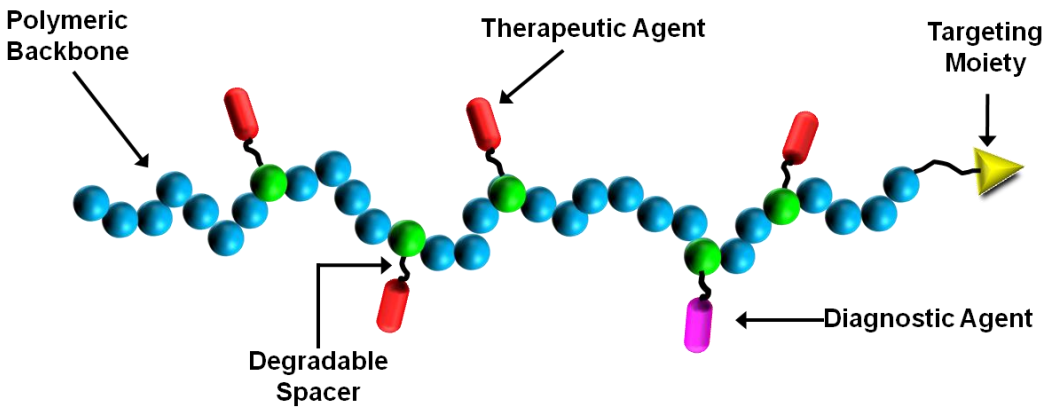

Figure 1.1. Ringsdorf "depot" model of idealized polymer-based therapeutic.

There are numerous barriers associated with polymer-facilitated cytosolic delivery of chemo- and gene-based therapeutics that must be overcome in order for polymer-based therapeutics to be a viable treatment option *in-vivo*.[3–9] These barriers include i) therapeutic agent degradation, ii) vascular circulation, iii) cell-specific targeting, iv) cellular internalization, v) endosomal escape, vi) controlled release of the therapeutic agent in its active form, and vii) polymer clearance/elimination from the body. The drug delivery "vehicle" must also be simultaneously biocompatible and non-immunogenic. Numerous polymer-based approaches have been developed to specifically address each of these issues with regard to drug/gene delivery but with varying degrees of success owing to the complex nature of drug delivery. Fully understanding each barrier to drug delivery is crucial to designing successful polymer therapeutics.

Therapeutic Agent Protection and Enhanced Vascular Circulation

Small molecule drug use *in-vivo* is largely inefficient due to rapid renal clearance in the kidneys and/or liver.[10,11] The reduced circulation half-lives of small molecule drugs necessitate high initial dosages and frequent administration which can result in unintended drug-induced side effects. *In-vivo* drug degradation also results in reduced therapeutic efficacy and may result in complete inhibition of therapeutic activity. For example, the extracellular half-life of unprotected small interfering ribonucleic acid (siRNA) is 3-5 minutes, making direct delivery of "naked" siRNA therapeutics completely ineffective.[12] It is therefore desirable to extend the circulation half-life of small molecule and nucleotide-based therapeutics by preventing degradation and increasing vascular retention.

Some of the earliest polymeric delivery vehicles encapsulated or sequestered therapeutic agents inside liposomes or micellar-like structures which simultaneously protected the therapeutic agent from degradation while also increasing circulation time before ultimate renal clearance.[13–15] However, these approaches did not specifically target cells, but rather relied upon non-specific cellular uptake and the enhanced permeation and retention (EPR) effect to direct the delivery vehicle to tumoral tissues.[16–20] As illustrated in Figure 1.2, the EPR effect enhances polymeric drug accumulation in tumoral tissue due to the combination of a leaky vascular system and poorly formed lymphatic drainage system, which are characteristic of rapidly growing tumors. In contrast, polymer therapeutics tend not to accumulate in healthy tissues due to tight endothelial junctions and improved lymphatic drainage compared to tumoral tissue.

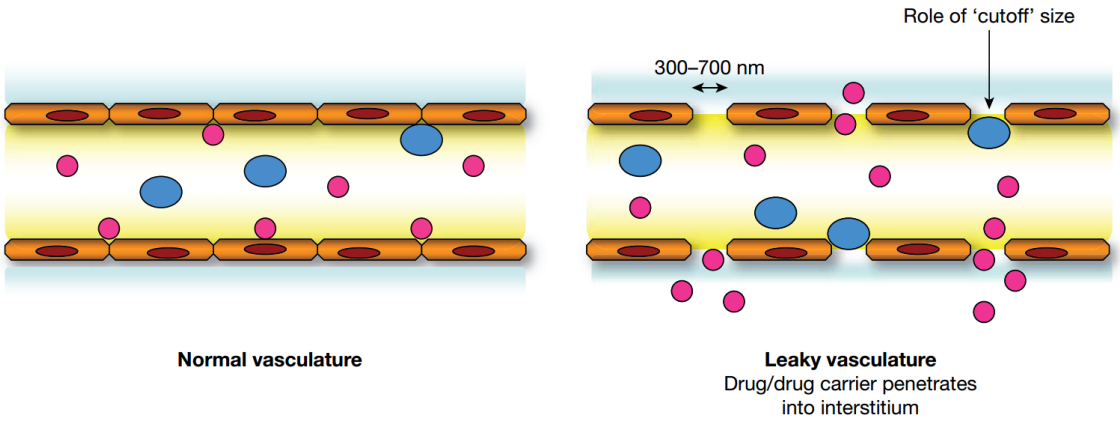

Figure 1.2. Enhanced permeation and retention (EPR) effect.[21]

Interpolyelectrolyte complex (IPEC) formation is a commonly used strategy to electrostatically bind negatively charged oligonucleic acids to cationic polymers, effectively shielding the nucleic acid from enzymatic degradation.[22–24] Traditionally, an excess of cationic charge is used to maintain water solubility of IPECs, but the overall

positive charge results in non-specific cellular uptake and high *in-vitro and in-vivo* cytotoxicity.[25–27] Recently, overall neutral block ionomer complexes (BICs) comprised of neutral-block-cationic copolymers and siRNA have shown adequate protection of siRNA while allowing for cell-specific uptake when used with appropriate targeting methods.[24,28]

Other approaches, aimed at improving therapeutic agent circulation time involve functionalization of nanoparticles or polymeric scaffolds with biocompatible water-soluble polymers such as poly(N-(2-hydroxypropyl)methacrylamide) (pHMPMA) or poly(ethylene glycol) (PEG).[29–32] This effectively shields the drug-containing core of the delivery vehicle from eliciting a potential immune response while simultaneously protecting the therapeutic agent from degradation.

The ultimate goal of limiting therapeutic agent degradation while increasing the circulation half-life of the delivery vehicle is to allow for suitable time to reach the site of intended therapeutic action. To this end, the EPR effect can be exploited as a passive tumor targeting mechanism; however, this approach will not specifically target any cell of interest when well-defined tumors are not present and does not facilitate cell-specific internalization. Therefore, to improve drug delivery specificity and avoid therapeutic accumulation in healthy tissue, a cell-specific and preferably modifiable targeting strategy is desired.

Cell-Specific Targeting

Polymeric drug carriers can be modified to contain targeting moieties through end group functionalization, incorporation along the polymer backbone, or side chains.[33] Availability of the targeting moiety on the surface of the polymer-drug conjugate is necessary to ensure appropriate contact with surface receptors expressed on the exteriors

of targeted cells. Common targeting moieties include antibodies and antibody fragments, peptides, oligosaccharides, and folate among others.[34–41] Antibodies represent a versatile targeting agent since it is possible to produce an antibody that can uniquely bind to a corresponding antigen expressed on any cell-type. Then, by conjugating the antibody to the polymer therapeutic, the delivery vehicle can be specifically targeted to the desired cell-type. It is also possible to cleave and isolate the variable regions of the antibody known as the fragment antigen binding (Fab) regions, which reduces the entire size of the targeting moiety from ~150 kDa per antibody to ~50 kDa per Fab.[42,43] Kopecek and coworkers have shown that Fab-targeted polymer therapeutics promote a 3-fold reduction in tumor size compared to the non-targeted therapeutics that relied exclusively upon the EPR effect for passive tumor targeting.[44] Despite their specificity, antibodies and Fab fragments are often recognized as being foreign biological molecules and can induce an immunological response that results in rapid elimination/degradation of the targeting moiety and the attached polymer therapeutic.

The use of oligosaccharides represents another attractive targeting option since all cells express saccharide-binding proteins on their surfaces called lectins.[45] Due to the large number of unique possible combinations of sugar residues in oligosaccharides, specific cellular targeting is possible if a unique lectin-oligosaccharide binding interaction is known for a particular cell-type. Although lectins exhibit high specificity of recognition, not all lectins induced cellular internalization of bound oligosaccharides such that an additional means of cellular internalization would be needed.

Folate-targeted polymer therapeutics have been used extensively *in-vitro* and *in-vivo*.[22,46,47] Folic acid is an essential vitamin required by cells and several cancer cell-

types are known to over-express folic acid receptors. Furthermore, folate is readily available compared to specifically targeted antibodies and other biomacromolecules which are more difficult to prepare and isolate. Despite the targeting method used, the polymer therapeutic must also be internalized by the cell. In some instances, the mode of targeting can result in cellular internalization, known as "piggy-back endocytosis," whereas other routes require an additional strategy to induce cell entry.

Cellular Internalization and Endosomal Escape

Cellular internalization is most often achieved via endocytosis, the process by which a portion of the cell membrane invaginates and separates from the rest of the cell membrane, subsequently internalizing extracelluar compounds (Figure 1.3). Endocytosis is usually triggered in response to an external stimulus, such as binding of a biomolecule to a particular cellular receptor.[47,48] This type of cellular entry is known as receptor-mediated endocytosis and is a readily exploited method to internalize polymer therapeutics that target cellular surface receptors. Following endocytosis, the internalized polymer therapeutic and extracellular media are isolated in endosomes, accompanied by a reduction in pH from physiological (7.4) to early endosomal (pH 6-6.5) to late endosomal (pH 5-6).[49,50] Within approximately 30 minutes of endocytosis, the endosomes fuse with or transform into lysozomes, which contain degradative enzymes that are particularly detrimental to most small molecule and nucleic acid-based therapeutics.[51] Furthermore, endosomes can fuse with the cell membrane via a process known as exocytosis, subsequently releasing their contents outside of the cell. For this reason, endosomal escape is often cited as the "bottle neck" of intracellular drug delivery thus making

escape of polymer-based therapeutics from the endosome prior to lysozomal fusion or exocytosis crucial for the successful application of polymer therapeutics.

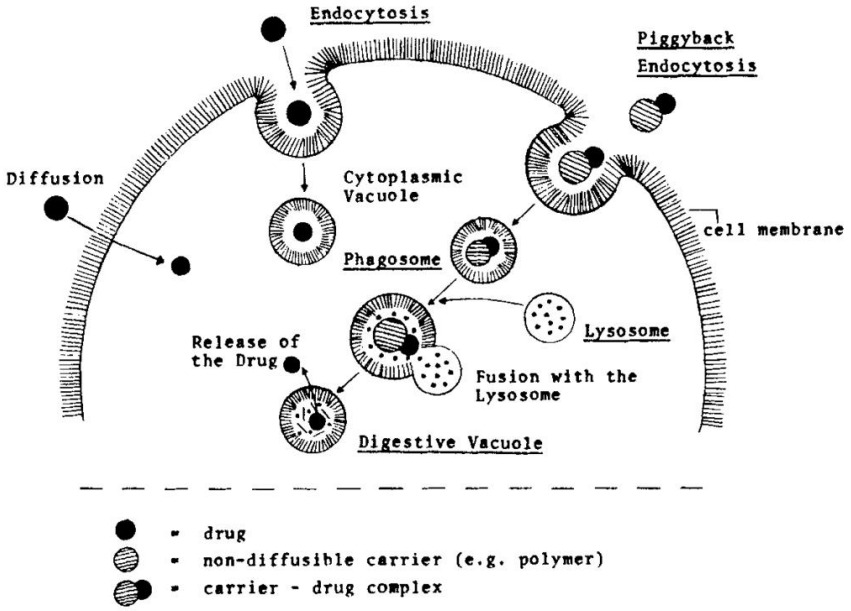

Figure 1.3. Cellular internalization of polymer therapeutics by endocytosis.[1]

Several methods of endosomal release have been developed that disrupt the structural integrity of the endosomal membrane, thus facilitating the release of its contents into the cytoplasm. One approach utilizes osmotoic swelling of the endosomal vesicle by promoting ion influx into the endosome by a process known as the proton sponge effect.[52] High buffer capacity polymers such as polyethylene imine (PEI), contain a large number of unprotonated amines and can act as "proton sponges" when exposed to the acidified environment of the endosome.[53] The resulting influx of counterions is further accompanied by an influx of water, subsequently swelling the endosome which results in either compromised membrane integrity or complete endosomal rupture, facilitating release of its contents, polymer therapeutic included. pH-responsive peptides and polymers that become hydrophobic at endosomal pH (5.0-6.5) have also been used to

destabilize the amphiphilic endosomal membrane facilitating the release of the endosomal contents.[54–57] Ultimately, the goal of endosomal escape is to release the polymer therapeutic into the cytoplasm, where triggered release of the therapeutic agent can elicit the desired pharmacological response.

Therapeutic Release and Ultimate Polymer Fate

The final role of a polymer therapeutic is to release the therapeutic agent upon cellular internalization. This is typically desired following escape from the endosome to avoid unwanted degradation by endosomal and lysosomal enzymes. For example, when delivering siRNA, release is preferred in the cytoplasm where it can then directly enter into the RNA interference (RNAi) pathway. Therefore, a number of approaches have been developed to promote release of therapeutic agents at a desired location within the cell.

A common strategy for intracellular-induced therapeutic release is to conjugate the therapeutic agent to a polymer scaffold using a degradable linkage. The most common types of degradable linkages used for intracellular drug release cleave in response to changes in pH, redox potential, or enzymatic degradation. Acid-labile linkages include esters, carbonates, carbamates, acetals, and hydrazones among others,[58–63] while enzymatically-degradable linkers comprised of specific ester- or peptide-containing sequences are selectively cleaved by esterases or peptidases, respectively, facilitating intracellular therapeutic release.[64–66] Disulfide linkages are the primary example of a chemical linkage that cleaves upon experiencing a change in redox potential.[67–69] Glutathione, the most abundant non-protein peptide in mammalian cells, is an efficient reducing agent meant to maintain the redox potential inside of the cell by

reducing reactive oxygen species but also has been shown to effectively reduce most forms of disulfide bonds.[70] This type of bond cleavage occurs readily and almost exclusively inside of the cytoplasm, which would promote therapeutic release from the polymeric carrier only after escaping the endosome. Also, higher levels of glutathione are observed in a number of cancer cell types compared to concentrations present in healthy tissues, which further promotes the likelihood of disulfide bond cleavage in these cancer cells.[71]

After the polymer "vehicle" has delivered its therapeutic payload to the appropriate location within the cell, it must be reabsorbed or eliminated from the body to avoid toxic *in vivo* accumulation. This can be accomplished using a polymer therapeutic in which the polymer component is partially or entirely degradable, or small enough to be excreted whole by the body. Examples of biodegradable polymers include poly(L-lactide/glycolide),[72] polypeptides,[73] and polysaccharides.[74] These polymers are capable of being completely degraded, or can be used as part of larger polymeric scaffolds which are reduced in size upon partial degradation of lactide or glycolide linkages, thus facilitating polymer clearance from the body. Polymers that are to be secreted based upon size are removed by renal filtration in the kidneys and typically must have hydrodynamic diameters less than ~15 nm for adequate removal without renal accumulation.[75] Thus, adequate control over the size of the delivery vehicle is necessary to avoid both rapid clearance from the body and to prevent perpetual accumulation by being too large for long term elimination to occur.

Reversible Addition-Fragmentation Chain Transfer Polymerization

The development of reversible-deactivation radical polymerization (RDRP) techniques including nitroxide-mediated polymerization (NMP),[76,77] atom transfer radical polymerization (ATRP),[78–81] and reversible addition-fragmentation chain transfer (RAFT)[82–87] polymerization has made possible the synthesis of polymers with precise compositions, predetermined molecular weights, and advanced architectures comprised of monomers possessing a wide variety of functional groups. RAFT polymerization is arguably the most versatile of the RDRP techniques owing to the increased tolerance of protic functional groups and solvents allowing for the polymerization of styrenics, (meth)acrylates, (meth)acrylamides, acrylonitriles, vinyl esters, and vinyl amides, in organic or aqueous media under homogeneous or heterogeneous conditions. In particular, the development of aqueous RAFT (aRAFT) polymerization has allowed for the direct synthesis of polymers containing biologically relevant functional groups such as amines, carboxylates, phosphates, sulfonates, and betaines among others.[88–98] For these reasons, RAFT is an ideal polymerization method for the synthesis of advanced polymer-based therapeutics.

The RAFT Mechanism

The mechanism of RAFT polymerization is fundamentally different from the mechanisms of NMP and ATRP in that the main active/dormant equilibrium is established by degenerative chain transfer between active (propagating) and dormant chain ends rather than reliance upon the persistent radical effect. Successful degenerative chain transfer is achieved when the product of chain transfer is also a chain transfer agent of equal or similar reactivity. Operating under these conditions, RAFT polymerization

exhibits similarities to pseudo-living polymerizations in that narrow molecular weight distributions can be obtained while molecular weight progresses linearly with monomer conversion and high chain-end fidelity is maintained throughout the reaction such that sequential monomer addition results in the formation of block copolymers.

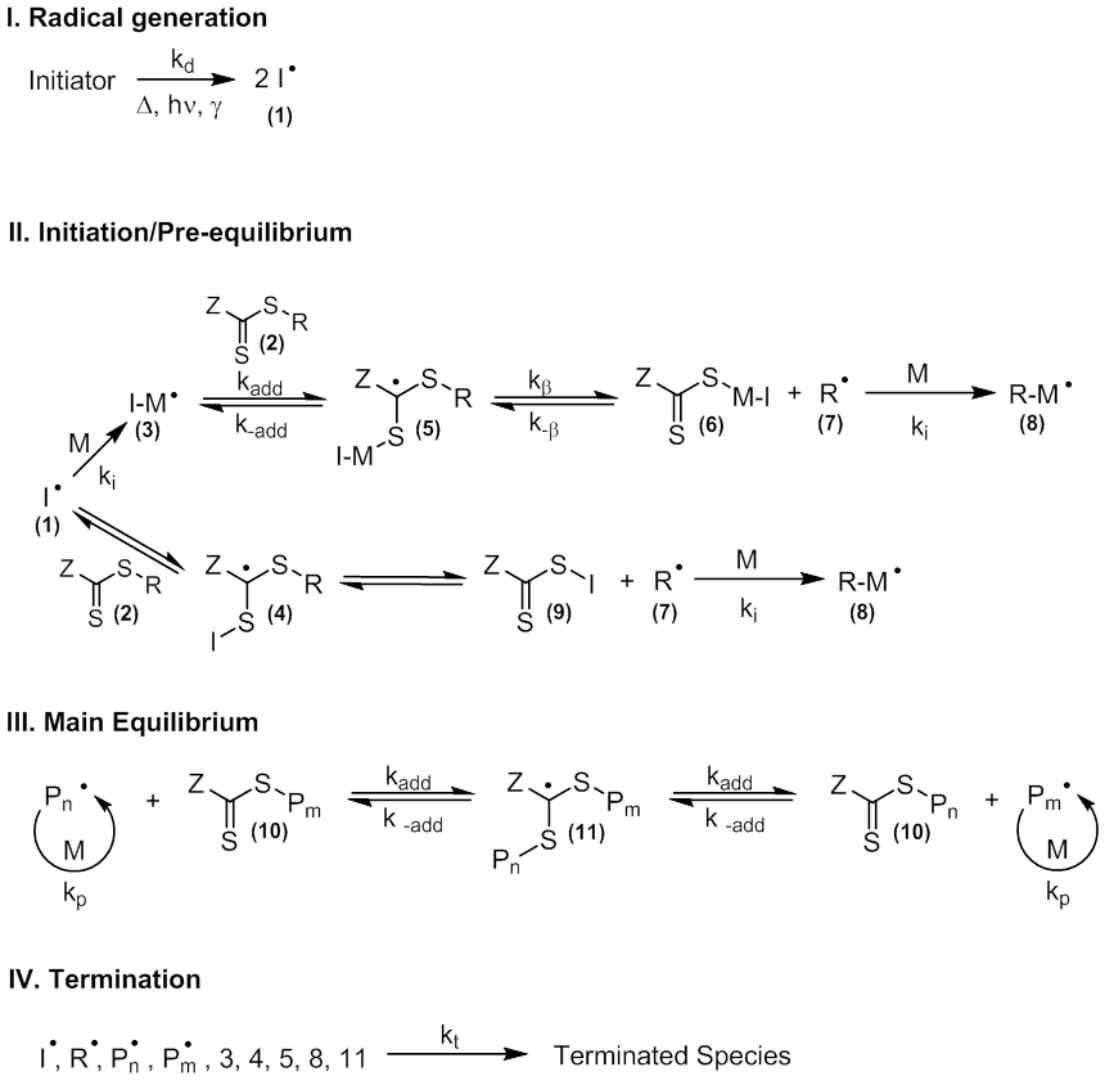

Scheme 1.1. Proposed mechanism of RAFT polymerization.

Like classical free radical polymerization, the first stage in the RAFT process involves decomposition of initiator into radicals (Scheme 1.1). However, the fate of initiator-derived radicals differs significantly during RAFT polymerization due to the presence of a thiocarbonylthio-containing chain transfer agent (CTA). The initiation/pre-equilibrium stage of RAFT consists of multiple kinetically distinct chain transfer reactions. During this period, initiator-derived radicals **1** can either initiate polymerization by direct addition to monomer to form the propagating species **3**, or add directly to CTA **2** to afford the radical intermediate **4**. Although the formation of **4** is also reversible, eventual fragmentation of the R-group yields a new initiator-derived CTA **9** and R-group-derived radical **7** capable of adding to monomer to form the propagating species **8**. Similarly, the initiator-derived propagating species **3** can add to CTA **2** with a rate constant k_{add} to yield the radical intermediate **5**. This intermediate can fragment in the reverse direction with rate constant k_{-add} or in the forward direction with rate constant k_{β} to form the macro-CTA **6** and the R-group-derived radical **7**, which can add to monomer forming the propagating species **8**. The pre-equilibrium period is complete when CTA **2** has been converted into the corresponding macro-CTA **6**. Similar to the initiation stage of other controlled/"living" polymerizations where $R_i > R_p$ must be met to achieve narrow molecular weight distributions, it is important that the duration of the pre-equilibrium period during RAFT be suitably short relative to the timescale of propagation such that the majority of polymer chains start growing at the same time.

Prolonged periods of little or no monomer conversion have often been observed during the pre-equilibrium stage of RAFT polymerizations.[99] Like conventional radical polymerizations, inhibition of RAFT is possible due to the presence of oxygen or other

impurities (e.g. thiol impurities originating from the CTA) that consume radicals early in the polymerization. Extended pre-equilibrium or inhibition periods in RAFT can also occur for certain CTA-monomer combinations because of slow reinitiation by R· due to preferred addition to the CTA thiocarbonyl (high $k_{-\beta}$) rather than addition to monomer (low k_i).[90,91,100–105] The cause of this initialization phenomena was first elucidated by McCleary, Klumperman, and coworkers using *in situ* ^{1}H NMR analysis during the 2-cyano-2-propyl dithiobenzoate-mediated polymerization of styrene.[106] As seen in Figure 1.4, complete conversion of the initial dithiobenzoate species (AD) to the corresponding single monomer unit adduct (ASD) was required before reaching the main RAFT equilibrium and thus observed as a period of minimal monomer conversion. Suppression or elimination of prolonged initialization periods can be accomplished by selection of CTA R- and Z-groups which favor fragmentation and reinitiation by R· (i.e. R-groups that are structurally similar to the propagating radical P_n·).

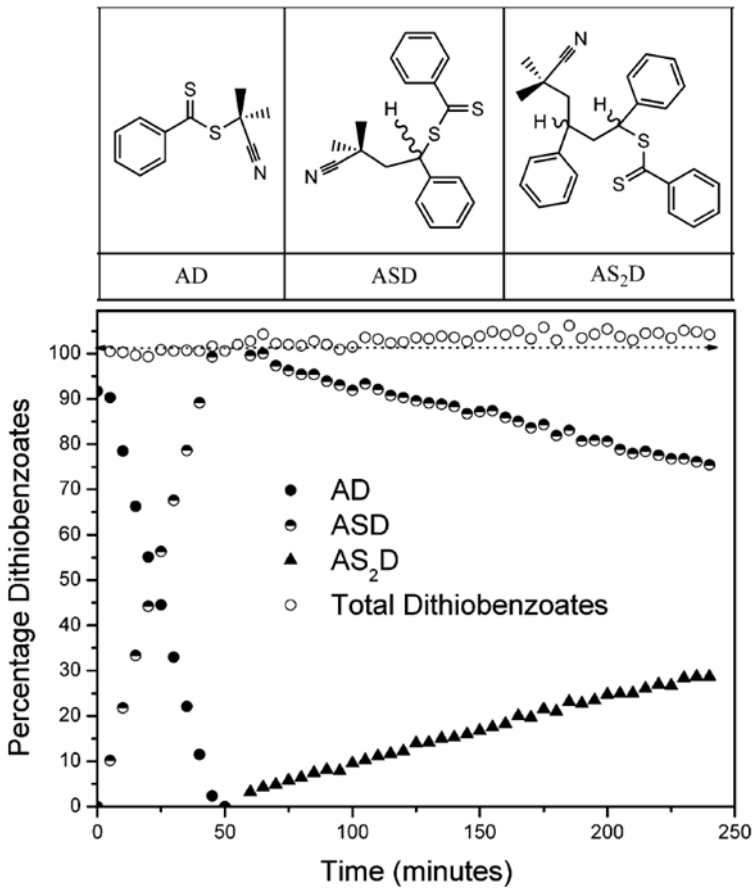

Figure 1.4. Percentage of dithiobenzoate species present during the AIBN-initiated polymerization of styrene in the presence of 2-cyano-2-propyl dithiobenzoate (AD).[106]

Propagation during the main RAFT equilibrium occurs as it does during conventional free radical polymerization where the rate of propagation (R_p) is expected to be first order with respect to both the concentration of monomer [M] and propagating radicals [P_n·] while independent of [CTA] as seen in equation 1. RAFT polymerizations often exhibit pseudo-first-order kinetic behavior when a steady state radical concentration is reached where $R_i \approx R_t$, allowing for simplification of equation 1 to equation 2 where k_{app} is the apparent propagation rate constant equal to $k_p[P_n\cdot]$.

$$R_p = k_p[P_n\cdot][M] \quad (1)$$

$$R_p = k_{app}[M] \quad (2)$$

Degenerative chain transfer during RAFT polymerization allows for the total number of polymer chains to greatly exceed the number of propagating radicals. This is a cornerstone feature of any RDRP technique since reducing [P_n·] by a factor of 10 will result in a 10-fold reduction in R_p but a 100-fold reduction in the rate of bimolecular radical termination (R_t) due to the second order dependence of R_t on [P_n·] (equation 3).

$$R_t = k_t[P_n \cdot]^2 \quad (3)$$

In theory, the introduction of CTA (RAFT agent) to a conventional free radical polymerization should have no effect on R_p as seen in equation 1. However, in practice R_p during RAFT polymerization is significantly reduced compared to the analogous free radical polymerization conducted in the absence of CTA with much debate over the exact cause of rate retardation.[107–110] One possible explanation for the differences in observed polymerization rates between conventional and RAFT polymerizations is due to extended lifetimes of the intermediate radical **11**, such that [P_n·] is lower than what would be predicted based upon the total radical concentration resulting from initiator-derived radicals.[111] While the intermediate radical **11** has been observed by electron spin resonance (ESR) spectroscopy, the observed concentrations were too low to completely explain the reduction in R_p for RAFT polymerizations.[112–115] Radical trapping or "sink" theories which suggest intermittent and reversible coupling of the transient species **11** with other radical species including P_n·, I·, and **11** have also been proposed with some spectroscopic evidence provided for the formation of these intermediates using electrospray ionization mass spectrometry (ESI-MS) and nuclear magnetic resonance

(NMR) spectroscopy, however, there is still much debate as to the exact cause of propagation rate retardation in RAFT polymerizations.[116–118]

Molecular Weight Control in RAFT Polymerization

In RAFT polymerization, the theoretical number average degree of polymerization ($X_{n,th}$) can be determined based upon the molar ratio of consumed monomer to the number of polymer chains formed during polymerization such that:

$$X_{n,th} = \frac{[M]_0 \rho}{[CTA]_0 + 2f[I]_0(1 - e^{-k_d t})} \quad (4)$$

where $[M]_0$ is the initial monomer concentration, ρ is the fractional monomer conversion, $[CTA]_0$ is the initial CTA concentration, f is the initiator efficiency, $[I]_0$ is the initial initiator concentration, k_d is the initiator dissociation constant, and t is the reaction time. In a typical RAFT polymerization, the $[CTA]_0$:$[I]_0$ is suitably high such that the total number of initiator-derived polymer chains is negligible allowing for omission of the second term in the denominator of equation 4.[110] The theoretical number average molecular weight ($M_{n,th}$) can then be calculated according to:

$$M_{n,th} = X_{n,th} M_{MW} + CTA_{MW} = \frac{[M]_0 \rho}{[CTA]_0} M_{MW} + CTA_{MW} \quad (5)$$

where M_{MW} and CTA_{MW} are the molecular weights of monomer and CTA respectively. It is worth noting that equation 5 assumes 100% of CTA results in formation of a polymer chain and has been shown to underestimate $M_{n,th}$ compared to experimentally determined M_n ($M_{n,exp}$) during RAFT polymerizations where incomplete consumption of CTA occurs during the pre-equilibrium period or due to CTA degradation during polymerization.[119]

RAFT Agent Design

Chain transfer agents possessing thiocarbonylthio functional groups (RAFT agents) have been utilized to mediate the polymerization of a wide variety of monomer types including styrenics, (meth)acrylates, (meth)acrylamides, acrylonitriles, vinyl esters, and vinyl amides among others. As shown in Figure 1.5, the RAFT agent consists of a reactive C=S double bond capable of addition to propagating radicals, a weak S-R bond to promote rapid fragmentation and reinitiation by the R-group, and Z-group that influences the stability of the intermediate radical. The R-group is only involved during the initialization period while the Z-group is present on the ω-terminus of dormant RAFT chains throughout the entire polymerization. Consequently, the Z-group has the greatest influence over polymerization control and must be chosen in accordance with monomer type. For this reason a number of Z-groups including dithioesters,[82] trithiocarbonates,[120] xanthates,[121] and dithiocarbamates[122] have been utilized to polymerize a range of monomers from "more activated monomers" (MAM) such as methyl methacrylate to "less activated monomers" (LAM) such as vinyl acetate. Furthermore, "universal" or "switchable" RAFT agents based upon 4-pyridinyl dithiocarbamates (Figure 1.5) have been designed to polymerize a wider range of monomers.[123–125] In the presence of acid, the pyridine ring is protonated and elelctron withdrawing, allowing for control over polymerization of MAMs. Alternatively, use of 4-pyridinyl dithiocarbamates in the electron donating neutral form facilitates polymerization control of LAMs. General guides for RAFT agent R- and Z-group selection for a given monomer-type are also now available as shown in Figure 1.6.

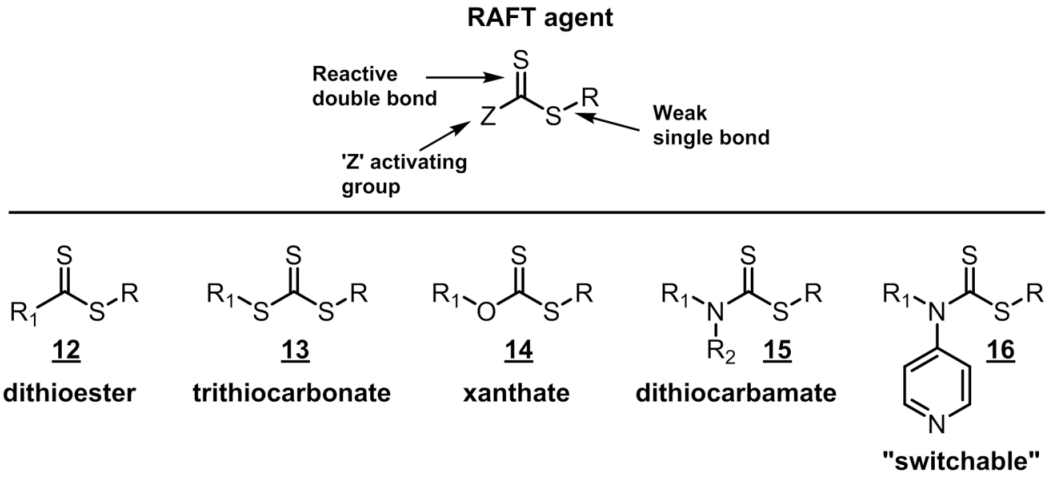

Figure 1.5. General structures of commonly used RAFT agents.

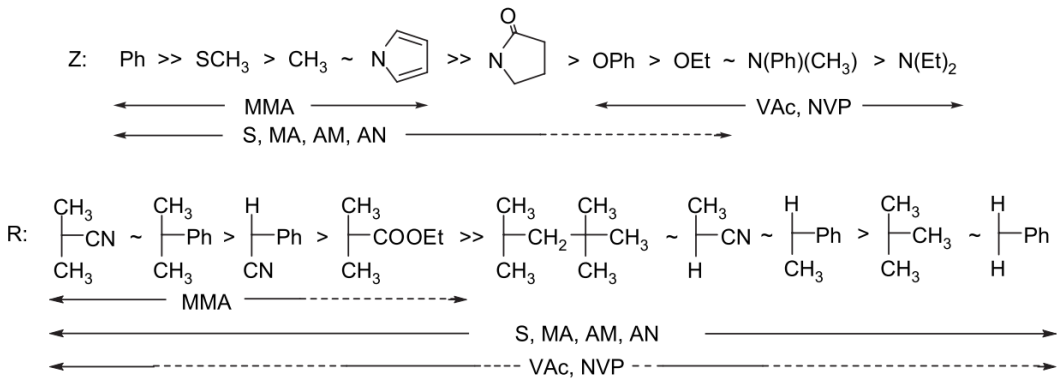

Figure 1.6. Guidelines for RAFT agent Z-group, R-group, and monomer selection based upon previously reported experimental results.[87] Dashed lines indicate marginal polymerization control.

End Group Functionalization of RAFT Polymers

It is often desirable or necessary to control polymer end group functionality. Inherent to polymers synthesized by RAFT is retention of the RAFT agent R-group on the α-terminus and the thiocarbonylthio moiety and Z-group on the ω-terminus (Figure 1.7). Accordingly, preparation of functional telechelic RAFT polymers is readily accomplished by incorporating the desired functionalities onto the RAFT agent R- and Z-groups.[126–129] However, precise control over end group functionality not directly

obtainable through R- and Z-group selection necessitates the use of post-polymerization end group transformations. Extensive efforts have thus been made toward end group functionalization of RAFT polymers by exploiting the latent reactivity of the thiocarbonylthio moeity.[130–137]

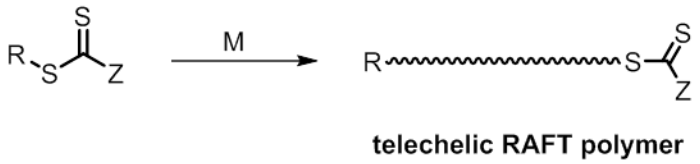

Figure 1.7. R/Z-group approach toward the synthesis of α,ω-telechelic polymers by RAFT.

While the reactive thiocarbonylthio ω-terminus of RAFT polymers functions as a useful chemical "handle" for subsequent end group transformations, the instability of this group may be undesirable depending upon the end-use of the RAFT polymer. Bulmus and coworkers recently studied the effect of RAFT agent type on cytotoxicity of the biocompatible polymer pHPMA. *In-vitro* cell viability assays showed that dithiobenzoate-functional pHPMA was significantly more toxic than analagous trithiocarbonate-terminated pHPMA.[138] This is likely due to the hydrolytic instability of dithiobenozoates relative to trithiocarbonates, with hydrolysis byproducts responsible for the decreased cell viability. A number of methods now exist whereby the reactive thiocarbonylthio moiety can be converted to a benign end group to minimize unintended consequences of RAFT agent reactivity.[139–142]

Stimuli-Responsive Polymers

Of particular interest in the field of polymeric drug carriers is the ability to design stimuli-responsive behavior into the delivery "vehicle" such that autonomous functions can be performed *in-vivo* that elicit a therapeutic effect. For example, the acidic

environment of tumoral tissue may be used as an environmental trigger for polymer-bound drug release.[143] Stimuli-responsive polymers in solution can exhibit changes in chain conformation, size, or solubility in response to biologically relevant stimuli such as changes in pH, redox potential, temperature, ionic strength, or specific molecular interactions.[144] Furthermore, externally applied stimuli such as electromagnetic radiation, changing magnetic fields, and mechanical forces (sonication) have also been used to elicit changes in polymer physical and chemical properties.[145] Such stimuli-responsive polymer properties can be exploited to passively/actively target polymeric drug carriers, promote cell-specific internalization, endosomal escape, site-specific drug release, trigger drug carrier degradation/elimination from the body, and allow polymers to function as combined therapeutic/diagnostic (theranostic) agents. It is therefore becoming ever more pertinent to design multipli-responsive polymeric carriers that can exhibit rapid and reversible changes in physical and chemical properties in response to discrete changes in orthogonal biologically relevant stimuli.

pH-Responsive Polymers

Polymers comprised of weakly acidic or basic functional groups (polyacids or polybases) make up a class of polyelectrolytes that exhibit pH-dependent aqueous solution properties and have been used extensively in a variety of applications including drug delivery.[97,146–157] A change in solution pH results in a corresponding change in the degree of ionization of the polyelectrolyte and subsequently its hydration state. This can ultimately lead to aggregation or self assembly of polyelectrolyte-containing polymers. Polyacids exist predominantly in the ionized form when the solution pH (pH_{sol}) is greater than the pK_a of the poly acid. Accordingly, polyacids are protonated and therefore neutral

(or nearly neutral) in charge and less hydrophilic when $pH_{sol} < pK_a$. Conversely, polybases are ionized and therefore water soluble when $pH_{sol} < pK_a$ and neutrally charged and less water soluble when $pH_{sol} > pK_a$. It is therefore possible to dictate whether increasing or decreasing the solution pH will increase or decrease polymer solubility depending upon whether the polymer is a weak polyacid or polybase Figure 1.8 shows some of the more common acid- and base-functional acrylic monomers that are readily polymerizable by RDRP techniques such as RAFT to afford the corresponding pH-responsive polymers.

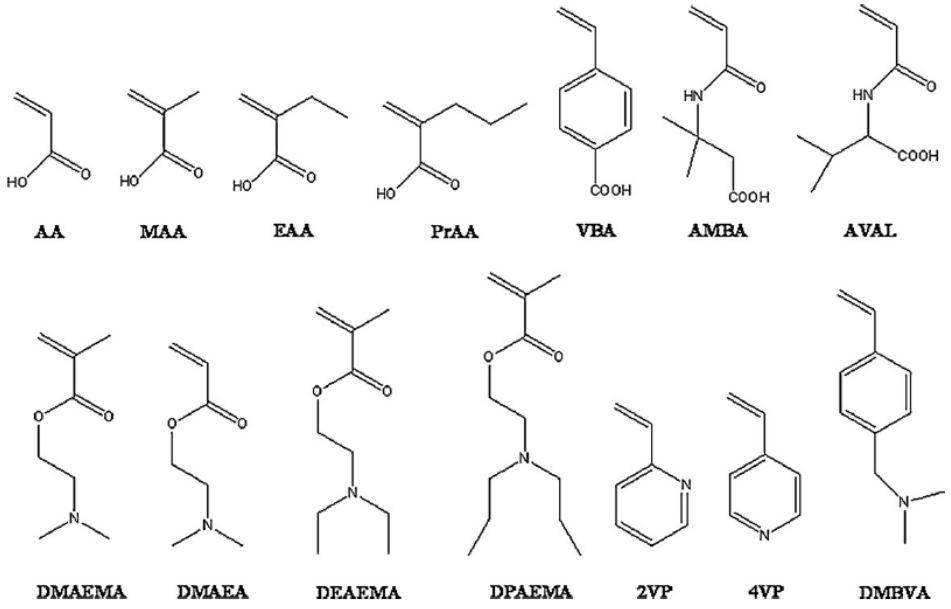

Figure 1.8. Common pH-responsive monomers polymerizable by RDRP techniques.[144]

Temperature-Responsive Polymers

Temperature-responsive polymers are those which exhibit a volume phase transition at a critical temperature. In solution, the influence of temperature on polymer solubility can be explained by the mutual influences of the enthalpy (ΔH) and entropy (ΔS) of mixing on the total free energy of mixing (ΔG) according to equation 6. Polymers

which exhibit a decrease in solubility in a given solvent upon heating possess a lower critical solution temperature (LCST), above which polymer-solution phase separation occurs. For these systems, ΔS is negative and an increase in temperature results in a corresponding increase in ΔG with the temperature at which ΔG = 0 defined as the LCST. Polymers that exhibit increased solubility in a given solvent upon heating possess an upper critical solution temperature (UCST) owing to a positive ΔS of mixing. In aqueous systems, entropic effects are driven by the ordering or disordering of water molecules at the polymer-water interface whereas the enthalpy of mixing is influenced by hydrogen bonding, dipole interactions, and hydrophobic effects.

$$\Delta G = \Delta H - T\Delta S \quad (6)$$

Figure 1.9 shows the more commonly used temperature-responsive monomers that have been polymerized by RAFT. The most extensively studied temperature-responsive polymers for biological applications are those derived from N-isopropylacrylamide (NIPAM) owing to the LCST of poly(NIPAM) (~32 °C) being near that of physiological temperature (37 °C).[158–161] A number of other N-substituted (meth)acrylamides have also been polymerized by RAFT to afford the corresponding temperature-responsive polymers and have seen applications in polymer-facilitated drug delivery.[146,162–166]

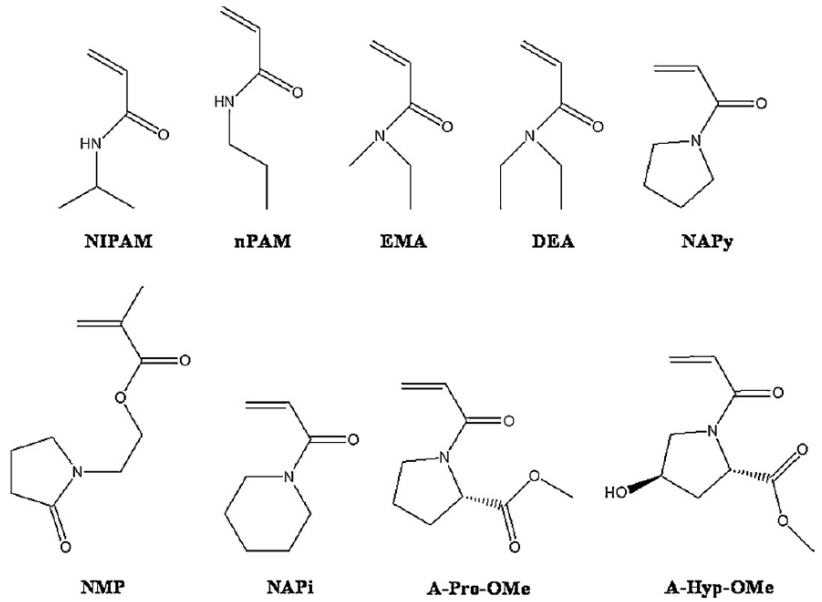

Figure 1.9. Common temperature-responsive monomers polymerizable by RDRP techniques.[144]

Redox-Responsive Polymers

Polymers exhibiting redox-responsive chemical and physical properties are actively being explored as stimuli-responsive drug carriers. Glutathione (GSH), the most abundant non-protein peptide in mammalian cells, is largely responsible for the reductive intracellular environment within cells.[71,167] The intracellular concentration of GSH (5-10 mM) is significantly higher than that outside of the cell (2- 20μM) resulting in a difference in redox potential that can be exploited as an intracellular-specific stimulus. Redox-responsive polymers for drug delivery are almost exclusively based upon disulfide linkages which are chemically stable in the oxidative extracellular environment while being rapidly reduced to the corresponding thiols by GSH upon cellular internalization.[46,168–174] Consequently, redox-responsive polymers differ from pH- and temperature-responsive polymers in that the "response" is cleavage of covalent disulfide linkages rather than a thermodynamic change in polymer hydration/solubility. This

makes possible the triggered release of covalently bound therapeutics such as thiol-functional siRNA as was recently demonstrated by York et al.[46] There are a number of reviews that address the potential applications of redox-responsive disulfide-containing polymer therapeutics.[168,171,172,174–176]

Advanced Macromolecular Architectures

While imparting stimuli-responsive behavior into polymer-drug conjugates through careful selection of monomer-type and end group functionality has the potential to address many of the barriers to drug delivery in a single delivery "vehicle," it is evident that multipli-responsive polymer therapeutics will likely be needed thus necessitating the use of branched or block copolymers where discrete blocks of the polymer are designed to respond to different stimuli. Furthermore, issues such as therapeutic agent protection, vascular circulation, tumoral accumulation, and ultimate polymer clearance from the body can be accomplished by controlling polymer architecture. Upon the advent of controlled/"living" polymerization techniques, a number of polymer architectures are now possible including alternating/statistical/gradient/multiblock copolymers, functional telechelics, stars, hyperbranched polymers, dendrimers, and molecular brushes (Figure 1.10).[177–185]

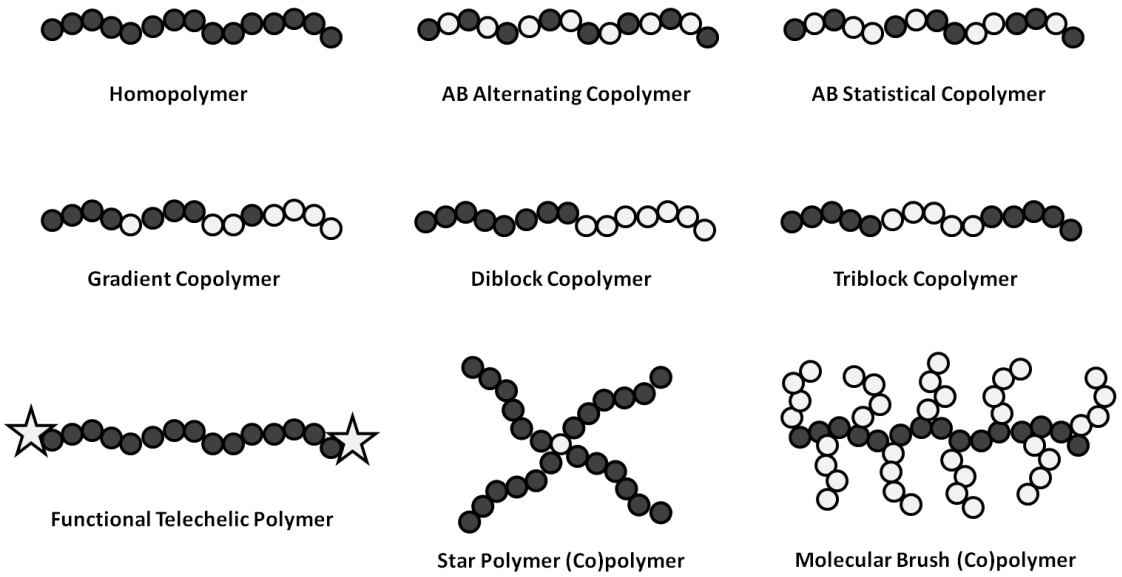

Figure 1.10. Polymer architectures accessible through the use of controlled/"living" polymerization techniques.

Highly branched architectures with tailorable shapes and sizes are of particular interest for polymer therapeutics. Compared to analogous linear polymers, highly branched polymers have been shown to exhibit increased vascular circulation and tumoral tissue accumulation.[186] While self-assembled polymer structures such as micelles and vesicles share many of the benefits of branched polymers, *in-vivo* usage is limited due to dilution-induced disassembly caused by polymer concentrations falling below the critical micelle concentration (CMC).[89,187] Consequently, branched polymer architectures that are assembled using permanent or reversible covalent linkages are desired.

Molecular Brush Copolymers

Molecular brush or "bottle-brush" copolymers are comprised of polymeric side-chains attached to a polymer backbone and can exhibit highly branched spherical or cylindrical morphologies with minimal intermolecular chain entanglement owing to the volume-exclusion interactions between sterically crowded polymeric side-chains.[188,189]

Molecular brush architectures are of particular interest as drug delivery "vehicles" due to their unique branched topology and readily tailorable dimensions. As stated previously, large, highly branched, and cylindrical polymer architectures exhibit increased *in-vivo* circulation times, enhanced accumulation in tumoral tissue due to the EPR effect, and improved biocompatibility compared to analogous linear polymers.[186] Molecular brush copolymers therefore represent an attractive polymer architecture that has the potential to simultaneously address numerous issues associated with drug delivery.

In general, molecular brush synthesis is accomplished by one of three routes referred to as "grafting from," "grafting onto," and "grafting through" (Figure 1.11). "Grafting from" molecular brush synthesis involves initial preparation of a multifunctional backbone (macroinitiator) followed by side chain growth from initiator side groups. Controlled polymerization techniques such as RAFT, ATRP, NMP, and ROP have been used to prepare molecular brush backbones, which typically require additional post-polymerization modification in order to attach the desired initiator groups along the backbone.[190–194] Side chain growth is most often accomplished using RDRP techniques such as ATRP. Limited use of RAFT polymerization to afford side chain growth is due in part to difficulties in attaching the RAFT agent to the brush backbone by post-polymerization modification and also because of the fragmentation-chain transfer nature of RAFT requiring that either a polymer side chain fragment from the backbone in order to propagate or necessitating the unlikely collision of sterically restricted polymer end groups in order for degenerate chain transfer to occur.[194] While there are some limitations regarding the synthesis of molecular brushes using "grafting from"

approaches, purification of molecular brushes synthesized in this fashion is typically simpler since the resulting molecular brush is the only polymeric product of the reaction.

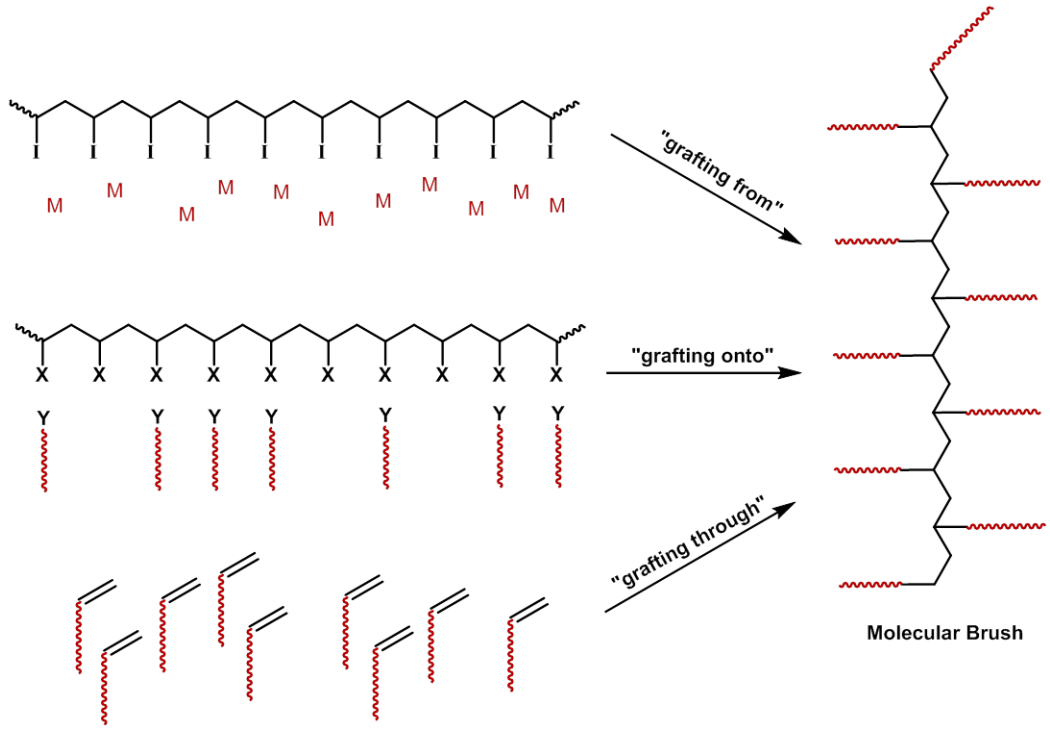

Figure 1.11. "Grafting from," "grafting onto," and "grafting through" synthetic routes toward molecular brush synthesis.

"Grafting onto" methods allow for preparation of molecular brush back bone and side chains separately.[195–197] Side chains are then grafted onto the brush backbone using efficient coupling or "click" type reactions to ensure high side chain grafting density. This approach makes possible the synthesis of well-defined side chains and backbones first, such that molecular brushes with predetermined backbone and side chain lengths are easier to prepare. In addition to covalent means of "grafting onto" molecular brush synthesis, supramolecular brushes based upon noncovalent interactions have been demonstrated which rely upon coordination bonding, hydrogen bonding, or ionic

interactions between side chains and backbones.[198–200] This type of supramolecular brush assemblage occurs naturally in proteoglycan aggregates found in cartilage tissues which are comprised of a positively charged polypeptide backbone electrostatically bound to glycosaminoglycan side chains.[201] While practical, the primary drawback to "grafting onto" methods is the near impossibility of achieving 100 % grafting density of the molecular brush backbone due to kinetic and thermodynamic restrictions resulting from steric exclusion of side chains as grafting density increases.

The third and arguably most versatile molecular brush synthetic route is referred to as "grafting through." This method relies upon first using a controlled polymerization technique to synthesize macromonomers (MMs) which possess polymerizable end groups that can then be reacted by a second polymerization technique to afford the corresponding molecular brush.[202–205] "Grafting through" is the only approach that affords molecular brushes with 100 % side chain graft density since each brush backbone repeat unit is inherently attached to a polymer side chain. However, this method often results in kinetically limited reactions with low MM conversions due to the steric constraints arising from the use of MMs and the low concentration of polymerizable end groups typically ranging from 0.01-0.1 M.

To overcome these issues, ring opening metathesis polymerization (ROMP)[206–209] has recently been used to successfully synthesize molecular brushes from norbornene-functional MMs while achieving near quantitative conversion of norbornene end groups owing to the high reactivity and functional group tolerance of the current generation of ruthenium-based metathesis catalysts (Figure 1.12).[189,202,210–217] This approach has since been used to synthesize a variety of molecular brushes with block-backbone and block-

side chain subarchitectures from a wide range of MMs derived from controlled polymerization techniques. While ROMP of MMs overcomes the previous limitations associated with "grafting through" molecular brush synthetic routes, the facile synthesis of norbornene-functional MMs still represents an ongoing challenge.

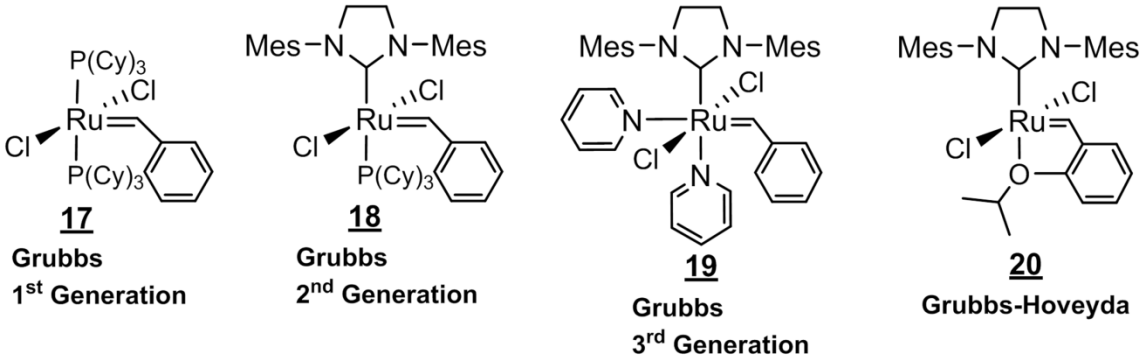

Figure 1.12. Ruthenium-based metathesis catalysts.

Synthesis of MMs can be accomplished by either "direct-growth" (DG-MM) or "growth-then-coupling" (GC-MM) methods as described recently by Xia and coworkers (Figure 1.13).[218] DG-MM synthesis has been accomplished through the use of norbornene-functional initiators during ROP, NMP, ATRP, and through the use of norbornene-functional chain transfer agents during RAFT polymerization.[202,219–226] The use of reversible deactivation radical polymerization techniques to synthesize MMs is particularly advantageous due to the wide variety of vinyl monomers available and ease of controlling end group functionality. However, DG-MM synthesis by RDRP techniques requires polymerization optimization for a given monomer to minimize radical addition to the norbornene olefin during polymerization.[214] Furthermore Xia and coworkers have demonstrated that even trace amounts of difunctional macromonomer impurities resulting from bimolecular radical coupling of α-norbornene-functional polymers can result in

undesired molecular brush branching and broadened molecular weight distributions.[218] Therefore, facile and efficient growth-then-coupling methods to synthesize RDRP-based MMs are needed.

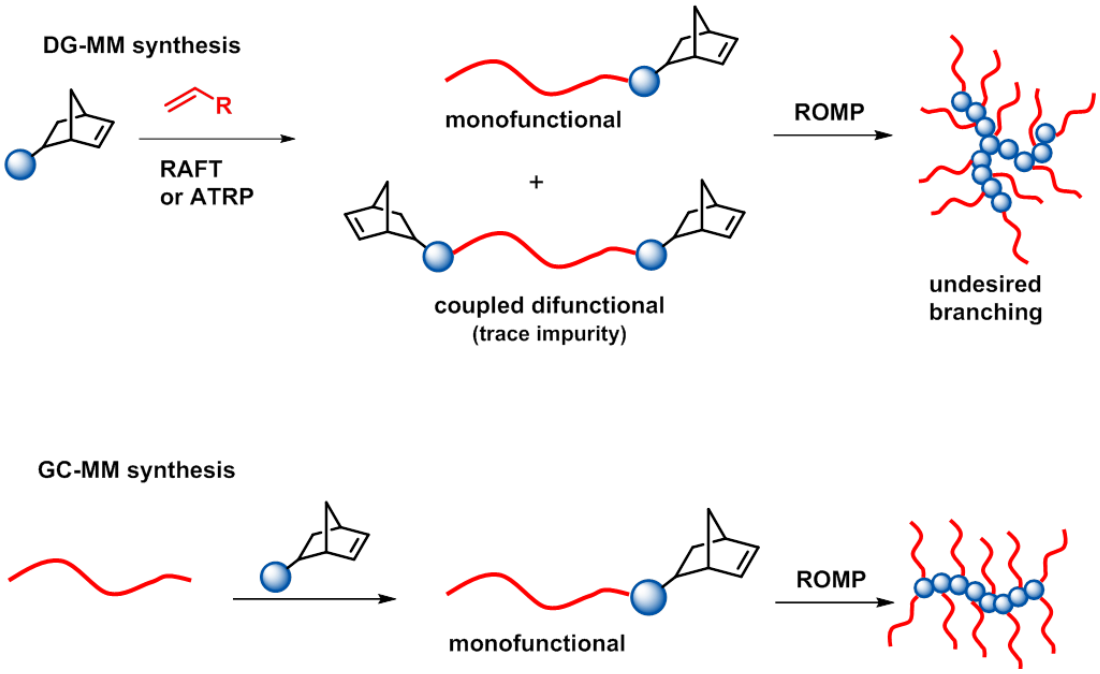

Figure 1.13. Norbornene-functional macromonomer synthesis by direct-growth (DG-MM) and growth-then-coupling (GC-MM) synthetic routes.

Due to recent improvements in molecular brush synthetic methods, a number of drug delivery applications have been developed that readily exploit the discrete sizes and highly branched morphologies of molecular brushes. Johnson, Grubbs and coworkers recently demonstrated the synthesis of drug-loaded, bivalent molecular brush copolymers that were synthesized using "grafting through" ROMP methodologies developed in the same lab (Figure 1.14).[212] Molecular brushes were comprised of polynorbornene backbones and PEG side chains with anticancer drugs doxorubicin (DOX) and camptothecin (CT) attached to the brush backbone using a photocleavable nitrobenzyloxycarbonyl linker. Subsequently, photolysis of the degradable linkages using

365 nm UV light afforded rapid release of DOX and CT with 50% drug release observed in 3.1 min and 10 min for each drug respectively. When irradiated with UV light, the molecular brush-cancer drug conjugates were shown to have similar half-maximum inhibitory concentrations to the free drugs whereas the PEG-based drug-bound molecular brushes showed minimal influence on cell viability due to steric shielding of the covalently attached anticancer drugs.

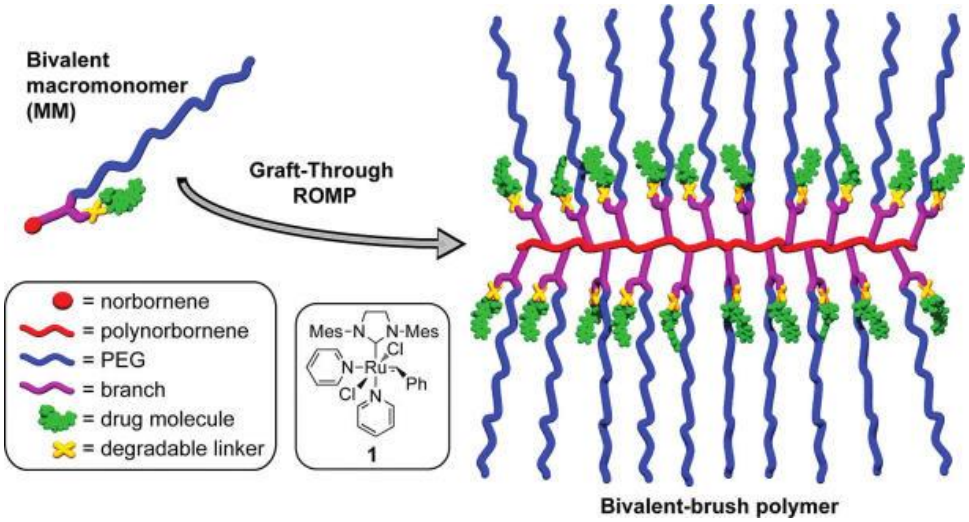

Figure 1.14. Drug-loaded, bivalent molecular brush polymers synthesized using "grafting through" ROMP of norbornene-functional macromonomers.[212]

CHAPTER II

OBJECTIVES OF RESEARCH

The original “depot” model proposed by Ringsdorf in 1975 was the first attempt at addressing the issues of drug delivery using a single macromolecular architecture. Initially, limitations in the available synthetic methods prevented the synthesis of well defined polymers comprised of functionally diverse monomers and advanced architectures such as block, star, and molecular brush copolymers. Upon the advent of controlled/”living” polymerization techniques such as reversible-deactivation radical polymerization (RDRP), facile preparation of (co)polymers with tailorable architectures, predetermined molecular weights, and of narrow molecular weight distributions has made possible the synthesis of a wide variety of interpretations of the Ringsdorf “depot” model. However, limitations still exist regarding the facile synthesis of polymers aimed at specifically addressing the issues of drug delivery.

The main work described in this dissertation focuses on the development of synthetic approaches toward novel stimuli-responsive polymers and advanced polymer architectures that specifically address the issues of *in vivo* drug delivery. Particular attention is given to understanding the fundamentals of the underlying chemistry used to synthesize the polymers discussed in this work.

The specific objectives of this research are to:

1. Synthesize a library of methacryloyl sulfonamide (MSA) monomers with pK_a values in the biologically relevant regime.
2. Develop conditions to control the RAFT polymerization of MSA monomers.

3. Investigate the tunable pH- and CO_2-responsive aqueous solution properties of MSA RAFT polymers.
4. Investigate temperature-dependent trithiocarbonate chain-end degradation observed during RAFT polymerization of N-arylmethacrylamides.
5. Synthesize RAFT polymer small molecule analogs by single monomer unit insertion in order to study the byproducts of trithiocarbonate degradation.
6. Use *in situ* ^{1}H NMR analysis to study the mechanism of N-arylmethacrylamide promoted trithiocarbonate chain-end degradation.
7. Develop complimentary mechanistic and kinetic models to explain the observed effects of N-arylmethacrylamide substitution on amide nucleophilicity.
8. Systematically investigate the effects of nucleophilic catalyst, reducing agent, and solvent on “one-pot” aminolysis/thiol-maleimide end-group functionalization of RAFT polymers.
9. Identify and prevent detrimental nucleophile-promoted thiol-maleimide side reactions.
10. Elucidate the mechanism(s) of base catalyzed maelimide polymerization initiated by thiols and thiol-maleimide adducts.
11. Optimize “one-pot” aminolysis/thiol-maleimide end-group functionalization reaction conditions to afford selective and quantitative end group functionalization efficiency of RAFT polymers with N-substituted maleimides.
12. Synthesize thiol-reactive maleimide- and methanethiosulfonate-functional oxanorbornenes.

13. Synthesize ω-oxanorbornenyl macromonomers by end-group modification of RAFT polymers with thiol-reactive oxanorbornenes.
14. Develop polymerization conditions for the controlled ROMP of RAFT-polymer derived macromonomers.
15. Demonstrate reduction-induced disassembly of disulfide-containing molecular brushes.

The work addressing these objectives is divided into four main sections. The first section is concerned with the synthesis of a novel class of tunable pH-responsive polymers by RAFT polymerization. These polymers are to be synthesized using a library of sulfadrug-based methacryloyl sulfonamide monomers possessing pK_a values in the range of the early-to-late endosomes (pH = 5-7). Future work regarding these polymers is aimed at developing pH-responsive endolytic polymers that could be incorporated into polymer therapeutics to aid in endosomal escape, which is often cited as the "bottle neck" of drug delivery.

Section 2 is concerned with investigating the poor RAFT polymerization control of methacryloyl sulfonamide monomers despite using "standard" methacrylamide polymerization conditions. Consequently, work in this section aims to provide an understanding of the factors influencing RAFT agent degradation during MSA polymerization by systematically studying the effects of methacrylamide structure and polymerization temperature on the rates and mechanisms of RAFT polymer chain-end degradation. In addition, on-going work regarding the development of a mechanistic and kinetic theory aimed at explaining the unique influence of N-arylsubstitution on amide nucleophilicity is further discussed in Appendix B.

Control over polymer end group functionality is typically necessary when synthesizing highly branched polymer architectures such as molecular brushes. Section 3 details the identification and prevention of deleterious side reactions that we observed during “one-pot” aminolysis/thiol-maleimide end group functionalization reactions of RAFT polymers. The effects of solvent, nucleophilic catalyst, reducing agent, and reagent order of addition on RAFT polymer end-group functionalization efficiency are investigated. Particular attention is also given to finding suitable reagents and reaction conditions that favor quantitative end group functionlization of RAFT polymers with N-substituted maleimides with minimal side reactions.

Section 4 is concerned with developing a facile synthetic route towards molecular brush copolymers derived from RAFT polymers for potential use as drug delivery “vehicles.” This work is particularly focused on synthesizing RAFT polymer-derived macromonomers using optimized end group functionalization techniques as discussed in Section 3. Furthermore, this work aims to develop a facile synthetic route towards molecular brushes capable of intracellular-induced disassembly via the incorporation of disulfide linkages between the molecular brush backbone and side chain. Macromonomer polymerization control by ROMP and reduction-induced molecular brush disassembly are discussed.

CHAPTER III

EXPERIMENTAL SECTION

Materials

Methacryloyl chloride (Aldrich, 97%), N,N-dimethylacrylamide (Aldrich, 99%), styrene (Aldrich, 99%), aniline (Aldrich, 99%), benzylamine (Aldrich, 98%), and furan (Aldrich, 99%) were vacuum distilled and stored under N_2 at -10 °C prior to use. 4,4-Azobis(4-cyanovaleric acid) and azobisisobutyronitrile (AIBN) (Aldrich, 98%) were recrystallized from methanol and stored at -10 °C. N,N'-dimethylformamide (Acros, extra dry w/ sieves) was stirred under vacuum at room temperature for 60 min prior to use in order to remove traces of dimethylamine. The following were used as received: 2, 2'-Azobis(4-methoxy-2-4-dimethyl valeronitrile) (V-70) (Wako, 96%); sulfacetamide (Aldrich, >98%); sulfamethazine (Aldrich, >99%); sulfamethizole (Aldrich, >99%); sulfadimethoxine (Aldrich, >98.5%); sulfadoxine (Aldrich, >95%); sulfabenzamide (TCI, >98%); trimesic acid (Aldrich, 95%); 1-dodecanethiol (Aldrich, 98%); ethane thiol (Aldrich, 97%); carbon disulfide (Aldrich, 99.9%); 2-bromoisobutyryl bromide (TCI, 98%); triethylamine (Aldrich, 99.5%); NaH (Aldrich, 95%); maleic anhydride (Aldrich, 99%); acetic anhydride (Fisher, 99.2%); sodium acetate (Fisher, anhydrous); N-methylmaleimide (Aldrich, 97%); ethyl 2-mercaptopropionate (Aldrich, >95%); benzyl mercaptan (Fluka, >99%); hexylamine (Aldrich, 99%); 1,8-diazabicyclo[5.4.0]undec-7-ene (DBU) (Aldrich >99.0%); triethylamine (Aldrich, >99.5%); tributylphosphine (Aldrich, 97%); trimethylphosphite (Aldrich, >99%); 2nd generation Grubbs catalyst (Aldrich); ethylenediamine (Aldrich > 99.5%); di-*tert*-butyl dicarboante (Aldrich, > 99%); maleimide (Aldrich, 99%); methylchlroformate (Aldrich, 99%); 4-

methylmorpholine (Aldrich, redist., > 99.5%); trifluoroacetic acid (Aldrich, 99%); 3-bromopropylamine hydrobromide (Aldrich, 98%); sodium methane sulfinate (Alfa Aesar, 95%); 0.1 N NaOH (Alfa Aesar, standardized); and 0.05 N HCl (Alfa Aesar, standardized); $CDCl_3$ (Cambridge Isotopes, 99.8%); acetone-d_6 (Cambridge Isotopes, 99.9%); N, N'-dimethylformamide-d_7 (Cambridge Isotope, 99.5%); dimethylsulfoxide-d_6 (Cambridge Isotopes, 99.9%); acetonitrile-d_3 (Cambridge Isotopes, 99.8%); methylene chloride-d_2 (Cambridge Isotopes, 99.8%); Ethanol-D (Cambridge Isotopes, D 99%, <6% D_2O); and Deuterium Oxide (Aldrich, 99.9%). All other chemicals were purchased from Aldrich in the highest available purity and used as received.

Characterization

NMR spectra for structural analysis and monomer conversions were obtained using a Varian INOVA 300 MHz NMR spectrometer. Polymer molecular weights and molecular weight distributions (M_w/M_n) were determined by size exclusion chromatography (SEC) using DMF 20 mM LiBr as the eluent at a flow rate of 1.0 mL/min in combination with two Agilent PolarGel-M columns heated to 50 °C and connected in series with a Wyatt Optilab DSP interferometric refractometer and Wyatt DAWN EOS multiangle laser light scattering (MALLS) detector (λ = 633 nm). Absolute molecular weights and M_w/M_n were calculated using a Wyatt ASTRA SEC/LS software package. The d*n*/d*c* values for each polymer derivative in the above eluent at 35 °C were determined offline using a Wyatt Optilab DSP interferometric refractometer and Wyatt ASTRA d*n*/d*c* software.

Chapter IV Section 1 Experimental

Dithiobenzoic acid **21**

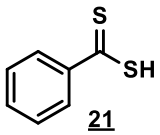

21

Magnesium (1.22 g, 50.0 mmol) was washed in anhydrous diethyl ether and dried in an oven prior to addition to a 250 mL round bottomed flask equipped with stir bar. The flask was flame dried under vacuum and backfilled with argon followed by the addition of anhydrous THF (25 mL). Bromobenzene (5.0 mL, 47.8 mmol) was then added dropwise via syringe over 15 min, upon which 75 mL of THF was added and the resulting Grignard solution transferred via cannula to a flame-dried 3-neck round bottomed flask equipped with condenser and heated to reflux (40 °C). Carbon disulfide (2.89 mL, 47.8 mmol) was then added dropwise over 15 min and the reaction stirred at 40 °C for an additional 2 h. Ice cold 0.5 N HCl (50 mL) was then added to the reaction followed by removal of approximately 75% of the THF/Et_2O by rotary evaporation. The pH of the aqueous solution was then adjusted to pH < 2 with 12 N HCl and transferred to a separatory funnel and extracted with diethyl ether (2 x 100 mL). The light pink aqueous layer was discarded and the dark pink/red ether layer kept in the separatory funnel, to which was added ice cold 10 wt. % NaOH (100 mL). Upon formation of distinct phases, the aqueous layer was removed and further washed with Et_2O (3 x 100 mL). The aqueous layer was again acidified (pH < 2) with 12 N HCl and the dithiobenzoic acid extracted into ether (2 x 100 mL) while discarding the aqueous layer. The Et_2O layer was dried over $MgSO_4$ and the solvent removed via rotary evaporation to give **21** as a purple oil (3.47 g, 47%).

Bis(thiobenzoyl)disulfide **22**

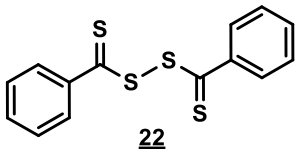

22

Dithiobenzoic acid **21** (3.47 g, 22.5 mmol) was dissolved in 2 N NaOH (150 mL) and transferred to a 1 L round bottomed flask equipped with stir bar. A solution of K_3FeCN_6 (15 g, mmol) in H2o (300 mL) was added dropwise over 1 h followed by stirring at room temperature for an additional hour. The resulting solids were removed by filtration and the solvent removed by rotary evaporation. **22** was further purified by recrystallization form EtOH to give deep purple crystals (1.71 g, 57%).

4-Cyanopentanoic acid dithiobenzoate **23**

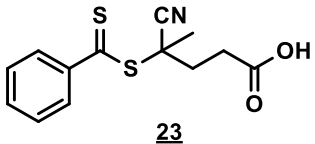

23

A solution of bis(thiobenzoyl)disulfide **22** (1.71 g, 5.6 mmol) and 4,4'-azobis(4-cyanopentanoic acid) (2.35 g, 8.4 mmol) in EtOAc (100 mL) was prepared in a 3-necked round bottomed flask equipped with stir bar and condenser. The reaction was degassed by purging with N_2 for 40 min prior to heating to reflux (77 °C) for 18 h. The reaction was quenched by exposure to air and freezing in liquid N_2 followed by solvent removal via rotary evaporation. The crude RAFT agent was purified by column chromatography (59:40:1 EtOAc:hexanes:AcOH). To remove residual AcOH, column fractions containing **23** were combined and transferred to a separatory funnel and washed with 0.05 N HCl (2 x 150 mL), brine (1 x 150 mL) and dried over $MgSO_4$ followed by solvent removal by

rotary evaporation to give **23** as a purple solid (2.22 g, 71%). ^{1}H NMR (300 MHz, $CDCl_3$): δ 7.91 (d, 2H), 7.57 (t, 1H), 7.40 (t, 2H), 2.77-2.40 (m, 4H), 1.94 (s, 3H).

Sodium ethyl trithiocarbonate **24**

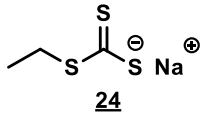

24

A suspension of NaH (2.11 g, 83.5 mmol) in anhydrous diethyl ether (150 mL) was cooled to 0 °C using an ice bath; ethane thiol (5.73 g, 92.3 mmol) was then added dropwise over 15 min accompanied by vigorous evolution of hydrogen gas. The reaction was stirred for an additional 15 min at 0 °C followed by dropwise addition of CS_2 (7.03g, 92.3 mmol) over 5 min and the reaction mixture stirred for an additional 60 min at room temperature and then diluted with pentane (100 mL). The resulting yellow precipitate was isolated by vacuum filtration before drying *in-vacuo* yielding **24** (12.07 g, 90%) as a hygroscopic yellow solid. ^{1}H NMR (300 MHz, D_2O): δ 3.15 (q, 2H), 1.27 (t, 3H). ^{13}C NMR δ: 35.36, 12.39.

Bisethyl trithiocarbonate **25**

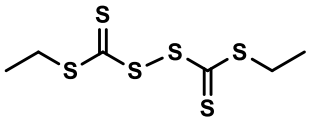

25

Sodium ethyl trithiocarbonate **24** (7.74 g, 48.3 mmol) was dissolved in H_2O (50 mL) in a 250 mL round bottomed flask equipped with magnetic stir bar. A solution of I_2 (13.49 g, 53.1 mmol) and potassium iodide (8.82 g, 53.1 mmol) in H_2O (100 mL) was subsequently added dropwise over 30 min to the stirred solution of sodium ethyl trithiocarbonate. The reaction mixture was stirred for an additional 60 min and transferred to a separatory funnel and extracted with ether (3 x 75 mL). The ether layers

were combined and washed with H_2O (2 x 150 mL), 5% $Na_2S_2O_3$ (2 x 150 mL) and brine (1 x 150 mL) before drying over $MgSO_4$ followed by solvent removal by rotary evaporation to give **25** as a yellow oil (6.29 g, 95%). ^{1}H NMR (300 MHz, $CDCl_3$): δ 3.30 (q, 4H), 1.35 (t, 6H).

4-cyano-4-(ethylsulfanylthiocarbonylsulfanyl)pentanoic acid **26**

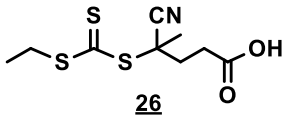

26

A solution of bisethyl trithiocarbonate **25** (5.00 g, 18.2 mmol) and 4,4'-azobis(4-cyanopentanoic acid) (7.66 g, 27.3 mmol) in EtOAc (250 mL) was prepared in a 500 mL 3-necked flask equipped with stir bar and condenser. The solution was purged with N_2 for 40 min prior to heating at reflux for 18 h. The reaction was then quenched via exposure to air and cooled to room temperature. The solvent was removed by rotary evaporation and the crude RAFT agent purified by column chromatography (60:35:5 hexanes:EtOAc:AcOH). To remove residual AcOH, column fractions containing **26** were combined and transferred to a separatory funnel and washed with 0.05 N HCl (2 x 150 mL), brine (1 x 150 mL) and dried over $MgSO_4$ followed by solvent removal by rotary evaporation to give **26** as a yellow solid (7.10 g, 74%).^{1}H NMR (300 MHz, $CDCl_3$): δ 3.37 (q, 2H), 2.70 (t, 2H), 2.60-2.30 (m, 2H) 1.89 (s, 3H), 1.36 (t, 3H).

General Procedure for Methacryloyl Sulfonamide Synthesis

Using a modified procedure, sulfa drug (40.0 mmol) was dissolved in 160 mL of a 1:1 (v:v) mixture of acetone and 0.5 N aqueous NaOH and stirred while cooling in an ice bath. Methacryloyl chloride (4.10 mL, 42.0 mmol) was then added dropwise over 30 min followed by removing the ice bath and stirring the reaction at room temperature for an

additional 60 min. The acetone was removed by rotary evaporation, followed by adjusting the solution to pH = 2 with 6 N HCl. The resulting solids were isolated using vacuum filtration and washed with 100 mL of dilute HCl (0.01 N) prior to drying *in-vacuo* for 48 h, yielding the desired monomers as colorless to off-white solids. The synthesis of methacryloyl sulfadoxine **30** required the use of 240 mL of a 1:2 (v:v) mixture of acetone and 0.5 N aqueous NaOH.

Methacryloyl sulfacetamide **27**

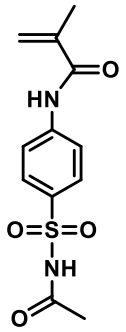

27

Yield: (10.29 g, 91%); mp 203-205 °C dec. ^{1}H NMR (300 MHz, DMSO-d_6): δ 11.99 (s, 1H), 10.20 (s, 1H), 8.11 – 7.65 (m, 4H), 5.84 (s, 1H), 5.58 (s, 1H), 1.93 (s, 3H), 1.89 (s, 3H). ^{13}C NMR (75 MHz, DMSO-d_6) δ 168.69, 167.34, 143.72, 139.99, 133.13, 128.67, 121.03, 119.50, 23.22, 18.63.

Methacryloyl sulfabenzamide **28**

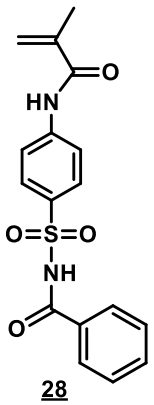

28

Yield: (12.89 g, 94%); mp 228-229 °C dec. ^{1}H NMR (300 MHz, DMSO-d_6): δ 12.46 (s, 1H), 10.22 (s, 1H), 8.02 – 7.87 (m, 4H), 7.83 (d, *J* = 7.2 Hz, 2H), 7.60 (t, *J* = 7.4 Hz, 1H), 7.47 (t, *J* = 7.6 Hz, 2H), 5.84 (s, 1H), 5.58 (s, 1H), 1.93 (s, 3H). ^{13}C NMR (75 MHz, DMSO-d_6) δ 167.36, 165.38, 143.79, 139.99, 133.24, 133.15, 131.54, 128.93, 128.61, 128.40, 121.03, 119.50, 18.62.

Methacryloyl sulfamethazine **29**

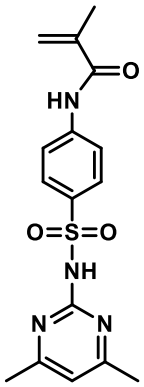

29

Yield: (13.39 g, 97%); mp 234-235 °C dec. ^{1}H NMR (300 MHz, DMSO-d_6): δ 11.47 (s, 1H), 10.10 (s, 1H), 7.86 (dd, *J* = 28.3, 8.6 Hz, 4H), 6.74 (s, 1H), 5.81 (s, 1H), 5.55 (s, 1H), 2.23 (s, 6H), 1.92 (s, 3H). ^{13}C NMR (75 MHz, DMSO) δ 167.61, 156.65, 143.19, 140.43, 135.08, 129.49, 121.24, 119.42, 113.97, 23.37, 19.04.

Methacryloyl sulfamethizole **30**

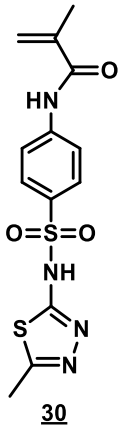

30

Yield: (12.42 g, 91%); mp 215-217 °C dec. ^{1}H NMR (300 MHz, DMSO-d_6): δ 13.90 (s, 1H), 10.12 (s, 1H), 7.77 (dd, *J* = 37.4, 8.4 Hz, 4H), 5.82 (s, 1H), 5.56 (s, 1H), 2.44 (s, 3H), 1.92 (s, 3H). ^{13}C NMR (75 MHz, DMSO-d_6) δ 167.80, 167.20, 154.46, 142.65, 140.03, 136.05, 126.71, 120.83, 119.70, 18.65, 16.10.

Methacryloyl sulfadimethoxine **31**

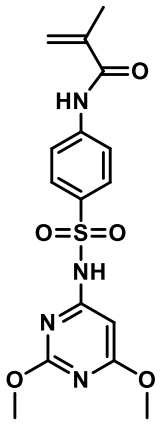

31

Yield: (14.72 g, 97%); mp 216-218 °C dec. ^{1}H NMR (300 MHz, DMSO-d_6): δ 11.50 (s, 1H), 10.17 (s, 1H), 7.86 (m, 4H), 5.92 (s, 1H), 5.82 (s, 1H), 5.57 (s, 1H), 3.77 (s, 3H), 3.73 (s, 3H), 1.92 (s, 3H). ^{13}C NMR (75 MHz, DMSO-d_6) δ 171.67, 167.30, 164.26, 159.90, 143.41, 139.98, 133.68, 128.30, 120.96, 119.64, 84.57, 54.54, 53.81, 18.59.

Methacryloyl sulfadoxine **32**

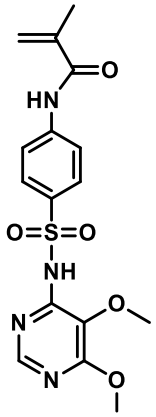

32

Yield (14.10 g, 93%); mp 198-199 °C. ^{1}H NMR (300 MHz, DMSO-d_6): δ 11.09 (s, 1H), 10.17 (s, 1H), 8.12 (s, 1H), 5.84 (s, 1H), 5.59 (s, 1H), 3.90 (s, 3H), 3.70 (s, 3H), 1.95 (s, 3H). ^{13}C NMR (75 MHz, DMSO-d_6) δ 167.32, 161.63, 150.43, 143.14, 140.06, 134.61, 129.88, 128.61, 127.21, 120.92, 119.40, 60.28, 54.08, 18.64.

General Procedure for RAFT Polymerization of Methacryloyl Sulfonamides

Briefly, methacryloylsulfonamide (5.0 x 10^{-3} mol, 150 equiv), CTA (**23** or **26**) (3.3 x 10^{-5} mol, 1 equiv), initiator (V-70 or V-501) (6.7 x 10^{-7} mol, 0.2 equiv), and trimesic acid (50 mg, ^{1}H NMR internal standard) were combined in a 10 mL graduated cylinder and DMF added to bring the final solution volume to 5.0 mL ($[M]_0$ = 1 M) or 6.0 mL (0.83 M) depending upon monomer solubility as indicated in Table 1. The solution was then transferred to a 10 mL test tube equipped with a magnetic stir bar and rubber septum followed by purging with N_2 for 40 mins. An initial aliquot (200 μL) was taken prior to heating the reaction vessel at the indicated temperature with subsequent aliquots taken at timed intervals and analyzed by ^{1}H NMR (DMSO-d_6) to determine monomer conversion by comparing the relative integral areas of the trimesic acid aromatic protons (8.64 ppm, 3H) to the monomer vinyl proton (5.84 ppm, 1H). SEC-MALLS (95% DMF/5% CH_3COOH, 20 mM LiBr) was used to monitor the progression of molecular weight and molecular weight distribution (M_w/M_n) throughout each polymerization. Polymers isolated for solubility studies were purified by precipitating the reaction mixture into a 10-fold excess of MeOH followed by isolating the resulting solids by ultracentrifugation. The isolated polymers were precipitated a total of three times from DMF into MeOH before drying overnight *in-vacuo*.

Methacryloyl Sulfonamide Monomer Titrations

Monomer stock solutions (1mM) were prepared by weighing each MSA (0.1 mmol) into separate 100 mL volumetric flasks, followed by the addition of 2.00 mL of 0.1 N NaOH (0.2 mmol) to each flask. Once the monomers were completely dissolved, DI H_20 (18.2 MΩ resistance) was added to each volumetric flask to achieve a final volume of 100 mL. Twenty-five mL of each stock solution was transferred to a 100 mL beaker containing a stir bar and titrated against 0.05 N HCl in volume increments of 5 μL at 25 °C using a Metrohm 848 Titrino Plus autotitrator. All titrations were performed in triplicate.

pH-dependent Polymer Solubility

Polymer solutions were first prepared by dissolving each pMSA derivative (1 eq. sulfonamide, 2.5 x 10^{-5} mol sulfonamide functional groups) in 1.00 mL 0.05 N NaOH (2 eq., 5 x 10^{-5} mol)) followed by dilution with DI H_2O (18.2 MΩ resistance) to a final volume of 2.50 mL ([SO_2NH] = 10 mM). The polymer solution was transferred into a quartz cuvette and the solution pH adjusted incrementally by adding 1-10 μL of 0.2 N HCl followed by measuring the % transmittance at λ = 500 nm using a UV-Vis spectrophotometer.

CO_2-dependent Polymer Solubility

In a 20 mL vial equipped with magnetic stir bar and pierceable cap, pMSA (1 eq. sulfonamide, 2.0 x 10^{-5} mol sulfonamide functional groups) was dissolved in 400 μL of 0.05 N NaOH (1.25 eq., 2.5 x 10^{-5} mol) and subsequently diluted to a final volume of 3.00 mL ([SO_2NH] = 6.7 mM) with DI H_2O (18.2 MΩ resistance). CO_2-dependent polymer solubility was examined between purge cycles by transferring the solutions to a

quartz cuvette and measuring the percent transmittance at 500 nm. Purge cycles consisted of purging the solution with CO_2 for 10 s or N_2 for 25 min.

Chapter IV Section 2 Experimental

*N-Phenylmethacrylamide **33***

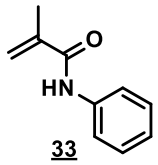

33

Methacryloyl chloride (11.83 mL, 121 mmol) was added dropwise over 15 min to a stirred solution of aniline (12.00 g, 121 mmol) and triethylamine (12.86 g, 127 mmol) in CH_2Cl_2 (250 mL) that was previously cooled using an ice bath. Upon complete addition of methacryloyl chloride, the reaction was stirred at 0 °C for 30 min followed by stirring at room temperature for an additional 60 min. The reaction mixture was then transferred to a separatory funnel and washed with 0.1 N HCl (1 × 200 mL), saturated $NaHCO_3$ (1 × 200 mL), and saturated NaCl (brine) (1 × 200 mL) before drying over $MgSO_4$. The solvent was removed via rotary evaporation and the isolated solids recrystallized from hot hexanes:THF (95:5) to yield **33** (17.52 g, 90%) as colorless needle-like crystals. mp 80-81 °C. ^{1}H NMR (300 MHz, $CDCl_3$): δ 7.60 (s, 1H), 7.57 (d, 2H), 7.32 (t, 2H), 7.11 (t, 1H), 5.78 (s, 1H), 5.44 (s, 1H), 2.05 (s, 3H). ^{13}C NMR ($CDCl_3$): δ 166.87, 141.05, 137.95, 129.15, 124.57, 120.24, 120.04, 18.96.

*N-Benzylmethacrylamide **34***

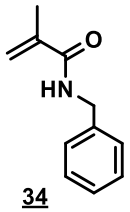

34

A synthetic procedure analogous to that described for **33** was used to prepare N-benzylmethacrylamide. The product was recrystallized from hot hexanes:THF (90:10) to yield **34** (17.88 g, 91%) as colorless needle-like crystals. mp 78-79 °C. ^{1}H NMR (300 MHz, $CDCl_3$): δ 7.30 (m, 5H), 6.13 (s, 1H), 5.71 (s, 1H), 5.34 (s, 1H), 4.50 (d, 2H), 1.97 (s, 3H). ^{13}C NMR ($CDCl_3$): δ 168.43, 140.03, 138.41, 128.87, 127.97, 127.67, 119.89, 43.86, 18.89.

*Sodium dodecyl trithiocarbonate **35***

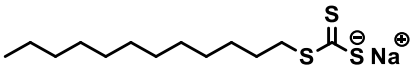

35

1-Dodecanethiol (15.0 g, 74.1 mmol) was added dropwise over 30 min to a stirred suspension of NaH (1.68 g, 70.0 mmol) in anhydrous diethyl ether (350 mL) resulting in slow evolution of hydrogen gas. The reaction mixture was vented and stirred overnight (12 h) at room temperature after which carbon disulfide (5.64 g, 74.1 mmol) was added dropwise over 10 min, followed by stirring at room temperature for 60 min. The reaction mixture was subsequently diluted with pentane (100 mL) and the solids isolated by vacuum filtration and further dried *in-vacuo* to yield **35** (18.55 g, 83%) as a yellow solid. ^{1}H NMR (300 MHz, DMSO-d_6): δ 2.97 (t, 2H), 1.49 (m, 2H), 1.23 (b, 18H), 0.85 (t, 3H). ^{13}C NMR (DMSO-d_6): δ 31.79, 29.55, 29.51, 29.27, 29.21, 29.14, 22.59, 14.45.

*Bisdodecyl trithiocarbonate **36***

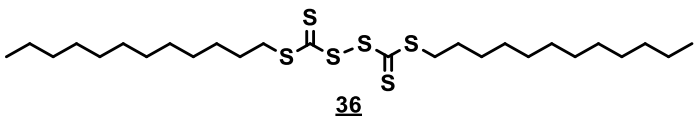

36

To a suspension of sodium dodecyl trithiocarbonate **35** (18.55 g, 61.7 mmol) in diethyl ether (200 mL) at room temperature was added solid I_2 (8.62 g, 34.0 mmol) over 5 min. The reaction was stirred for 60 min at room temperature followed by removal of the precipitated NaI salts by vacuum filtration. The filtrate was transferred to a separatory funnel and washed with 5% $Na_2S_2O_4$ (1 × 150 mL), H_2O (1 × 150 mL), and brine (1 × 150 mL) before drying over $MgSO_4$. The solvent was removed via rotary evaporation to yield **36** (16.36 g, 96%) as a yellow oil that solidified upon cooling to -10 °C. ^{1}H NMR (300 MHz, $CDCl_3$): δ 3.28 (t, 4H), 1.68 (m, 4H), 1.24 (b, 36H), 0.87 (t, 6H). ^{13}C NMR ($CDCl_3$): δ 221.74, 38.52, 32.13, 29.85, 29.77, 29.64, 29.57, 29.31, 29.16, 27.57, 22.91, 14.36.

*2-Cyano-2-propyl dodecyl trithiocarbonate **37***

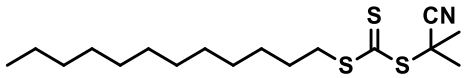

37

Bisdodecyl trithiocarbonate **36** (7.88 g, 14.2 mmol) and AIBN (2.33 g, 14.2 mmol) were dissolved in EtOAc (250 mL) and the solution purged with N_2 for 40 min before heating to 77 °C. After 12 h, a degassed solution of AIBN (2.33 g, 14.2 mmol) in EtOAc (100 mL) was subsequently added and the reaction stirred for an additional 12 h at 77 °C. Purification by column chromatography (95:5 Hexanes:EtOAc) yielded **37** (7.36 g, 75%) as a yellow oil that solidified upon cooling to 0 °C. ^{1}H NMR (300 MHz, $CDCl_3$): δ 3.32 (t, 2H), 1.86 (s, 6H), 1.68 (m, 2H), 1.25 (b, 18H), 0.87 (t, 3H). ^{13}C NMR ($CDCl_3$): δ 217.96, 120.66, 42.54, 37.13, 32.11, 29.82, 29.74, 29.62, 29.54, 29.27, 29.12, 27.91, 27.25, 22.90, 14.35.

*2-(Ethylthiocarbonylthio)-2-methylpropionic acid **38***

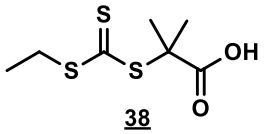

38

Ethane thiol (12.4 g, 0.200 mol), acetone (96.4 g, 1.66 mol), and trioctylmethylammonium chloride (aliquat 336) (3.23 g, 8.00 mmol) were charged into a 500 mL round bottomed flask equipped with magnetic stir bar and the solution cooled to 0-5 °C using an ice bath. 50 wt. % NaOH (16.8 g, 0.210 mol) was then added dropwise over 20 min, followed by the dropwise addition of a solution of carbon disulfide (15.2 g, 0.200 mol) in acetone (20.0 g, 0.344 mol) over 20 min. The reaction mixture was stirred at 0 °C for 20 min, upon which chloroform (35.8 g, 0.300 mol) was added in a single portion immediately followed by the dropwise addition of 50 wt. % NaOH (80.0 g, 1.00 mol) over 30 min. The ice bath was then removed and the reaction mixture stirred overnight (18 h) at room temperature, after which the remaining acetone was removed by rotary evaporation. The resulting viscous residue was diluted with 250 mL H_2O and cooled with an ice bath before acidification with 12 N HCl to pH = 2. Upon acidification, the aqueous component was transferred to a separatory funnel and extracted with hexane (4 x 250 mL) and the aqueous layer discarded. The combined hexane layers were subsequently washed with 0.1 N HCl (1 x 250 mL), brine (1 x 250 mL), and dried over Na_2SO_4 before isolating the crude product by rotary evaporation. Purification by column chromatography (60:38:2 Hexanes:EtOAc:AcOH, R_f = 0.33) yielded a dark yellow oil that was further purified by recrystallization from hot hexanes to give **38** (16.01 g, 36%) as bright yellow crystals. ^{1}H NMR (300 MHz, $CDCl_3$) δ 3.31, 1.73, 1.34.

*2-Bromoisobutyranilide **39***

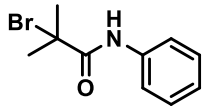

39

2-Bromoisobutyryl bromide (15.00 mL, 124 mmol) was added dropwise over 15 min to a stirred solution of aniline (12.03 g, 124 mmol) and triethylamine (12.28 g, 124 mmol) in CH_2Cl_2 (500 mL) that was previously cooled using an ice bath. Upon complete addition of 2-bromoisobutyryl bromide, the reaction was stirred at 0 °C for 30 min followed by stirring at room temperature for an additional 60 min. The reaction mixture was then transferred into a separatory funnel and washed with 0.1 N HCl (1 × 400 mL), saturated $NaHCO_3$ (1 × 400 mL), and brine (1 × 400 mL) before drying over $MgSO_4$ and removal of the solvent by rotary evaporation. The isolated solids were recrystallized from hot hexanes to yield **39** (29.13 g, 97%) as colorless needle-like crystals. mp 82-23 °C. ^{1}H NMR (300 MHz, $CDCl_3$): δ 8.45 (s, 1H), 7.55 (d, 2H), 7.35 (t, 2H), 7.14 (t, 1H), 2.04 (s, 6H). ^{13}C NMR ($CDCl_3$): δ 170.12, 137.53, 129.24, 125.06, 120.11, 63.37, 32.75.

*N-phenyl-2-(ethylsulfanylthiocarbonylsulfanyl)propanamide **40***

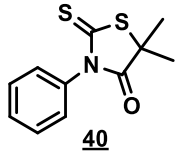

40

A solution of sodium ethyl trithiocarbonate **24** (1.32 g, 8.3 mmol), 2-bromoisobutyrylanilide **39** (2.00 g, 8.3 mmol), and NaI (0.124 g, 0.83 mmol) in absolute EtOH (10 mL) was prepared and stirred at 22 °C for 48 h. The reaction mixture was then precipitated twice into water (100 mL) and the precipitate isolated by vacuum filtration and further purified by recrystallization from absolute EtOH resulting in large needle-like crystals. The product, isolated by recrystallization, was determined to be 5,5-dimethyl-3-

phenyl-2-thioxothiazolidin-4-one (**40**).[227] Conducting the reaction at 60 °C for 12 h allowed for isolation of **40** in higher yields for use in additional studies. mp 108-110 °C. ^{1}H NMR (300 MHz, $CDCl_3$): δ 7.50 (m, 3H), 7.22 (d, 2H), 1.79 (s, 6H). ^{13}C NMR ($CDCl_3$) δ 199.80, 179.64, 135.43, 129.82, 129.70, 128.54, 55.59, 27.55.

*Synthesis of **41***

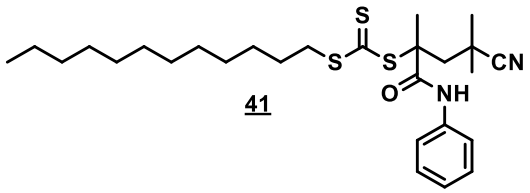

41

A solution of 2-cyano-2-propyl dodecyl trithiocarbonate **37** (3.41 g, 9.9 mmol), **33** (1.59 g, 9.9 mmol), and V-70 (0.609 g, 2.0 mmol) in DMF (35 mL) was prepared in a round bottomed flask equipped with magnetic stir bar and the reaction degassed via three freeze-pump-thaw cycles and backfilled with argon. The reaction mixture was heated at 30 °C in an oil bath for 48 h, followed by exposure to air and freezing in liquid N_2. The reaction mixture was then diluted with EtOAc (250 mL) and transferred to a separatory funnel and washed with 75% brine (1 × 200 mL), H_2O (1 × 200 mL), brine (1 × 200 mL), and dried over $MgSO_4$. The crude product was then purified by column chromatography (8:2 Hexanes:EtOAc, R_f = 0.30) yielding **41** (0.511 g, 10%) as a yellow solid. ^{1}H NMR (300 MHz, $CDCl_3$): δ 8.44 (s, 1H), 7.45 (d, 2H), 7.32 (t, 2H), 7.12 (t, 1H), 3.26 (t, 2H), 2.55 (q, 2H), 2.02 (s, 3H), 1.64 (m, 2H), 1.47 (s, 3H), 1.46 (s, 3H), 1.23 (b, 18H), 0.87 (t, 3H). ^{13}C NMR ($CDCl_3$): δ 219.02, 169.43, 137.45, 129.02, 124.83, 120.51, 60.48, 45.13, 37.33, 31.91, 30.45, 29.62, 29.54, 29.42, 29.35, 29.10, 29.07, 28.90, 28.69, 27.62, 23.81, 22.70, 14.15.

*Synthesis of **42***

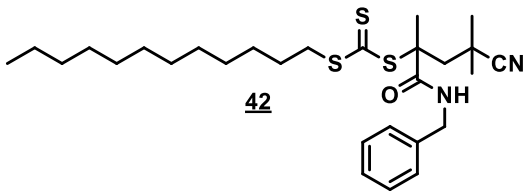

42

A solution of 2-cyano-2-propyl dodecyl trithiocarbonate **37** (2.00 g, 5.8 mmol), **34** (1.01 g, 5.8 mmol), and AIBN (0.190 g, 1.2 mmol) in DMF (20 mL) was prepared in a round bottomed flask equipped with magnetic stir bar and degassed via three freeze-pump-thaw cycles and backfilled with argon. The reaction mixture was heated at 60 °C in an oil bath for 24 h, followed by exposure to air and freezing in liquid N_2. The reaction mixture was then diluted with EtOAc (150 mL) and transferred to a separatory funnel and washed with 75% brine (1 × 150 mL), H_2O (1 × 150 mL), brine (1 × 150 mL), and dried over $MgSO_4$. The crude product was first purified by column chromatography (8:2 Hexanes:EtOAc, R_f = 0.25) followed by recrystallization from MeOH:H_2O (98:2) at -10 °C yielding **42** (0.475 g, 16%) as yellow crystals. ^{1}H NMR (300 MHz, $CDCl_3$): δ 7.31 (m, 5H), 6.79 (t, 1H), 4.42 (q, 2H), 3.25 (t, 2H), 2.56 (q, 2H), 1.96 (s, 3H), 1.64 (m, 2H), 1.47 (s, 3H), 1.45 (s, 3H), 1.27 (b, 18H), 0.89 (t, 3H). ^{13}C NMR ($CDCl_3$): δ 219.32, 171.33, 137.62, 128.87, 128.38, 127.84, 125.04, 60.16, 45.04, 37.28, 32.12, 30.66, 29.84, 29.76, 29.64, 29.55, 29.47, 29.29, 29.14, 28.72, 27.87, 24.16, 22.90, 14.35.

*RAFT Polymerization of **33** and **34***

Briefly, monomer (**33** or **34**) (10.0 mmol, 200 equiv), **37** (5.0×10^{-5} mol, 1 equiv), initiator (V-70 or V501) (1.0×10^{-5} mol, 0.2 equiv), and trimesic acid (50 mg, ^{1}H NMR internal standard) were combined in a 10 mL graduated cylinder and DMF added to bring the final solution volume to 5.0 mL ($[M]_0$ = 2 M). The solution was then transferred to a 10 mL test tube equipped with a magnetic stir bar and rubber septum, degassed via three

freeze-pump-thaw cycles, and backfilled with argon. An initial aliquot (200 μL) was taken prior to heating the reaction vessel at the indicated temperature with subsequent aliquots taken at timed intervals and analyzed by ^{1}H NMR (DMSO-d_6) to determine monomer conversion by comparing the relative integral areas of the trimesic acid aromatic protons (8.64 ppm, 3H) to the vinyl proton of **33** (5.86 ppm, 1H) or **34** (5.79 ppm, 1H). SEC-MALLS (DMF 20 mM LiBr) analysis of aliquots was used to monitor molecular weight and molecular weight distribution progression throughout each polymerization.

Trithiocarbonate Degradation Analysis by UV-Vis Spectroscopy

Reactions (final volume = 2500 μL) were performed using $[\mathbf{37}]_0 = 5 \times 10^{-3}$ M and $[M]_0$:$[\mathbf{37}]_0$:$[V501]_0$ = 10:1:0.2 in DMF. A typical procedure was as follows: **34** (250 μL of an 87.6 mg/mL stock soln. in DMF, 10 equiv), **37** (250 μL of a 17.3 mg/mL stock soln. in DMF, 1 equiv), V501 (25 μL of a 28.0 mg/mL stock soln. in DMF, 0.2 equiv), and DMF (1975 μL) were combined in a 4 mL test tube equipped with magnetic stir bar and rubber septum. The reaction was then degassed via 4 freeze-pump-thaw cycles and backfilled under argon. An initial aliquot (50 μL) was taken using an argon-purged gas-tight syringe and subsequently diluted into a quartz cuvette containing 2500 μL of acetonitrile before measuring the absorbance at λ = 320 nm using a Lambda 35 UV-vis spectrometer. Subsequent aliquots (50 μL) were taken and analyzed in the same manner.

In situ ^{1}H NMR Analysis

Samples of **41** and **42** (2×10^{-2} M) in DMF-d_7 were prepared immediately prior to analysis by first adding DMF-d_7 (0.60 mL) into an NMR tube equipped with pierceable rubber septum and the solvent degassed by two freeze-pump-thaw cycles to remove

possible traces of dimethyl amine. The appropriate amount of **41** or **42** was then added as a solid directly into the NMR tube containing the previously degassed DMF-d_7 and the resulting solution degassed by two additional freeze-pump-thaw cycles and backfilled with argon. ^{1}H NMR spectra were acquired at 70 °C using a Bruker Ascend™ 600 MHz spectrometer.

Chapter IV Section 3 Experimental

Reactions of N- and P-based Nucleophiles with N-Methylmaleimide

A solution of N-methylmaleimide (25.0 mg, 2.23×10^{-4} mol, 10 eq.) and CH_2Cl_2 (10 μL, ^{1}H NMR internal standard) in DMSO-d_6 (1.00 mL) was prepared in an NMR tube in the presence of air. An initial ^{1}H NMR spectrum was taken upon which the appropriate nucleophile (2.23×10^{-5} mol, 1 eq.) was added to the NMR tube and the solution mixed by inverting three times. Subsequent spectra were taken at timed intervals and the fractional change in maleimide concentration measured by comparing the relative integrated peak areas of the maleimide olefin protons (DMSO-d_6, 7.02 ppm, 2H) to the CH_2Cl_2 protons (DMSO-d_6, 5.76 ppm, 2H).

Reaction of Ethyl 2-Mercaptopropionate with N-Methylmaleimide

A solution of N-methylmaleimide (25.0 mg, 2.23×10^{-4} mol, 10 eq.), triethylamine (3.13 μL, 2.23×10^{-5} mol 1.0 eq.) and CH_2Cl_2 (10 μL, ^{1}H NMR internal standard) in DMSO-d_6 (1.00 mL) was prepared in an NMR tube in the presence of air. An initial ^{1}H NMR spectrum was taken upon which ethyl 2-mercaptopropionate () was added to the NMR tube and the solution mixed by inverting three times. Subsequent spectra were taken at timed invervals and the fractional change in maleimide concentration

measured by comparing the relative integrated peak areas of the maleimide olefin protons (DMSO-d_6, 7.02 ppm, 2H) to the CH_2Cl_2 protons (DMSO-d_6, 5.76 ppm, 2H).

*Synthesis of 3-Benzylsulfanyl-1-Methylmaleimide **43***

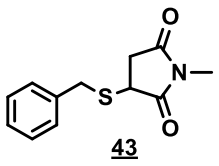

43

An initially colorless solution of benzylmercaptan (2.64 g, 21.2 mmol) and N-methylmaleimide (2.36 g, 21.2 mmol) in MeCN (50 mL) was first prepared at room temperature followed by the addition of TEA (0.281 mL, 2.12 mmol) via syringe. The resulting red solution was stirred at room temperature for 30 min followed by quenching with acetic acid (1.0 mL) resulting in the solution becoming colorless. The solvent was removed by rotary evaporation and the crude reaction mixture redissolved in diethyl ether (100 mL) and washed with 0.1 M HCl (100 mL), H_2O (100 mL), and saturated NaCl (100 mL). The product was further purified by column chromatography (65:35 hexanes:EtOAc, R_f = 0.35), yielding **43** (4.55 g, 91%) as a colorless viscous oil that solidified into a waxy solid after 7 days; mp 47-52 °C. ^{1}H NMR (600 MHz, DMSO-d_6): δ 7.31 (m, 4H), 7.24 (m, 1H), 3.93 (dd, *J* = 62.3, 13.1 Hz, 2H), 3.76 (dd, *J* = 9.0, 3.9 Hz, 1H), 3.06 (dd, *J* = 18.5, 9.0 Hz, 1H), 2.78 (s, 3H), 2.45 (dd, *J* = 18.5, 3.9 Hz, 1H).

*Reaction of **43** with N-Methylmaleimide.*

A solution of N-methylmaleimide (25.0 mg, 2.23×10^{-4} mol, 10 eq.), **43** (5.29 mg, 2.23×10^{-5} mol, 1.0 eq.), and CH_2Cl_2 (10 μL, ^{1}H NMR internal standard) in DMSO-d_6 (1.00 mL) was prepared in an NMR tube in the presence of air. An initial ^{1}H NMR spectrum was taken upon which TEA (3.13 μL, 2.23×10^{-5} mol, 1 eq) was added to the NMR tube and the solution mixed by inverting three times. Subsequent spectra were

taken at timed intervals and the fractional change in maleimide concentration measured by comparing the relative integrated peak areas of the maleimide olefin protons (DMSO-d_6, 7.02 ppm, 2H) to the CH_2Cl_2 protons (DMSO-d_6, 5.76 ppm, 2H).

*Hydrogen-Deuterium Exchange Kinetics of **43***

NMR Spectra were recorded with a Bruker Ascend™ 600 MHz spectrometer at 23 °C. Briefly, a solution of **7** (10.0 mg, 4.25×10^{-5}, 1 eq) and D_2O (100 μL, 5.54 mmol, 130 eq) in DMSO-d_6 (0.600 mL) was prepared in an NMR tube in the presence of air and an initial ^1H NMR spectrum was acquired (t = 0 min). TEA (5.93 μL, 1 eq) was then added to the NMR tube and the solution mixed by inverting three times. Subsequent spectra were acquired at timed intervals and the fractional change in peak area (A_t/A_0) of protons H_a (3.80 – 3.75 ppm, 1H), H_b (3.10 – 3.00 ppm, 1H), and H_c (2.50 – 2.40 ppm, 1H) were measured relative to the peak area of the benzylsulfanyl aromatic protons (7.30 - 7.20 ppm, 5H).

*2-cyano-2-propyl benzodithioate **44***

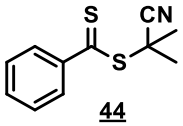

44

A solution of bis(thiobenzoyl)disulfide **22** (1.00 g, 3.3 mmol) and AIBN (1.07 g, 6.6 mmol) in EtOAc (40 mL) was prepared in a 3-necked round bottomed flask equipped with stir bar and condenser. The reaction was degassed by purging with N_2 for 40 min prior to heating to reflux (77 °C) for 18 h. The reaction was quenched by exposure to air and freezing in liquid N_2 followed by solvent removal via rotary evaporation. The crude RAFT agent was purified by column chromatography (9:1 hexanes:EtOAc, R_f = 0.25) to

give **44** as a dark red oil that solidified upon cooling to - 10 °C (0.87 g, 60%). ^{1}H NMR (200 MHz, $CDCl_3$): δ 7.90 (d, 2H), 7.57 (t, 1H), 7.40 (t, 2H), 1.94 (s, 6H).

Synthesis of pDMA-CPDB ***45***

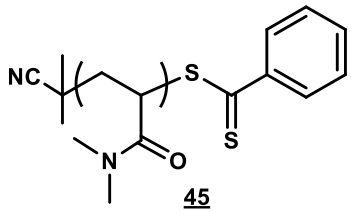

45

N,N-dimethylacrylamide (28.0 g, 282 mmol), 2-cyano-2-propyl benzodithioate **44** (298.0 mg, 1.34 mmol), AIBN (44.1 mg, 0.27 mmol), and benzene (100 mL) were combined in a 250 mL round bottomed flask equipped with magnetic stir bar and sealed with a rubber septum before purging with N_2 for 45 mins. The reaction vessel was then heated in an oil bath at 60 °C for 5 h, upon which the reaction was quenched via exposure to air and freezing in liquid nitrogen. The solvent was removed by rotary evaporation and the polymer precipitated 4 times into pentane, redissolving in a minimal amount of CH_2Cl_2 between precipitations. The final product **45** was dried overnight *in-vacuo* before characterizing via ^{1}H NMR (D_2O) and SEC-MALLS (DMF 20 mM LiBr). M_n(NMR) = 3220 g/mol, M_n(SEC) = 3360 g/mol, Đ = 1.06.

N-Benzylmaleimide ***46***

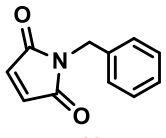

46

A solution of maleic anhydride (20.00 g, 204 mmoL) in anhydrous diethyl ether (250 mL) was first prepared at room temperature in a 3-necked 1L round bottom flask equipped with magnetic stir bar, condenser, and addition funnel. A solution of

benzylamine (21.86 g, 204 mmol) in anhydrous diethyl ether (100 mL) was added dropwise via addition funnel over 30 mins such that the exothermic reaction produced a mild reflux of the solvent. The reaction mixture was stirred for 1 h at room temperature before isolating the resulting solids by vacuum filtration followed by washing with anhydrous diethyl ether (100 mL). The resulting N-benzylmaleamic acid intermediate was dried *in-vacuo* and used without further purification (40.70 g, 97%).

N-benzylmaleamic acid (40.70 g, 198 mmol) was added as a solid to a stirred solution of acetic anhydride (90.00 g, mmol) and anhydrous sodium acetate (13.00 g, mmol) and the reaction heated at 100 °C for 30 min resulting in formation of a dark brown homogenous solution. The reaction mixture was then poured into a vigorously stirred solution of ice cold water (600 mL) and stirred for 30 min. The resulting brown precipitate was isolated by vacuum filtration and washed with water (3 × 100 mL). The solids were resuspended in water (500 mL) and stirred vigorously for 30 min before isolation again by vacuum filtration. The crude compound was further purified by recrystallization from EtOH:H_2O (2:1, v:v) to afford **46** (27.02 g, 73%) as fine beige crystals; mp 67-69 °C. ^{1}H NMR (300 MHz, $CDCl_3$): δ 7.22 (b, 5H), 6.64 (s, 2H), 4.61 (s, 2H). ^{13}C NMR ($CDCl_3$): δ 170.41, 136.17, 134.19, 128.69, 128.38, 127.86, 41.42.

*Simultaneous "One-Pot" Aminolysis/Thiol-Maleimide End Group Modification of **45** with **46** (Method 1)*

A representative procedure is as follows: **45** (100.0 mg, 3.10×10^{-5} mol, 1 eq) and N-benzylmaleimide (29.0 mg, 1.55×10^{-4} mol, 5 eq) were measured into a 5 mL test tube equipped with rubber septum and dissolved in 1.00 mL of DMSO. The reaction mixture was degassed via three freeze-pump-thaw cycles and backfilled with argon. 100 μL of a

solution of hexylamine in DMSO (102 μL/mL, 7.75×10^{-5} mol, 2.5 eq) and 100 μL of a solution of DBU in DMSO (40.0 μL/mL, mol, 1 eq) were then added via gas tight syringe and the reaction stirred for 12 h at room temperature (23 °C). End-modified pDMA was purified by precipitation into diethyl ether (3 × 50 mL) and dried overnight *in-vacuo*. End group analysis was performed using ^{1}H NMR (D_2O) by comparing the integrated peak area of the benzyl aromatic protons (7.50 - 7.15 ppm, 5H) to the integrated peak area of the pDMA N,N-dimethyl side chain and methyne backbone protons (3.30 – 2.20 ppm, 213.22H). NMR samples were filtered through a 0.20 μm Millex PTFE filter prior to analysis.

*Sequential "One-Pot" Aminolysis/Thiol-Maleimide End Group Modification of **45** with **46** (Method 2)*

A representative procedure is as follows: **45** (100.0 mg, 3.10×10^{-5} mol, 1 eq) and trimethylphosphite (18.3 μL, 1.55×10^{-4} mol, 5 eq) were measured into a 5 mL test tube equipped with rubber septum and dissolved in 1.00 mL of DMSO. The reaction mixture was degassed via three freeze-pump-thaw cycles and backfilled with argon. 100 μL of a solution of hexylamine in DMSO (102 μL/mL, 7.75×10^{-5} mol, 2.5 eq) was then added via gas tight syringe and the reaction stirred for 30 min at room temperature (23 °C) upon which a previously degassed solution of **46** (29.0 mg, 1.55×10^{-4} mol, 5 eq) in DMSO (0.5 mL) was added and the reaction stirred for 12 h at room temperature. End-modified **45** was purified by precipitation into diethyl ether (3 × 50 mL) and dried overnight *in-vacuo*. End group analysis was performed using ^{1}H NMR (D_2O) by comparing the integrated peak area of the benzyl aromatic protons (7.50 - 7.15 ppm, 5H) to the integrated peak area of the **45** N,N-dimethyl side chain and methyne backbone protons

(3.30 – 2.20 ppm, 213.22H). NMR samples were filtered through a 0.20 μm Millex PTFE filter prior to analysis.

Chapter IV Section 4 Experimental

tert-butyl 2-aminoethylcarbamate ***47***

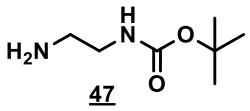

47

To a 1 L flask equipped with a magnetic stir bar was added 1,2-diaminoethane (7.7 mL, 114 mmol) and dichloromethane (450 mL). The solution was cooled using an ice bath, upon which a solution of di-*tert*-butyl dicarbonate (5.00 g, 22.9 mmol) in dichloromethane (50 mL) was added dropwise via addition funnel over 2 h. Following complete addition, the ice bath was removed and the reaction stirred at room temperature for 12 h, after which the solution was filtered of solids and the filtrate concentrated via rotary evaporation to ~250 mL. The filtrate was then washed with half saturated brine (3 x 150 mL), brine (1 x 150 mL), dried using $MgSO_4$, and the solvent removed via rotary evaporation to yield the desired compound **47** as a colorless oil (3.25 g, 89%). ^{1}H NMR (300 MHz, $CDCl_3$): δ 3.12 (dd, *J* = 11.6, 5.8 Hz, 2H), 2.75 (t, *J* = 5.9 Hz, 2H) 1.40 (s, 9H).

N-(methoxycarbonyl) maleimide ***48***

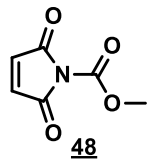

48

A solution of maleimide (7.00 g, 72.1 mmol) in dichloromethane (250 mL) was prepared and cooled using an ice bath. A solution of N-methylmorpholine (7.92 mL, 72.1 mmol) in dichloromethane (50 mL) was added dropwise to the solution of maleimide

over 10 min while stirring. Subsequently, a solution of methylchloroformate (6.69 mL, 86.5 mmol) in dichloromethane (50 mL) was added dropwise over 1 h, upon which the ice bath was removed and the reaction stirred for 1 h at room temperature. The heterogeneous solution was then poured into a separatory funnel and washed with 1 x 250 mL each of saturated $NaHCO_3$, water, and brine, before drying over $MgSO_4$. The solvent was removed via rotary evaporation and the product further dried *in vacuo* to yield **48** as an off white solid (10.26 g, 92%). ^{1}H NMR (300 MHz, $CDCl_3$): δ 6.80 (s, 2H), 3.88 (s, 3H).

*tert-Butyl N-[2-(2,5-dioxo-2,5-dihydro-1H-pyrrol-1-yl)ethyl]carbamate **49***

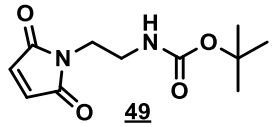

49

A solution of **47** (3.25 g, 20.3 mmol) in saturated $NaHCO_3$ (120 mL) was prepared and stirred at room temperature for 10 min before vacuum filtering to remove the resulting solids. The filtrate was subsequently cooled using an ice bath followed by the solid addition of finely ground N-(methoxycarbonyl) maleimide **48** (3.15 g, 20.3 mmol). After 30 min, the ice bath was removed and the reaction stirred at room temperature for an additional 30 min. The resulting precipitate was filtered, washed with 100 mL water, and dried overnight *in vacuo* to yield the desired compound **49** as a white solid (3.87 g, 79%). ^{1}H NMR (300 MHz, $CDCl_3$): δ 6.69 (s, 2H), 3.78 – 3.53 (m, 2H), 3.31 (dd, *J* = 11.1, 5.8 Hz, 2H), 1.38 (s, 9H).

*tert-Butyl N-{2-[(2R,6S)-3,5-dioxo-10-oxa-4-azatricyclo[5.2.1.0^{2,6}]dec-8-en-4-yl]ethyl} carbamate **50***

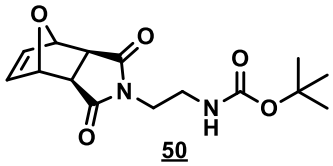

50

A round bottomed flask equipped with a magnetic stir bar and condenser was charged with **49** (3.87 g, 16.1 mmol), freshly distilled furan (20 mL, 275 mmol), and benzene (80 mL) and heated to reflux for 12 h, upon which the reaction was concentrated via rotary evaporation and further dried *in vacuo* resulting in isolation of **50** as a white solid that required no further purification (4.65 g, mmol, 96%). ^{1}H NMR (300 MHz, $CDCl_3$): δ 6.49 (s, 2H), 5.24 (s, 2H), 3.75 – 3.51 (m, 2H), 3.28 (dd, *J* = 11.1, 5.3 Hz, 2H), 2.83 (s, 2H), 1.40 (s, 9H).

2-[(2R,6S)-3,5-dioxo-10-oxa-4-azatricyclo[5.2.1.0^{2,6}]dec-8-en-4-yl]ethan-1-amonium trifluoroacetate ***51***

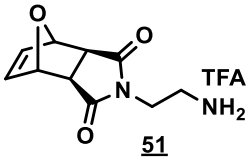

51

N-bocethyl oxanorbornene **50** (4.60 g, 14.9 mmol) was dissolved in dichloromethane (40 mL) and cooled using an ice bath. Trifluoroacetic acid (10 mL) was then added via syringe over 10 min followed by stirring of the reaction overnight (12 h) at room temperature. Diethyl ether (250 mL) was then added to the reaction and the heterogeneous solution cooled using an ice bath for 30 min before isolating the resulting precipitate by vacuum filtration. The isolated solids were further dried *in vacuo*, yielding **51** as a white solid (4.64 g, 97%). ^{1}H NMR (300 MHz, D_2O): δ 6.64 (s, 2H), 5.36 (s, 2H), 3.84 (t, *J* = 5.8 Hz, 2H), 3.23 (t, *J* = 5.9 Hz, 2H), 3.19 (s, 2H).

(2R,6S)-4-[2-(2,5-dioxo-2,5-dihydro-1H-pyrrol-1-yl)ethyl]-10-oxa-4 azatricyclo[5.2.1.0^{2,6}] dec-8- ene-3,5-dione ***52***

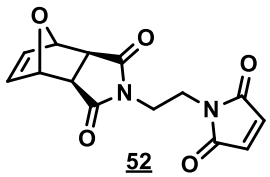

52

Oxanorbornene ethylamine TFA **51** (4.72 g, 14.6 mmol) was dissolved in saturated $NaHCO_3$ (200 mL) and cooled using an ice bath. The solution was stirred while purging with N_2 for 10 min at 0 °C to dispel any dissolved CO_2. Subsequently, finely ground N-(methoxycarbonyl) maleimide **48** (2.27 g, 14.6 mmol) was then added as a solid to the solution of **51**, followed by stirring for 30 min at 0 °C, upon which the ice bath was removed and the reaction stirred for an additional 3 h at room temperature. The resulting precipitate was isolated via vacuum filtration and the filtrand washed with water (50 mL) before drying overnight *in vacuo* to yield the desired compound **52** as an off-white solid (2.09 g, 48%). ^{1}H NMR (300 MHz, $CDCl_3$): δ 6.65 (s, 2H), 6.47 (d, J = 0.7 Hz, 2H), 5.19 (t, J = 0.8 Hz, 2H), 3.84 – 3.59 (m, 4H), 2.81 (s, 2H).

N-(3-bromopropyl)maleimide ***53***

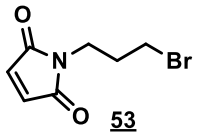

53

3-Bromopropylamine hydrobromide (2.00 g, 9.1 mmol) was dissolved in saturated $NaHCO_3$ (100 mL) and cooled using an ice bath. The solution was allowed to stir for 10 min at 0 °C while purging with N_2 to dispel any dissolved CO_2. Subsequently, finely ground N-(methoxycarbonyl) maleimide **48** (1.42 g, 9.1 mmol) was added as a solid to the solution of 3-bromopropylamine, followed by stirring for 30 min at 0 °C,

upon which the ice bath was removed and the reaction stirred for an additional 1 h at room temperature. The resulting precipitate was isolated via vacuum filtration and the filtrand washed with water (50 mL) before drying overnight *in vacuo* to yield the desired compound **53** as a white solid (1.23 g, 62%). Note: after ~1 hr, additional **53** formed in the filtrate as colorless plate-like crystals. This additional product was isolated by vacuum filtration followed by drying *in-vacuo*. ^{1}H NMR (300 MHz, $CDCl_3$): δ 6.70 (s, 2H), 3.65 (t, *J* = 6.9 Hz, 2H), 3.34 (t, *J* = 6.6 Hz, 2H), 2.15 (p, *J* = 6.7 Hz, 2H).

(2R,6S)-4-(3-bromopropyl)-10-oxa-4-azatricyclo[5.2.1.0^{2,6}]dec-8-ene-3,5-dione ***54***

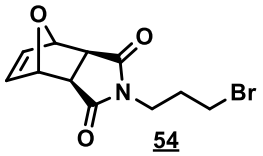

54

A round bottomed flask equipped with a magnetic stir bar and condenser was charged with 3-bromopropyl maleimide **53** (5.16 g, 23.7 mmol), freshly distilled furan (30 mL, 413 mmol), and benzene (150 mL) and heated to reflux for 12 h, upon which the reaction was concentrated via rotary evaporation and further dried *in vacuo* resulting in isolation of **54** as a white solid that required no further purification (6.16 g, 91%). ^{1}H NMR (300 MHz, $CDCl_3$): δ 6.49 (s, 2H), 5.25 (s, 2H), 3.61 (t, *J* = 6.9 Hz, 2H), 3.31 (t, *J* = 6.7 Hz, 2H), 2.83 (s, 2H), 2.12 (p, *J* = 6.8 Hz, 2H).

Sodium Methanethiosulfonate ***55***

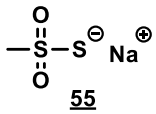

55

Sodium methanesulfinate (5.00 g, 49 mmol) and elemental sulfur (1.57 g, 49 mmol) were combined in anhydrous methanol (500 mL) and heated to reflux. After 30 min, a homogenous solution was observed and the reaction cooled to room temperature,

followed by solvent removal via rotary evaporation. The resulting crude solid was triturated with absolute ethanol (2 x 30 mL) and further dried *in vacuo* yielding **55** as a white crystalline solid (6.27 g, 95%) m.p. 271-272 °C (lit. 272-273 °C) ^{1}H NMR (300 MHz, D_2O): δ 3.36 (s, 3H).

(2R,6S)-4-[3-(methanesulfonylsulfanyl)propyl]-10-oxa-4-azatricyclo[5.2.1.0^{2,6}]dec-8-ene-3,5-dione ***56***

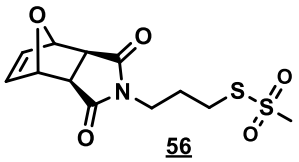

56

Oxanorbornene propylbromide **54** (5.24 g, 18.3 mmol) and sodium methanethiosulfonate **55** (3.69 g, 27.5 mmol) were dissolved in DMF (40 mL) and heated at 50 °C for 18 h. Most of the solvent was removed via rotary evaporation and the crude product was dissolved in EtOAc (100 mL) and washed with water (2 x 50 mL) and brine (1 x 50 mL) before drying over $MgSO_4$. The solvent was then removed *in vacuo* to yield the product **56** as a yellow solid (5.00 g, 86%). ^{1}H NMR (300 MHz, $CDCl_3$): δ 6.50 (s, 2H), 5.25 (s, 2H), 3.61 (t, *J* = 6.5 Hz, 2H), 3.31 (s, 3H), 3.07 (t, *J* = 7.3 Hz, 2H), 2.84 (s, 2H), 2.15 – 1.99 (m, 2H).

Synthesis of ***57***

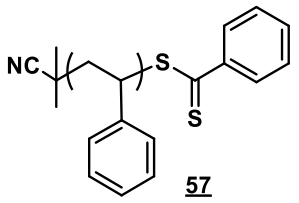

57

Styrene (15.00 g, 120 eq.), **44** (246.0 mg, 1 eq.), and AIBN (29.6 mg, 0.15 eq.) were combined in a 25 mL Schlenk tube equipped with magnetic stir bar and sealed

before degassing by three freeze-pump-thaw cycles and backfilled under argon. The reaction vessel was then heated in an oil bath at 65 °C for 5.25 h, upon which the reaction was quenched via exposure to air and freezing in liquid nitrogen. The polymer was precipitated 3 times in to methanol, redissolving in a minimal amount of CH_2Cl_2 between precipitations. The final product **57** was dried overnight *in-vacuo* before characterizing via NMR and DMF SEC-MALLS. M_n(NMR) = 3090 g/mol, M_n(SEC) = 2980 g/mol, Đ = 1.03, d*n*/d*c* = 0.160 mL/g.

*Synthesis of **58***

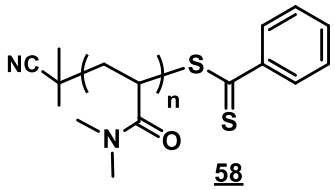

58

N,N-dimethylacrylamide (28.0 g, 282 mmol), **44** (298.0 mg, 1.34 mmol), AIBN (44.1 mg, 0.27 mmol), and benzene (100 mL) were combined in a 250 mL round bottomed flask equipped with magnetic stir bar and sealed with a rubber septum before purging with N_2 for 45 mins. The reaction vessel was then heated in an oil bath at 60 °C for 6 h, upon which the reaction was quenched via exposure to air and freezing in liquid nitrogen. The solvent was removed by rotary evaporation and the polymer precipitated 4 times into pentane, redissolving in a minimal amount of CH_2Cl_2 between precipitations. The final product **58** was dried overnight *in-vacuo* before characterizing via ^{1}H NMR (D_2O) and SEC-MALLS (DMF 20 mM LiBr). M_n(NMR) = 3700 g/mol, M_n(SEC) = 3630 g/mol, Đ = 1.05, d*n*/d*c* = 0.086 mL/g.

*End group functionalization of **57** with **52** (**59**)*

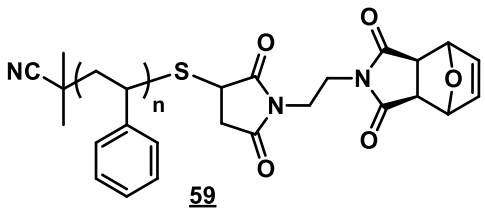

59

57 (600 mg, 1.94×10^{-4} mol, 1 eq), THF (2.00 mL) and trimethylphosphite (114.4 μL, 9.69×10^{-4} mol, 5 eq) were measured into a 10 mL test tube equipped magnetic stir bar and sealed with a rubber septum. The reaction mixture was degassed via three freeze-pump-thaw cycles and backfilled with argon. Propylamine (39.9 μL, 4.85×10^{-4} mol, 2.5 eq) was then added via gas tight syringe and the reaction stirred for 60 min at room temperature upon which a previously degassed solution of **52** (280.0 mg, 9.69×10^{-4} mol, 5 eq) in THF (4.0 mL) was added and the reaction stirred for 12 h at room temperature. **59** was purified by precipitation into MeOH (3 × 50 mL) and dried overnight *in-vacuo*. End group analysis was performed using ^{1}H NMR (acetone-d_6) by comparing the integrated peak area of the norbornene bridgehead methyne protons (5.25 – 4.95 ppm, 2H) to the integrated peak area of the polystyrene aromatic side chain protons (7.50 – 6.25 ppm, 137.92 H).

*End group functionalization of **57** with **56** (**60**)*

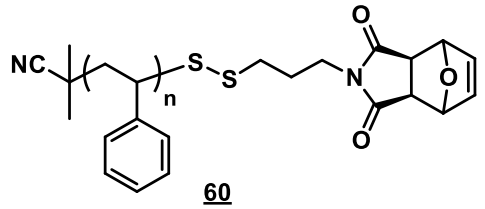

60

57 (500 mg, 1.6×10^{-4} mol, 1 eq), **56** (307 mg, 9.7×10^{-4} mol, 6 eq), and THF (2 mL) were combined in a 5 mL test tube equipped with magnetic stir bar and sealed with a rubber septum. The reaction mixture was degassed via three freeze-pump-thaw cycles and backfilled with argon. Propylamine (200 μL, 2.4×10^{-3} mol, 15 eq) was then added

by gas-tight syringe and the reaction stirred for 12 h at room temperature. **60** was purified by precipitation into MeOH (3 x 50 mL) and dried overnight *in-vacuo*. End group analysis of **60** was performed in analogous fashion to that described for analysis of **58**.

*End group functionalization of **58** with **52** (**61**)*

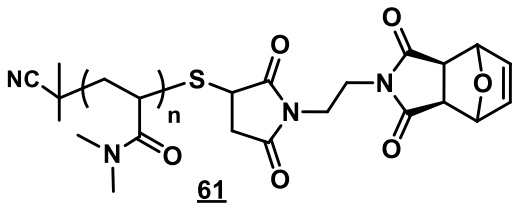

61

58 (500 mg, 1.35×10^{-4} mol, 1 eq), THF (2.00 mL) and trimethylphosphite (79.5 μL, 7.74×10^{-4} mol, 5 eq) were measured into a 10 mL test tube equipped magnetic stir bar and sealed with a rubber septum. The reaction mixture was degassed via three freeze-pump-thaw cycles and backfilled with argon. Hexylamine (35.4 μL, 4.85×10^{-4} mol, 2.0 eq) was then added via gas tight syringe and the reaction stirred for 30 min at room temperature upon which a previously degassed solution of **52** (194.0 mg, 7.74×10^{-4} mol, 5 eq) in THF (4.0 mL) was added and the reaction stirred for 12 h at room temperature. The reaction mixture was then dialyzed against water (3 x 200 mL), changing the water every hour. The aqueous solution was reclaimed from the dialysis bag and filtered through a 0.2 uM Millipore filter and then further dialyzed against MeOH (5 x 100 mL), changing the solvent every hour. **61** was subsequently isolated by rotary evaporation as a colorless solid. End group analysis was performed using ^{1}H NMR (D_2O) by comparing the integrated peak area of the norbornenyl olefin protons (6.65 – 6.55 ppm, 2H) to the integrated peak area of the pDMA N,N-dimethyl side chain and methyne backbone protons (3.30 – 2.20 ppm, 246.26H).

*End group functionalization of **58** with **56** (**62**)*

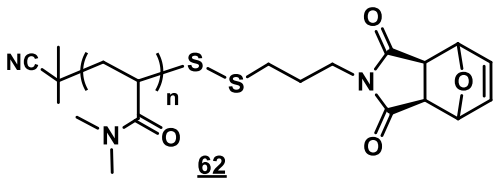

62

58 (500 mg, 1.6×10^{-4} mol, 1 eq), **56** (307 mg, 9.7×10^{-4} mol, 6 eq), and THF (2 mL) were combined in a 5 mL test tube equipped with magnetic stir bar and sealed with a rubber septum. The reaction mixture was degassed via three freeze-pump-thaw cycles and backfilled with argon. Propylamine (200 μL, 2.4×10^{-3} mol, 15 eq) was then added by gas-tight syringe and the reaction stirred for 12 h at room temperature. The reaction mixture was then dialyzed against water (3 x 200 mL), changing the water every hour. The aqueous solution was reclaimed from the dialysis bag and filtered through a 0.2 uM Millipore filter and then further dialyzed against MeOH (5 x 100 mL), changing the solvent every hour. **62** was isolated by rotary evaporation as an off-white solid. End group analysis of **62** was performed in analogous fashion to that described for analysis of **61**.

*Synthesis of 3rd Generation Grubbs Catalyst **19***

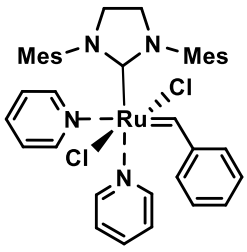

19

Grubbs 2nd generation catalyst (500 mg, 0.12 mmol) was weighed into a scintillation vial containing a small magnetic stir bar followed by the addition of pyridine

(0.474 mL, 5.88 mmol) in the presence of air. After 5 min, pentane (20 mL) was added to the vial resulting in precipitation of a bright green solid. The vial was placed in the refrigerator (5 °C) overnight upon which the green 3rd generation Grubbs catalyst **19** was isolated by vacuum filtration and washed with pentane (20 mL) before drying *in-vacuo*. **19** was subsequently stored under argon in the dark at 5 °C. Yield: 400 mg, 93%.

*ROMP of RAFT-Derived Macromonomers **58**, **59**, **60**, or **61***

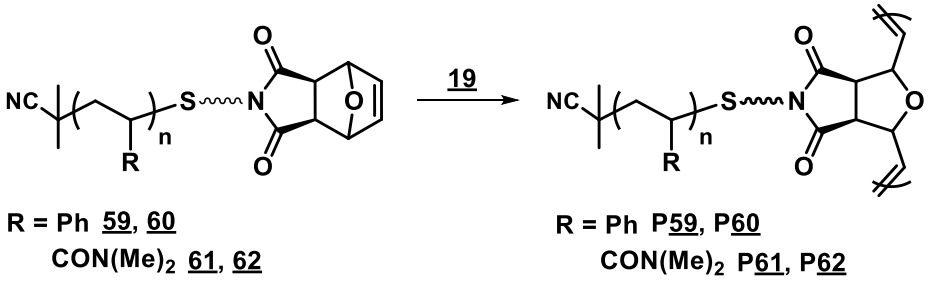

A representative procedure is as follows: A stock solution of **19** (1 eq.) in CH_2Cl_2 (degassed by 4 x freeze-pump-thaw cycles and backfilled with argon) was measured into a vial that was previously degassed with argon. A separate vial containing **59** (100.0 mg, 50 eq,) was evacuated and backfilled with argon. Degassed CH_2Cl_2 (200 uL) was added to the vial of **59**, upon which the solution was transferred by gas tight syrige to the vial of **19**. The reaction was stirred for 6 h at room temperature before being terminated via the addition of one drop of ethyl vinyl ether followed by precipitation in MeOH.

CHAPTER IV

RESULTS AND DISCUSSION

Section 1. Tunable pH- and CO_2-Responsive Sulfonamide-Containing Polymers by RAFT Polymerization

Overview

Lately, extensive research efforts have been directed toward the synthesis of well-defined (co)polymers capable of rapid and reversible changes in solubility and/or conformation in response to external stimuli including pH,[144,228,229] temperature,[230,231] or ionic strength,[232] among others.[233–235] Of particular interest are "smart" nanocarriers for drug and gene delivery that exploit discrete changes in physiological pH to elicit the desired therapeutic effect.[236–240] Designing such polymeric systems requires that the morphological transitions occur over a very narrow designated pH range. Commonly, this specificity is achieved by the selection of a monomer with a pK_a at or near the target transition pH; however, polymer design is accordingly restricted by the limited choice in monomers and their respective pK_a values. Consequently, a facile method of specifically tuning polymer pH-responsiveness while maintaining a narrow transition range is needed.

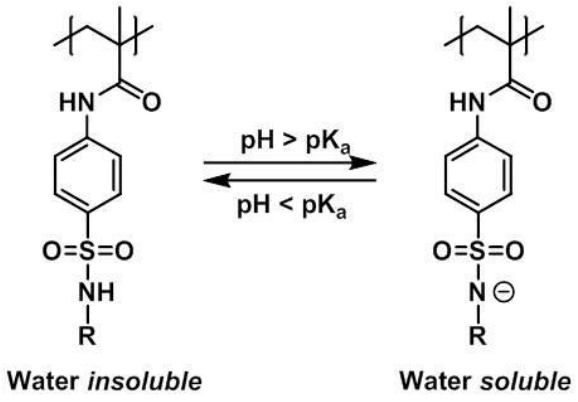

Scheme 4.1. pH-dependent solubility of pMSAs.

A number of attempts have been made to systematically vary the pH-responsiveness of polymers.[57,241] One versatile approach towards modification of polymer pK_a was reported by Ringsdorf in seminal work in which a library of sulfonamide-containing polymers derived from sulfa drugs was synthesized by classical free radical or Michael-addition techniques.[242] Variation of the sulfonamide R-group afforded facile, tunable control over polymer pK_a and subsequent pH-dependent solubility (Scheme 4.1). Recently, Bae and coworkers further demonstrated this versatility in pK_a selection for a variety of polymer-based therapeutic applications.[237,243–245] However, until now the uncontrolled nature of the polymerization methods used to prepare such polymers has limited the ability to attain well-defined polymer architectures with the specific molecular weights and narrow molecular weight distributions required for responsive nanotherapeutics.

Reversible-deactivation radical polymerization (RDRP) techniques such as nitroxide-mediated polymerization (NMP), atom transfer radical polymerization (ATRP), and reversible addition-fragmentation chain transfer (RAFT) polymerization have made possible the synthesis of (co)polymers of a wide variety of architectures with predictable molecular weights and narrow molecular weight distributions.[76,246,247] In particular, RAFT has been used to directly polymerize a variety of cationic, anionic, and other functional monomers in organic or aqueous media without the necessity of protecting group chemistries or post-polymerization modification.[89,247] The facility of polymerization and excellent functional group tolerance of RAFT polymerization have driven our current objectives of synthesizing sulfonamide-containing polymers in a controlled fashion.

In this chapter we report, to our knowledge, the first controlled RAFT polymerization of a library of methacryloyl sulfonamide (MSA) monomers possessing pK_a values in the biologically relevant regime (pH = 4.5-7.4). In this work we show that temperature has a significant influence on the polymerization of MSAs, with lower reaction temperatures affording improved molecular weight control and functional chain end retention. Varying the sulfonamide R-group is shown to be an effective means of adjusting monomer pK_a and subsequently the pH-dependent solubility of the resulting polymethacryloyl sulfonamides (pMSAs). During our study of the weakly acidic/basic nature of the MSA derivatives chosen, we found a remarkably facile and reversible CO_2-induced solubility transition in aqueous solutions. The demonstrated control over RAFT polymerization of MSAs now allows new routes for the synthesis of advanced polymer architectures with tunable pH- and CO_2-responsive properties for ultimate use in biological and therapeutic applications.

RAFT Polymerization of Methacryloyl Sulfonamides (MSAs) at 70 °C

The MSA monomers **27**-**32** (R-groups shown in Scheme 4.2) were targeted for this work based upon their respective pK_a values (Table 4.3) that reside within the biologically relevant pH range of 4.5-7.4. Utilizing a modified literature procedure,[237] high monomer yields (>90%) were obtained from the reaction of methacryloyl chloride and the appropriate sulfa drug precursor, as outlined in the experimental section.

Achieving controlled RAFT polymerization of a given monomer requires appropriate choice of CTA and polymerization conditions. Previously, our group successfully utilized the trithiocarbonate 4-cyano-4-(ethylsulfanylthiocarbonylsulfanyl)pentanoic acid (**26**) and the dithioester 4-

cyanopentanoic acid dithiobenzoate (**23**) to polymerize a wide variety of (meth)acrylamide monomers in aqueous or organic media in a controlled fashion.[153,248] Based on that work, we have investigated the RAFT polymerization of MSAs using **26** and **23** as outlined in Scheme 4.2. It is worth noting that although these monomers are water soluble, polymerizations were conducted in DMF in order to avoid CTA hydrolysis or aminolysis.[119]

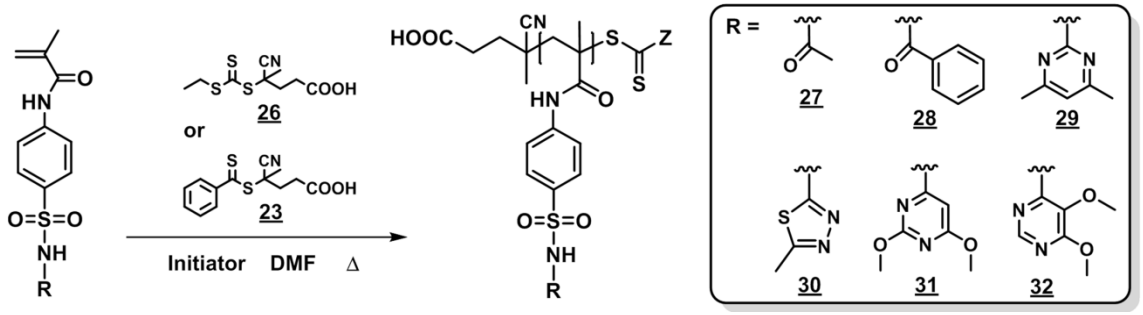

Scheme 4.2. Synthetic pathway for the **23**- or **26**-mediated RAFT polymerization of MSAs in DMF.

Initially, **26**- and **23**-mediated RAFT polymerizations of methacryloyl sulfacetamide (**27**) were carried out at 70 °C in DMF using V-501 as the initiator at molar ratios of $[M]_0:[CTA]_0:[I]_0 = 150:1:0.2$. As illustrated in Figure 4.1, a near linear pseudo-first-order kinetic plot is observed for the polymerization of **27** with **26** at 70 °C. After an initialization period of approximately 30 min, monomer conversion reached 81% after 600 min. The **23**-mediated polymerization of **27** at 70 °C under analogous conditions was significantly slower, reaching only 12% monomer conversion after 600 min. Retardation in rate of dithiobenzoate-mediated polymerizations as compared to analogous reactions mediated by trithiocarbonates has been observed previously for styrenics, acrylates, and acrylamides with some monomers failing to polymerize in the presence of a dithiobenzoate RAFT agent.[107,249]

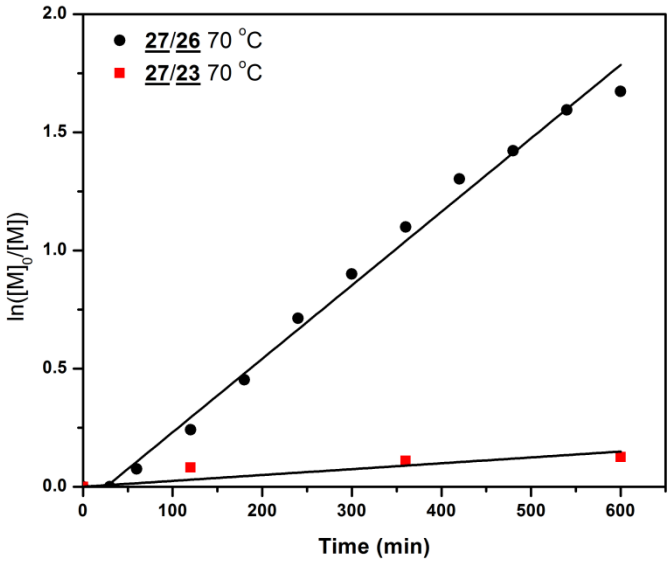

Figure 4.1. Kinetic plots for the **23**- and **26**-mediated RAFT polymerization of **27** at 70 °C in DMF ($[M]_0$:$[CTA]_0$:$[I]_0$ = 150:1:0.2).

Despite near ideal linear pseudo-first-order kinetic behavior, the **26**-mediated polymerization of **27** at 70 °C produced polymers with M_w/M_n of 1.27 or higher (Table 4.1). Similarly, the polymerization of **27** with **23** yielded polymers with M_w/M_n >1.20. The increased conversions achieved during the **26**-mediated polymerization of **27** prompted our use of this CTA to polymerize each monomer derivative in order to ascertain what influences the sulfonamide R-group might have on conversion, molar mass, and molecular weight distribution (Table 4.1). As with the **26**-mediated polymerization of **27** at 70 °C, each substituted monomer derivative also yielded moderately broad molecular weight distributions, typically increasing with conversion, and indicative of limited polymerization control.

Table 4.1

Conversion, molar mass, and molecular weight distribution data for the RAFT polymerization of MSAs in DMF at 70 °C.[a]

entry	monomer	CTA	time (min)	conv.[b] (%)	$[M]_0$ (mol/L)	$M_{ntheory}$[c] (g/mol)	M_{nexp}[d] (g/mol)	M_w/M_n[d]
1a	**27**	**23**	120	7	1.0	3200	4400	1.19
1b	**27**	**23**	360	10		4500	5800	1.18
1c	**27**	**23**	600	12		5400	6200	1.27
2a	**27**	**26**	120	22	1.0	9400	14 600	1.27
2b	**27**	**26**	360	67		28 500	26 400	1.41
2c	**27**	**26**	600	81		34 700	29 700	1.44
3a	**28**	**26**	120	13	1.0	7000	7400	1.27
3b	**28**	**26**	360	48		25 000	22 000	1.24
3c	**28**	**26**	600	66		34 200	28 100	1.26
4a	**29**	**26**	120	16	0.83	8800	13 900	1.22
4b	**29**	**26**	360	51		26 800	29 800	1.27
4c	**29**	**26**	600	69		36 300	35 500	1.29
5a	**30**	**26**	120	35	1.0	18 000	22 000	1.55
5b	**30**	**26**	420	79		40 600	34 900	1.78
5c	**30**	**26**	600	85		43 300	35 200	1.81
6a	**31**	**26**	120	12	0.83	6900	15 100	1.23
6b	**31**	**26**	360	47		26 800	34 600	1.20
6c	**31**	**26**	600	73		41 900	44 400	1.28
7a	**32**	**26**	120	15	0.83	8800	11 100	1.10
7b	**32**	**26**	420	62		35 500	25 900	1.45
7c	**32**	**26**	600	67		38 500	27 100	1.47

[a]Sulfonamide monomers were polymerized at 70 °C in DMF ($[M]_0$:$[CTA]_0$:$[I]_0$ = 150:1.0:0.2) using V-501 as the initiator. [b]Conversions were determined by ^{1}H NMR (DMSO-d_6) by comparing the relative integral areas of trimesic acid (internal standard) aromatic protons (8.64 ppm, 3H) to the vinyl proton of the sulfonamide monomer (5.84 ppm, 1H). [c]Theoretical number average molecular weights were calculated according to the following equation: $M_n=(\rho \cdot MW_{mon} \cdot [M]/[CTA]) + MW_{CTA}$ where ρ is the fractional monomer conversion, MW_{mon} is the molecular weight of the monomer, and MW_{CTA} is the molecular weight of the CTA. [d]As determined by SEC-MALLS (95:5 (v:v) DMF:CH_3COOH 20 mM LiBr).

*Chain Extension of **P<u>27</u>** macroCTA at 70 °C*

The degree of "living" chain end retention was investigated by synthesizing and isolating a **P<u>27</u>** macroCTA using **<u>26</u>** (**P<u>27</u>-<u>26</u>**) (M_n = 7 300 g/mol, M_w/M_n = 1.35), followed by chain extension with **<u>27</u>** to yield the corresponding chain extended polymer (**P<u>27</u>**-*b*-**P<u>27</u>-<u>26</u>**). Figure 4.2 shows the SEC traces of both the initial monomodal **P<u>27</u>-<u>26</u>** macroCTA and the corresponding **P<u>27</u>**-b-**P<u>27</u>-<u>26</u>** polymer after chain extension with **<u>27</u>**. The latter exhibits multimodality and broad molecular weight distribution, indicating extensive loss of "living" polymer chain ends during the initial polymerization of the **P<u>27</u>** macroCTA. Loss of "living" polymer chains is most often attributed to irreversible radical termination, undesirable chain transfer events, or degradation of the thiocarbonylthio chain ends. During the **<u>23</u>**- and **<u>26</u>**-mediated polymerizations of MSAs at 70 °C, we observed a loss of the characteristic color of **<u>23</u>** (pink) and **<u>26</u>** (yellow) after extended polymerization times, qualitatively indicating degradation of the dithiobenzoate and trithiocarbonate moieties, respectively.

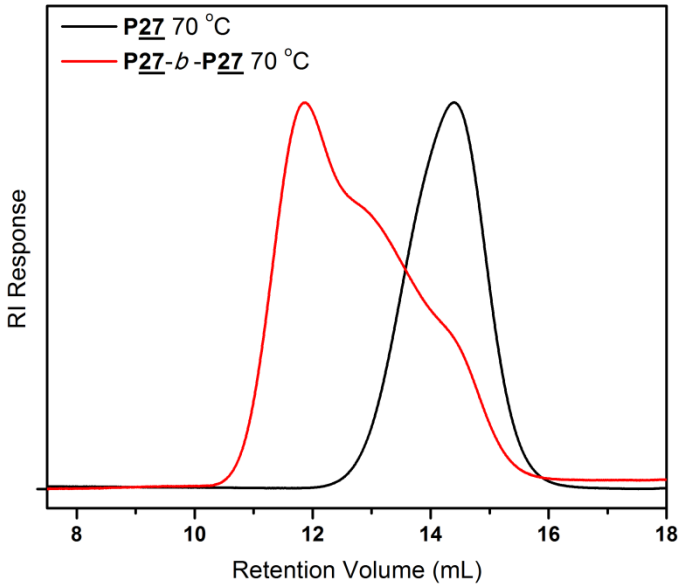

Figure 4.2. SEC traces of **P27** macroCTA (M_n = 7300 g/mol, M_w/M_n = 1.35) and **P27**-*b*-**P27** after chain extension at 70 °C in DMF.

RAFT Polymerization of Methacryloyl Sulfonamides at 30 °C

Hypothesizing that a deleterious side reaction was competing with chain extension during the CTA-mediated polymerization, we lowered the reaction temperature. Such approaches have been previously successful in RAFT polymerizations, yielding well-defined copolymers that maintained a high degree of chain end functionality.[158,250,251] Figure 4.3 shows the comparative SEC chromatograms of the **26**-mediated polymerizations of **27** at 70 °C and 30 °C under the polymerization conditions outlined in Table 4.1. It should be noted that the 30 °C reaction utilized the low decomposition temperature initiator 2,2'-azobis(4-methoxy-2-4-dimethyl valeronitrile) (V-70). While both reactions produced polymers with similar number average molecular weights, the resulting molecular weight distribution of the polymer synthesized at 30 °C (58 % conversion, M_n = 29 700 g/mol, M_w/M_n = 1.05) was substantially lower than the polymer prepared at 70 °C (67% conversion, M_n = 26 400 g/mol, M_w/M_n = 1.41).

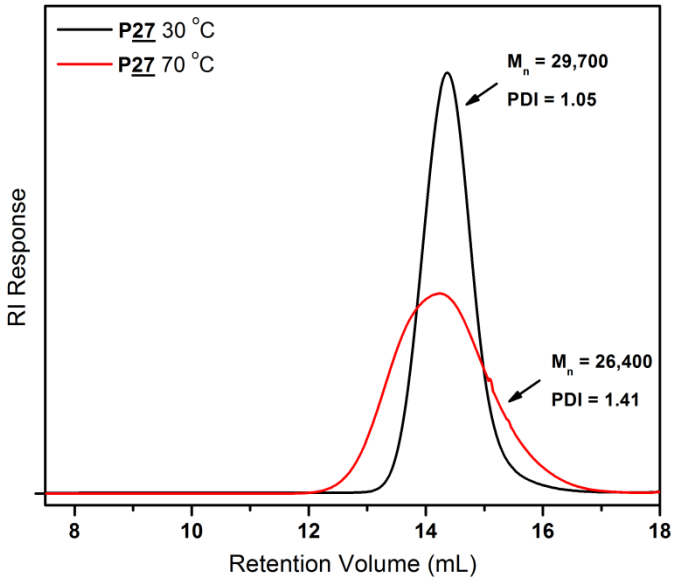

Figure 4.3. DMF SEC RI traces of **P27** polymerized at 30 °C and 70 °C using V-70 and V-501, respectively.

Figure 4.4a shows the kinetic plots for the respective **26**- and **23**-mediated polymerizations of **27** at 30 °C. The former exhibited a longer pre-equilibrium (initialization) period (~60 min) as compared to polymerization at 70 °C; however, linear pseudo-first-order kinetic behavior was observed up to 600 min. Deviation from linearity at longer times in this particular case is possibly due to the reduced radical flux observed as the initiator concentration decreases substantially at prolonged reaction times, as we have previously reported.[95] Figure 4.4b shows the SEC chromatogram overlay at specified times during the 30 °C polymerization of **27** with **26**. The progression of the polymer traces to lower elution volumes with corresponding increases in RI intensity, without high molecular weight shouldering, is indicative of controlled polymerization behavior and thus maintenance of thiocarbonylthio functionality. This is further indicated by the narrow molecular weight distributions (Figure 4.4c) and linear progression of M_n vs. monomer conversion (Figure 4.4d) observed for the 30 °C polymerization of **27**.

While M_n increases in a linear fashion during the RAFT polymerization of **27** at 30 °C, experimentally determined molecular weights (M_{nexp}) are marginally higher than those theoretically predicted ($M_{ntheory}$) based upon monomer conversion. The higher than expected molecular weights determined by MALLS directly of aliquots taken from the polymerization could be indicative of irreversible coupling of CTA intermediate radicals during the initialization stage.[106,252,253]

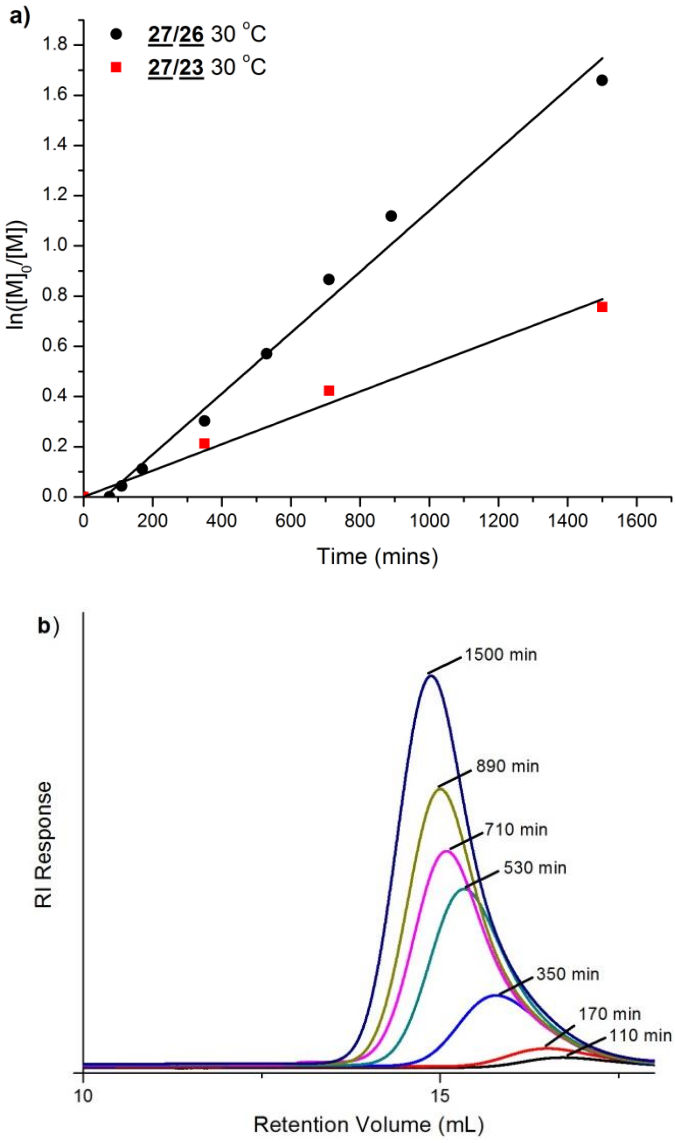

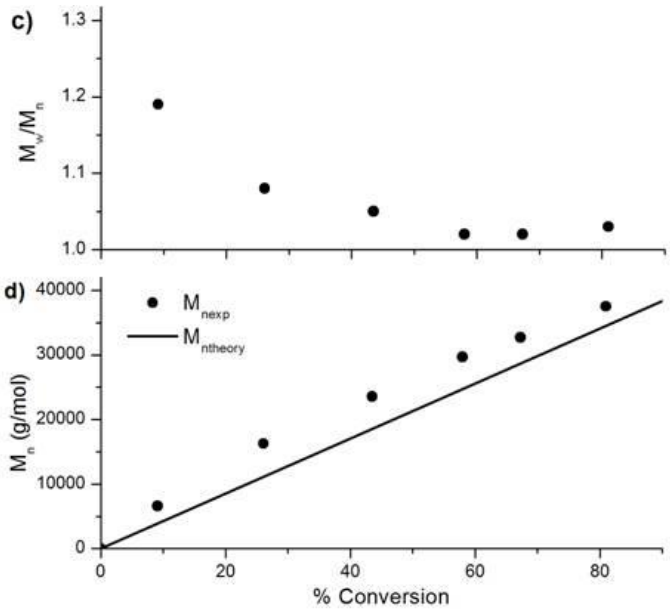

Figure 4.4. a) Pseudo-first-order kinetic plots for the **26**- and **23**-mediated RAFT polymerization of **27** at 30 °C in DMF ($[M]_0$:$[CTA]_0$:$[I]_0$ = 150:1:0.2). b) SEC overlay for **26**-mediated polymerization of **27** at 30 °C in DMF. c) M_w/M_n versus conversion. d) M_n versus conversion.

Table 4.2 summarizes the conversion, molar mass, and molecular weight distribution data for the RAFT polymerization of each MSA derivative in DMF at 30 °C using either **26** or **23** as the RAFT agent and V-70 as the initiator. Reducing the polymerization temperature to 30 °C results in M_w/M_n values typically below 1.10 for all monomer derivatives. M_n values determined by DMF SEC-MALLS are in reasonable agreement with theoretical values calculated from monomer conversion; however, M_{nexp} exceeds $M_{ntheory}$ in a similar manner to that discussed earlier. Furthermore, all polymerizations conducted at 30 °C maintained the characteristic color of the parent CTA, indicating limited degradation as compared to that at 70 °C.

The **23**-mediated polymerization of **27** conducted at 30 °C resulted in 34% monomer conversion after 710 min and narrow molecular weight distributions even after 1500 min of polymerization (53% conversion, M_n = 20 500 g/mol, M_w/M_n = 1.03) (Table

4.2) with the M_n values determined by DMF SEC-MALLS agreeing well with the theoretical values. The analogous reaction conducted at 70 °C yielded 12% monomer conversion after 600 min and relatively broad molecular weight distributions (M_n = 6 200 g/mol, M_w/M_n = 1.27) (Table 4.1). The strikingly higher rate of polymerization observed for the **23**-mediated polymerization of **27** performed at 30 °C as compared to 70 °C is consistent with effectively minimizing (though not completely eliminating) competing dithioester degradation and limiting the accumulation of potentially rate-retarding degradation byproducts.

Table 4.2

Conversion, molar mass, and molecular weight distribution data for the RAFT polymerization of MSAs in DMF at 30 °C.[a]

entry	monomer	CTA	time (min)	conv.[b] (%)	$[M]_0$ (mol/L)	$M_{ntheory}$[c] (g/mol)	M_{nexp}[d] (g/mol)	M_w/M_n[d]
1a	**27**	**23**	350	19	1.0	8300	9500	1.02
1b	**27**	**23**	710	34		14 700	16 700	1.01
1c	**27**	**23**	1500	53		22 700	20 500	1.03
2a	**27**	**26**	350	26	1.0	11 300	16 300	1.08
2b	**27**	**26**	710	58		24 800	29 700	1.05
2c	**27**	**26**	1500	81		34 600	37 500	1.03
3a	**28**	**26**	350	10	1.0	5600	8100	1.19
3b	**28**	**26**	710	30		15 900	14 500	1.12
3c	**28**	**26**	1500	69		36 000	28 600	1.02
4a	**29**	**26**	350	11	0.83	5700	10 300	1.12
4b	**29**	**26**	710	35		18 200	22 100	1.06
4c	**29**	**26**	1500	61		32 200	35 400	1.06
5a	**30**	**26**	240	8	1.0	4200	8100	1.16

Table 4.2 (continued).

entry	monomer	CTA	time (min)	conv.[b] (%)	$[M]_0$ (mol/L)	$M_{ntheory}$[c] (g/mol)	M_{nexp}[d] (g/mol)	M_w/M_n[d]
5b	**30**	**26**	360	14		7500	12 200	1.06
5c	**30**	**26**	780	54		28 200	33 200	1.05
6a	**31**	**26**	240	7	0.83	6300	10 800	1.11
6b	**31**	**26**	360	13		14 800	16 700	1.05
6c	**31**	**26**	780	44		35 500	43 800	1.04
7a	**32**	**26**	240	11	0.83	4200	8700	1.10
7b	**32**	**26**	360	26		7500	11 800	1.06
7c	**32**	**26**	780	62		25 000	30 100	1.07

[a]Sulfonamide monomers were polymerized at 30 °C in DMF ($[M]_0$:$[CTA]_0$:$[I]_0$ = 150:1.0:0.2) using V-70 as the initiator. [b]Conversions were determined by 1H NMR (DMSO-d_6) by comparing the relative integral areas of trimesic acid (internal standard) aromatic protons (8.64 ppm, 3H) to the vinyl proton of the sulfonamide monomer (5.84 ppm, 1H). [c]Theoretical number average molecular weights were calculated according to the following equation: $M_n=(\rho \cdot MW_{mon} \cdot [M]/[CTA]) + MW_{CTA}$ where ρ is the fractional monomer conversion, MW_{mon} is the molecular weight of the monomer, and MW_{CTA} is the molecular weight of the CTA. [d]As determined by SEC-MALLS (95:5 (v:v) DMF:CH_3COOH 20 mM LiBr).

*Chain Extension of **P27**macroCTA at 30 °C*

To further demonstrate the controlled RAFT polymerization of MSAs at low temperatures, a **P27**macroCTA was prepared at 30 °C using V-70 as the initiator and isolated before chain extending with additional **27** at 30 °C. Figure 4.5 shows the SEC chromatogram of the **P27** macroCTA (M_n = 25 100 g/mol, M_w/M_n = 1.09) and a distinct decrease in elution volume of the chain-extended polymer (**P27**-*b*-**P27**) (M_n = 49 600 g/mol, M_w/M_n = 1.07). The monomodal SEC chromatogram and absence of low molecular weight tailing at higher elution volumes of the chain extended polymer is additional evidence of improved chain end retention during the polymerization of MSAs at 30 °C as compared to the analogous chain extension conducted at 70 °C (Figure 4.2).

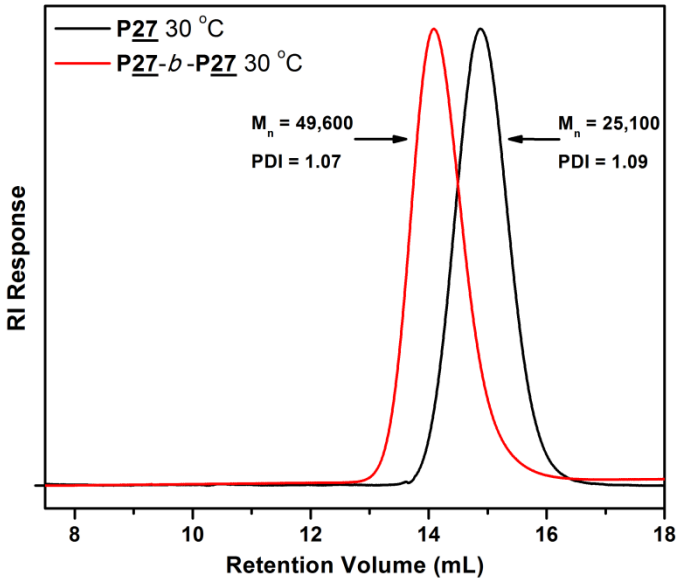

Figure 4.5. SEC traces of **P27** macroCTA (M_n= 25 100 g/mol, M_w/M_n = 1.09) and **P27**-*b*-**P27** (M_n = 49 600 g/mol, M_w/M_n = 1.07) after chain extension in DMF. Both polymerizations were conducted at 30 °C.

Methacryloyl Sulfonamide Monomer pK_a Studies

MSA monomer titrations were performed to determine the pK_a of each monomer derivative after converting the respective sulfa drug precursors into the corresponding methacrylamides. The pK_a of the sulfonamide (SO_2NH) group of each monomer derivative was determined by equation 7 where $pH_{EP1/2}$ is the pH corresponding to the half equivalence point ($EP_{1/2}$) of the titration curve. The volume of HCl titrant required to reach the $EP_{1/2}$ ($Vol_{EP1/2}$) was determined by equation 8 where Vol_{EP} is the volume of HCl titrant required to reach the equivalence point of the titration curve, [SO_2NH] is the sulfonamide concentration, [HCl] is the concentration of HCl titrant used, and Vol_{sol} is the initial volume of the monomer solution being titrated. Figure 4.6 shows the positions of EP and $EP_{1/2}$ on the titration curve for **27**.

$$pK_a = pH_{EP1/2} \quad (7)$$

$$Vol_{EP1/2} = Vol_{EP} + \frac{1}{2}\frac{[SO_2NH]}{[HCl]}Vol_{sol} \quad (8)$$

Table 4.3 contains the pK_a values for each monomer calculated using equation 1 along with the literature reported pK_a values for the corresponding sulfa drug precursors. A general trend is observed whereby the pK_a of the MSA is lower than that of the sulfa drug precursor which is consistent with the decrease in pK_a observed upon acetylation of the *p*-amino group of sulfa drugs.[254]

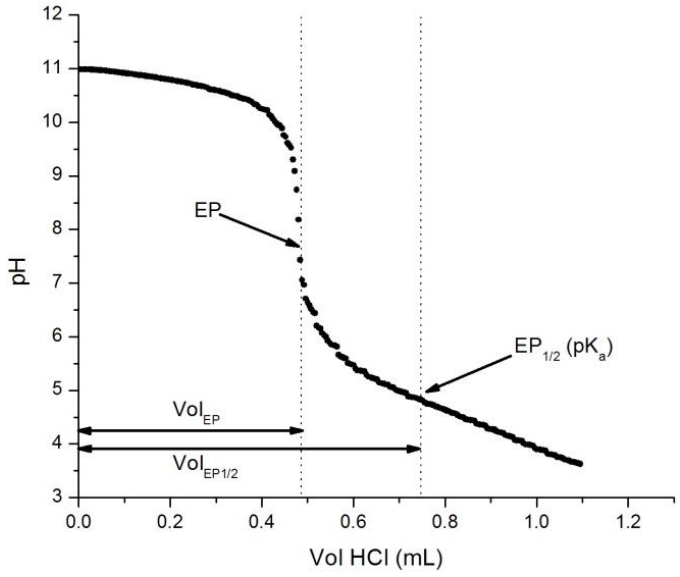

Figure 4.6. EP and $EP_{1/2}$ locations on the titration curve of **27** (1 mM) titrated against HCl (0.05 N) at 25 °C using a Metrohm 848 Titrino Plus autotitrator.

pH-dependent Solubility of Poly(methacryloyl sulfonamides)

The titration curves (Figure 4.7) demonstrate the facility by which the pH-dependent solubility of pMSAs can be "tuned" by simply varying the sulfonamide R-group of the monomer. The changes in polymer solubility occur over a very narrow range of typically 0.5 pH units. Table 4.3 summarizes the pH-dependent solubility of each

MSA derivative. The critical onset of precipitation (pH*), is defined as the pH corresponding to 90% light transmittance. For each of the MSA derivatives, pH* of the polymer is greater than the pK_a of the corresponding monomer. The pH* of a particular pMSA is dependent upon the monomer pK_a and the relative hydrophobicity of the monomer derivative, both influenced by the sulfonamide R-group. The mutual influence of these two parameters is readily apparent by comparing the pH* and pK_a values for **P27** and **P28** (Table 4.3). While the pK_a of **28** (4.51) is lower than that of **27** (4.88), the pH* for **P28** (5.3) is higher than that of **P27** (5.1) due to the greater hydrophobicity of the benzoyl R-group.

Table 4.3

MSA monomer and polymer titration data.

polymer	M_{nexp} (g/mol)	M_w/M_n	sulfadrug pK_a	monomer pK_a	pH*
P27	31 400	1.04	5.38	4.88 ± 0.01	5.3
P28	27 500	1.03	4.57	4.51 ± 0.01	5.7
P29	32 000	1.05	5.29	5.19 ± 0.03	6.3
P30	24 400	1.03	6.16	5.44 ± 0.01	6.7
P31	43 800	1.04	6.70	5.75 ± 0.01	7.5
P32	34 400	1.08	7.49	7.33 ± 0.02	7.9

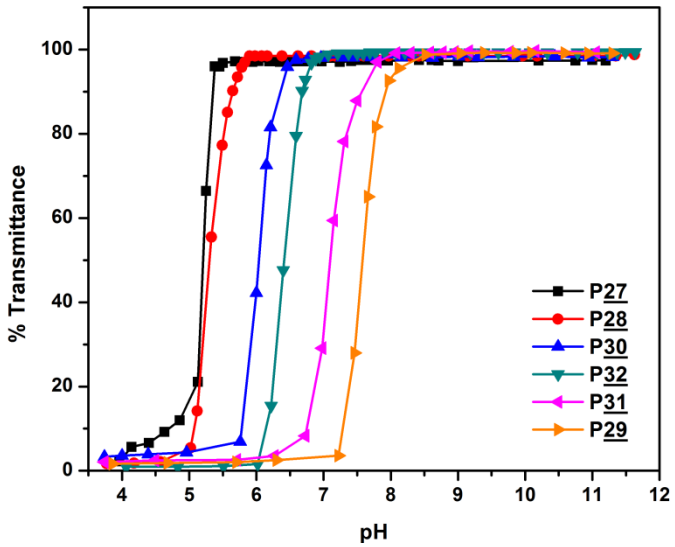

Figure 4.7. Substituent effects on pH-dependent solubility transitions of sulfonamide-containing polymers. Percent transmittance was measured using a UV-Vis spectrophotometer (λ = 500 nm).

CO_2-dependent Solubility of Poly(methacryloyl sulfonamides)

To date, CO_2-responsive polymers rely almost exclusively upon protonation of amine or amidine functional groups by carbonic acid (produced upon dissolution of CO_2 in water) that alters polymer solubility and conformation in solution.[235,255] However, there are very few examples of CO_2-responsive polymers based upon acidic functional groups.[256] In order for acid-functional polymers to exhibit CO_2-induced changes in phase or conformation, the pK_a of the acidic functional group and more importantly the pH* of the corresponding polymer, must be greater than the pH of the solution upon production of carbonic acid via dissolution of CO_2. Therefore, weakly acidic polyacids that exhibit pH-responsive behaviors above pH = 4 (the pH of an aqueous solution in equilibrium with 1 atm of CO_2 at 25 °C) should also exhibit similar changes in properties upon CO_2-induced solution acidification.

The weakly acidic pMSA derivatives we report here exhibit pH* values above pH = 5.0, making these ideal candidates as CO_2-responsive polymers. To demonstrate the

reversible CO_2-responsiveness of pMSAs, polymethacryloyl sulfamethazine (**P29**) (M_n = 34 400 g/mol, M_w/M_n = 1.08) (1 eq sulfonamide functional group) was dissolved in 0.05 N NaOH (1.25 eq) and diluted with DI H_2O to yield a final [SO_2NH] = 6.7 mM and [NaOH] = 8.4 mM. The solution was purged with CO_2 (10 s) and then N_2 (25 min) and the % transmittance (λ = 500 nm) of the polymer solution measured before and after each purge cycle using a UV-Vis spectrophotometer. Figure 4.8 shows % transmittance as a function of purge cycle and illustrates the reversible CO_2-triggered change in aqueous solubility of **P29**.

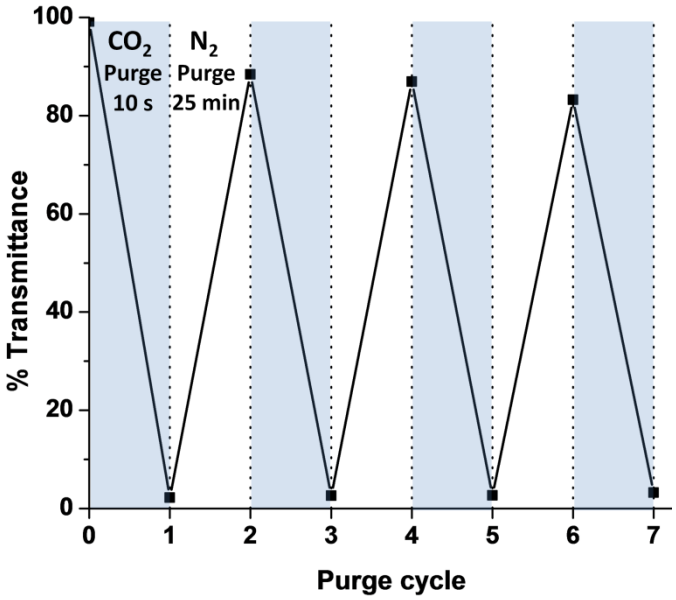

Figure 4.8. Reversible solubility of **P29** in response to presence or absence of CO_2. Solutions were purged with either CO_2 for 10 s (shaded regions) or N_2 for 25 min (unshaded regions) and % transmittance measured using a UV-Vis spectrophotometer (λ = 500 nm).

Section 2. Mechanistic Insights into Temperature-Dependent Trithiocarbonate Chain-End Degradation during the RAFT Polymerization of N-Arylmethacrylamides

Overview

The acknowledged utility of reversible-deactivation radical polymerization (RDRP) is the facile synthesis of polymers with precise compositions, predetermined molecular weights, and well-defined architectures while incorporating monomers possessing a wide variety of functional groups.[76,89,246,247] The success of any RDRP technique depends greatly upon maintaining "living" chain end fidelity. In particular, the reversible addition-fragmentation chain transfer (RAFT) process must retain thiocarbonylthio end groups in order to maintain the active/dormant equilibrium necessary for polymerization control. While thiocarbonylthio reactivity has often been exploited as a facile means of post-polymerization end group modification of RAFT polymers,[257–263] a number of deleterious side reactions involving the thiocarbonylthio moiety can occur including hydrolysis,[119] aminolysis,[95,119] thermolysis,[264] oxidation,[265,266] and irreversible coupling of intermediate radicals.[252,267,268] It is therefore important to fully understand the nature of any degradative reactions involving thiocarbonylthio end groups in order to extend the current capabilities of RAFT polymerization.

Recently, we reported the RAFT polymerization of a library of pH-responsive methacryloyl sulfonamide (MSA) monomers derived from sulfa drugs.[97] Loss of chain end functionality was observed during the polymerization of MSAs at the commonly used temperature of 70 °C as evidenced, in part, by broad molecular weight distributions ($M_w/M_n > 1.3$) and failure to successfully chain extend a poly(MSA) macro chain transfer agent (macroCTA). However, narrow molecular weight distributions and controlled

molecular weights were ultimately achieved by conducting the polymerizations at 30 °C. The poor polymerization control of MSAs at 70 °C surprisingly contrasts numerous literature reports of successful RAFT polymerizations of (meth)acrylamides in organic and aqueous media at temperatures greater than 60 °C,[91,95,100,269–271] thus prompting our current investigation.

Since our initial report,[97] we have conducted the RAFT polymerization of N-phenylmethacrylamide (**33**), an MSA analog lacking the sulfonamide functional group (vide infra). Notably, the trithiocarbonate-mediated polymerization of **33** at 70 °C also results in relatively broad molecular weight distributions (M_w/M_n = 1.30), indicating that the sulfonamide functional group is not the primary cause for chain end degradation during polymerization of MSAs. Previous reports regarding the atom transfer radical polymerization (ATRP) of (meth)acrylamides attributed loss of "living" chain ends to nucleophilic displacement of the terminal bromine by the penultimate amide unit.[272–274] Similarly, oxazolone formation during peptide synthesis occurs by an amide "back-biting" reaction.[275] There is also literature precedent for the effects of N-aryl substitution on the cyclization of (thio)carbamoyl derivatives formed during sequencing of peptides by Edman's degradation[276] as well as the cyclization of γ-bromobutyranilides.[277] From these observations, we have hypothesized that a similar reaction involving nucleophilic attack on the ω-thiocarbonyl by the terminal methacrylamide unit may be responsible for thiocarbonylthio degradation during the RAFT polymerization of N-arylmethacrylamides.

In this contribution we report the influences of methacrylamide structure and reaction temperature on trithiocarbonate degradation during the RAFT polymerization of

N-substituted methacrylamides. A detailed study of the trithiocarbonate-mediated polymerizations of **33** and N-benzylmethacrylamide (**34**) using SEC-MALLS and UV-vis spectroscopy has now provided a clear understanding of the influence of methacrylamide structure on CTA degradation. Furthermore, *in situ* ^{1}H NMR analysis of RAFT polymer small molecule analogs, prepared by single monomer unit insertion, affords additional mechanistic insight into the specific degradation pathway.

33 *and* ***34*** *Polymerization Kinetics*

To our knowledge, there are no reports detailing the effects of N-aryl substitution on RAFT-mediated polymerization control of (meth)acrylamides. To this end, we chose to compare the RAFT polymerizations of **33** and **34** under analogous conditions (Scheme 4.3). **34** was chosen based upon its structural similarity to **33** while lacking direct N-aryl substitution.

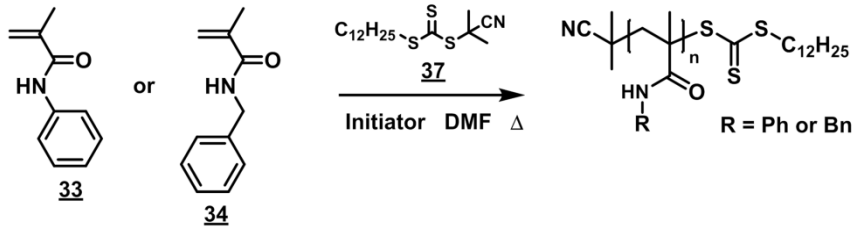

Scheme 4.3. Synthetic route for **37**-mediated polymerization of **33** and **34** in DMF at 70 or 30 °C.

Table 4.4 summarizes the conversion, molar mass, and molecular weight distribution data for the polymerizations of **33** and **34** in DMF at 70 and 30 °C, using the RAFT agent 2-cyano-2-propyl dodecyl trithiocarbonate (**37**). The effect of methacrylamide structure on polymerization control is initially apparent by comparing the increase in molecular weight distribution of **P33** (M_w/M_n = 1.30) relative to that of **P34** (M_w/M_n = 1.15) synthesized under identical reaction conditions. Limited molecular

weight control during polymerization of **33** at 70 °C can also be seen in the M_n vs conversion plot (Figure A1, Appendix A) which shows a decrease in $M_{n,exp}$ relative to $M_{n,th}$ at higher conversions. By contrast, for the polymerization of **34** at 70 °C, $M_{n,exp}$ values mirror $M_{n,th}$ values, indicating that the number of active/dormant chain ends remain constant during polymerization (Figure A2, Appendix A).

Table 4.4

*Conversion, Molar Mass, and Molecular Weight Distribution Data for the RAFT Polymerizations of **33** and **34** in DMF at 70 and 30 °C.*[a]

entry	monomer	temp. (°C)	time (min)	conv.[b] (%)	$M_{n,th}$[c] (g/mol)	$M_{n,exp}$[d] (g/mol)	M_w/M_n[d]
1a	**33**	70	240	37	12400	14800	1.09
1b	**33**	70	360	48	16000	17300	1.16
1c	**33**	70	480	55	18200	18100	1.24
1d	**33**	70	600	59	19500	18900	1.30
2a	**34**	70	240	24	8900	11700	1.06
2b	**34**	70	360	32	11500	13400	1.11
2c	**34**	70	480	37	13400	15000	1.15
2d	**34**	70	600	41	14600	16100	1.15
3a	**33**	30	300	9	3200	6000	1.07
3b	**33**	30	420	14	4900	7400	1.05
3c	**33**	30	600	23	7800	10500	1.02
3d	**33**	30	1380	50	16600	18800	1.02
4a	**34**	30	300	7	2700	3400	1.13
4b	**34**	30	420	10	3700	4100	1.07
4c	**34**	30	600	14	5100	5900	1.05
4d	**34**	30	1380	29	10400	11200	1.04

[a]Polymerizations were conducted at 70 or 30 °C in DMF ($[M]_0$:$[CTA]_0$:$[I]_0$ = 200:1.0:0.2) using V501 or V-70 as the initiators respectively. [b]Conversions were determined by ^{1}H NMR (DMSO-d_6) by comparing the relative integral areas of trimesic acid (internal standard) aromatic protons (8.64 ppm, 3H) to the vinyl proton of **33** (5.86 ppm, 1H) or **34** (5.79 ppm, 1H). [c]Theoretical M_n values were calculated according to the equation $M_{n,th}=(\rho MW_{mon}[M]_0/[CTA]_0) + MW_{CTA}$ where ρ is the fractional monomer conversion, MW_{mon} is the molecular weight of the monomer, and MW_{CTA} is the molecular weight of the CTA. [d]Experimental M_n and M_w/M_n values were determined by SEC-MALLS (DMF 20 mM LiBr).

Figure 4.9 shows the kinetic plots for the 70 °C polymerizations of **33** (black) and **34** (red); each plot shows an initialization period of approximately 30 min followed by pseudo-first-order kinetic behavior up to 300 min with the differences in slope of the curves indicative of the relative propagation rate coefficients (k_p) for each monomer derivative. Similar initialization periods were observed previously for the trithiocarbonate-mediated polymerizations of N-aryl MSAs and are indicative of slow fragmentation/reinitiation by the RAFT agent R-group.[97,106] Interestingly, the first-order kinetic plots for the homopolymerizations of **33** and **34** at 70 °C show similar minimal decreases in slope beyond 300 min despite limited molecular weight control observed during the same time period for the polymerization of **33**. It might be expected that RAFT agent degradation during polymerization of **33** would result in a decrease in the slope ($k_p[P_n\cdot]$) of the pseudo-first-order kinetic plot due to chain transfer to thiol-containing degradation byproducts. However, efficient chain transfer can take place without influencing the rate of polymerization if the rate of reinitiation by thiyl radicals is greater than the rate of propagation (i.e. $k_{iT} > k_p$).[278] The decrease in $M_{n,exp}$ relative to $M_{n,th}$ throughout the 70 °C polymerization of **33** (Figure A1, Appendix A) is evidence of an increasing number of polymer chains resulting from efficient chain transfer.

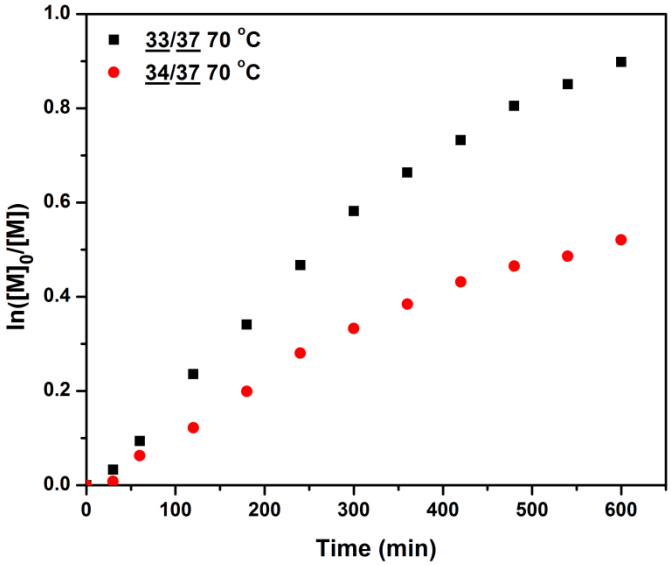

Figure 4.9. Kinetic plot for the **37**-mediated polymerization of **33** and **34** in DMF at 70 °C ($[M]_0$ = 2.0 M, $[M]_0$:$[CTA]_0$:$[I]_0$ = 200:1:0.2).

Recently we demonstrated that improved chain end retention and narrow molecular weight distributions can be achieved during the RAFT polymerization of N-aryl MSAs by reducing the reaction temperature.[97] Likewise, as seen in Figure 4.10, the molecular weight distribution of **P33** synthesized at 30 °C (M_w/M_n = 1.02, M_n = 18800) was markedly narrower than that of **P33** synthesized under analogous conditions at 70 °C (M_w/M_n = 1.30, M_n = 18900). Reduced polymerization temperature also afforded improved molecular weight control during the polymerization of **33** as evidenced by the linear progression of $M_{n,exp}$ with conversion and good correlation between $M_{n,exp}$ and $M_{n,th}$ values (Figure A3, Appendix A). As shown in Table 4.4, narrower molecular weight distributions were also obtained during the polymerization of **34** at 30 °C ($M_w/M_n < 1.10$) but the additional decrease was minimal due to already narrow M_w/M_n achieved during polymerization at 70 °C.

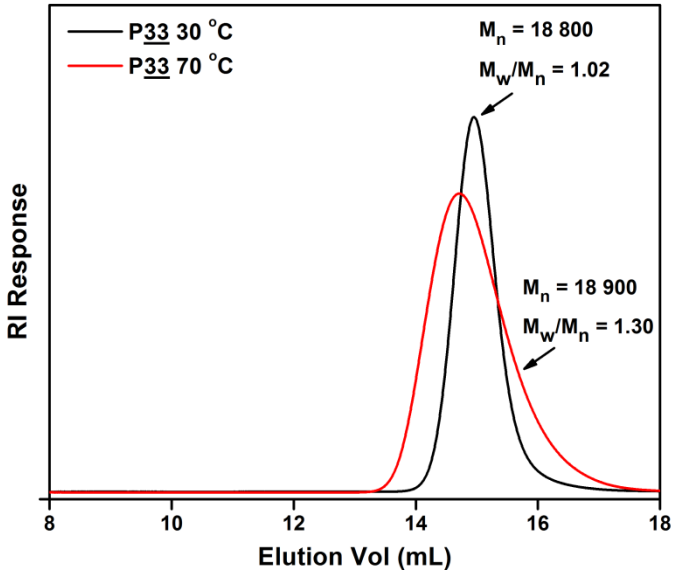

Figure 4.10. SEC RI chromatogram showing the effect of temperature on molecular weight distribution for the **37**-mediated RAFT polymerization of **33** at 70 and 30 °C.

The kinetic plots for the **37**-mediated polymerizations of **33** and **34** at 30 °C (Figure 4.11) exhibit initialization times of 100 min and 60 min respectively, while demonstrating near pseudo-first-order kinetic behavior up to at least 1380 min. The increase in initialization time with decreasing temperature for the RAFT polymerizations of **33** and **34** is consistent with observations made by McLeary et al.[106] The improved linearity of the first-order kinetic plots is also consistent with previous low temperature RAFT polymerizations of (meth)acrylamides and is generally attributed to increased thiocarbonylthio chain end retention.[158,250]

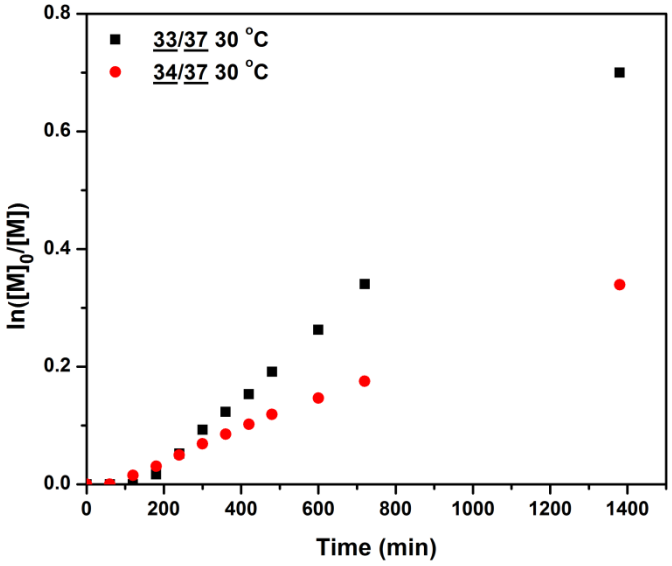

Figure 4.11. Kinetic plot for the **37**-mediated polymerization of **33** and **34** in DMF at 30 °C ($[M]_0$ = 2.0 M, $[M]_0$:$[CTA]_0$:$[I]_0$ = 200:1:0.2).

*Trithiocarbonate Degradation during the **37**-mediated Polymerizations of **33** and **34***

It is evident from the molecular weight data summarized in Table 4.4 that chain end degradation is likely occurring during the 70 °C polymerization of **33**. Meanwhile, polymerization of **34** at the same temperature affords narrower molecular weight distributions with good correlation between $M_{n,th}$ and $M_{n,exp}$ values. In order to ascertain the influences of each polymerization component (i.e. solvent, monomer, and initiator) on temperature-dependent trithiocarbonate degradation, reactions were performed in DMF using combinations of **37**, monomer (**33** or **34**), and initiator (V501) at relative concentrations of $[\mathbf{37}]_0$:$[M]_0$:$[I]_0$ = 10:1.0:0.2 as illustrated in the figures of Figure 4.12. The fractional change in total trithiocarbonate (TTC) concentration ($[TTC]/[TTC]_0$) was measured by comparing the absorbance (λ = 320 nm) of diluted aliquots taken at timed intervals to that of an initial aliquot at t = 0. It is worth noting that only minimal change in the molar extinction coefficient (ε) of **37** at λ = 320 nm occurs after covalent addition of **33** or **34**, allowing for accurate measurement of the total [TTC] during polymerization.

Figure A5 in Appendix A shows the Beer-Lambert plots and ε values at λ = 320 nm for **37** (ε_{320} = 9380 M^{-1} cm^{-1}) and the corresponding single monomer unit insertion (SMUI) adducts of **37** and **33** (**41**) (ε_{320} = 9560 M^{-1} cm^{-1}) and the SMUI adduct of **37** and **34** (**42**) (ε_{320} = 10300 M^{-1} cm^{-1}).

Examination of Figure 4.12a reveals no measureable influences of DMF (▼), **33** (▲), or V501 (●) independently on [TTC]/[TTC]$_0$ at 70 °C. However, a 60 % decrease in [TTC]/[TTC]$_0$ is observed after 12 h when **37**, **33**, and V501 are combined at 70 °C (■) such that monomer addition to **37** takes place. This result supports terminal monomer unit-induced degradation in which the ultimate methacrylamide unit is in a favored orientation for O-5 or N-5 nucleophilic attack on the terminal thiocarbonyl (Scheme 4.4). In this case "5" denotes the number of atoms between the amide oxygen or nitrogen and the thiocarbonyl carbon. By contrast, identical experiments performed with **34** showed minimal trithiocarbonate degradation during polymerization with only a 3 % decrease in [TTC]/[TTC]$_0$ observed after 12 h (Figure 4.12b).

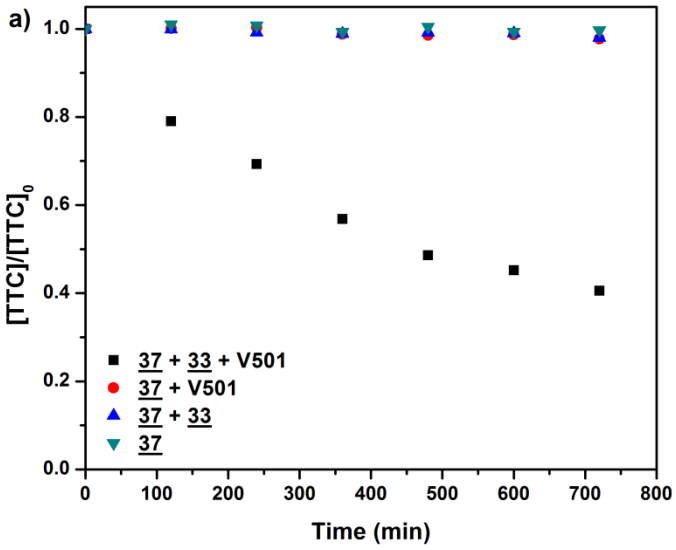

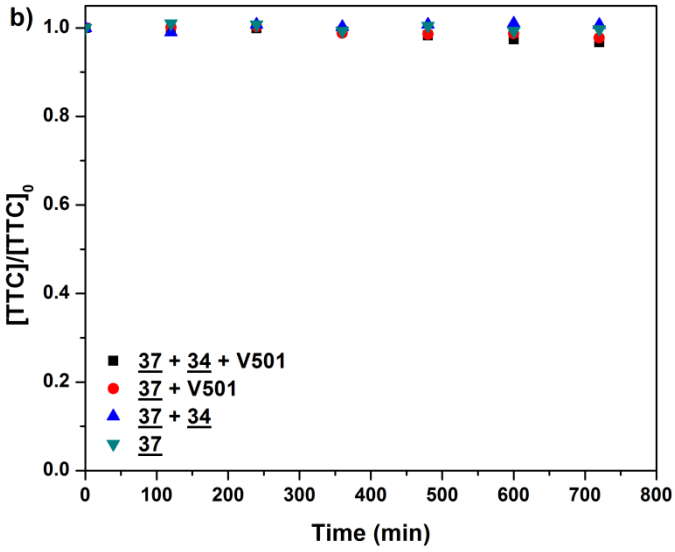

Figure 4.12. Individual and combined influences of solvent, initiator, and monomer on the time-dependent change in [TTC]/[TTC]$_0$ as measured by UV-Vis spectroscopy ([M]$_0$:[CTA]$_0$:[I]$_0$ = 10:1:0.2). Trithiocarbonate degradation experiments were performed using (a) **33** or (b) **34** as the monomer.

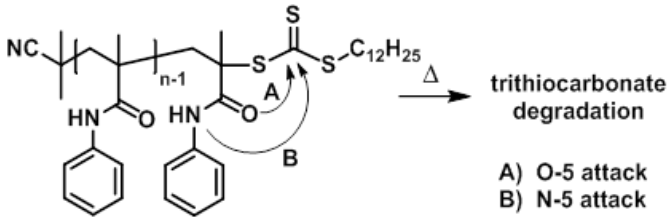

Scheme 4.4. Proposed trithiocarbonate degradation by O-5 or N-5 nucleophilic attack by the terminal methacrylamide unit.

Previously, we attributed the substantially improved polymerization control of MSAs and **33** at 30 °C to increased chain end retention.[97] As seen in Figure 4.13, the effect of temperature on trithiocarbonate degradation was confirmed by measuring [TTC]/[TTC]$_0$ during polymerization of **33** at 30 °C under analogous conditions used for experiments in Figure 4.12a. At 30 °C, only 8 % trithiocarbonate degradation was observed after 720 min compared to 60 % degradation for the same time period at 70 °C.

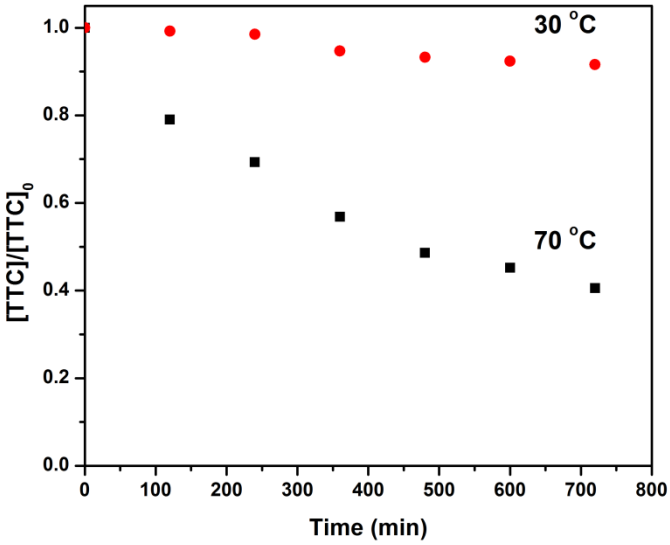

Figure 4.13. Trithiocarbonate degradation during the **37**-mediated polymerization of **33** ($[M]_0$:$[CTA]_0$:$[I]_0$ = 10:1:0.2) at 70 and 30 °C using V501 and V-70 as initiators respectively.

Small Molecule Analog Synthesis

In order to better study the mechanism and byproducts of N-arylmethacrylamide-promoted trithiocarbonate degradation, we attempted to synthesize a small molecule analog of trithiocarbonate-terminated poly(N-phenylmethacrylamide). According to Scheme 4.5, the desired product **40a** should result from the SN_1 reaction of sodium ethyl trithiocarbonate (**24**) and 2-bromoisobutyrylanilide (**39**). Despite the reaction being performed at room temperature (22 °C), isolation of **40a** proved unsuccessful. Recrystallization of the crude reaction mixture afforded 5,5-dimethyl-3-phenyl-2-thioxothiazolidin-4-one (**40**), the N-5 cyclization product of **40a** (Scheme 4.5). The structure of **40** was confirmed in part by analysis of the ^{1}H NMR spectrum (Figure 4.14) which is absent of ethylsulfanyl –SCH_2CH_3 and amide -N-*H* ^{1}H resonances. The ^{1}H and ^{13}C chemical shifts of **40** also match those reported previously.[227] ^{1}H NMR analysis of aliquots sampled during the reaction (Scheme 4.5) showed rapid formation of **40**,

indicating that under these conditions, N-5 cyclization/elimination of the transient species **40a** occurs even at temperatures below 30 °C.

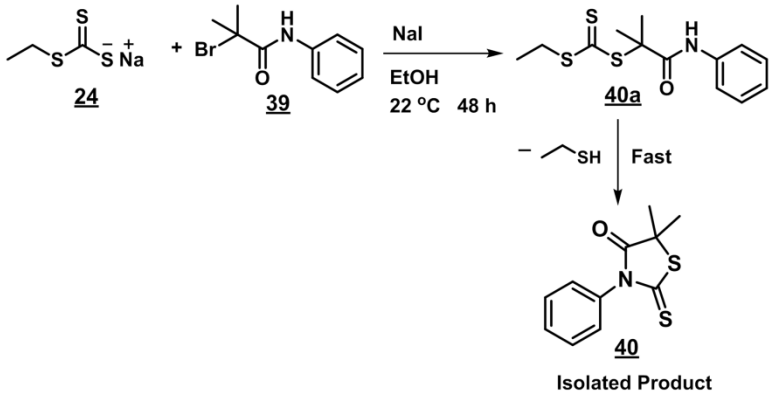

Scheme 4.5. Synthetic route for small molecule analog **40a**.

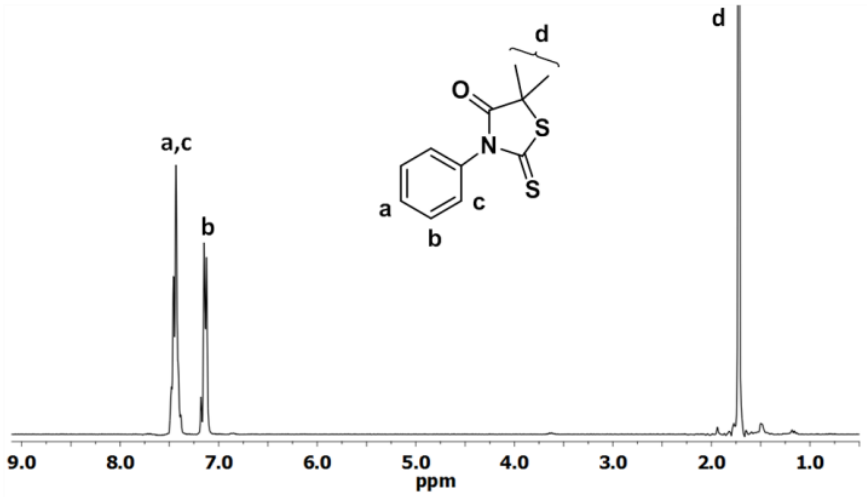

Figure 4.14. ^{1}H NMR (300 MHz, $CDCl_3$) spectrum of isolated N-5 cyclization/elimination product **40**.

Small Molecule Analog Synthesis via Single Monomer Unit Insertion

Minimal degradation of **37** during the polymerization of **33** at 30 °C indicates that covalent adducts of **33** and **37** are stable at low temperatures and can be formed by free radical processes. Recently, single monomer unit insertion[279,280] has become a facile method for CTA synthesis, exploiting the "initialization" phenomenon previously

described by McLeary, Klumperman, and coworkers.[106] We found that the SMUI adduct of **37** and **33** (**41**) could be marginally favored by stoichiometric control of monomer, CTA, and initiator at 30 °C as outlined in Scheme 4.6. The SMUI adduct of **37** and **34** (**42**) was synthesized at 60 °C using AIBN as the initiator owing to the lower nucleophilicity of the N-benzylamide at higher temperatures as previously demonstrated. The labeled ^{1}H NMR spectra of **41** and **42** are shown in Figures 4.15a and 4.15b respectively.

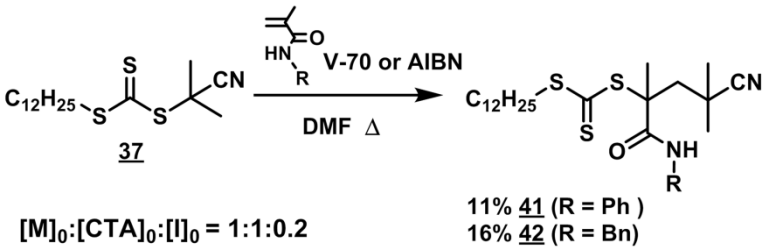

Scheme 4.6. Synthesis of **41** and **42** by single monomer unit insertion.

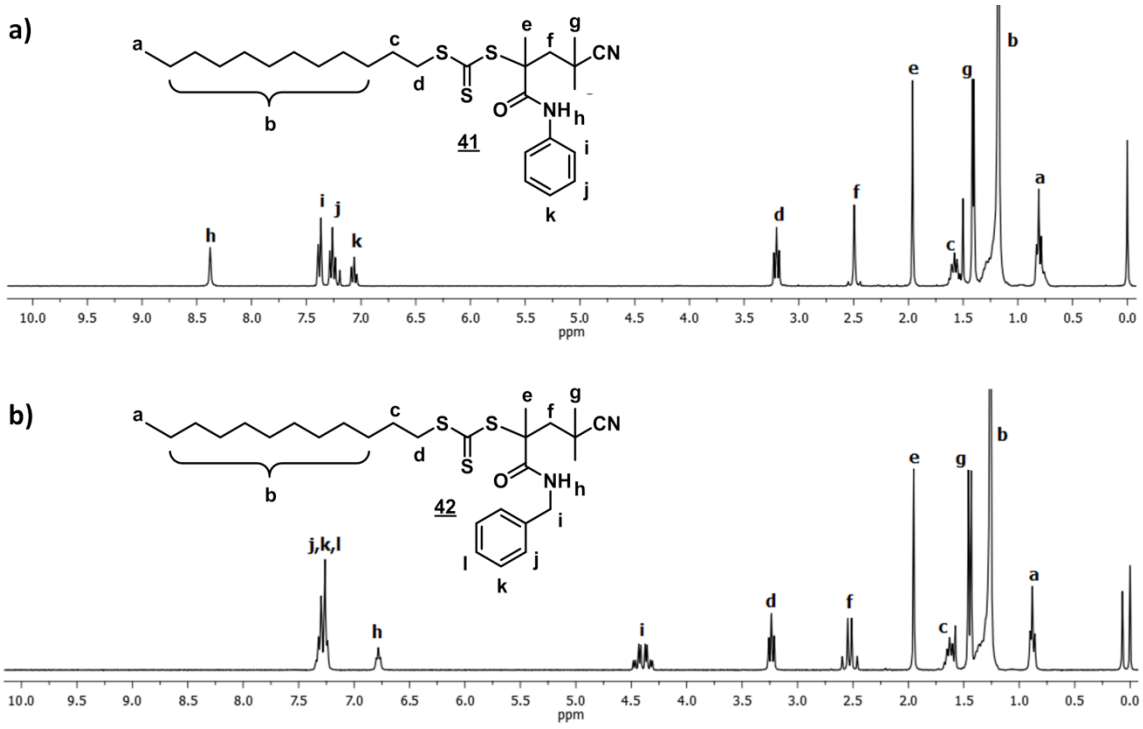

Figure 4.15. ^{1}H NMR (300 MHz, $CDCl_3$) spectra of (a) **41** and (b) **42** SMUI adducts.

In situ [1]*H NMR Analysis of* ***41*** *and* ***42*** *Degradation at 70 °C*

In situ ^{1}H NMR analysis was used to gain further insight into the mechanism and kinetics of **41** and **42** degradation. The labeled ^{1}H NMR spectra at select time points during the degradation analysis of **41** at 70 °C in DMF-d_7 are shown in Figure 4.16. After 5 min, only the ^{1}H resonances **41** are observed. Subsequently, new signals in the aromatic (7.4-7.7 ppm) and aliphatic (1.5-2.7 ppm) regions corresponding to degradation byproducts appear and increase in intensity with time. Comparison of the ^{1}H NMR chemical shifts of the degradation byproducts (Figure 4.16) with those of 1-dodecanethiol and 5,5-dimethyl-3-phenyl-2-thioxothiazolidin-4-one (**40**) (Figures A6, A7 and A8, Appendix A) indicates that the byproducts of **41** degradation are those formed exclusively by N-5 cyclization/elimination. Labeled resonances corresponding to N-5 cyclization/elimination degradation byproducts are given prime designation in the NMR spectrum (Figure 4.16) obtained at 491 min.

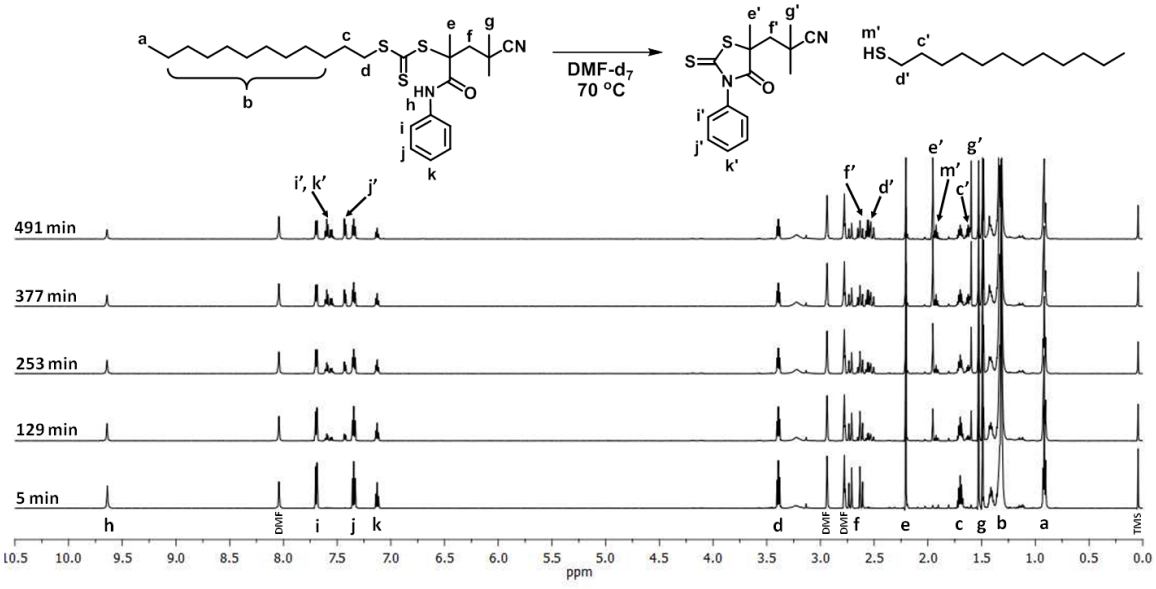

Figure 4.16. ^{1}H NMR (600 MHz, DMF-d_7) overlay following the time-dependent degradation of **41** at 70 °C.

Degradation of **42** at 70 °C (Figure 4.17) was also monitored using *in situ* ^{1}H NMR analysis. After 491 min, minimal degradation was observed as shown in the expanded regions of the ^{1}H NMR spectrum in Figure 4.17 corresponding to the 3-benzyl-2-thioxothiazolidin-4-one methylene (peak i') and the cyclized benzylmethacrylamide methyl (peak e'). Also visible is the characteristic methylene of 1-dodecanethiol (peak d') which is additional evidence of degradation by N-5 cyclization/elimination.

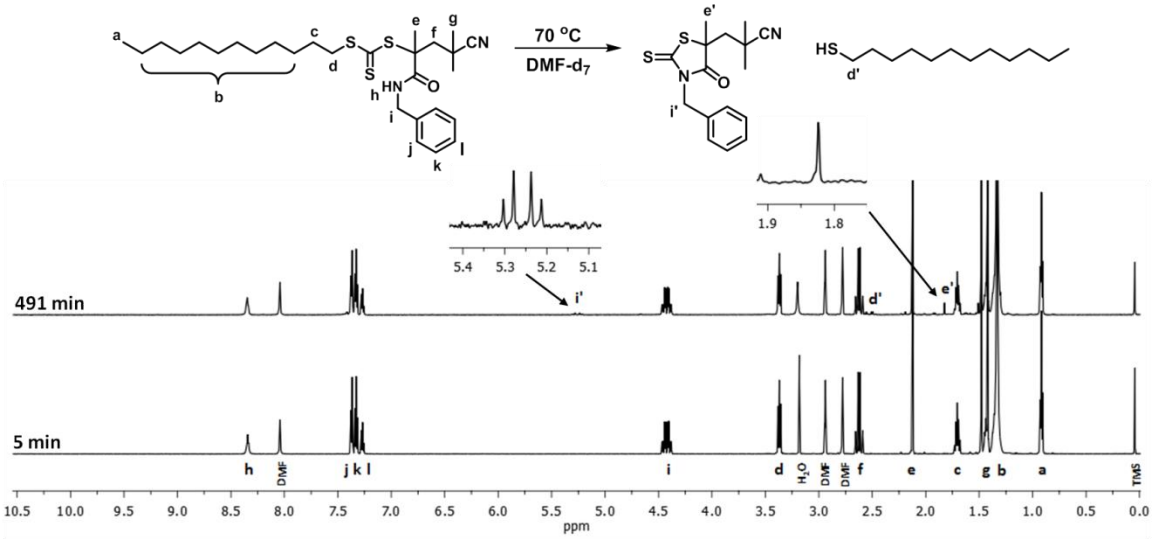

Figure 4.17. ^{1}H NMR (600 MHz, DMF-d_7) overlay following the time-dependent degradation of **42** at 70 °C.

Kinetic analysis of **41** degradation also provides additional evidence for exclusive N-5 cyclization/elimination. As shown in Scheme 4.7, intramolecular N-5 nucleophilic attack of the trithiocarbonate by adjacent methacrylamide can occur by either cyclization/elimination (pathway A) or rearrangement (pathway B) depending upon which C-S bond is cleaved. The total rate of degradation of **41** by pathways A and B is equal to the rate of change in area of the phenyl ^{1}H resonances (Figure 4.16, peaks i, j, and k) as N-5 nucleophilic attack results in loss of the N-phenylamide. The exclusive rate of N-5 cyclization/elimination (pathway A) is equal to the rate of change in area of the –

C*H*$_2$-S- ^{1}H resonance (Figure 4.16, peak d) as elimination of 1-dodecanethiol occurs. As shown in Figure 4.18a, the fractional changes in area (A_t/A_0) of peaks i (7.70 ppm) and d (3.39 ppm) are essentially identical throughout the 491 min experiment indicating that pathway A is responsible for the degradation of **41** at 70 °C.

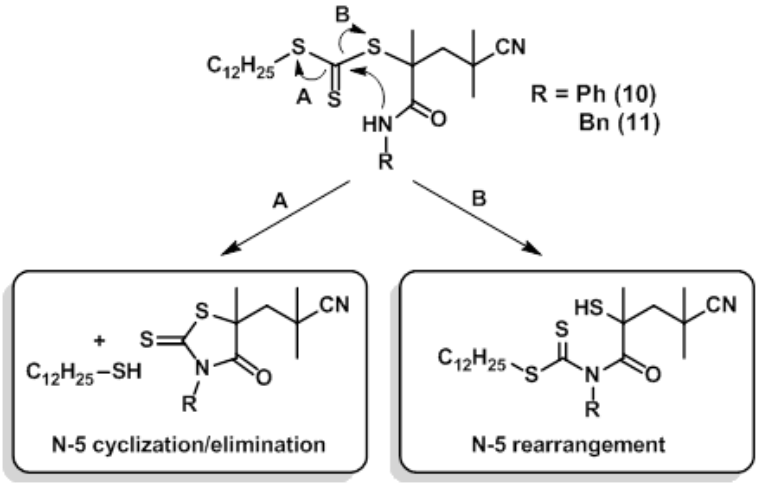

Scheme 4.7. Possible N-5 nucleophilic attack degradation pathways.

Kinetic analysis of **42** degradation (Figure 4.18b) additionally supports the proposed degradation pathway of N-5 cyclization/elimination as shown by the comparable change in A_t/A_0 of peaks i (4.42 ppm) and d (3.37 ppm) (Peak assignments in Figure 4.17).

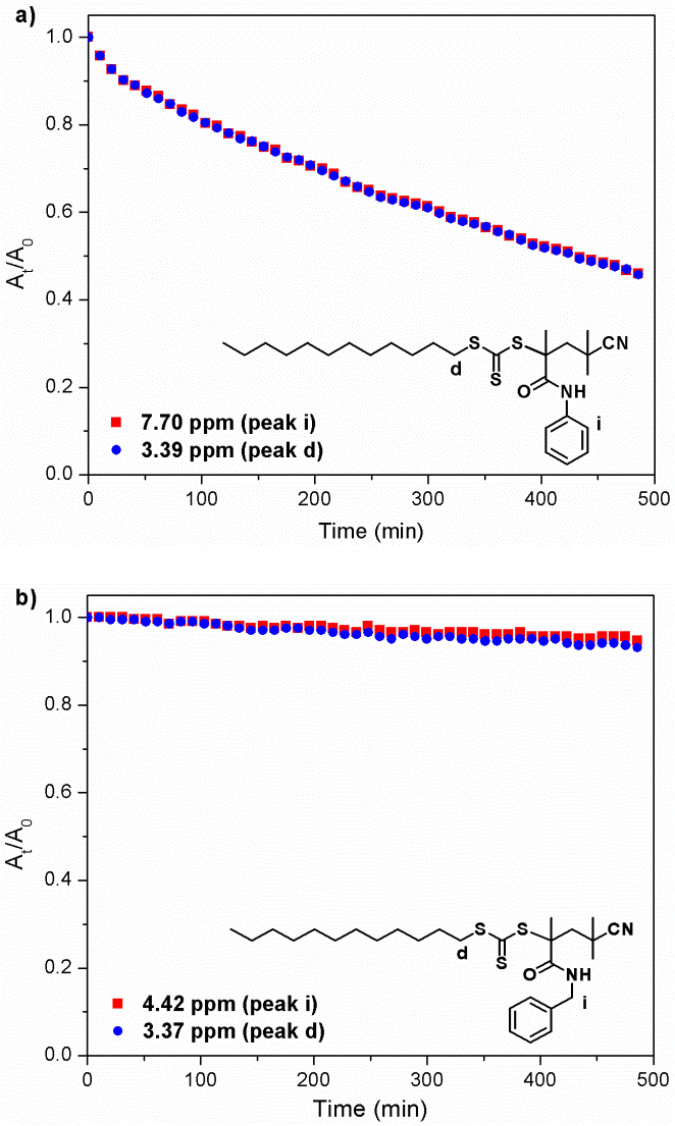

Figure 4.18. Time-dependent fractional change in the area of select ^{1}H chemical shifts during the degradation of (a) **41** and (b) **42** in DMF-d_7 at 70 °C.

As seen in Figure 4.19, excellent agreement is observed between the time-dependent fractional changes in [TTC] measured during the **37**-mediated polymerizations of **33** and **34** by UV-Vis spectroscopy (open data points) and during **41** and **42** degradation measured by *in situ* ^{1}H NMR analysis (solid data points). The half lives ($t_{1/2}$) of **41** and **42** at 70 °C in DMF were calculated to be $t_{1/2}$ = 7.18 h and $t_{1/2}$ = 78.5 h respectively based upon the degradation rates measured using ^{1}H NMR.

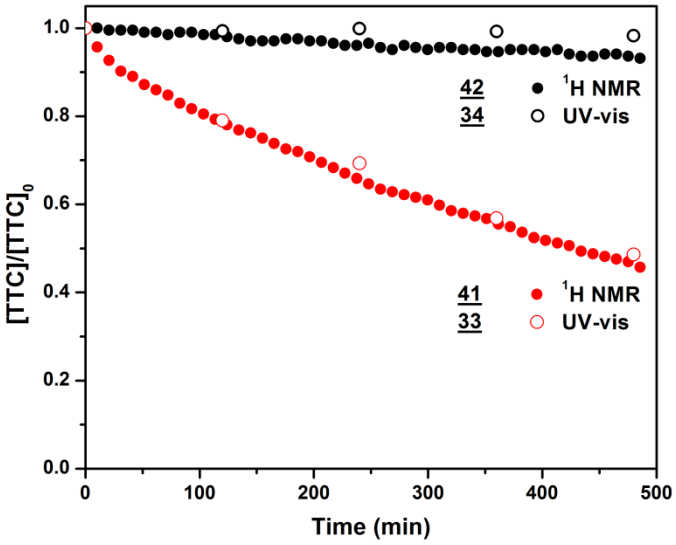

Figure 4.19. Time-dependent change in $[TTC]/[TTC]_0$ at 70 °C in DMF as measured by UV-vis spectroscopy during polymerization (open circles) and as measured by *in situ* ^{1}H NMR during SMUI adduct degradation analysis (closed circles).

It is important to note that while we have determined that significant trithiocarbonate degradation occurs by N-5 cyclization/elimination during the RAFT polymerization of **33** at 70 °C, this work does not specifically address the influence of N-phenyl substitution on increased amide nucleophilicity and how this affects the observed reaction mechanism. We are currently examining the influences of N-aryl substitution on both reaction mechanism and rate of N-5 cyclization/elimination and will report this in a future manuscript.

*Influence of 3-phenyl-2-thioxothiazolidin-4-one Chain Ends on the RAFT Polymerization of **33***

Typically, RAFT agent degradation during polymerization results in the loss of active thiocabonylthio chain ends affording "dead" polymer chains that can no longer participate in the RAFT process. However, we have shown that trithiocarbonate degradation by N-5 cyclization/elimination during the polymerization **33** results in

formation of a new cyclic thiocarbonylthio end group. To date, there are few examples of RAFT polymerizations mediated by cyclic thiocarbonylthio compounds.[281–283] However, Zhan and coworkers recently reported the RAFT polymerization of vinyl acetate using **40** as the RAFT agent, which resulted in incorporation of thiocarbonylthio functionality into the polymer backbone.[227] Similarly, it is plausible that the 3-phenyl-2-thioxothiazolidin-4-one chain ends formed as a result of N-5 cyclization/elimination could participate during the RAFT polymerization of **33** as shown in Scheme 4.8.

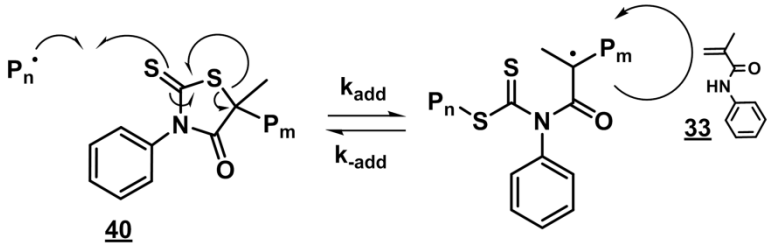

Scheme 4.8. Proposed mechanism for radical addition to 3-phenyl-2-thioxothiazolidin-4-one chain ends during RAFT polymerization of **33** at 70 °C.

We investigated the possibility of 3-phenyl-2-thioxothiazolidin-4-one chain ends participating in the RAFT process by conducting the polymerization of **33** at 70 °C in the presence of **40**, a small molecule analogue of N-5 cyclized poly(N-phenylmethacrylamide) chain ends. Figure 4.20a shows the kinetic plot for the **40**-mediated polymerization of **33** in DMF at 70 °C. Linear pseudo-first-order kinetic behavior was observed up to 140 min with no initialization period. By contrast, the **37**-mediated polymerization of **33** under identical conditions exhibited a 30 min initialization period, consistent with similar results first reported by Klumperman and coworkers.[106] While the linear pseudo-first-order kinetic behavior indicates a constant $k_p[P_n\cdot]$, the SEC RI overlay shown in Figure 4.20b demonstrates that molecular weight control is not achieved during the **40**-mediated polymerization of **33** at 70 °C. The intensities of the

SEC RI chromatograms shown in Figure 4.20b increase with conversion but the unchanging peak elution volumes, which occur at the exclusion limit of the SEC system (~11.0 mL), are representative of uncontrolled polymerization behavior where M_n does not scale linearly with monomer conversion. While the polymers presented in Figure 4.20b were too large to characterize by our SEC-MALLS system, it is worth noting that a polyvinylpyridine standard of M_n = 475,000 g/mol (M_w/M_n = 1.06) elutes at a volume of 11.5 mL. These results suggest that 3-phenyl-2-thioxothiazolidin-4-one-terminated polymers do not participate in the normal CTA-mediated RAFT polymerization of **33** at 70 °C.

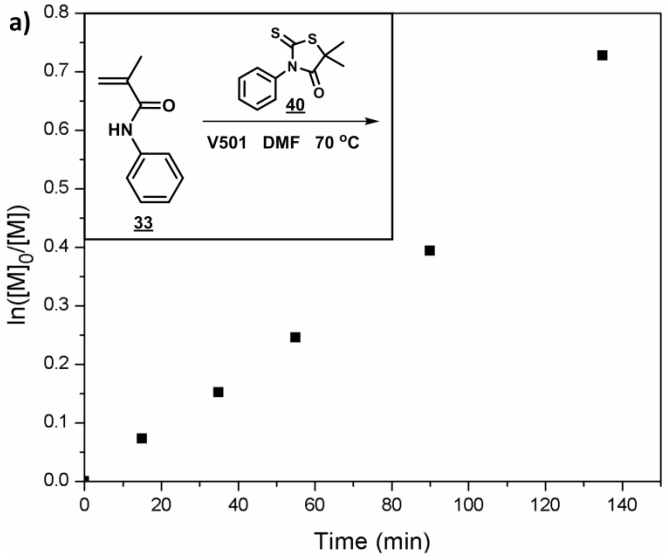

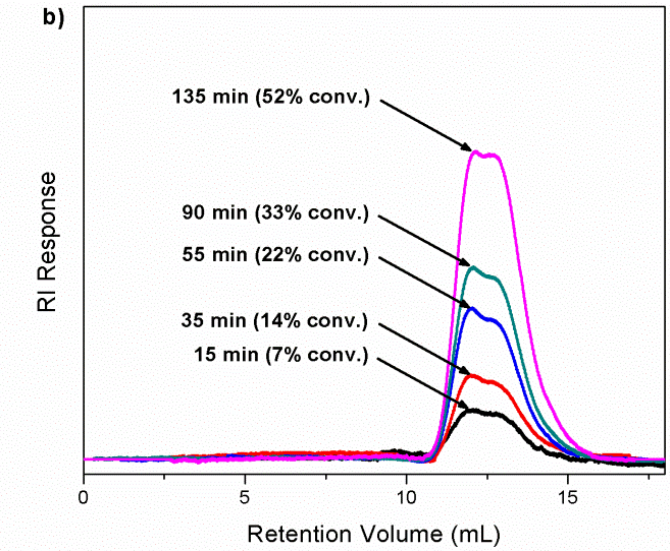

Figure 4.20. (a) Kinetic plot and (b) SEC RI chromatogram overlay for the **40**-mediated polymerization of **33** in DMF at 70 °C ([**33**]$_0$ = 2.0 M, [**33**]$_0$:[**40**]$_0$:[V501]$_0$ = 200:1.0:0.2).

Section 3. "One-Pot" Aminolysis/Thiol-Maleimide End Group Functionalization of RAFT Polymers: Identifying and Preventing Michael Addition Side Reactions

Overview

Reversible addition-fragmentation chain transfer (RAFT) polymerization has made possible the synthesis of functionally-diverse polymers with predetermined molecular weights and low dispersities (Đ) using a wide variety of monomer types and polymerization conditions (e.g. aqueous and organic media).[89,284,285] The versatility of RAFT in synthesizing tailor-made polymers also stems from the fidelity by which polymer end-functionality can be controlled. Such end-functionalized polymers have been used to prepare advanced macromolecular architectures including block copolymers,[286] star copolymers,[287] molecular brushes,[202,213] and polymer bioconjugates.[172,288] Telechelic RAFT polymers can be synthesized directly by controlling the RAFT agent R- and Z-group functionality[263] or by post-polymerization end group modification.[289–291] The latter approach often exploits the inherent reactivity of

the residual thiocarbonylthio moiety present on RAFT polymers, allowing for simultaneous removal and replacement of the unstable RAFT agent with a benign or functional end group.

In recent years, reduction or aminolysis of thiocarbonylthio-terminated RAFT polymers to the corresponding polymeric thiol has afforded a myriad of thiol "click" end group functionalization routes including thiol-isocyanate,[292] thiol-epoxy,[293] thiol-halogen,[294] thiol-disulfide,[295,296] and thiol-ene reactions.[257,258,262,297–299] Particularly advantageous are thiol-maleimide Michael addition reactions which proceed to near quantitative conversions at room temperature in the presence of oxygen and water and typically occur much more rapidly than analogous thiol-acrylate or thiol-acrylamide reactions.[260,300–305] Furthermore, thiol-maleimide end group modification of RAFT polymers can be performed as "one-pot" reactions without isolation of the intermediate polymeric thiol (Scheme 4.9).

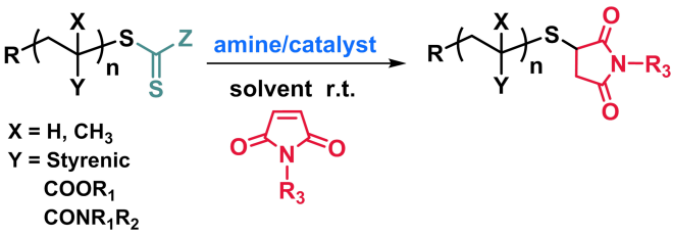

Scheme 4.9. "One-pot" aminolysis/thiol-maleimide end group functionalization of RAFT polymers.

To ensure quantitative polymer end group functionalization, an excess of maleimide relative to polymeric thiol is required. It is therefore desirable to optimize the reaction conditions to favor rapid and efficient polymer conjugation with minimal excess of maleimide, especially when using costly biologic, therapeutic, or diagnostic agents. One potential way to maximize end group functionalization efficiency while minimizing

the required excess of maleimide is through the use of nucleophilic catalysts. Thiol-Michael addition reactions typically employ a base catalyst (e.g. tertiary amine) to generate the nucleophilic thiolate species.[305] However, nucleophilic catalysts such as phosphines, amines, and amidines have been used to initiate Michael addition reactions and can increase reaction rates of these reactions by several orders of magnitude compared to analogous base-catalyzed reactions.[300,306–312] The proposed mechanism of nucleophile-initiated thiol-maleimide Michael addition is illustrated in Scheme 4.10.[312] Rather than direct deprotonation of thiol, conjugate addition of the nucleophile to the maleimide double bond **60** forms the zwitterionic enolate **61**, which in turn functions as a strong base ($pK_a \approx 25$) capable of generating the nucleophilic thiolate species while also forming a nucleophile-succinimide byproduct **62**. In this regard, the nucleophile does not function as a catalyst which would be regenerated during each catalytic cycle, but rather serves as an initiator that generates the steady state enolate/thiolate concentration necessary for the thiol-ene chain transfer mechanism to operate. Subsequent propagation occurs by thiolate addition to maleimide forming the corresponding enolate **63**, which abstracts a proton from thiol, regenerating the thiolate along with the desired thiol-maleimide Michael addition product **64**.

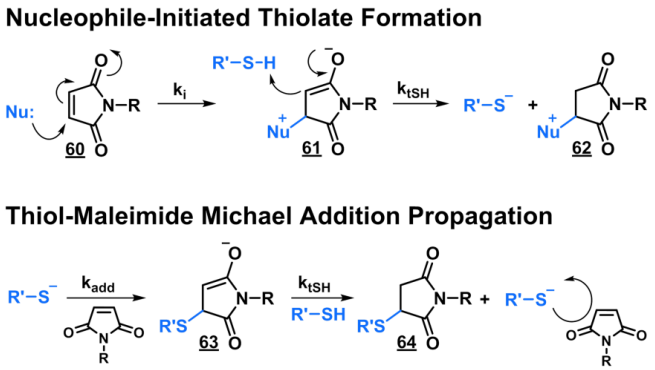

Scheme 4.10. Mechanism of nucleophile-initiated thiol-maleimide Michael addition.

Recently, while investigating the use of nucleophilic initiators to improve the efficiency of RAFT polymer end group functionalization with N-substituted maleimides, we discovered that in certain instances, nucleophilic initiators *reduced* the degree of end group functionalization compared to reactions performed using only a base catalyst. Reagent order of addition and solvent-type were also determined to have marked effects on end group functionalization efficiency (vide infra). These observations have prompted this study aimed at understanding the influences of nucleophile type, solvent, and reaction conditions on the efficacy of "one-pot" aminolysis/thiol-maleimide end group functionalization of RAFT polymers. Furthermore, the results discussed herein offer mechanistic insights into potentially detrimental side reactions that can occur during thiol-maleimide Michael addition reactions.

Nucleophile-Promoted Michael Addition Side Reactions

Preliminary efforts in our lab to catalyze the "one-pot" aminolysis/thiol-maleimide end group modification of acrylamido RAFT polymers in DMSO using the amidine 1,8-diazabicyclo[5.4.0]undec-7-ene (DBU) resulted in i) low end group functionalization efficiencies compared to reactions performed in the absence of DBU, ii) quantitative maleimide consumption, and iii) the formation of high molecular weight impurities observable by SEC-MALLS. From these observations we hypothesize that a low polymeric thiol concentration relative to maleimide concentration in the presence of a strong nucleophile (DBU), results in anionic propagation of maleimide occuring faster than the desired thiol-maleimide Michael addition. It is also possible that other nucleophiles (e.g. amines and phosphines) commonly used during "one-pot" aminolysis/thiol-maleimide modification of RAFT polymers could promote similar side

reactions. Azechi et al. showed that 1°, 2°, and 3° amines can initiate the anionic polymerization of N-substituted maleimides in highly polar aprotic solvents (DMSO and DMF) whereas no polymerization was observed in less polar solvents (THF).[313] Also, phosphines have been used as initiators for the anionic polymerizations of methylene malonic esters,[314] cyanoacrylates,[315] and N-substituted maleimides.[316] It is therefore plausible that during "one-pot" aminolysis/thiol-maleimide modification of RAFT polymers, amine- and phosphine-initiated polymerization of maleimide could also outcompete the desired thiol-maleimide Michael reaction and account for the poor end group functionalization efficiencies observed under certain reaction conditions.

Reaction of N- and P-Based Nucleophiles with N-Methylmaleimide

A number of nucleophile types including amines (aminolysis), phosphines (reducing agent), and amidines (nucleophilic initiator) can be present during "one-pot" aminolysis/thiol-maleimide end group reactions of RAFT polymers. Accordingly, we chose to first investigate the effect of solvent on the reactions of representative N- and P-based nucleophiles with N-methylmaleimide (**65**) in the absence of thiol as outlined in Figure 4.21. A stoichiometric excess of maleimide relative to nucleophile ($[Nu]_0$:$[Mal]_0$ = 1.0:10) was chosen to reflect the relative concentrations of these reagents used during "one-pot" RAFT polymer aminolysis/thiol-maleimide reactions and to make apparent whether or not maleimide polymerization is occurring. *In situ* ^{1}H NMR analysis was used to monitor the time-dependent fractional change in maleimide concentration ($[Mal]/[Mal]_0$) by comparing the area of the maleimide olefin peak to the peak area of an internal standard (CH_2Cl_2).

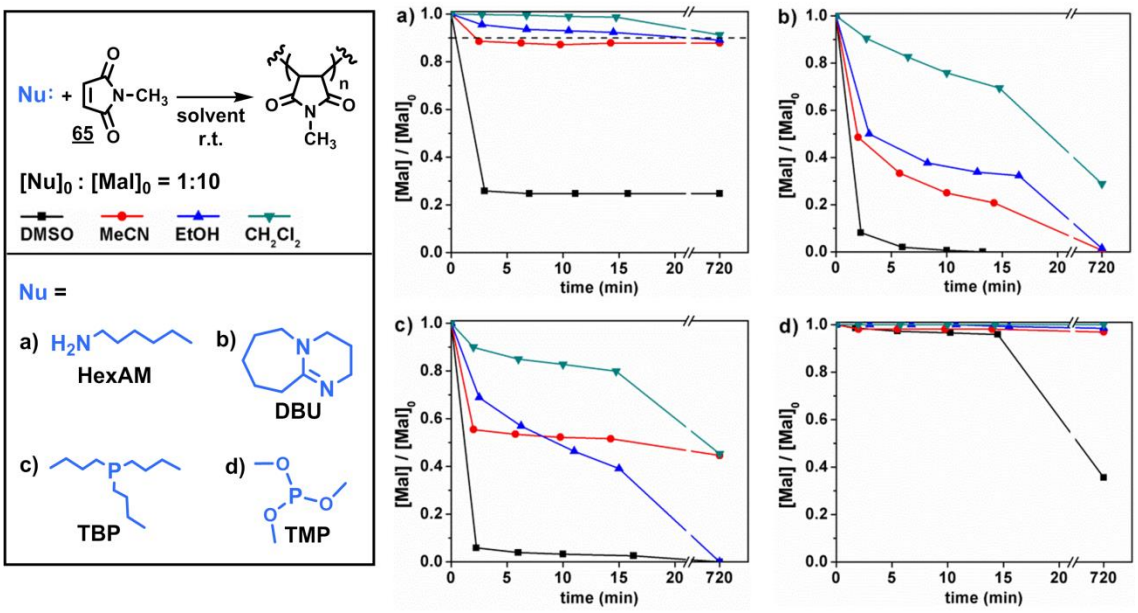

Figure 4.21. Effect of solvent on the time-dependent fractional change in $[Mal]/[Mal]_0$ upon reaction of **65** with representative nucleophiles a) hexylamine (HexAM), b) 1,8-diazabicyclo[5.4.0]undec-7-ene (DBU), c) tributylphosphine (TBP), and d) trimethylphosphite (TMP) as measured by *in situ* ^{1}H NMR analysis.

Figure 4.21a shows the time-dependent $[Mal]/[Mal]_0$ plots for the reactions of hexylamine (HexAM) with **65** in different solvents with the dashed line ($[Mal]/[Mal]_0$ = 0.9) representing the theoretical decrease in $[Mal]/[Mal]_0$ predicted for the reaction of HexAM and **65** via single aza-Michael addition. Reactions conducted in MeCN, EtOH, and CH_2Cl_2 show decreases in $[Mal]/[Mal]_0$ to a value of 0.9, beyond which no change in $[Mal]/[Mal]_0$ is observed up to 12 h, indicating exclusive aza-Michael addition takes place in these solvents. Conversely, reaction of HexAM with **65** in DMSO results in rapid maleimide consumption, corresponding to 7.5 maleimides consumed on average per amine within the first 3 min. Subsequently, no change in $[Mal]/[Mal]_0$ is observed up to 12 h. These results are consistent with those reported by Azechi et al.[313] and confirm that HexAM can initiate the anionic polymerization of **65** in polar solvents such as DMSO whereas exclusive aza-Michael addition takes place in less polar solvents. Furthermore,

the effect of solvent polarity on the reaction of HexAM with **65** is readily observed in Figure 4.21a by noting the increase in reaction rate with increasing solvent polarity in the order of CH_2Cl_2 ($\varepsilon = 8.93$) < EtOH ($\varepsilon = 24.5$) < MeCN ($\varepsilon = 37.5$) < DMSO ($\varepsilon = 46.7$).

The time-dependent $[Mal]/[Mal]_0$ plots for the reactions of DBU and **65** are shown in Figure 4.21b. Reaction rate increases with increasing solvent polarity with 100 % **65** conversion reached in < 10 min in DMSO. Quantitative consumption of **65** was also observed for reactions performed in EtOH and MeCN while 71% maleimide conversion was measured in CH_2Cl_2 after 12 h. Interestingly, the kinetic plots in Figure 4.21b do not rapidly reach a constant value of $[Mal]/[Mal]_0$ as was observed during the reaction of HexAM and **65** in Figure 4.21a. Unlike protic nucleophiles (e.g. 1°, 2° amines, and thiols), aprotic nucleophiles such as DBU cannot undergo complete Michael addition due to the lack of a transferable hydrogen from the nucleophile. Therefore, if an active hydrogen-containing compound (e.g. thiol) is in low concentration or completely absent, the nucleophile-derived zwitterionic enolate **61** can undergo reaction with additional maleimide without enolate termination by proton transfer, allowing for a "living-like" polymerization process to occur. Noteworthy is that precipitation was observed during the reaction of DBU and **65** in CH_2Cl_2 after ~30 min. Limited solubility of the propagating macro zwitterionic enolate in CH_2Cl_2 likely prevents the propagating chain-end from reacting with **65** in solution, accounting for the non-quantitative maleimide conversion obtained in this solvent. Nonetheless, these results indicate that DBU-initiated polymerization of **65** occurs rapidly and extensively in both polar and nonpolar solvents.

Similarly, the aprotic nucleophile tributylphosphine (TBP) was shown to initiate polymerization of **65** in all solvents tested (Figure 4.21c). Reaction rates increase with solvent polarity with 95% maleimide conversion reached within 2.5 min in DMSO. Precipitation was also observed during reactions performed in EtOH and CH_2Cl_2 after ~5 min following the addition of TBP. Poor solubility of the propagating phosphonium zwitterionic enolate is again a likely explanation for the non-quantitative maleimide conversions achieved in EtOH and CH_2Cl_2 during the time frame of these kinetic experiments.

From these results it is apparent that maleimide polymerization initiated by DBU or TBP is unavoidable, even in low polarity solvents. While DBU is optional during "one-pot" aminolysis/thiol-maleimide modification of RAFT polymers, mild reducing agents such as phosphines are generally required to prevent disulfide formation from occurring between polymeric thiols during the RAFT agent aminolysis step.[258,301] Initially, we explored triphenylphoshine as a more sterically hindered, and therefore less nucleophilic phosphine, but maleimide polymerization was again observed in each of the four solvents tested in this work (data not shown). Recently, Ho et al. reported on trialkylphosphites as cheaper and less toxic alternatives to trialkylphosphines as reducing agents during "one-pot" RAFT polymer aminolysis/thiol-ene reactions.[317] Trialkylphosphites can undergo conjugate addition to electron deficient olefins but are less nucleophilic than phosphines and typically require elevated temperatures (100 °C) for reaction to take place.[318,319] As seen in Figure 4.21d, the reaction of trimethylphosphite (TMP) with **65** results in no measureable change in $[Mal]/[Mal]_0$ in MeCN, EtOH, and CH_2Cl_2. Only after prolonged reaction times (12 h) in DMSO is a 65

% decrease in [Mal]/[Mal]$_0$ observed. Consequently, TMP is a suitable alternative to phosphines as a reducing agent during thiol-maleimide reactions when used in less polar solvents. It should also be noted that trace amounts of water must be present for trialkylphosphite (and phosphine) reduction of disulfides to occur.[320] Therefore, rigorous anhydrous conditions should be avoided during RAFT polymer aminolysis when using trialkylphosphites as reducing agents.

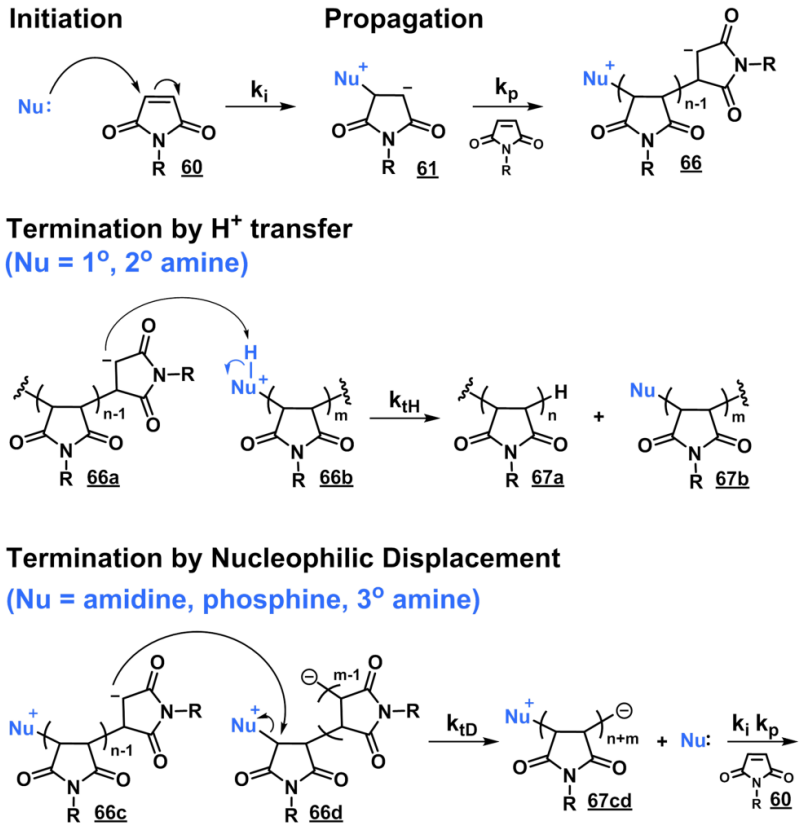

Scheme 4.11. Proposed mechanisms of initiation, propagation, and termination for the nucleophile-initiated anionic polymerization of N-substituted maleimides.

The proposed mechanisms of initiation, propagation, and termination for the anionic polymerization of N-substituted maleimides initiated by protic or aprotic nucleophiles are illustrated in Scheme 4.11. Conjugate addition of the nucleophile to the maleimide double bond to form the zwitterionic enolate **61** in identical fashion to first

step of nucleophile-initiated thiol-maleimide reactions. However, if the thiol concentration is suitably low relative to maleimde concentration ([Mal] > [thiol]), propagation can occur faster than proton transfer to the enolate **61**, resulting in the formation of the propagating macrozwitterionic species **66**. For maleimide polymerization initiated by protic nucleophiles (e.g. 1° or 2° amines), termination can occur by proton transfer from the nucleophile to afford a terminated chain **67a**. Conversely, aprotic nucleophiles do not posess a transferable proton and consequently can not under go "long range" Michael addition. However, termination by nucleophilic displacement of the positively charged nucleophilic residue (**66d**) by the enolate terminus of an adjacent chain (**66c**) could result in regeneration of the nucleophile while also producing a new macrozwitterionic polymer chain (**67cd**) equal in mass to the sum of **66c** and **66d**. These differences in termination mechanisms adequately describe the continued decrease in $[Mal]/[Mal]_0$ observed during reaction of aprotic nucleophiles with **65** whereas reaction of a protic nucleophile (HexAM) rapidly reach a constant value of $[Mal]/[Mal]_0$ owing to termination by proton transfer. Additional evidence of termination by nucleophilic displacement was also obtained by noting that the solution viscosity of the reaction of **65** with DBU continues to increase for several days after complete maleimide consumption, eventually leading to complete vitrification. This continued increase in solution viscosity would be expected if the macrozwitterions formed from the reaction of DBU and **65** were functioning as macro A-B monomers capable of continued step-growth polymerization resulting in a continued increase in molecular weight.

*Reaction of Thiols with N-Methylmaleimide (**65**)*

It is evident from the kinetic plots shown in Figure 4.21 that strong N- and P-based nucleophiles can react with maleimides to form either the Michael addition product or polymaleimide depending upon the nucleophile type (protic or aprotic) and solvent polarity. Therefore, it is plausible that other strong nucleophiles such as thiolates can initiate the anionic polymerization of maleimides in polar solvents. To this end, we chose to investigate the reaction of ethyl 2-mercaptopropionate (E2MP) with **65** under conditions identical to those outlined in Figure 4.21, except with the addition of TEA to generate the nucleophilic thiolate species. E2MP was chosen as a model thiol due to its structural similarity to the polymeric thiol that would be produced upon aminolysis of a polyacrylate RAFT polymer.

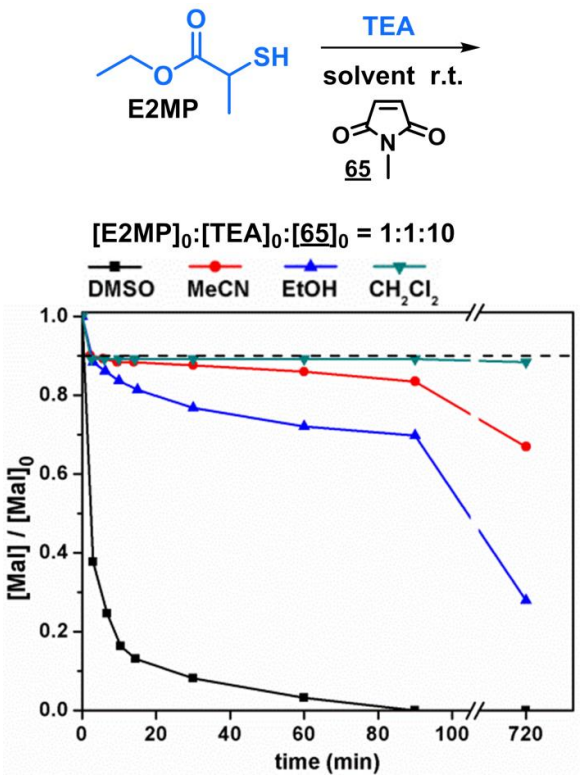

Figure 4.22. Effect of solvent on the time-dependent fractional change in [Mal]/[Mal]$_0$ during the TEA-catalyzed reaction of E2MP with **65** as measured by *in situ* ^{1}H NMR analysis.

As shown in Figure 4.22, only the reaction of E2MP and **65** in CH_2Cl_2 gives the change in [Mal]/[Mal]$_0$ expected for exclusive thiol-maleimide Michael addition ([Mal]/[Mal]$_0$ = 0.9, dashed line). Meanwhile, the reactions conducted in more polar solvents (DMSO, EtOH, and MeCN) show a continued decrease in [Mal]/[Mal]$_0$ up to 12 h, with 100% maleimide conversion reached in 90 min in DMSO. Initially, we anticipated the kinetic profiles for the reactions of E2MP and **65** (Figure 4.22) to rapidly reach a constant [Mal]/[Mal]$_0$ value due to rapid enolate termination by means of proton transfer, as previously observed for the reactions of HexAM and **65** (Figure 4.21a). However, a continued decrease in [Mal]/[Mal]$_0$ up to 12 h is evidence of either slow reaction of thiol or an additional reaction pathway.

Closer inspection of the kinetic profiles for reactions conducted in EtOH and MeCN reveals an inflection point at the first time point (2.5 min) when [Mal]/[Mal]$_0$ ≈ 0.9, indicating that thiol-maleimide Michael addition likely occurs faster than subsequent maleimide propagation in these solvents. Furthermore, *in situ* ^{1}H NMR indicated 100% thiol conversion prior to the first time point (2.5 min) for reactions conducted in DMSO, MeCN, and CH_2Cl_2 (Figures A9-A11, Appendix A) whereas thiol conversion could not be measured for the reaction performed in EtOH-d_6 due to deuterium exchange between the solvent and thiol proton. Quantitative thiol consumption early in each reaction requires that proton transfer from thiol to enolate also occurs rapidly. Therefore, the continued decrease in [Mal]/[Mal]$_0$ observed at longer reaction times in more polar solvents is not likely attributable to slow reaction of thiol and is suggestive of an alternate maleimide reaction pathway.

One plausible explanation for the continued decrease in $[Mal]/[Mal]_0$ at longer reaction times is TEA-initiated maleimide polymerization. The time-dependent change in $[Mal]/[Mal]_0$ plots (Figure A12, Appendix A) for the reactions of TEA with **65** in DMSO and EtOH show a decrease in $[Mal]/[Mal]_0$ of 0.07 and 0.04 respectively after 12 h. Meanwhile, no change in $[Mal]/[Mal]_0$ was observed in MeCN and CH_2Cl_2 after 12 h. Accordingly, TEA-initiated maleimide polymerization is insufficient to account for the significant decrease in $[Mal]/[Mal]_0$ that occurs within the same time period during the reactions of E2MP with **65** in these solvents.

Another potential explanation for the continued decrease in $[Mal]/[Mal]_0$ observed in the kinetic plots of Figure 4.22 involves deprotonation of the thiol-maleimide Michael adduct by TEA to regenerate the nucleophilic enolate species. Initially, this seems unlikely since the pK_a of TEA (10.75) is much lower than that of most succinimide-derived enolates (~25). However, enolate formation of 2-aminosuccinimide residues in peptides has been shown to occur under mildly basic conditions in aqueous media (pH = 7.4), indicating that heteroatom-substitution of the succinimide α-carbon can reduce enolate pK_a compared to unsubstituted succinimides.[321]

To test whether thiol-maleimide Michael addition products are capable of reinitiating maleimide polymerization in the presence of TEA, the Michael adduct of benzyl mercaptan and N-methylmaleimide (**43**) was synthesized and purified by column chromatography. The Michael adduct of E2MP and **65** was not synthesized due to potential complications arising from the presence of chemically distinct diastereomers and the complexity in identifying the ^{1}H NMR chemical shifts of the resulting four

stereoisomers. Meanwhile, the synthesis of **43** from benzyl mercaptan and **65** affords a racemic mixture of chemically indistinct enantiomers.

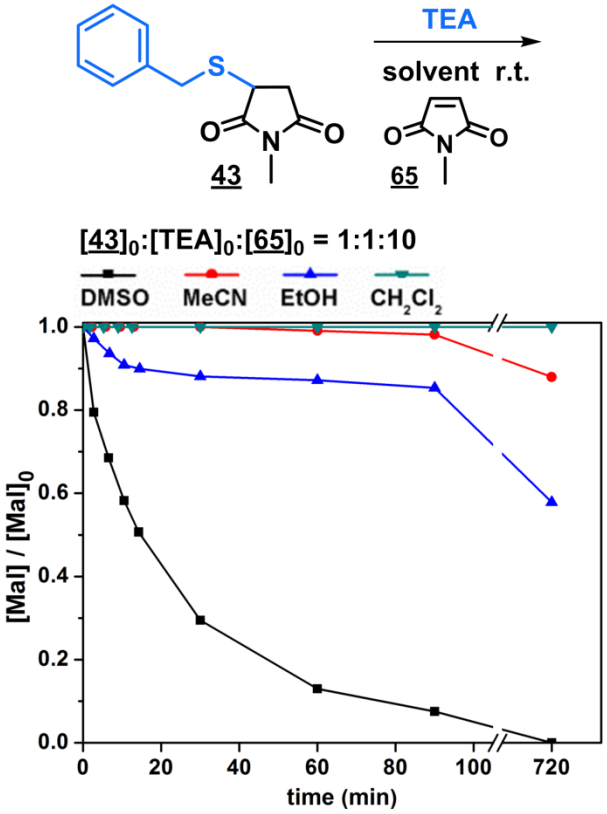

Figure 4.23. Effect of solvent on the time-dependent fractional change in $[Mal]/[Mal]_0$ during the TEA-catalyzed reaction of **43** with **65** as measured by *in situ* ^{1}H NMR analysis.

Figure 4.23 shows that $[Mal]/[Mal]_0$ decreases with time during the TEA-catalyzed reactions of **43** and **65** in DMSO, EtOH, and MeCN whereas no change in $[Mal]/[Mal]_0$ is observed in CH_2Cl_2 up to 12 h. The kinetic profiles obtained in each solvent for the reactions of **43** and **65** in Figure 4.23 accurately reflect the kinetic profiles observed below $[Mal]/[Mal]_0 = 0.9$ (dashed line) for the analogous reactions of E2MP and **65** shown in Figure 4.22. This is not a surprising result since the dashed line in Figure 4.22 represents the change in $[Mal]/[Mal]_0$ predicted for formation of the thiol-maleimide Michael adduct. Any decrease in $[Mal]/[Ma]_0$ below a value of 0.9 in Figure

4.22 would presumably occur as a result of TEA-promoted regeneration of the nucleophilic enolate species and therefore resemble the kinetic profiles in Figure 4.23.

Also worth noting is that TEA has little influence on the time-dependent $[Mal]/[Mal]_0$ plots for the reaction of HexAM and **65** in DMSO as shown in Figure A13 in Appendix A. This indicates that the amine-maleimide adduct is not capable of reinitiation of maleimide polymerization under these reaction conditions and that reinitiation is likely unique to thiol-maleimide adducts.

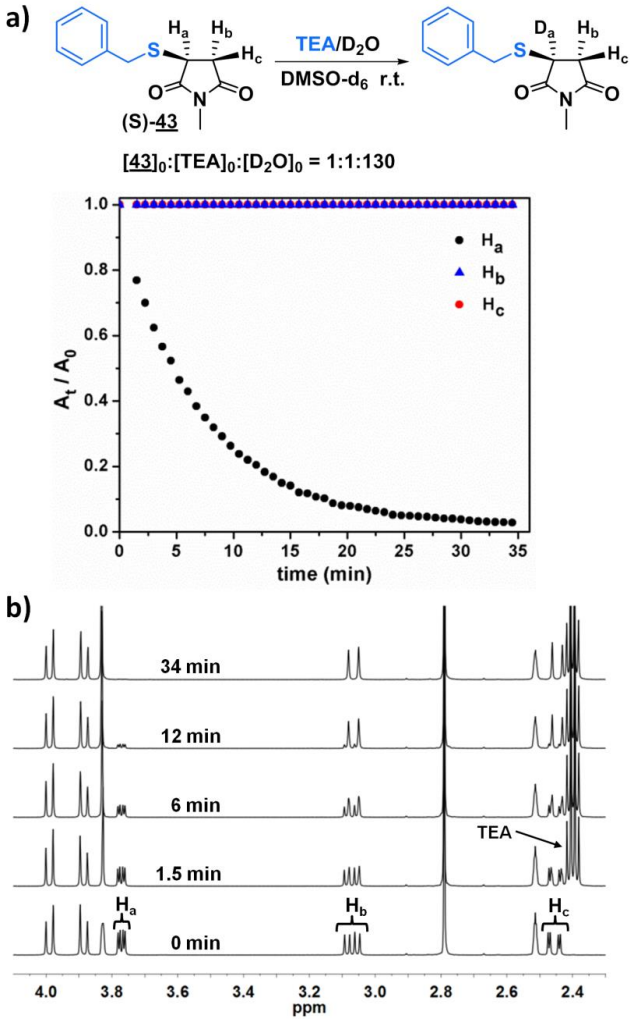

Figure 4.24. a) Time-dependent fractional change in peak area (A_t/A_0) for protons H_a, H_b, and H_c during TEA-catalyzed H-D exchange of **43** in DMSO. b) ^{1}H NMR spectral overlay of select time points during H-D exchange experiments with **43**.

We next sought to provide direct evidence that TEA is a strong enough base to generate the enolate of **43** in polar solvents. To this end, we used *in situ* ^{1}H NMR analysis to measure the relative rates of hydrogen-deuterium exchange (H-D) of **43** in a DMSO/D_2O mixture in the presence of TEA. Figure 4.24a shows the time-dependent fractional change in peak area (A_t/A_0) for the three chemically distinct protons of **43** which could be abstracted by TEA to form an enolate on either the α-carbon (H_a) or the β-carbon (H_b and H_c) relative to the benzylsulfanyl group. For simplicity, only the structure of the S enantiomer is shown in Figure 4.24a, whereas **43** is actually comprised of a racemic mixture of enantiomers. The kinetic plot of Figure 4.24a reveals that H-D exchange was only observed for proton H_a with a 97% decrease in A_t/A_0 occurring by 35 min. Sigma withdrawing effects by the adjacent thioether are most likely responsible for the increased acidity of H_a, leading to exclusive enolate formation at the α-carbon. Figure 4.24b shows the ^{1}H NMR spectral overlay of select time points during the H-D exchange experiments with **43**. The peak corresponding to H_a decreases in area with time while maintaining the doublet of doublets (dd) splitting pattern that arises from spin-spin coupling with H_b and H_c. Meanwhile, the peaks corresponding to the geminal protons H_b and H_c do not change in area, but rather show changes in splitting pattern from dd to d as spin-spin coupling of H_b and H_c with H_a are diminished through deuterium exchange. Also apparent in Figure 4.24b is the significant downfield chemical shift of H_a (3.78 ppm) relative to H_b (3.07 ppm) and H_c (2.46 ppm) that arises from the deshielding (sigma withdrawing) effects of the benzylsulfanyl group.

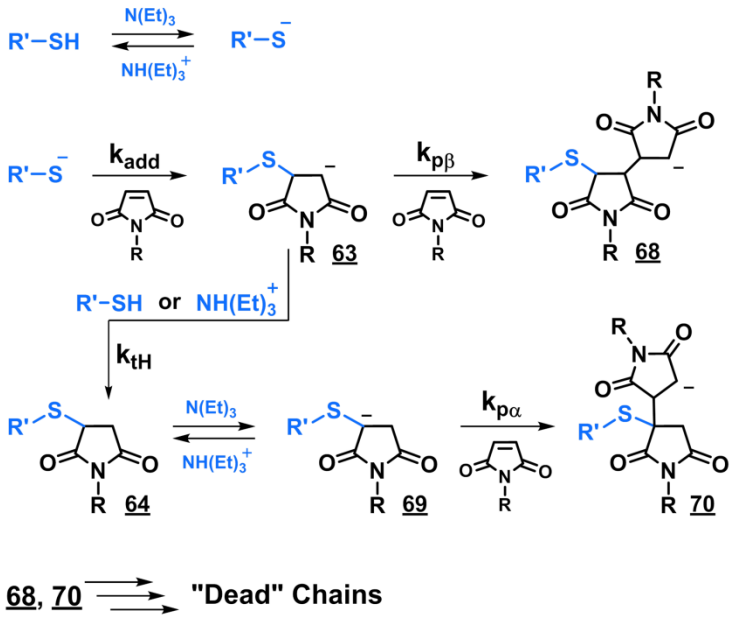

Scheme 4.12. Proposed reaction pathways for the TEA-catalyzed thiol-maleimide reaction in which reversible enolate formation is operational.

Scheme 4.12 shows the proposed reaction pathways for the TEA-catalyzed thiol-maleimide reaction when a stoichiometric excess of maleimide relative to thiol is employed in polar solvents. Thiolate addition to maleimide forms the β-enolate **63** which can either abstract a proton from thiol or $^{+}NH(Et)_3$ to give the thiol-maleimide adduct **64**, or react directly with maleimide to form the propagating species **68** when conditions favor propagation over termination (i.e. [Mal]>>[thiol]). Deprotonation of **64** by TEA forms the α-enolate **69** which can reversibly terminate by proton transfer or react with maleimide to form the propagating species **70**. The propagating species **68** and **70** derived from β- and α-enolates respectively can continue to react with maleimide until termination occurs by proton transfer. Also, the termination products of **68** can in theory reinitiate maleimide polymerization by α-enolate formation. These additional reaction pathways can account for the continued decrease in $[Mal]/[Mal]_0$ following initial formation of the thiol-maleimide Michael adduct for the TEA-catalyzed reactions of

E2MP with **65** shown in Figures 4.23. It should also be noted that exclusive enolate formation at the α-carbon rules out the possibility of TEA-catalyzed β-elimination (retro Michael addition) as a means of regenerating the nucleophilic thiolate species after formation of the thiol-maleimide Michael adduct.

"One-pot" Aminolysis/Thiol-Maleimide End Group Functionalization of RAFT Polymers

It is apparent that many of the reagents (e.g. amines and phosphines) commonly used during "one-pot" RAFT polymer aminolysis/thiol-maleimide reactions can react with maleimides to form polymaleimide or Michael addition byproducts and potentially outcompete the desired polymeric thiol-maleimide Michael reaction. Also, we have shown that intermediate strength bases such as TEA can deprotonate thiol-maleimide Michael adducts in polar solvents to form a nucleophilic α-enolate capable of subsequent reaction with maleimide. However, the effects of these side reactions on RAFT polymer end group functionalization efficiency are not yet well understood. Also not well understood is the influence of aminolysis method on end group functionalization efficiency. The simplest method involves simultaneous aminolysis of the RAFT polymer in the presence of maleimide and does not require the use of a reducing agent to prevent disulfide formation. However, the competing amine-maleimide aza-Michael addition could prevent quantitative RAFT agent aminolysis and subsequently reduce the degree of end group functionalization. Alternatively, the sequential method allows for complete aminolysis of the RAFT agent to occur prior to the addition of maleimide in a second step. This route limits side reactions between the amine and maleimide but necessitates

the use of a reducing agent to prevent polymeric disulfide formation from occurring during the aminolysis stage.

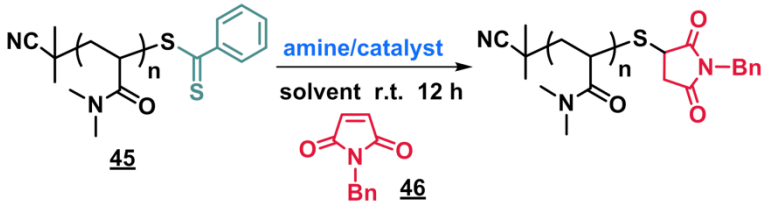

Scheme 4.13. "One-pot" aminolysis/thiol-maleimide modification of **45** with **46**.

To investigate the effects of solvent, catalyst, reducing agent, and aminolysis method on RAFT polymer end group functionalization efficiency, we first synthesized the water soluble polymer poly(N,N-dimethylacrylamide) (**45**) using the RAFT agent 2-cyano-2-propyl benzodithioate (**44**). Low dispersities (Đ = 1.06) and excellent agreement between the number average molecular weights determined by size exclusion chromatography (M_n(SEC) = 3360 g/mol) and by ^{1}H NMR (M_n(NMR) = 3220 g/mol) are evident of a controlled polymerization and high dithiobenzoate chain-end fidelity. "One-pot" reactions of **45** with N-benzylmaleimide (**46**) were conducted at room temperature for 12 h using the initial molar ratios of [**45**]$_0$:[HexAM]$_0$:[**46**]$_0$ = 1.0:2.5:5.0 as outlined in Scheme 4.13. End group analysis by ^{1}H NMR was performed in D_2O by comparing the integrated peak area of the benzyl aromatic protons (7.50 – 7.15 ppm) to the known integrated peak area of the N,N-dimethyl side chain and methyne backbone protons (3.30 – 2.20 ppm) of **45** (Figures A14-A15, Appendix A). The poor solubility of **46** and its nucleophile-initiated byproducts (i.e. poly(**46**)) in D_2O allows for accurate quantification of only **46** that is covalently attached to **45**.

Table 4.5

*"One-pot" aminolysis/thiol-maleimide reactions of **45** with **46**.*[a]

entry	method[b]	solvent	catalyst/ red agent	funct.[e] (%)	CTA[f] (%)	color[g] (12 h)
1a	1	CH_2Cl_2	DBU[c]	93	0	R
1b	1	MeCN	DBU	37	0	R
1c	1	EtOH	DBU	25	15	R
1d	1	DMSO	DBU	0	0	R
2a	1	CH_2Cl_2	-	89	0	Y
2b	1	MeCN	-	81	3	O
2c	1	EtOH	-	8	90	O
2d	1	DMSO	-	31	46	R
3a	2	CH_2Cl_2	-	95	0	Y
3b	2	MeCN	-	95	0	R
3c	2	EtOH	-	84	0	Y
3d	2	DMSO	-	72	0	R
4a	2	CH_2Cl_2	TBP[d]	89	0	R
4b	2	MeCN	TBP	86	0	R
4c	2	EtOH	TBP	84	0	R
4d	2	DMSO	TBP	72	0	R
5a	2	CH_2Cl_2	TMP[d]	98	0	Y
5b	2	MeCN	TMP	99	0	Y
5c	2	EtOH	TMP	86	0	Y
5d	2	DMSO	TMP	89	0	Y

[a]$[\mathbf{45}]_0$:$[HexAM]_0$:$[\mathbf{46}]_0$ = 1.0:2.5:5.0. [b]Method 1: simultaneous aminolysis/thiol-maleimide; Method 2: sequential aminolysis/thiol-maleimide. [c]$[\mathbf{45}]_0$:$[DBU]_0$ = 1.0:1.0. [d]$[\mathbf{45}]_0$:[TBP or TMP]$_0$ = 1.0:5.0. [e]Percent end group functionalization of **45** with **46** as measured by ^{1}H NMR. [f]Percent CTA remaining after reaction of **45** with **46** as measured by ^{1}H NMR. [g]Reaction color after 12 h: red (R), orange (O), or yellow (Y).

Table 4.5 summarizes the results of the "one-pot" aminolysis/thiol-maleimide reactions of **45** with **46** with the last column indicating the color exhibited by each reaction after 12 h. Entries 1a-d reflect our initial attempts to catalyze thiol-maleimide end group functionalization reactions with DBU as a catalyst and were performed using the simultaneous aminolysis method (method 1). A distinct trend of decreasing end group functionalization efficiency with increasing solvent polarity was observed with 0% functionalization achieved in DMSO. These results are relatable to the trend observed for the reactions of DBU and **65** shown in Figure 4.21b, where the rate of DBU-initiated maleimide polymerization increases with solvent polarity. From these results, we conclude that in polar solvents, DBU-initiated maleimide polymerization is outcompeting the desired polymeric thiol-maleimide reaction.

Table 4.5 entries 2a-d show the effect of simultaneous aminolysis/thiol-maleimide Michael addition in the absence of DBU on end group functionalization efficiency. Incomplete aminolysis was observed in all solvents except CH_2Cl_2 (2a) with reactions performed in DMSO (2d) and EtOH (2c) retaining 46% and 90% respectively of the original dithiobenzoate functionality. Accordingly, only 31% and 8% end group functionalization was observed in DMSO EtOH respectively. These results show that the amine-maleimide aza-Michael addition can occur faster than CTA aminolysis in more polar solvents and are consistent with the effect of solvent polarity on the reaction rates of HexAM with **65** shown in Figure 1a.

The reactions performed in Table 4.5 entries 3a-d were identical to those performed in entries 2a-d except the HexAM was allowed to react with **45** for 30 min prior to the addition of **46** (Method 2). CTA aminolysis was qualitatively confirmed to

occur within 30 min by noting the change in color that takes place as the dithiobenzoate end groups (orange) are aminolyzed to the corresponding N-hexylthiobenzamide (yellow). Entries 3a-d show that 100% CTA aminolysis was acheived in all solvents while end group functionalization efficiencies were significantly improved compared to reactions conducted using the simultaneous aminolysis method (entries 2a-2d). High end group functionalization (95%) was achieved in the less polar aprotic solvents CH_2Cl_2 (3a) and MeCN (3b) while moderate degrees of functionalization were obtained in EtOH (84%, 3c) and DMSO (72%, 3d). While these results are promising, it is well known that disulfide coupling of polymeric thiols can occur during CTA aminolysis, resulting in both reduced end group functionalization efficiencies and high molecular weight impurities, thus necessitating the use of a reducing agent.[258]

Table 4.5 entries 4a-d show the use of TBP as a reducing agent results in decreased end group functionalization efficiencies for reactions performed in CH_2Cl_2 (4a) and MeCN (4b) compared to analogous reactions conducted without TBP (entries 3a and 3b respectively). Meanwhile, no effect of TBP was observed on the functionalization efficiencies of reactions performed in EtOH and DMSO (entries 4c and 4d respectively). From these results and the kinetic plots in Figure 4.21c, we conclude that trialkylphosphines are not suitable reducing agents during thiol-maleimide end group modification of RAFT polymers due to competing phosphine-initiated maleimide polymerization. Alternatively, using the less nucleophilic TMP as a reducing agent affords substantially increased degrees of end group functionalization in all solvents as seen in Table 4.5 entries 5a-d with 98% and 99% end group functionalization acheived in CH_2Cl_2 (5a) and MeCN (5b) respectively.

Stoichiometric Considerations

Efficient and quantitative end group functionalization of RAFT polymers using aminolysis/thiol-maleimide chemistry also requires consideration of the reactant feed ratios. Ideally, minimal excess of maleimide should be used relative to polymeric thiol to limit the waste of potentially costly maleimide compounds. However, inevitable side reactions such as amine-maleimide aza-Michael addition must be taken into account when choosing reactant stoichiometry such that $[Mal]_0 > [P_nSH] + [amine]$; $[P_nSH]$ and [amine] are the polymeric thiol and unreacted amine concentrations respectively after complete RAFT agent aminolysis has occurred. In this work, we found that aminolysis of **45** with HexAM using a molar ratio of $[\mathbf{45}]_0$:$[HexAM]_0$ = 1.0:2.5 results in complete loss of dithiobenzoate end groups within 30 min. However, other work conducted by our group (not reported herein) has shown that dithiobenzoate-functional polystyrene synthesized by RAFT requires several hours for complete aminolysis to occur using the same dithiobenzoate to amine ratio. Therefore, the reactant feed ratios reported herein should be considered as a starting point for stoichiometric optimization of different RAFT polymer systems.

The type of RAFT agent being aminolyzed must also be considered when choosing reactant stoichiometry. Dithiobenzoate-terminated polymers react with one equivalent of amine to yield polymeric thiol and thiobenzamide byproducts in equimolar amounts. Conversely, trithiocarbonate-terminated polymers can react with two equivalents of amine to give the polymeric thiol, Z-group derived thiol, and thiourea byproduct in equimolar amounts. In this case, the reactant stoichiometry must allow for

$[Mal]_0 > [P_nSH] + [amine] + [ZSH]$ where [ZSH] is the concentration of small molecule Z-group derived thiol.

Section 4. Growth-Then-Coupling Method of Molecular Brush Synthesis from RAFT Polymers and Thiol-Reactive Oxanorbornenes

Overview

In recent years, extensive efforts have been made towards developing synthetic methodologies to prepare functionally diverse and structurally complex molecular brush copolymers. Molecular brush or "bottle-brush" copolymers are comprised of polymeric side-chains attached to a polymer backbone and exhibit highly branched spherical or cylindrical morphologies with minimal intermolecular chain entanglement owing to the volume-exclusion interactions between sterically crowded polymeric side-chains.[322] Consequently, molecular brush (co)polymers have been used as polymer nanotherapeutics,[212] rheological modifiers,[323] surfactants,[324] and as discrete nanostructures.[325] The increased interest in molecular brushes has driven current efforts towards developing facile and versatile synthetic routes.

Molecular brush copolymers can be synthesized using grafting-to, grafting-from, grafting-through, or more recently by transfer-to routes.[322,326] Of these approaches, grafting-through ensures the highest grafting density with 100% of polymer backbone repeat units bearing a polymeric side-chain. Lately, the strong thermodynamic driving force of ring opening metathesis polymerization (ROMP) of norbornene-functional macromonomers (MMs) has been demonstrated as an effective method of overcoming the issues of steric hindrance and low concentration of polymerizable end groups typically associated with grafting-through synthetic approaches.[202,211]

Norbornene-functional macromonomers can be synthesized using either "direct-growth" (DG-MM) or "growth-then-coupling" (GC-MM) methods as reviewed recently by Xia and coworkers.[218] DG-MM synthesis has been accomplished using norbornene-functional initiators during ring opening polymerization (ROP)[189] and atom transfer radical polymerization (ATRP).[211] In addition, norbornene-functional chain transfer agents have been used to prepare macromonomers using RAFT polymerization.[201,212,213] Synthesizing MMs by RAFT is particularly advantageous due to the wide variety of vinyl monomers available and ease of controlling end-group functionality. However, DG-MM synthesis by RDRP techniques such as RAFT requires polymerization optimization for a given monomer-type to minimize radical addition to the norbornene olefin during polymerization.[214] Furthermore Xia and coworkers have demonstrated that trace amounts of difunctional macromonomer impurities resulting from radical-radical coupling of α-norbornene-functional polymers can result in undesired molecular brush branching and broadened molecular weight distributions.[218] Consequently, facile and efficient GC-MM synthetic routes are desired.

New Synthetic Route Toward Norbornene-Functional RAFT Polymer Macromonomers

We envisioned a GC-MM synthetic route that exploits the latent reactivity of thiocarbonylthio-terminated RAFT polymers. In Chapter IV Section III we demonstrated the efficient and quantitative end group functionalization of RAFT polymers using "one-pot" aminolysis/thiol-maleimide chemistry. Accordingly, norbornene end-functional RAFT polymers should be accessible using thiocarbonylthio end-functional RAFT polymers and a maleimide-functional oxanorbornene (**52**) as illustrated in Scheme 4.14. Furthermore, it should be possible to end-functionalize RAFT polymers using a

methanethiosulfonate (MTS)-functional oxanorbornene (**56**) to give the corresponding disulfide-containing macromonomer. Molecular brushes comprised of side chains attached by disulfide linkages are of particular interest for drug delivery applications where selective intracellular reduction of disulfides would trigger molecular brush disassembly and favor polymer clearance *in vivo*.

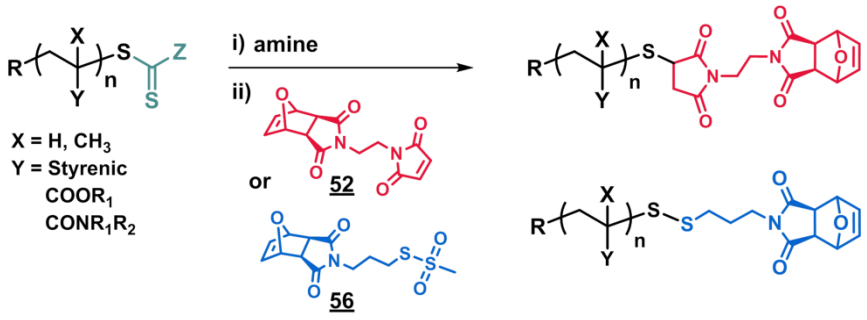

Scheme 4.14. "One-pot" end group functionalization of RAFT polymers with thiol-reactive oxanorbornenes **52** and **56**.

Synthesis of Thiol-Reactive oxaNorbornenes.

Maleimide-functional (**52**) and MTS-functional (**56**) oxanorborne derivatives were synthesized according to Schemes 4.15 and 4.16 respectively. Substituted oxanorbornedicarboximides are readily synthesized from the Diels-Alder reaction of furan and N-substituted maleimides. However, subsequent chemical reactions of oxanorbornene intermediates must be conducted at temperatures below 100 °C in order to avoid the furan-maleimide retro Diels-Alder reaction.[327] Consequently, low temperature imide forming reactions were utilized for the synthesis of **52** and **56**. Using the method developed by Keller and Rudinger,[328] reaction of N-methoxycarbonylmaleimide (**48**) with primary amines in saturated $NaHCO_3$ at 0-23 °C affords the corresponding N-substituted maleimides which precipitated out of the aqueous reaction mixture in moderate to high yields and required no additional purification.

Reaction of sodium methanethiosulfonate (**55**) with primary bromide-functional oxanorbornenedicarboximide (**54**) affords in good yield the MTS-functional product **56**. In contrast to symmetric disulfides which undergo thiol-disulfide exchange to form a mixture of mixed and homo disulfide products, reaction of MTS activated disulfides with thiols gives exclusively the mixed disulfide owing to the excellent leaving group ability and poor nucleophilicity of the methanesulfinic acid group. Consequently, this selectivity has been extensively used to prepared disulfide end-functional RAFT polymers.[296]

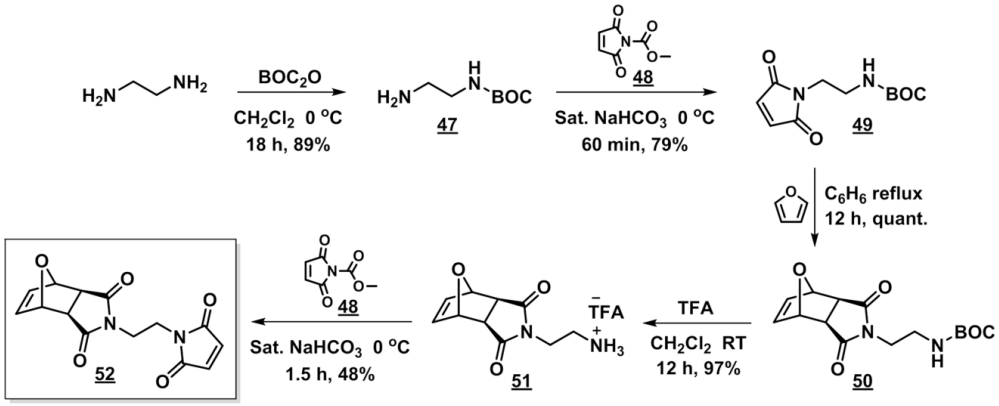

Scheme 4.15. Synthetic route for **52**.

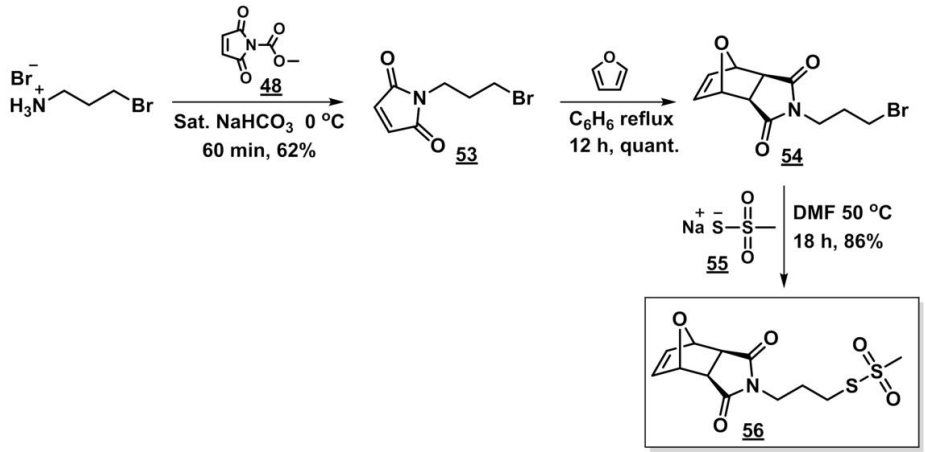

Scheme 4.16. Synthetic route for **56**.

"One-pot" Synthesis of RAFT Polymer Macromonomers from Thiol-Reactive oxaNorbornenes

We first synthesized dithiobenzoate-terminated poly(styrene) (**57**) and poly(N,N-dimethylacrylamide) (**58**) as representative RAFT polymers for end group functionalization with thiol-reactive oxanorbornenes. Low dispersities and excellent agreement between the molecular weights determined by NMR and SEC-MALLS for **57** (M_n(NMR) = 3090 g/mol, M_n(SEC) = 2980 g/mol, Đ = 1.03) and **58** (M_n(NMR) = 3710 g/mol, M_n(SEC) = 3630 g/mol, Đ = 1.05) are indicative of controlled RAFT polymerization and high dithiobenzoate chain end fidelity.

The work in Chapter IV Section III of this dissertation shows that quantitative end group functionalization of RAFT polymers using "one-pot" aminolysis/thiol-maleimide chemistry is attainable using sequential aminolysis/maleimide addition, less polar solvents (e.g. CH_2Cl_2), and mild reducing agents (e.g. trimethylphosphite) while avoiding the use of aprotic nucleophilic catalysts such as amidines and phosphines. Similar reaction conditions were used for the reactions of **57** or **58** with **52** as outlined in the experimental section. Figure 4.25 shows the ^{1}H NMR spectra of **57** before end group modification (Figure 4.25c) and after reaction with **52** (Figure 4.25b). Complete aminoylsis of the dithiobenzoate end groups of **57** is observed by noting the disappearance of the aromatic protons at 8.0 – 7.3 ppm (Figure 4.25b). Ultimately, 98% end functionalization of **57** is achieved with the characteristic oxanorbornene peaks a, b, and c visible in Figure 4.25b. Similarly, reaction of the RAFT polymer **58** with **52** results in complete dithiobenzoate aminolysis and near-quantitative (>99%) end group functionalization efficiency as determined by ^{1}H NMR (Figure 4.26). Minimal change in

M_n(SEC) and Đ of end-modified polymers (**59** and **61**) compared to the starting RAFT polymers (**57** and **58**) indicates little or no polymeric disulfide coupling (Table 4.6).

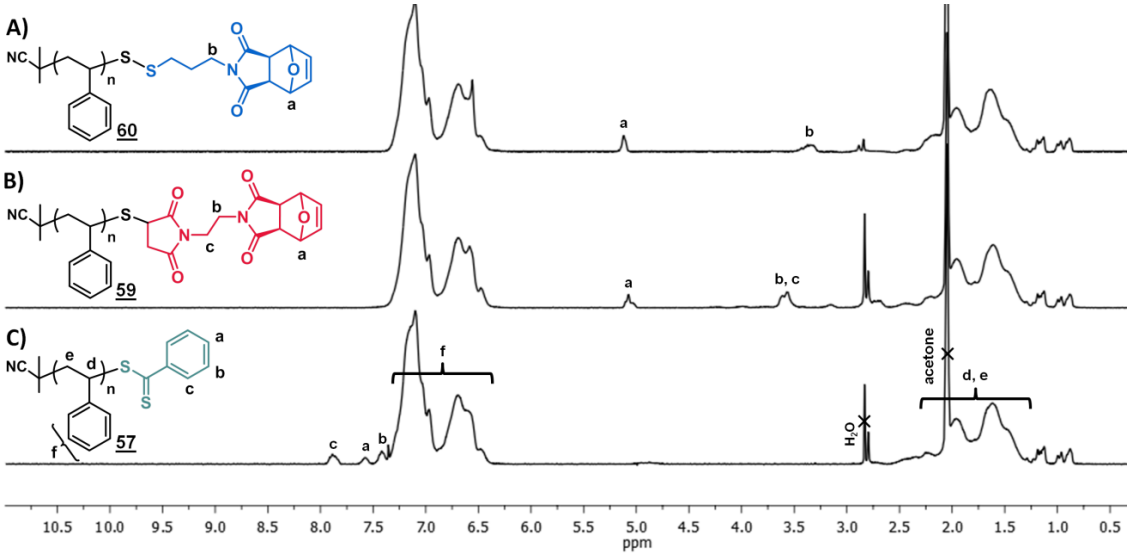

Figure 4.25. ^{1}H NMR (300 MHz, acetone-d_6) end group analysis of **57**, **59**, and **60**.

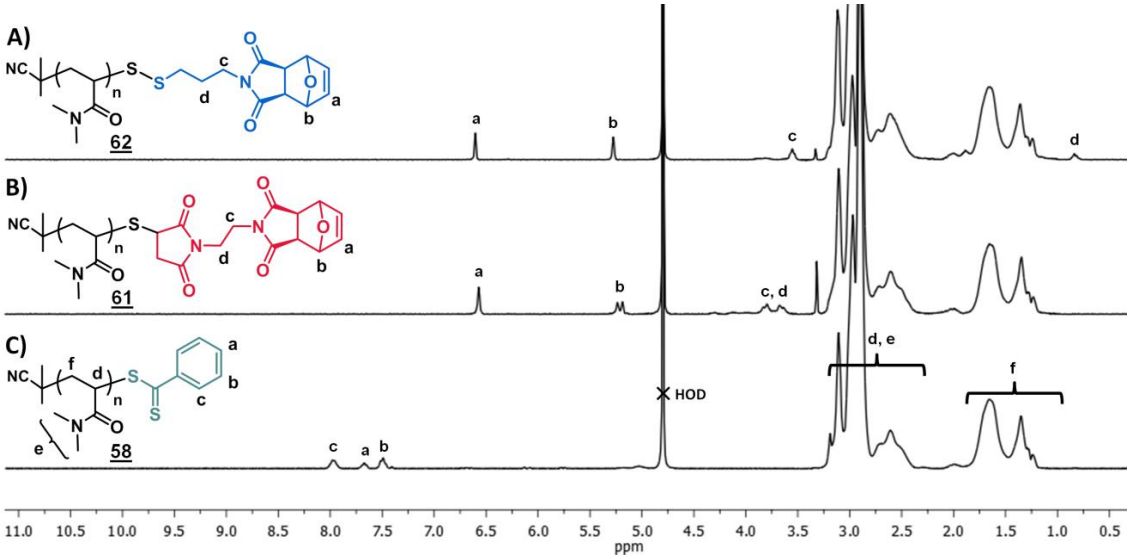

Figure 4.26. ^{1}H NMR (300 MHz, D_2O) end group analysis of **58**, **61**, and **62**.

End group functionalization of RAFT polymers **57** or **58** with **56** were also performed as "one-pot" reactions. RAFT polymer aminolysis was conducted in the presence of **56** using relative ratios of [**57**/**58**]$_0$:[**56**]$_0$:[amine]$_0$ = 1.0:6.0:10. ^{1}H NMR end

group analysis of **56**-modified RAFT polymers (**60** and **62** respectively) confirms quantitative aminolysis of dithiobenzoate end groups along with the appearance of the characteristic oxanorbornene peaks. Reactions of **57** or **58** with **62** afforded moderately high end group functionalization efficiencies (95% and 94% respectively) with no significant change in M_n or Đ compared to the parent RAFT polymers indicating little or no polymeric disulfide coupling (Table 4.6).

Table 4.6

*Summary of end group functionalization of RAFT polymers **57** and **58** with thiol-reactive oxanorbornenes **52**[a] and **56**.[b]*

entry	RAFT polymer	M_n(NMR)[c] (g/mol)	M_n(SEC)[d] (g/mol)	Đ[d]	norb. deriv.	funct.[e] (%)	M_n(SEC)[f] (g/mol)	Đ[f]
1 (**59**)	**57**	3090	2980	1.03	**52**	98	3290	1.06
2 (**60**)	**57**	3090	2980	1.03	**56**	96	3360	1.05
3 (**61**)	**58**	3710	3630	1.05	**52**	>99	3950	1.07
4 (**62**)	**58**	3710	3630	1.05	**56**	94	3930	1.05

[a][**57**/**58**]$_0$:[**52**]$_0$:[amine]$_0$ = 1.0:5.0:2.5. [b][**57**/**58**]$_0$:[**56**]$_0$:[amine]$_0$ = 1.0:6.0:10. [c] M_n(NMR) was determined by comparing the integral area of the dithibenzoate aromatic protons (5H) to either the aromatic protons of **57** or the N,N-dimethyl and methyne protons of **58**. [c]Theoretical M_n values were calculated according to the equation $M_{n,th}=(\rho MW_{mon}[M]_0/[CTA]_0) + MW_{CTA}$ where ρ is the fractional monomer conversion, MW_{mon} is the molecular weight of the monomer, and MW_{CTA} is the molecular weight of the CTA. [d]M_n(SEC) and Đ values of **57** and **58** were determined by SEC-MALLS (DMF 20 mM LiBr). [e]Determined by ^{1}H NMR. [f]M_n(SEC) and Đ values measured after end group modification.

Ring Opening Metathesis Polymerization of oxaNorbornene End-Functional RAFT Polymers

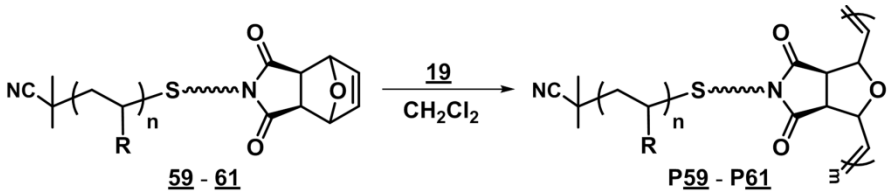

Scheme 4.17. ROMP of ω-oxanorbornenyl-functionalized macromonomers (**59**–**62**) into the corresponding molecular brushes (**P59**–**P62**).

The ω-oxanorbornenyl-functionalized macromonomers (**59-62**) were next polymerized by ROMP using the 3rd Generation Grubbs catalyst (**19**) (Scheme 4.17). Polymerizations were conducted in CH_2Cl_2 using stoichiometric ratios of $[MM]_0$:$[\mathbf{19}]_0$ = 50:1.0 and allowed to proceed for 6 h prior to termination via the addition of ethyl vinyl ether. SEC-MALLS analysis of aliquots taken during preliminary experiments confirmed that all reactions reached maximal MM conversion within 6 h. Figure 4.27a shows the RI traces for dithiobenzoate-terminated poly(styrene) RAFT polymer before (**57**) and after (**59**) end-functionalization with **52**. 91% MM conversion was reached during the ROMP of **59**, affording the corresponding molecular brush (**P59**) of low dispersity and with reasonable agreement between M_{nth} and M_{nexp} (M_{nexp} = 159,600 g/mol, Đ = 1.06) (Table 4.7). Similarly, ROMP of the disulfide-containing MM (**60**) resulted in 87% MM conversion and produced the molecular brush **P60** of low dispersity (M_n = 198,200 g/mol, Đ = 1.04) (Table 4.7). Worth noting is the bimodal shape of the residual MM peak following ROMP of **59** and **60** as shown in Figures 4.27a and 4.27b respectively. The residual MM peak appearing at longer elution volumes corresponds well with the peak elution volume of the respective MM. Meanwhile, the peak exhibiting a lower elution volume corresponds well with the high molecular weight shoulder exhibited by the RAFT polymer **57** and the resulting MMs (**59** and **60**). Consequently, the higher elution volume peak is likely due to coupled polymer resulting from termination by radical-radical coupling during RAFT polymerization. Such coupled polymer would not retain the RAFT agent end group and would not be functionalizable by **52** or **56**. Nonetheless, these results show that macromonomers derived from **57** and thiol-reactive oxanorbornene

derivatives **52** and **56** can be polymerized by ROMP to give the corresponding molecular brush of low dispersity and of relatively high MM conversion.

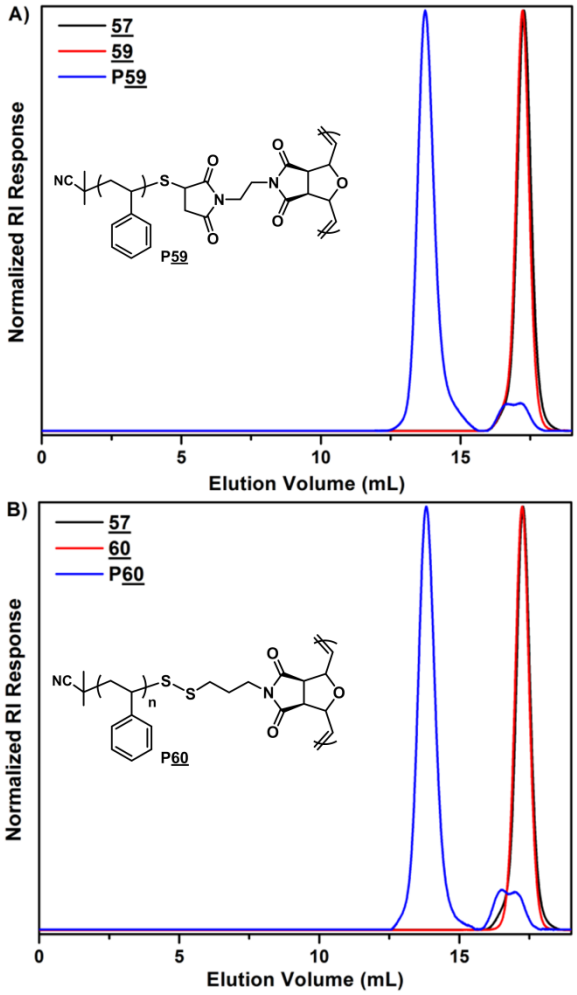

Figure 4.27. a) SEC RI traces of the parent RAFT polymer (— **57**), **52**-functional macromonomer (— **59**), and corresponding molecular brush (— **P59**). b) SEC RI traces of the parent RAFT polymer (— **57**), **56**-functional macromonomer (— **60**), and corresponding molecular brush (— **P61**).

SEC RI traces of macromonomers (**61** and **62**) synthesized from the water soluble RAFT polymer poly(N,N-dimethylacrylamide) (**58**) are shown in Figures 4.28a and 4.28b respectively. In contrast to the ROMP of poly(styrene)-based MMs (**59** and **60**), ROMP of **61** and **62** exhibited limited MM conversion and yielded molecular brushes of broad dispersities as shown in Table 4.7. Despite >99% oxanorbornenyl end group

functionalization of **61** and 94% functionalization of **62**, ROMP of **61** and **62** only reached 57% and 76% conversion respectively in 6 h. Furthermore, extending the reaction time beyond 6 h (data not shown) was determined to have no influence on MM conversion for the ROMP of **61** or **62**. From these observations we hypothesize that catalyst **19** is likely degrading due to residual oxygen or as a result of some unforeseen degradation reaction. It is well known that polar solvents and functional groups can coordinate with Ru-based metathesis catalysts, consequently competing with monomer for the catalyst binding site and slowing the rate of ROMP.[329] Indeed, the rate of polymerization measured during the ROMP of **61** and **62** is slower than that measured for the ROMP of the poly(styrene)-based MMs **59** and **60** (data not shown). Therefore it is plausible that the dimethylacrylamide side chains coordinate with **19** and slow the rate of polymerization enough for degradation of **19** (e.g. oxidation) to occur before complete consumption **61** or **62**.

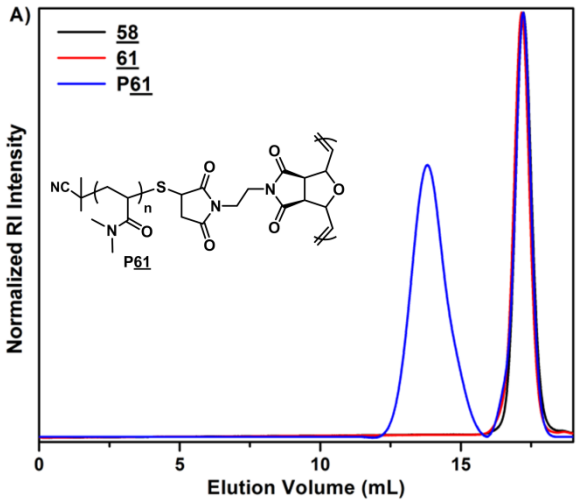

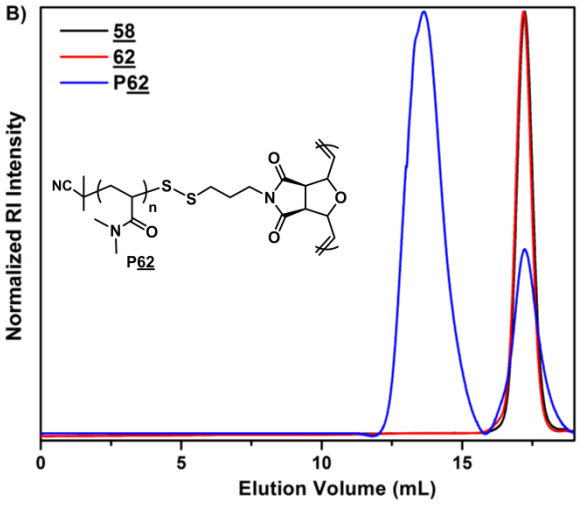

Figure 4.28. a) SEC RI traces of the parent RAFT polymer (— **58**), **52**-functional macromonomer (— **61**), and corresponding molecular brush (— **P61**). b) SEC RI traces of the parent RAFT polymer (— **58**), **56**-functional macromonomer (— **62**), and corresponding molecular brush (— **P62**).

Table 4.7

ROMP of RAFT-derived macromonomers summary.

entry	MM	MM conv.[a] (%)	M_{nth}[b] (g/mol)	M_{nexp}[c] (g/mol)	Đ[c]
1	**59**	91	135,600	159,600	1.06
2	**60**	87	129,600	198,200	1.04
3	**61**	57	103,500	161,000	1.24
4	**62**	76	137,900	141,700	1.23

[a]Macromonomer conversion was determined from the relative integral areas of the SEC RI traces at t = 0 min and t = 6 h. [b]Theoretical M_n values were calculated according to the equation $M_{nth}=(\rho MW_{MM}[MM]_0/[\mathbf{19}]_0)$ where ρ is the fractional macromonomer conversion and MW_{MM} is the molecular weight of the macromonomer. [c]Experimental M_n and M_w/M_n values were determined by SEC-MALLS (DMF 20 mM LiBr).

Reduction-Induced Molecular Brush Disassembly

Polymer therapetuics have made extensive use of disulfide reduction as an intracellular specific bond-breaking reaction in order to trigger therapeutic agent release

and polymer disassembly/degradation following cellular internalization.[171] Similarly, we envision the use of disulfide-containing molecular brushes as highly branched "delivery vehicles" which would exhibit extended circulation times *in vivo* and undergo reduction-induced disassembly upon cellular internalization to promote subsequent polymer clearance from the body. Accordingly, we investigated the reduction-induced disassembly of **P62**, which is comprised of water soluble poly(N,N-dimethylacrylamide) side chains attached to a poly(oxanorbornenedicarboximide) backbone via disulfide linkages, under physiological conditions (pH = 7.4 PBS buffer) (Scheme 4.18). DL-dithiothreitol (DTT) was used as a representative reducing agent at [DTT] = 5 mM in accordance with the natural concentration range of glutathione found in mammalian cells (1-10 mM). Residual macromonomer present after ROMP of **62** (Figure 4.28) was removed by dialysis against water (MWCO = 15 kDa) followed by lyophilization. Figure 4.29 shows the monomodal SEC RI trace of **P62** after dialysis (black trace).

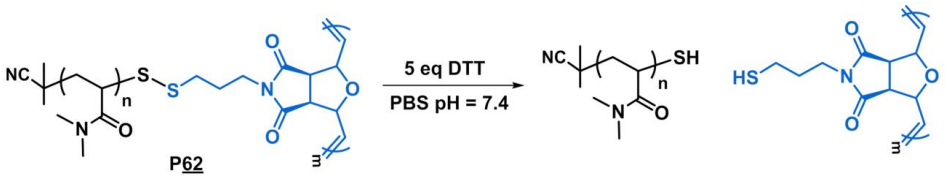

Scheme 4.18. DTT reduction of **P62** in pH = 7.4 PBS buffer (10 mM) at 23 °C.

DTT reduction of **P62** was monitored by SEC-MALLS (DMF 20 mM LiBr) by injecting aliquots at timed intervals using an autosampler. A solution of **P62** in pH = 7.4 PBS was initially prepared in a GPC vial equipped with piercable cap to give a final disulfide concentration of 1 mM. Subsequently, a stock solution of DTT in PBS was added to the GPC vial to give a final [DTT] = 5 mM. The first aliquot, which was injected 5 min after addition of DTT, is shown in Figure 4.29 (red trace). Remarkably,

disappearance of the peak corresponding to **P62** is observed by the first aliquot. The appearance of a new peak at ~17.5 mL is nearly equivalent to the elution volume of **62** (elution volume = 17.4 mL). The second new peak with elution volume = 20.2 mL is that of the PBS buffer salts. Also worth noting is that precipitation was observed in the GPC vial following the addition of DTT and is likely due to the insolubility of the poly(oxanorbornenedicarboximide) backbone (Scheme 4.18) in PBS.

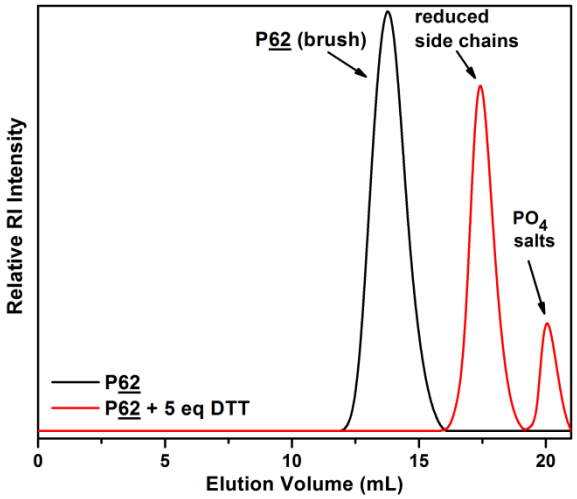

Figure 4.29. SEC RI trace of the disulfide-containing molecular brush after purification by dialysis (— **P62**) and SEC RI trace (—) of **P62** 5 min after the addition of DTT (5 eq.). **P62** molecular brush reduction reactions were performed in pH = 7.4 phosphate buffered saline (10 mM) at 23 °C.

CHAPTER V

CONCLUSIONS

Section 1. Tunable pH- and CO_2-Responsive Sulfonamide-Containing Polymers by RAFT Polymerization

A series of pMSA polymers with tunable, pH-dependent solubility in aqueous media has been synthesized by RAFT polymerization. Initially, polymerizations conducted in DMF at 70 °C gave polymers with broad molecular weight distributions, but upon reducing the polymerization temperature to 30 °C and employing the low decomposition temperature initiator V-70, polymers of narrow molecular weight distribution and increased thiocarbonylthio chain end functionality were obtained. Selection of the sulfonamide R-group of MSA monomers is a facile means of adjusting pK_a and ultimately the critical onset of precipitation pH (pH*) of the corresponding pMSA. Thus it is possible to "fine tune" pH-dependent polymer solubility in the biologically relevant regime (pH = 4.5-7.4). Additionally, we demonstrated, the reversible CO_2-responsiveness of pMSAs in aqueous media, further indicating the potential of pMSAs in biological and nanotherapeutic applications.

Section 2. Mechanistic Insights into Temperature-Dependent Trithiocarbonate Chain-End Degradation during the RAFT Polymerization of N-Arylmethacrylamides

Methacrylamide-induced trithiocarbonate degradation during RAFT polymerization has been investigated. N-phenyl-promoted nucleophilic attack of the terminal trithiocarbonate by the ultimate methacrylamide unit was shown to occur by N-5 cyclization/elimination, resulting in rapid loss of active chain ends in DMF at 70 °C. The 3-phenyl-2-thioxothiazolidin-4-one RAFT polymer chain ends resulting from N-5 cyclization/elimination were shown to have little direct influence on the RAFT process

and thus function as “dead” chain ends. Suppression of methacrylamide-induced trithiocarbonate degradation during the RAFT polymerization of N-arylmethacrylamides can be achieved by reducing the reaction temperature to 30 °C. Work is currently underway in our labs to study the influence of N-aryl amide substitution on both the reaction mechanism and rate of N-5 cyclization/elimination.

Section 3. “One-Pot” Aminolysis/Thiol-Maleimide End Group Functionalization of RAFT Polymers: Identifying and Preventing Michael Addition Side Reactions

In this work we have elucidated a number of deleterious nucleophile-promoted side reactions that occur during the “one-pot” aminolysis/thiol-maleimide end group modification of RAFT polymers. Nucleophilic thiol-ene Michael addition catalysts including amines, amidines, and phosphines were shown to initiate the anionic polymerization of N-methylmaleimide in a range of solvents with the rate of reaction increasing with solvent polarity. We also demonstrated that in more polar solvents, thiols can initiate the anionic polymerization of maleimides when [Mal] > [thiol]. Mechanistic evidence of TEA-catalyzed enolate formation of the thiol-maleimide adduct was acquired using proton-deuterium exchange experiments of thiol-maleimide adducts and used to prove that thiol-maleimide adducts were capable of direct initiation of maleimide polymerization in the presence of a weak base. Ultimately, optimal reaction conditions for the selective and near quantitative “one-pot” end group modification of RAFT polymers using thiol-maleimide chemistry was identified

Section 4. Growth-Then-Coupling Method of Molecular Brush Synthesis from RAFT Polymers and Thiol-Reactive Oxanorbornenes

This section details a new “grafting through” synthetic route towards molecular brushes capable of intracellular-induced disassembly. RAFT polymer-derived macromonomers were synthesized using “one-pot” aminolysis/thiol reactions with maleimide- or methanethiosulfonate-functional oxanorbornenes. Subsequent ring opening metathesis polymerization (ROMP) of the resulting macromonomers afforded molecular brushes with RAFT polymer side chains attached to a polyoxanorbornene backbone via either permanent thioether linkages or reversible disulfide linkages. Molecular brushes comprised of disulfide linkages were shown to undergo reduction-induced disassembly and show promise a new class of stimuli-responsive polymer therapeutics.

APPENDIX A

SUPPORTING INFORMATION

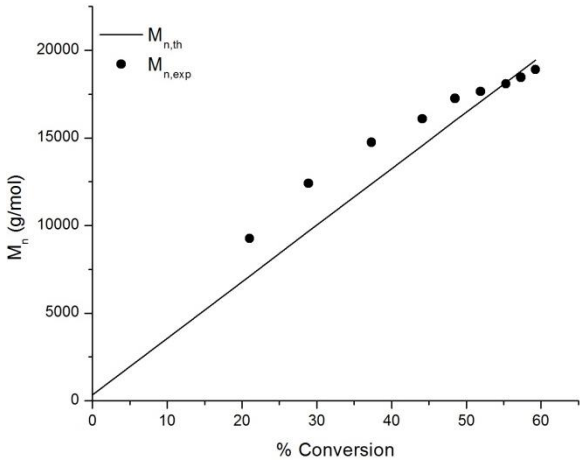

Figure A1. M_n versus % conversion for **37**-mediated polymerization of **33** at 70 °C.

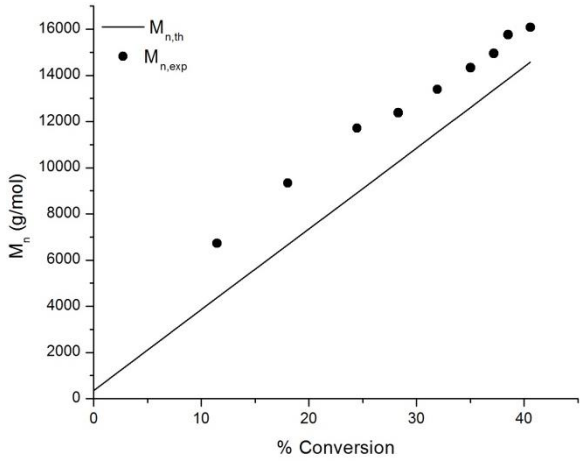

Figure A2. M_n versus % conversion for **37**-mediated polymerization of **34** at 70 °C.

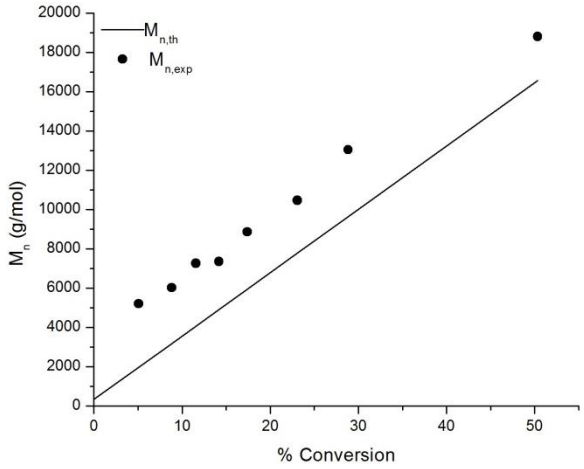

Figure A3. M_n versus % conversion for **37**-mediated polymerization of **33** at 30 °C.

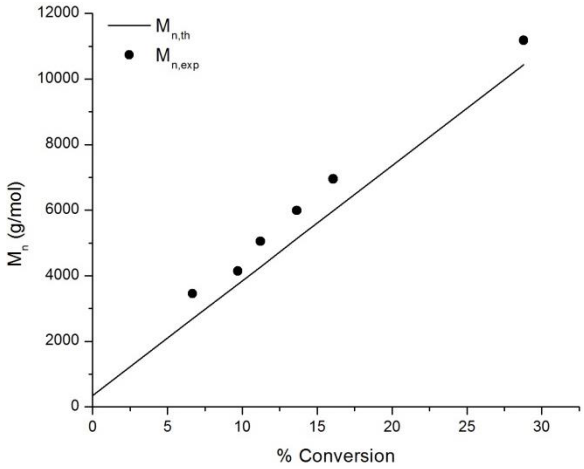

Figure A4. M_n versus % conversion for **37**-mediated polymerization of **34** at 30 °C.

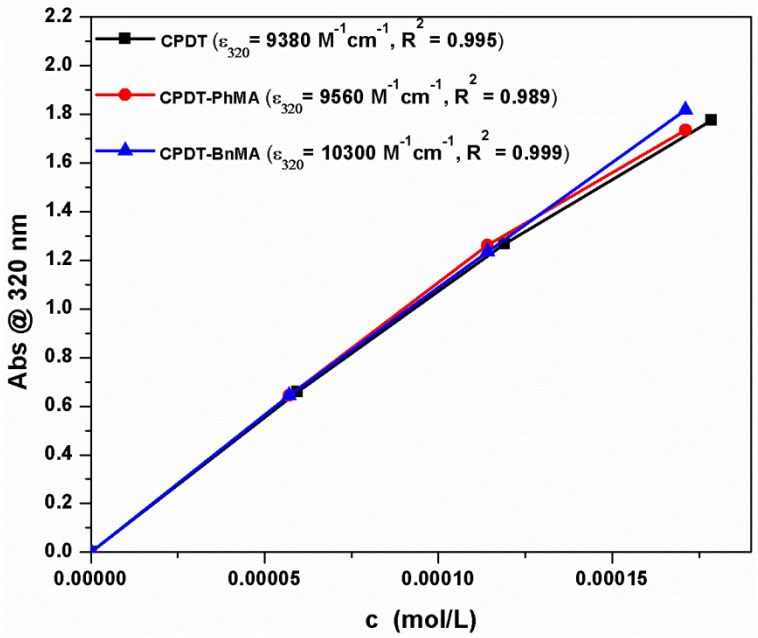

Figure A5. Beer-Lambert plot and molar extinction coefficients (ε) for **37**, **41**, and **42** in acetonitrile measured using a Lambda 35 UV-vis spectrometer (λ = 320 nm).

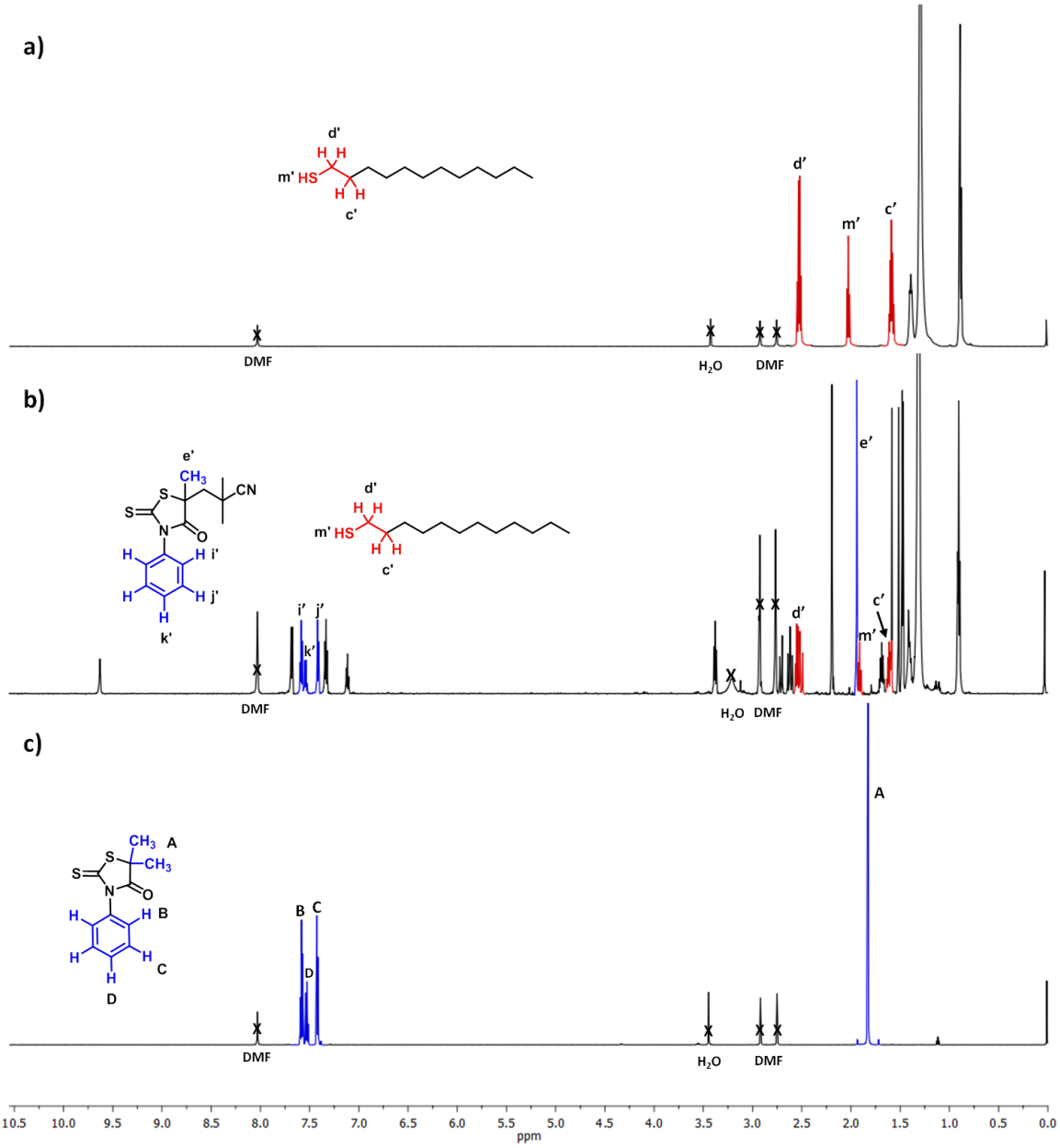

Figure A6. (a) ^{1}H NMR (600 MHz, DMF-d_7) spectrum of 1-dodecanethiol, (b) ^{1}H NMR (600 MHz, DMF-d_7) spectrum acquired at t = 491 min during the *in situ* degradation analysis of **41** at 70 °C, (c) ^{1}H NMR (600 MHz, DMF-d_7) spectrum of **40**. Peaks of interest corresponding to degradation byproducts formed during *in situ* degradation analysis (Figure A6b) are colored red and blue and correspond well with key peaks of analogous compounds 1-dodecanethiol (red) and **40** (blue) (Figures A6a and A6c respectively).

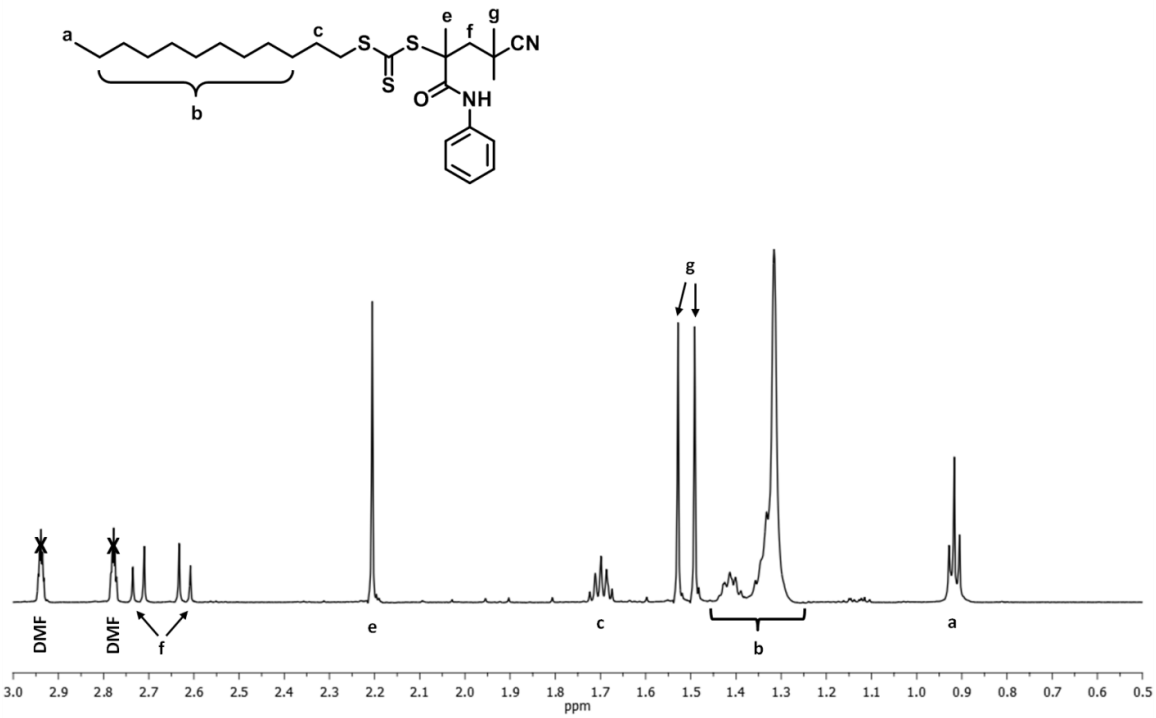

Figure A7. Expanded region (3.00 - 0.5 ppm) of the ^{1}H NMR (600 MHz, DMF-d_7) spectrum acquired at t = 5 min during *in situ* degradation analysis of **41** at 70 °C.

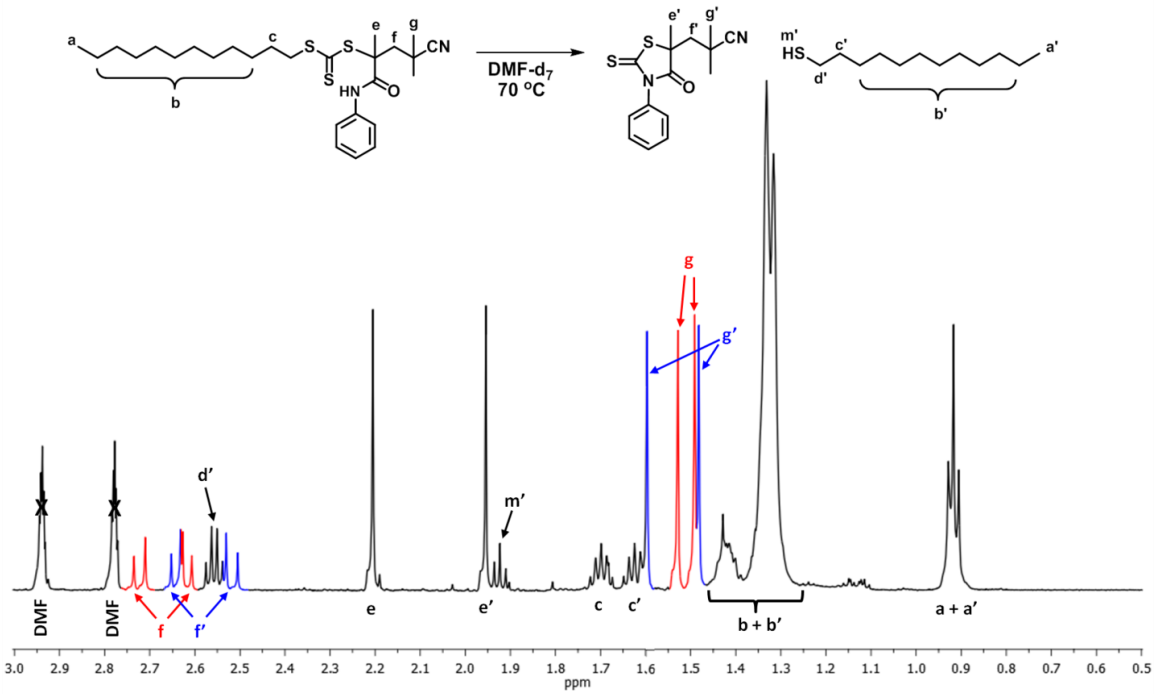

Figure A8. Expanded region (3.00 - 0.5 ppm) of the ^{1}H NMR (600 MHz, DMF-d_7) spectrum acquired at t = 491 min during *in situ* degradation analysis of **41** at 70 °C. Overlapping peaks are colored red or blue for improved visualization.

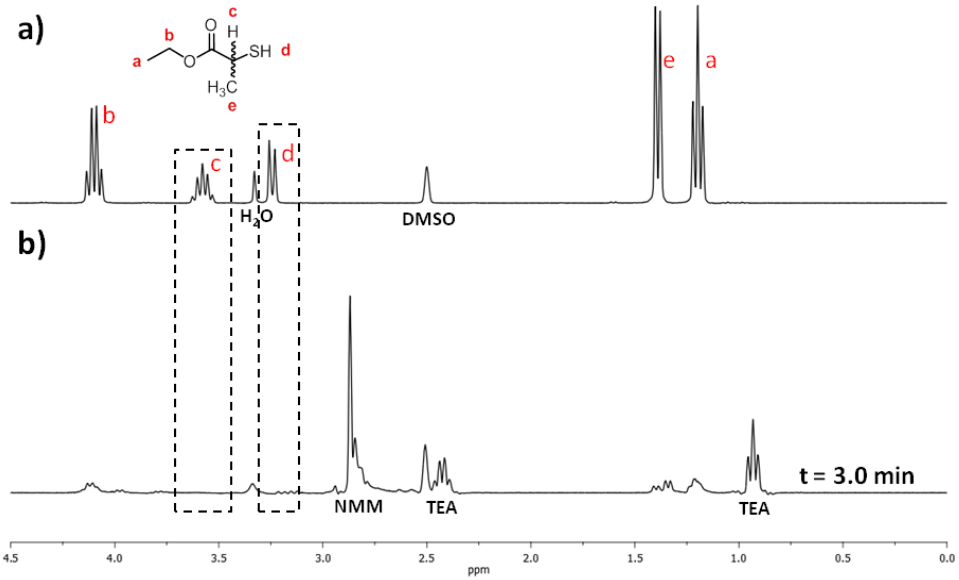

Figure A9. a) ^{1}H NMR spectrum of E2MP in DMSO-d_6 at T = 0 min. b) ^{1}H NMR spectrum during the reaction of E2MP and **65** in DMSO-d_6 at T = 3 min. Disappearance of the thiyl (peak c) and methyne (peak d) protons of E2MP confirm quantitative thiol conversion by 3.0 min.

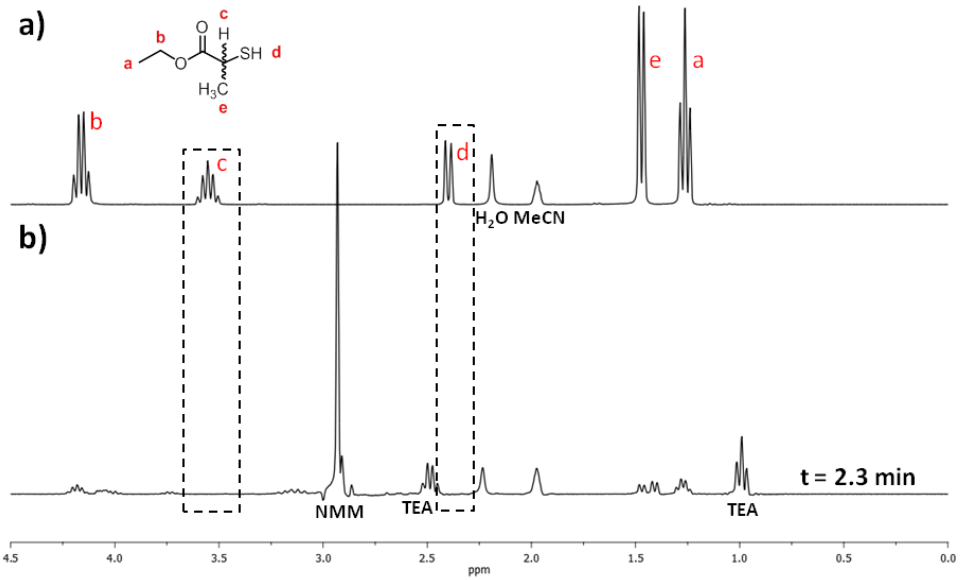

Figure A10. a) ^{1}H NMR spectrum of E2MP in MeCN-d_3 at T = 0 min. b) ^{1}H NMR spectrum during the reaction of E2MP and **65** in MeCN-d_3 at T = 2.3 min. Disappearance of the thiyl (peak c) and methyne (peak d) protons of E2MP confirm quantitative thiol conversion by 2.3 min

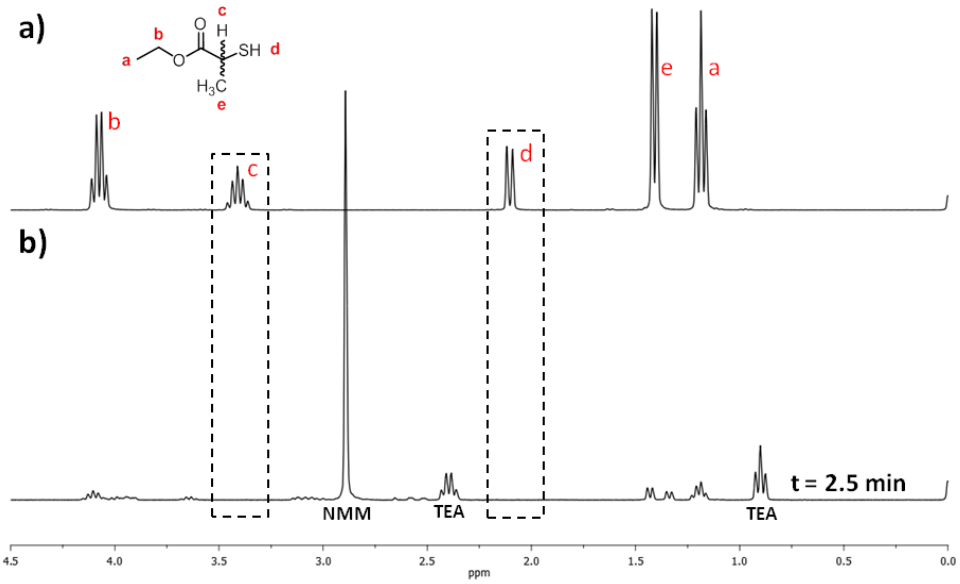

Figure A11. a) ^{1}H NMR spectrum of E2MP in CD_2Cl_2 at T = 0 min. b) ^{1}H NMR spectrum during the reaction of E2MP and **65** in CD_2Cl_2 at T = 2.5 min. Disappearance of the thiyl (peak c) and methyne (peak d) protons of E2MP confirm quantitative thiol conversion by 2.5 min.

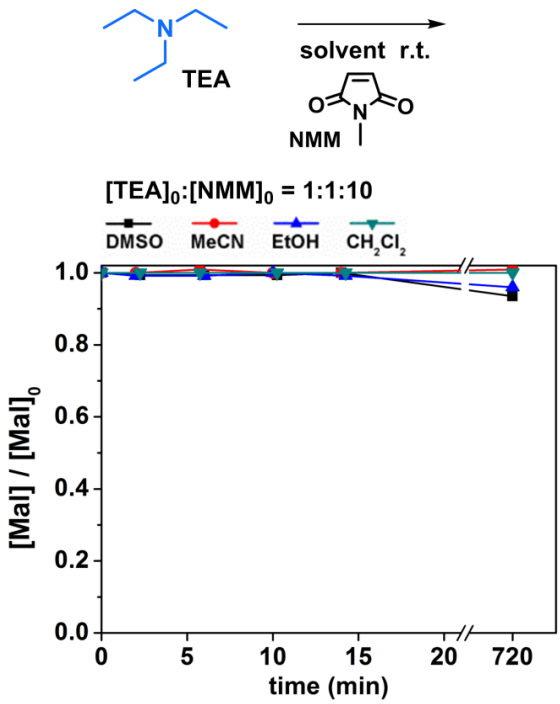

Figure A12. Effect of solvent on the time-dependent fractional change in $[Mal]/[Mal]_0$ during the reaction of TEA with **65** as measured by *in situ* ^{1}H NMR analysis.

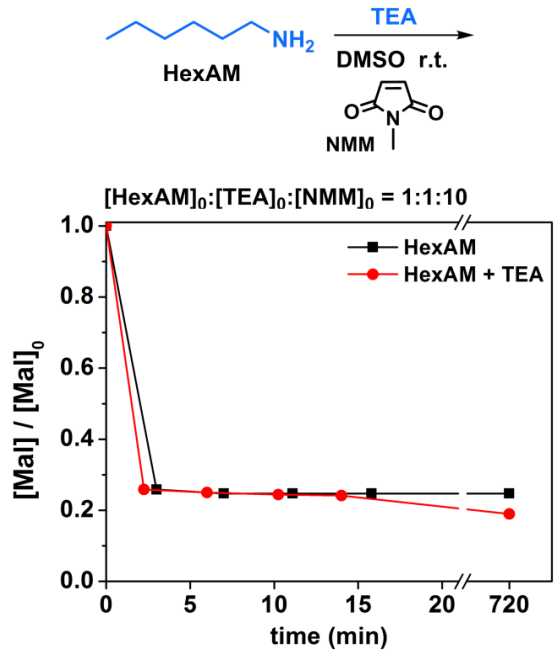

Figure A13. Effect of solvent on the time-dependent fractional change in $[Mal]/[Mal]_0$ during the TEA-catalyzed reaction of HexAM with **65** as measured by *in situ* ^{1}H NMR analysis.

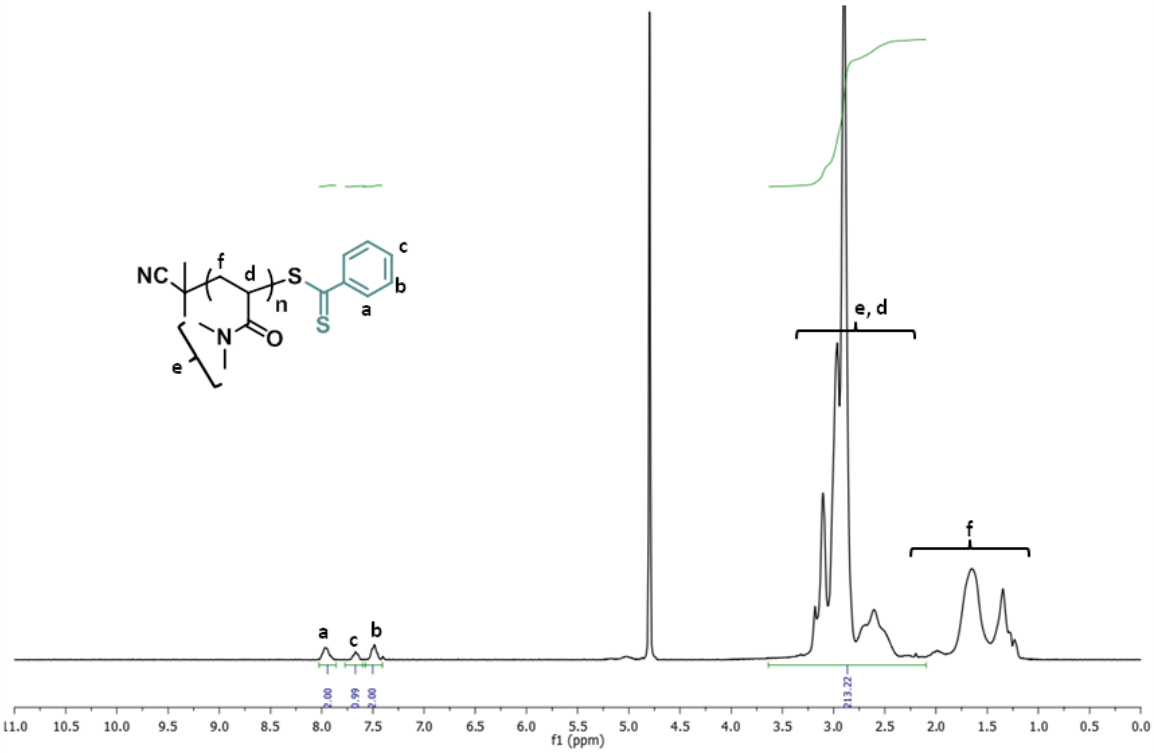

Figure A14. ^{1}H NMR (300 MHz, D_2O) spectrum of **45**.

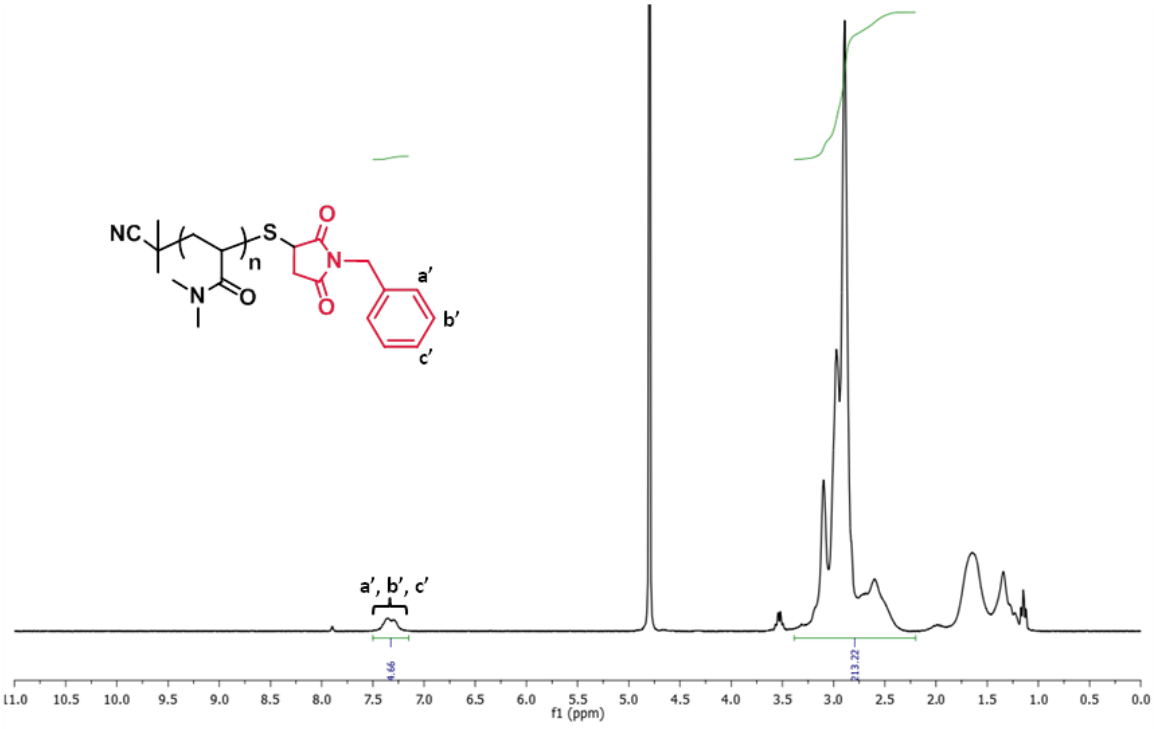

Figure A15. Representative ^{1}H NMR (300 MHz, D_2O) spectrum of **46**-functionalized **45** (Table 4.5 entry 1a).

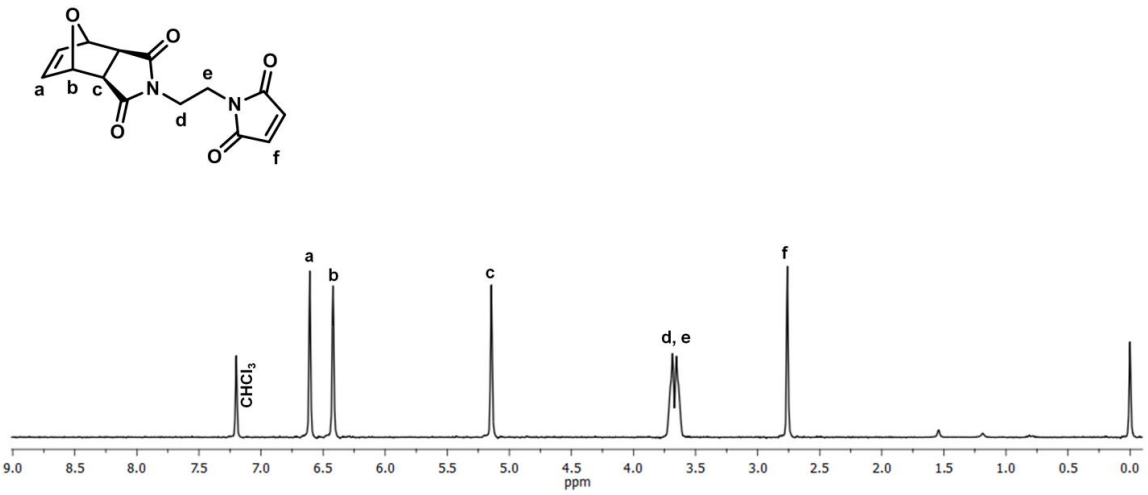

Figure A16. ^{1}H NMR spectrum (300 MHz, $CDCl_3$) of **52**.

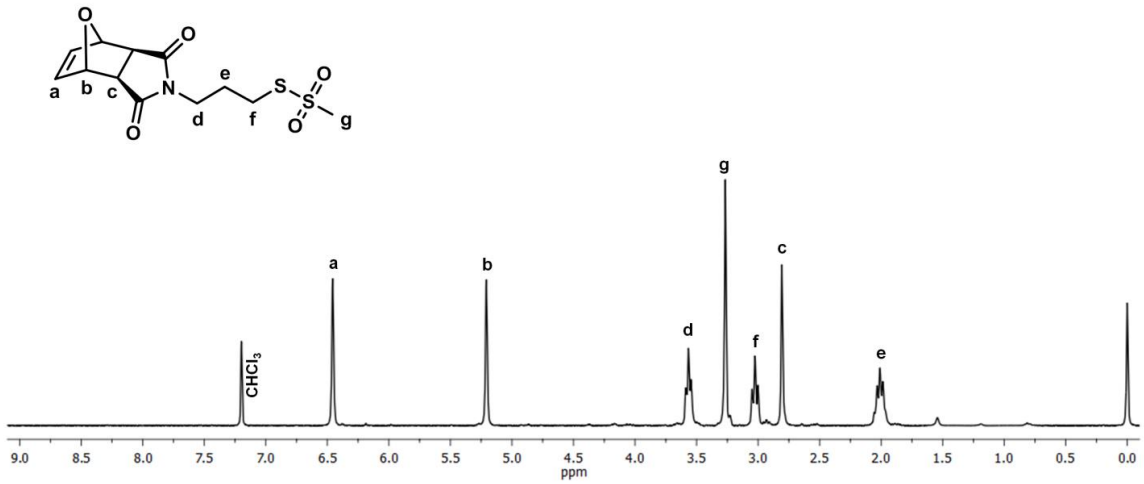

Figure A17. ^{1}H NMR spectrum (300 MHz, $CDCl_3$) of **56**.

APPENDIX B

N-ARYLAMIDE NUCLEOPHILICITY

Overview

Previously, we described the unique influence of N-phenyl methacrylamide substitution on the limited RAFT polymerization control of methacryloylsulfonamides (**27**-**32**)[97] and N-phenylmethacrylamide (**33**)[330] at 70 °C in DMF. We showed that chain end degradation during the trithiocarbonate-mediated polymerization of **33** at elevated temperatures occurs by N-5 nucleophilic attack of the terminal thiocarbonyl moiety by the ultimate methacrylamide unit. Although mechanistic insights were gained into the specific degradation pathway (N-5 cyclization/elimination) as discussed in Chapter IV Section II, the nature of the true nucleophilic species involved in N-5 cyclization and the influence of N-phenyl amide substitution is still not understood. The purpose of this work is to better understand the influences of N-phenyl substitution on amide nucleophilicty and develop a fundamental understanding of how substituents influence the mechanism of amide-based nucleophilic reactions.

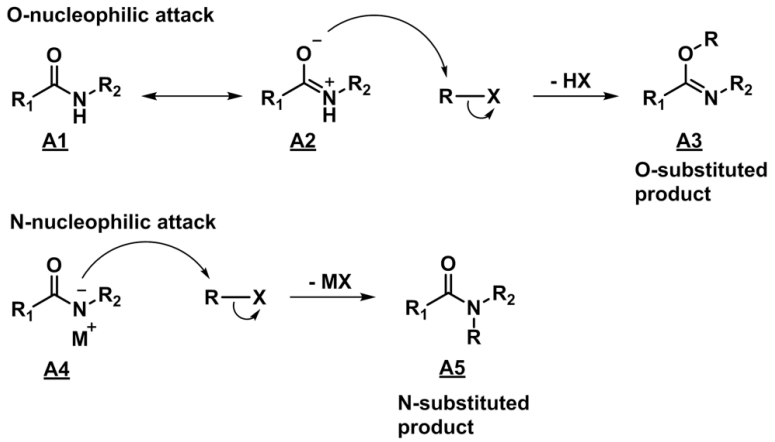

Scheme A1. Influence of ionized (**A2**) or conjugate base (**A4**) resonance forms on amide nucleophilicity.

The structures and reactivity of neutral amides (**A1**) are greatly influenced by the ionized resonance form (**A2)** whereby the lone pair on nitrogen is delocalized onto the carbonyl oxygen, increasing the double bond character of the C-N bond and increasing the electron density of the carbonyl oxygen atom (Scheme A1). Consequently, N-substituted amides exhibit planar structures due to restricted C-N bond rotation and react with electrophiles via the oxygen atom to afford the O-substituted product (**A3**). Alternatively, amide anions derived from protic amides and strong bases (e.g. NaH) (**A4**), react with electrophiles almost exclusively via the nitrogen atom to give the N-substituted product (**A5**). Selective reaction of amide anions at the nitrogen atom has been rationalized using the "hard and soft Lewis acids and bases" (HSAB) theory which attempts to predict/explain the outcomes of substitution reactions involving ambident nucleophiles (i.e. nucleophiles with two potential nucleophilic sites). HSAB theory can be applied to ambident nucleophiles such as amide anions by way of Kornblum's rule which states:

> "… hard acids prefer hard bases and soft acids prefer soft bases. In an SN_1 mechanism, the nucleophile attacks a carbocation, which is a hard acid. In an SN_2 mechanism, the nucleophile attacks the carbon atom of a molecule, which is a softer acid. The more electronegative atom of an ambident nucleophile is a harder base than the less electronegative atom. Therefore, as the character of a given reaction changes from SN_1 to SN_2 like, an ambident nucleophile becomes more likely to attack with its less electronegative atom."[331]

In other words, SN_2 reactions involving amide anions will proceed via the less electronegative nitrogen atom (χ = 3.0) rather than more electronegative oxygen atom (χ = 3.5), where χ is the Pauling electronegativity value. This adequately describes the selectivity in forming the N-substituted product **A5** upon reaction of amide anion **A4** with an electrophilic species by an SN_2 mechanism as shown in Scheme A1. However, according to these theories, the neutral amide of **41** should react via the oxygen atom to give O-5 cyclization/elimination products (**41B**) rather than the observed N-5 cyclization/elimination products (**41A**) as shown in Scheme A2. The key to understanding this mechanism and its products must therefore lie in the role of N-aryl substitution on amide nucleophilicity.

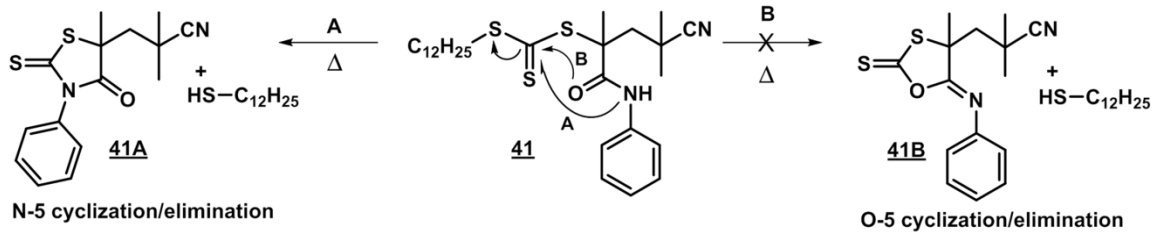

Scheme A2. Proposed degradation of **41** by N-5 cyclization/elimination (pathway A).

In Chapter IV Section II we show that i) N-phenyl methacrylamide substitution increases the observed rate of trithiocarbonate degradation of **41** compared to N-benzyl substitution (**42**) and ii) degradation of **41** proceeds by N-5 cyclization/elimination. We can rationalize these observations if N-phenyl substitution promotes amide N-H dissociation to give the amide anion (and solvated proton) where the amide anion is the true nucleophilic species. As shown in Scheme A3, dissociation of an N-arylamide (**A6**) affords the corresponding amide anion with O- and N-based resonance structures **A7** and

A8 respectively. However, direct N-aryl substitution provides additional resonance forms **A9**-**A11** that can further stabilize the amide anion. These additional resonance forms should reduce the pK_a of **A6** by stabilizing the conjugate base and consequently shift the equilibrium towards the dissociated amide anion species ([CON$^-$Ph]) compared to an analogous amide with N-alkyl substituents. Indeed, comparison of the literature pK_a values of N-methylacetamide (pK_a = 25.9, DMSO)[332] and N-phenylacetamide (pK_a = 21.5, DMSO)[333] confirms the influence of N-aryl substitution on increased amide acidity in polar organic solvents. From these observations, we hypothesize that N-aryl substitution decreases the pK_a of **41** and consequently increases [CON$^-$Ph], accounting for the increased rate of degradation by N-5 cyclization/elimination as compared to **42**.

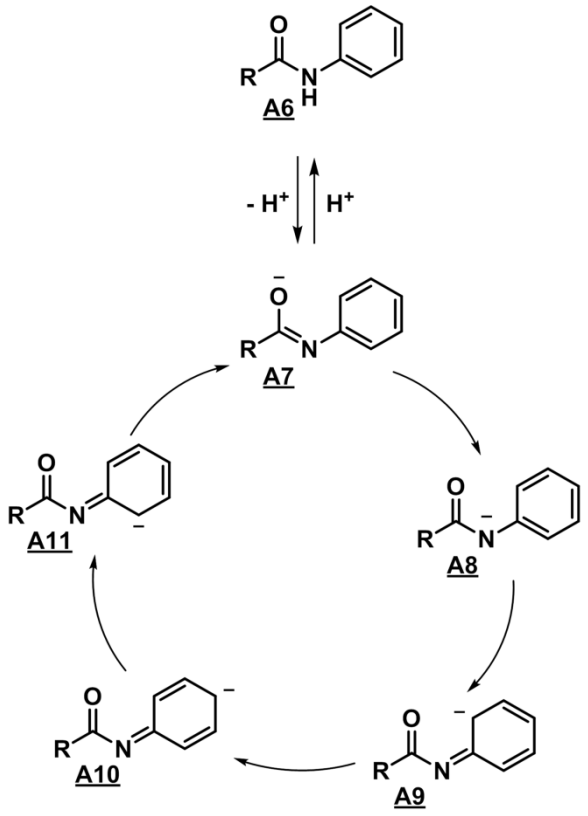

Scheme A3. Possible N-arylamide conjugate base resonance forms.

To test this hypothesis, we have synthesized single monomer unit insertion adducts **A12** and **A13** which possess either electron withdrawing p-chloro or electron donating p-methoxy groups respectively (Figure A18). According to our theory, the electron withdrawing p-chloro substituent of **A12** should decrease the amide pK_a and consequently increase the amide anion concentration ([CON^-PhCl]) resulting in an increased rate of degradation by N-5 cyclization/elimination as compared to **41**. Conversely, electron donating p-methoxy substitution should increase the amide pK_a of **A13** relative to **41** and decrease the rate of degradation by N-5 cyclization/elimination as compared to **41**. Meanwhile we have already shown in Chapter IV Section II that **41** degrades significantly faster than **42** by N-5 cyclization/elimination. It should therefore hold true that $pK_{a41} < pK_{a42}$. Indirect evidence of the relative pK_a values of **41** and **42** can be inferred by noting the relative chemical shifts of the amide N-H protons in Figures 4.16 and 4.17 respectively (Chapter IV Section II). The N-H chemical shift (600 MHz, DMF-d_7) of **41** (9.64 ppm) is significantly downfield shifted compared to the N-H chemical shift of **42** (8.34 ppm). Greater deshielding of the N-H proton of **41** relative to **42** is indicative of increased acidity (lower pK_a).

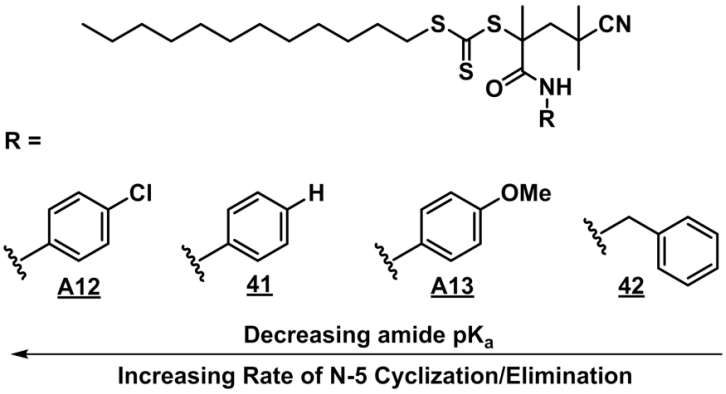

Figure A18. Proposed inverse relationship between amide pK_a and apparent amide nucleophilicity.

In this work, we will study the influence of amide substituent, solvent polarity, temperature, and acid/base catalysis on the kinetics of N-5 cyclization/elimination of the SMUI adducts **41**, **42**, **A12**, and **A13** in order to test our theory of N-arylamide nucleophilicity. This work is currently on-going and therefore the following results and conclusions are incomplete. However, the results reported herein thus far support our current theory of N-arylamide nucleophilicity.

Experimental

4-Chlorophenylmethacrylamide ***A14***

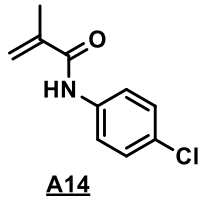

A14

Methacryloyl chloride (5.83 mL, 59.7 mmol) was added dropwise over 15 min to a stirred solution of 4-chloroaniline (7.25 g, 56.8 mmol) and triethylamine (8.32 mL, 59.7 mmol) in CH_2Cl_2 (150 mL) that was previously cooled using an ice bath. Upon complete addition of methacryloyl chloride, the reaction was stirred at 0 °C for 30 min followed by stirring at room temperature for an additional 60 min. The reaction mixture was then transferred to a separatory funnel and washed with 0.1 N HCl (1 × 150 mL), saturated $NaHCO_3$ (1 × 150 mL), and saturated NaCl (brine) (1 × 150 mL) before drying over $MgSO_4$. The solvent was removed via rotary evaporation and the isolated solids recrystallized from hot hexanes:THF (90:10) to yield **A14** (10.05 g, 90%) as colorless needle-like crystals. ^{1}H NMR (300 MHz, $CDCl_3$): δ 7.52 (s, 1H), 7.43 (d, 2H), 7.23 (d, 2H), 5.72 (s, 1H), 5.40 (s, 1H), 1.98 (s, 3H).

4-Methoxyphenylmethacrylamide ***A15***

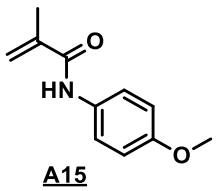

A15

Methacryloyl chloride (5.83 mL, 59.7 mmol) was added dropwise over 15 min to a stirred solution of p-anisidine (7.00 g, 56.8 mmol) and triethylamine (8.32 mL, 59.7 mmol) in CH_2Cl_2 (150 mL) that was previously cooled using an ice bath. Upon complete

addition of methacryloyl chloride, the reaction was stirred at 0 °C for 30 min followed by stirring at room temperature for an additional 60 min. The reaction mixture was then transferred to a separatory funnel and washed with 0.1 N HCl (1 × 150 mL), saturated $NaHCO_3$ (1 × 150 mL), and saturated NaCl (brine) (1 × 150 mL) before drying over $MgSO_4$. The solvent was removed via rotary evaporation and the isolated solids recrystallized from hot hexanes:THF (90:10) to yield **A15** (7.60 g, 70%) as colorless needle-like crystals. ^{1}H NMR (300 MHz, $CDCl_3$): δ 7.38 (d, 3H), 6.79 (d, 2H), 5.71 (s, 1H), 5.37 (s, 1H), 3.73 (s, 2H), 1.99 (s, 3H).

*Synthesis of **A12***

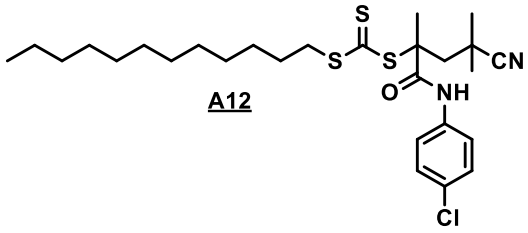

A12

A solution of **27** (3.41 g, 9.9 mmol), **A14** (1.93 g, 9.9 mmol), and V-70 (0.609 g, 2.0 mmol) in DMF (35 mL) was prepared in a round bottomed flask equipped with magnetic stir bar and the reaction degassed via three freeze-pump-thaw cycles and backfilled with argon. The reaction mixture was heated at 30 °C in an oil bath for 48 h, followed by exposure to air and freezing in liquid N_2. The reaction mixture was then diluted with EtOAc (150 mL) and transferred to a separatory funnel and washed with 75% brine (1 × 150 mL), H_2O (1 × 150 mL), brine (1 × 150 mL), and dried over $MgSO_4$. The crude product was then purified by column chromatography (85:15 Hexanes:EtOAc, R_f = 0.20) yielding **A12** (0.427 g, 8%) as a yellow solid. ^{1}H NMR (300 MHz, $CDCl_3$): δ 8.41 (s, 1H), 7.32 (d, 2H), 7.23 (d, 2H), 3.20 (t, 2H), 2.47 (s, 2H), 1.95 (s, 3H), 1.56 (b, 2H), 1.41 (d, 6H), 1.18 (b, 18H), 0.81 (t, 3H).

*Synthesis of **A13***

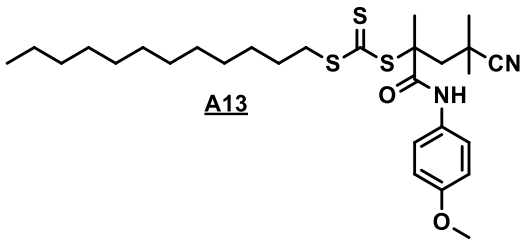

A13

A solution of **27** (3.41 g, 9.9 mmol), **A15** (1.89 g, 9.9 mmol), and V-70 (0.609 g, 2.0 mmol) in DMF (35 mL) was prepared in a round bottomed flask equipped with magnetic stir bar and the reaction degassed via three freeze-pump-thaw cycles and backfilled with argon. The reaction mixture was heated at 30 °C in an oil bath for 48 h, followed by exposure to air and freezing in liquid N_2. The reaction mixture was then diluted with EtOAc (150 mL) and transferred to a separatory funnel and washed with 75% brine (1 × 150 mL), H_2O (1 × 150 mL), brine (1 × 150 mL), and dried over $MgSO_4$. The crude product was then purified by column chromatography (75:25 Hexanes:EtOAc, R_f = 0.28) yielding **A13** (0.452 g, 9%) as a yellow solid. ^{1}H NMR (300 MHz, $CDCl_3$): δ 8.26 (s, 1H), 7.26 (d, 2H), 6.78 (d, 2H), 3.72 (s, 3H), 3.21 (t, 2H), 2.48 (s, 2H), 1.96 (s, 3H), 1.58 (b, 2H), 1.40 (d, 6H), 1.18 (b, 18H), 0.81 (t, 3H).

In situ ^{1}H NMR Analysis

A representative procedure is as follows: A solution of **41** (2×10^{-2} M) in DMSO-d_6 (0.6 mL) was prepared in an NMR tube equipped with pierceable rubber septum and the solvent degassed by two freeze-pump-thaw cycles followed by backfilling the NMR tube with argon. ^{1}H NMR spectra were acquired at predetermined temperatures using a Bruker Ascend™ 600 MHz spectrometer.

Results and Discussion

If the rate determining step of N-5 cyclization/elimination of **41** is dependent upon [CON$^-$Ph], a non-nucleophilic base should catalyze the reaction by promoting the formation of the nucleophilic CON$^-$Ph species. To this end, we examined the effect of triethylamine (TEA) (pK_a = 9.00, DMSO)[334] as a base catalyst for N-5 cyclization/elimination of **41** in DMSO-d_6 at room temperature (23 °C). As shown in Figure A19, 100% degradation of **41** was observed within the time required to obtain the first spectrum (5 min) with peaks corresponding to the degradation byproducts given prime designation. In contrast, the half life of **41** in DMF-d_7 at 70 °C in the absence of TEA was measured to be $t_{1/2}$ = 7.18 h (Chapter IV Section II).

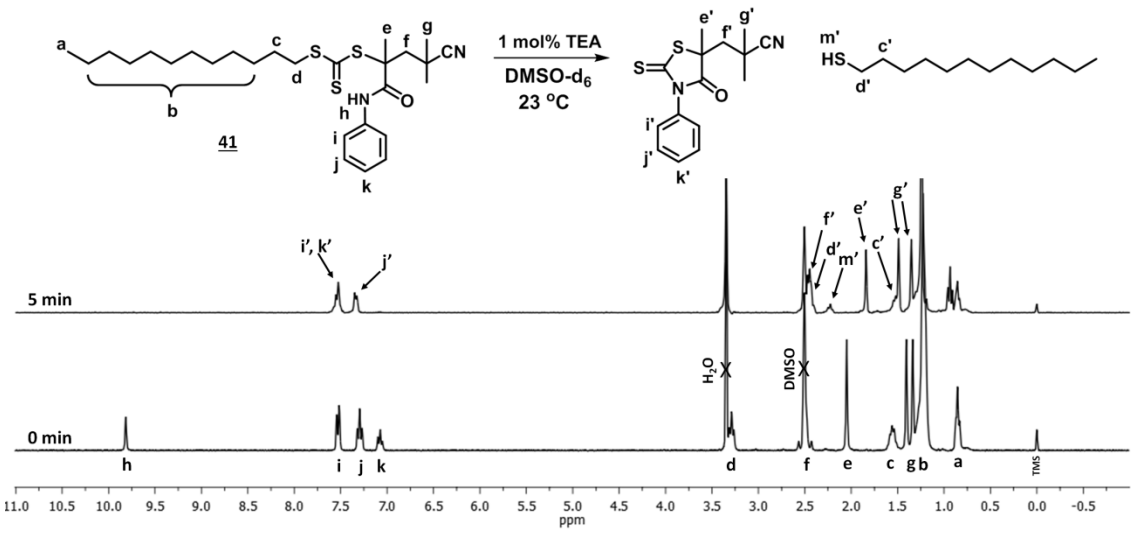

Figure A19. ^{1}H NMR (300 MHz, DMSO-d_6) overlay following the TEA-catalyzed degradation of **41** at room temperature.

Base-catalyzed degradation of **41** is evidence of the rate determining step of N-5 cyclization/elimination being dependent upon [CON$^-$Ph]. Consequently, we can develop a kinetic theory based upon Scheme A2 where the rate of irreversible trithiocarbonate

(TTC) degradation due to intramolecular nucleophilic attack by an adjacent amide can be expressed as follows:

$$Rate = -\frac{d[TTC]}{dt} = k_{app}[CONHR]_{tot} \quad \text{(A1)}$$

where [TTC] is the concentration of **41**, $[CONHR]_{tot}$ is the total concentration of associated and dissociated amide, and k_{app} is the apparent rate constant for intramolecular nucleophilic attack. Assuming that nucleophilic attack (pathway A and/or B, Scheme A2) is the rate determining step, the total rate of trithiocarbonate degradation can be expressed as the sum of the rates of degradation by both N-5 and O-5 intramolecular nucleophilic attack:

$$-\frac{d[TTC]}{dt} = k_1[CON^-R] + k_2[CONHR] \quad \text{(A2)}$$

where $[CON^-R]$ is the concentration of amide anion, [CONHR] is the concentration of neutral amide, and k_1 and k_2 are the first order rate constants for N-5 and O-5 nuclephilic attack respectively. We have shown that degradation of **41** occurs exclusively by N-5 cyclization such that $k_2 = 0$. This allows for simplification of Eq A2 to the following:

$$-\frac{d[TTC]}{dt} = k_1[CON^-R] \quad \text{(A3)}$$

The quantity $[CON^-R]$, which cannot be measured directly, can be determined from the measurable quantity [CONHR] and the dissociation constant (K_a) according to the equilibrium shown in Eq A4.

$$[CONHR] \leftrightarrows [CON^-R][H^+] \quad \text{(A4)}$$

$$K_a = \frac{[CON^-R][H^+]}{[CONHR]} \tag{A5}$$

In the absence of external acid or base, $[CON^-R] = [H^+]$ such that:

$$[CON^-R] = K_a^{\frac{1}{2}}[CONHR]^{\frac{1}{2}} \tag{A6}$$

Substitution of Eq A6 into Eq A3 gives:

$$-\frac{d[TTC]}{dt} = k_1 K_a^{\frac{1}{2}}[CONHR]^{\frac{1}{2}} \tag{A7}$$

The total trithiocarbonate concentration [TTC], which is equal to the total amide concentration ($[CONHR]_{tot}$) can be expressed as:

$$[TTC] = [CONHR]_{tot} = [CONHR] + [CON^-R] \tag{A8}$$

When K_a is small and $[CONHR] >> [CON^-R]$, Eq A8 simplifies to [TTC] = [CONHR] and can be substituted into Eq A7 to give:

$$-\frac{d[TTC]}{dt} = k_1 K_a^{\frac{1}{2}}[TTC]^{\frac{1}{2}} \tag{A9}$$

Integration of Eq. A9 using the integral form of an n^{th} order rate equation (Eq A10) gives the final integrated rate equation of trithiocarbonate degradation by N-5 cyclization (Eq. A11).

$$\frac{1}{[A]^{n-1}} = \frac{1}{[A]_0^{n-1}} + (n-1)kt \tag{A10}$$

$$[\boldsymbol{TTC}]^{\frac{1}{2}} = [\boldsymbol{TTC}]_{\boldsymbol{0}}^{\frac{1}{2}} - \frac{\boldsymbol{1}}{\boldsymbol{2}}\boldsymbol{k_1 K_a^{\frac{1}{2}} t} \qquad \text{(A11)}$$

According to Eq A11, plotting $[TTC]^{1/2}$ versus time will give the y-intercept = $[TTC]_0^{1/2}$ and slope = $-(1/2)k_1K_a^{1/2}$.

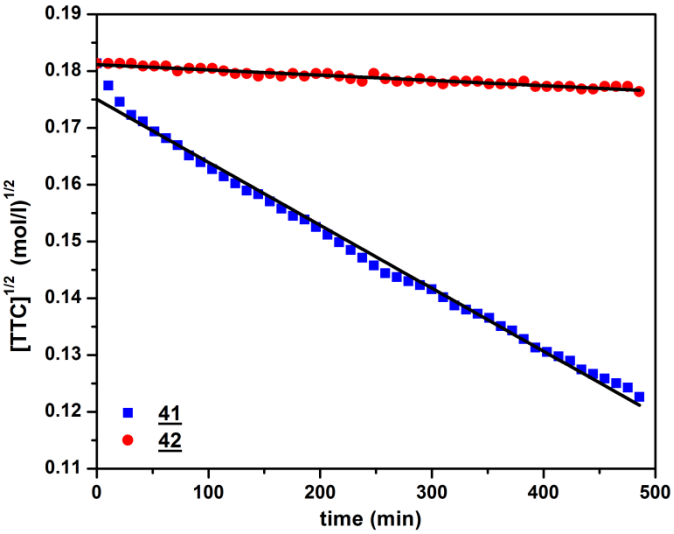

Figure A20. $[TTC]^{1/2}$ vs time plots for the degradation of **41** and **42** in DMF-d_7 at 70 °C ($[TTC]_0$ = 0.0329 M).

We next used Eq A11 to replot the kinetic data obtained previously for the degradation reactions of **41** and **42** from Figures 4.18a and 4.18b respectively (Chapter IV Section II). As shown in Figure A20, the graph of $[TTC]^{1/2}$ vs time yields linear plots for the degradation of **41** and **42** in DMF-d_7 at 70 °C. The $k_1K_a^{1/2}$ values for **41** and **42** in DMF at 70 °C were calculated from the slopes of the linear plots in Figure A20 to be 2.22×10^{-4} $M^{1/2}$ s^{-1} and 1.86×10^{-5} $M^{1/2}$ s^{-1} respectively. However, in order for k_1 to be determined, K_a for the amide must be known.

While K_a for the amides of interest in this study (**41**, **42**, **A12**, **A13**) could be measured by potentiometric or photometric titrations in DMSO using a strong base such as sodium dimsyl,[335] rapid trithiocarbonate degradation would likely occur due to nucleophilic attack of the thiocarbonyl by the dimsyl anion and also as a result of base-catalyzed N-5 cyclization. Therefore an alternative method of determining K_a *in situ* is desired. This can be accomplished by disturbing the amide dissociation equilibrium (Eq 4) via the addition of a known amount of strongly dissociating "super acid," such as bis trifluoromethanesulfonimide, and measuring the effect of $[H^+]$ on k_{app} (Eq 1) which is a function of both k_1 and K_a. If the dissociation constant of the acid ($K_{a,acid}$) is suitably large compared to K_a of the amide, $[H^+] \approx [HX]$ where [HX] is the concentration of externally added acid. The relationship between [HX] and $[CON^-R]$ can then be expressed as follows:

$$[CON^-R] = \frac{K_a[CONHR]}{[HX]} \tag{A12}$$

Combination of Eq A1, Eq A3, and Eq A12 gives:

$$k_{app}[TTC] = \frac{k_1 K_a[CONHR]}{[HX]} \tag{A13}$$

Recalling that [TTC]≈[CONHR], Eq A13 can be simplified to:

$$\boldsymbol{k_{app} = \frac{k_1 K_a}{[HX]}} \tag{A14}$$

Plotting k_{app} vs. $[HX]^{-1}$ would yield a slope = k_1K_a. K_a can then be determined by combining the slopes from Eq A11 and Eq A14:

$$k_1 = \frac{-2slope_1}{K_a^{\frac{1}{2}}} \text{ (from Eq 11)} \quad \text{(A15)}$$

$$k_1 = \frac{slope_2}{K_a} \text{ (from Eq 14)} \quad \text{(A16)}$$

$$\boldsymbol{K_a = \frac{1}{4}\left(\frac{slope_2}{slope_1}\right)^2} \quad \text{(A17)}$$

where $slope_1$ is the slope of $[TTC]^{1/2}$ vs. time plot (Eq A11) and $slope_2$ is the slope of k_{app} vs. $[HX]^{-1}$ plot (Eq A14).

Despite not yet knowing the K_a values for the amides of interest in this study, we can make the following predictions regarding the influence of amide substituents on the values of k_1 and K_a for uncatalyzed N-5 cyclization/elimination reactions.

1) Electron withdrawing substituents will *increase* the value of K_a.

Electron withdrawing substituents will stabilize the conjugate base of the amide and thus shift the equilibrium towards the dissociated amide anion thus increasing the value of K_a.

2) Electron withdrawing substituents will *reduce* the value of k_1.

At first this seems counterintuitive since we predict that electron withdrawing substituents will increase the rate of degradation by N-5 cyclization/elimination. However, k_1 is a function of the relative nucleophilicity of the amide anion. Electron withdrawing substituents will increase the stability of the amide anion relative to electron donating substituents and consequently reduce the nucleophilicity (and reduce k_1) of the amide anion. Accordingly, we predict that electron withdrawing stubstituents will cause

$K_a^{1/2}$ to increase *more* than k_1 will decrease, such that the product of $k_1K_a^{1/2}$, which is directly proportional to the rate of degradation by N-5 cyclization, will increase. In other words, the increase in concentration of the nucleophilic species [CON^-Ph] more than compensates for the reduced nucleophilicity of that species.

We can initially evaluate these predictions if we assume the pK_a values of **41** and **42** in DMF-d_7 are similar to the pK_a values of N-phenylacetamide (pK_a = 21.5, DMSO) and N-methylacetamide (pK_a = 25.9, DMSO) respectively. Using these estimated pK_a values for **41** and **42** along with the $k_1K_a^{1/2}$ values determined previously from the slopes of the kinetic plots in Figure A20, we calculated the k_1 values for degradation by N-5 cyclization/elimination of **41** and **42** to be 1.25×10^7 $M^{1/2}$ s^{-1} and 1.66×10^8 $M^{1/2}$ s^{-1} respectively. As predicted, the k_1 value of the more acidic amide (**41**) is lower (by ~1 order of magnitude) than the k_1 value for the less acidic amide (**42**) despite the rate of N-5 cyclization/elimination of **41** being greater than that of **42**.

Conclusions

We have estabilised a mechanistic theory in order to explain the influence of N-aryl substitution on the observed relative rates of N-5 cyclization/elimination of **41** and **42** at elevated temperatures. In addition, we have developed a kinetic model based upon the "amide dissociation mechanism" which thus far fits the previously obtained kinetic data. We also show that degradation by N-5 cyclization/elimination is base catalyzed and we are currently investigating the influence of electron withdrawing/donating substituents and solvent polarity on the N-5 cyclization/elimination rate constants (k_1) and dissociation constants (K_a) of select amides. Ultimately, this work has the potential to provide greater insights into the nucleophilic character of amides.

REFERENCES

(1) Ringsdorf, H. *J. Polym. Sci. Polym. Symp.* **1975**, *51*, 135–153.

(2) Vicent, M. J.; Ringsdorf, H.; Duncan, R. *Adv. Drug Deliv. Rev.* **2009**, *61*, 1117–1120.

(3) Christie, R. J.; Nishiyama, N.; Kataoka, K. *Endocrinology* **2010**, *151*, 466–473.

(4) Grigsby, C. L.; Leong, K. W. *J. R. Soc. Interface* **2010**, *7*, S67–S82.

(5) Higuchi, Y.; Kawakami, S.; Hashida, M. *BioDrugs* **2010**, *24*, 195–205.

(6) Oh, Y.; K. Park, T. G. *Adv. Drug Deliv. Rev.* **2009**, *61*, 850–862.

(7) Pichon, C.; Billiet, L.; Midoux, P. *Curr. Opin. Biotechnol.* **2010**, *21*, 640–645.

(8) Roth, C. M. *Biotechnol. Prog.* **2008**, *24*, 23–28.

(9) Wang, X.; Zhou, L.; Ma, Y.; Li, X.; Gu, H. *Nano Res.* **2009**, *2*, 365–372.

(10) Markovsky, E.; Baabur-Cohen, H.; Eldar-Boock, A.; Omer, L.; Tiram, G.; Ferber, S.; Ofek, P.; Polyak, D.; Scomparin, A.; Satchi-Fainaro, R. *J. Control. Release* **2012**, *161*, 446–460.

(11) Marschall, A. L.; Frenzel, A.; Schirrmann, T.; Schungel, M.; Dube, S. *MAbs* **2011**, *3*, 3–16.

(12) Wang, J.; Lu, Z.; Wientjes, G.; Au, J. L.-S. *Am. Assoc. Pharm. Sci.* **2010**, *12*, 492–503.

(13) Bader, H.; Ringsdorf, H.; Schmidt, B. *Angew. Makromol. Chemie* **1984**, *123*, 457–485.

(14) Liu, S.; Armes, S. P. *J. Am. Chem. Soc.* **2001**, *123*, 9910–9911.

(15) McCormick, C. L.; Lowe, A. B. *Acc. Chem. Res.* **2004**, *37*, 312–325.

(16) Fang, J.; Nakamura, H.; Maeda, H. *Adv. Drug Deliv. Rev.* **2011**, *63*, 136–151.

(17) Matsumura, Y.; Maeda, H. *Cancer Res.* **1986**, *46*, 6387–6392.

(18) Christie, R. J.; Grainger, D. W. *Adv. Drug Deliv. Rev.* **2003**, *55*, 421–437.

(19) Etrych, T.; Jelinkova, M.; Rihova, B.; Ulbrich, K. *J. Control. Release* **2001**, *73*, 89–102.

(20) Ulbrich, K.; Subr, V. *Adv. Drug Deliv. Rev.* **2004**, *56*, 1023–1050.

(21) Lembo, D.; Cavalli, R. *Antivir. Chem. Chemother.* **2010**, *21*, 53–70.

(22) York, A. W.; Zhang, Y.; Holley, A. C.; Guo, Y.; Huang, F.; McCormick, C. L. *Biomacromolecules* **2009**, *10*, 936–943.

(23) Gebhart, C. L.; Kabanov, A. V. *J. Control. Release* **2001**, *73*, 401–416.

(24) Kabanov, A. V; Kabanov, V. A. *Adv. Drug Deliv. Rev.* **1998**, *30*, 49–60.

(25) Merdan, T.; Kunath, K.; Fischer, D.; Kopecek, J.; Kissel, T. *Pharm. Res.* **2002**, *19*, 140–146.

(26) Dash, P. R.; Read, M. L.; Barrett, L. B.; Wolfert, M. A.; Seymour W. L. *Gene Ther.* **1999**, *6*, 643–650.

(27) Zou, S. M.; Erbacher, P.; Remy, J. S.; Behr, J. P. *J. Gene Med.* **2000**, *2*, 128–134.

(28) Kabanov, A. V.; Vinogradov, S. V.; Suzdaltseva, Y. G.; Alakhov, V. Y. *Bioconjug. Chem.* **1995**, *6*, 639–643.

(29) Greenwald, R. B. *J. Control. Release* **2001**, *74*, 159–171.

(30) Etrych, T.; Jelnkova, M.; Rihova, B.; Ulbrich, K. *J. Control. Release* **2001**, *73*, 89–102.

(31) Kovar, M.; Kovar, L.; Subr, V.; Etrych, T.; Ulbrich, K.; Mrkvan, T.; Loucka, J.; Rihova, B. *J. Control. Release* **2004**, *99*, 301–314.

(32) Subr, V.; Konak, C.; Laga, R.; Ulbrich, K. *Biomacromolecules* **2006**, *7*, 122–130.

(33) Liechty, W. B.; Kryscio, D. R.; Slaughter, B. V.; Peppas, N. A. *Annu Rev Chem Biomol Eng.* **2010**, *1*, 149–173.

(34) Simone, E.; Ding, B. S.; Muzykantov, V. *Cell Tissue Res.* **2009**, *335*, 283–300.

(35) Fischbach, C.; Mooney, D. J. *Biomaterials* **2007**, *28*, 2069–2076.

(36) Jensen, M.; Berthold, F. *Cancer Lett.* **2007**, *258*, 9–21.

(37) Qian, Z. M.; Li, H.; Sun, H.; Ho, K. *Pharmacol. Rev.* **2002**, *54*, 561–587.

(38) Pasqualini, R.; Koivunen, E.; Kain, R.; Lahdenranta, J.; Sakamoto, M.; Stryhn, A.; Ashmun, R. A.; Shapiro, L. H.; Arap, W.; Ruoslahti, E. *Cancer Res.* **2000**, *60*, 722–727.

(39) Pierschbacher, M. D.; Ruoslahti, E. *Proc. Natl. Acad. Sci.* **1984**, *81*, 5985–5988.

(40) Ulbrich, K.; Etrych, T.; Chytil, P.; Jelinkova, M.; Rihova, B. *J. Drug Target.* **2004**, *12*, 477–489.

(41) Miller, K.; Erez, R.; Segal, E.; Shabat, D.; Satchi-Fainaro, R. *Angew. Chem. Int. Ed.* **2009**, *48*, 2949–2954.

(42) Chapman, A. P. *Adv. Drug Deliv. Rev.* **2002**, *54*, 531–545.

(43) Lu, Z.-R.; Kopecková, P.; Kopecek, J. *Nat. Biotechnol.* **1999**, *17*, 1101–1104.

(44) Lu, Z.-R.; Shiah, J.-G.; Kopecková, P.; Kopecek, J. *J. Control. Release* **2001**, *74*, 263–268.

(45) Gabius, H. J.; Siebert, H. C.; Andre, S.; Jimenez-Barbero, J.; Ruediger, H. *ChemBioChem* **2004**, *5*, 740–764.

(46) York, A. W.; Huang, F.; McCormick, C. L. *Biomacromolecules* **2010**, *11*, 505–514.

(47) Lu, Y.; Low, P. S. *Adv. Drug Deliv. Rev.* **2002**, *54*, 675–693.

(48) Rejman, J.; Oberle, V.; Zuhorn, I. S.; Hoekstra, D. *Biochem. J.* **2004**, *377*, 159–169.

(49) Rybak, S. L.; Murphy, R. F. *J. Cell. Physiol.* **1998**, *176*, 216–222.

(50) Rybak, S. L.; Lanni, F.; Murphy, R. F. *Biophys. J.* **1997**, *73*, 674–687.

(51) Gaynor, J. W.; Campbell, B. J.; Cosstick, R. *Chem. Soc. Rev.* **2010**, *39*, 4169–4184.

(52) Pack, D. W.; Hoffman, A. S.; Pun, S.; Stayton, P. S. *Nat. Rev. Drug Discov.* **2005**, *4*, 581–593.

(53) Merdan, T.; Kopecek, J.; Kissel, T. *Adv. Drug Deliv. Rev.* **2002**, *54*, 715–758.

(54) Funhoff, A. M.; van Nostrum, C. F.; Koning, G. A.; Schuurmans-Nieuwenbroek, N. M. E.; Crommelin, D. J. A.; Hennink, W. E. *Biomacromolecules* **2004**, *5*, 32–39.

(55) Henry, S. M.; El-Sayed, M. E. H.; Pirie, C. M.; Hoffman, A. S.; Stayton, P. S. *Biomacromolecules* **2006**, *7*, 2407–2414.

(56) Wang, X.-L.; Xu, R.; Lu, Z.-R. *J. Control. Release* **2009**, *134*, 207–213.

(57) Jones, R. a; Cheung, C. Y.; Black, F. E.; Zia, J. K.; Stayton, P. S.; Hoffman, A. S.; Wilson, M. R. *Biochem. J.* **2003**, *372*, 65–75.

(58) Gillies, E. R.; Goodwin, A. P.; Frechet, J. M. J. *Bioconjug. Chem.* **2004**, *15*, 1254–1263.

(59) Ulbrich, K.; Etrych, T.; Chytil, P.; Pechar, M.; Jelinkova, M.; Rihova, B. *Int. J. Pharm.* **2004**, *277*, 63–72.

(60) Hoste, K.; De Winne, K.; Schacht, E. *Int. J. Pharm.* **2004**, *277*, 119–131.

(61) Ulbrich, K.; Subr, V. *Adv. Drug Deliv. Rev.* **2010**, *62*, 150–166.

(62) Murthy, N.; Campbell, J.; Fausto, N.; Hoffman, A. S.; Stayton, P. S. *Bioconjug. Chem.* **2003**, *14*, 412–419.

(63) Murthy, N.; Campbell, J.; Fausto, N.; Hoffman, A. S.; Stayton, P. S. *J. Control. Release* **2003**, *89*, 365–374.

(64) Etrych, T.; Krakovicova, H.; Sirova, M.; Rihova, B.; Ulbrich, K. *J. Control. Release* **2008**, *132*, 184–192.

(65) Yang, N.; Ye, Z.; Li, F.; Mahato, R. I. *Bioconjug. Chem.* **2009**, *20*, 213–221.

(66) Omelyanenko, V.; Kopeckova, P.; Gentry, C.; Kopecek, J. *J. Control. Release* **1998**, *53*, 25–37.

(67) Jia, Z.; Wong, L.; Davis, T. P.; Bulmus, V. *Biomacromolecules* **2008**, *9*, 3106–3113.

(68) Wong, L.; Boyer, C.; Jia, Z.; Zareie, H. M.; Davis, T. P.; Bulmus, V. *Biomacromolecules* **2008**, *9*, 1934–1944.

(69) Zhang, L.; Liu, W.; Lin, L.; Chen, D.; Stenzel, M. H. *Biomacromolecules* **2008**.

(70) Balendiran, G. K.; Dabur, R.; Fraser, D. *Cell Biochem. Funct.* **2004**, *22*, 343–352.

(71) Nori, A.; Kopecek, J. *Adv. Drug Deliv. Rev.* **2005**, *57*, 609–636.

(72) Campolongo, M. J.; Luo, D. *Nat. Mater.* **2009**, *8*, 447–448.

(73) Ang, G.; Uludag, H. *Expert Opin. Drug Deliv.* **2008**, *5*, 499–515.

(74) Shrivastava, P. K. Shrivastava, S. K. *Int. J. Pharm. Sci.* **2009**, *1*, 353–368.

(75) Lammers, T. *Adv. Drug Deliv. Rev.* **2010**, *62*, 203–230.

(76) Hawker, C. J.; Bosman, A. W.; Harth, E. *Chem. Rev.* **2001**, *101*, 3661–3688.

(77) Grubbs, R. B. *Polym. Rev.* **2011**, *51*, 104–137.

(78) Kato, M.; Kamigaito, M.; Sawamoto, M.; Higashimura, T. *Macromolecules* **1995**,

28, 1721–1723.

(79) Wang, J.-S.; Matyjaszewski, K. *J. Am. Chem. Soc.* **1995**, *117*, 5614–5615.

(80) Matyjaszewski, K.; Xia, J. *Chem. Rev.* **2001**, *101*, 2921–2990.

(81) Matyjaszewski, K. *Macromolecueles* **2012**, *45*, 4015–4039.

(82) Chiefari, J.; Chong, Y. K. B.; Ercole, F.; Krstina, J.; Jeffery, J.; Le, T. P. T.; Mayadunne, R. T. A.; Meijs, G. F.; Moad, C. L.; Moad, G.; Rizzardo, E.; Thang, S. H.; South, C. *Macromolecules* **1998**, *9297*, 5559–5562.

(83) Moad, G.; Rizzardo, E.; Thang, S. H. *Aust. J. Chem.* **2005**, *58*, 379–410.

(84) Moad, G.; Rizzardo, E.; Thang, S. H. *Aust. J. Chem.* **2006**, *59*, 669–692.

(85) Moad, G.; Rizzardo, E.; Thang, S. H. *Polymer* **2008**, *49*, 1079–1131.

(86) Moad, G.; Rizzardo, E.; Thang, S. H. *Acc. Chem. Res.* **2008**, *41*, 1133–1142.

(87) Moad, G.; Rizzardo, E.; Thang, S. H. *Aust. J. Chem.* **2009**, *62*, 1402–1472.

(88) Lowe, A. B.; McCormick, C. L. *Acs Symp. Ser.* **2006**, *937*, 65–78.

(89) Lowe, A. B.; McCormick, C. L. *Prog. Polym. Sci.* **2007**, *32*, 283–351.

(90) Sumerlin, B. S.; Donovan, M. S.; Mitsukami, Y.; Lowe, A. B.; McCormick, C. L. *Macromolecules* **2001**, *34*, 6561–6564.

(91) Donovan, M. S.; Sanford, T. A.; Lowe, A. B.; Sumerlin, B. S.; Mitsukami, Y.; McCormick, C. L. *Macromolecules* **2002**, *35*, 4570–4572.

(92) Donovan, M. S.; Sumerlin, B. S.; Lowe, A. B.; McCormick, C. L. *Macromolecules* **2002**, *35*, 8663–8666.

(93) Lowe, A. B.; Sumerlin, B. S.; McCormick, C. L. *Polymer* **2003**, *44*, 6761–6765.

(94) Thomas, D. B.; Sumerlin, B. S.; Lowe, A. B.; McCormick, C. L. *Macromolecules* **2003**, *36*, 1436–1439.

(95) Thomas, D. B.; Convertine, A. J.; Myrick, L. J.; Scales, C. W.; Smith, A. E.; Lowe, A. B.; Vasilieva, Y. A.; Ayres, N.; McCormick, C. L. *Macromolecules* **2004**, *37*, 8941–8950.

(96) Scales, C. W.; Vasilieva, Y. a; Convertine, A. J.; Lowe, A. B.; McCormick, C. L. *Biomacromolecules* **2005**, *6*, 1846–1850.

(97) Abel, B. A.; Sims, M. B.; McCormick, C. L. *Macromolecules* **2015**, *48*, 5487–5495.

(98) Treat, N. J.; Smith, D.; Teng, C.; Flores, J. D.; Abel, B. A.; York, A. W.; Huang, F.; McCormick, C. L. *ACS Macro Lett.* **2011**, *1*, 100–104.

(99) Donovan, M. S.; Lowe, A. B.; Sanford, T. A.; McCormick, C. L. *Polymer* **2003**, *41*, 1262–1281.

(100) Donovan, M. S.; Lowe, A. B.; Sumerlin, B. S.; McCormick, C. L. *Macromolecules* **2002**, *35*, 4123–4132.

(101) Stenzel, M. H.; Cummins, L.; Roberts, G. E.; Davis, T. P.; Vana, P.; Bamer-Kowollik, C. *Macromol. Chem. Phys.* **2003**, *204*, 1160–1168.

(102) Perrier, S.; Bamer-Kowollik, C.; Quinn, J. F.; Vana, P.; Davis, T. P. *Macromolecules* **2002**, *35*, 8300–8306.

(103) Vana, P.; Davis, T. P.; Bamer-Kowollik, C. *Macromol. Theory Simul.* **2002**, *11*, 823–835.

(104) Schilli, C.; Lanzendoerfer, M. G.; Mueller, A. H. E. *Macromolecules* **2002**, *35*, 6819–6827.

(105) Bamer-Kowollik, C.; Quinn, J. F.; Morsley, D. R.; Davis, T. P. *J. Polym. Sci. Part A Polym. Chem.* **2001**, *39*, 1353–1365.

(106) McLeary, J. B.; Calitz, F. M.; McKenzie, J. M.; Tonge, M. P.; Sanderson, R. D.; Klumperman, B. *Macromolecules* **2004**, *37*, 2383–2394.

(107) Barner-Kowollik, C.; Buback, M.; Charleux, B.; Coote, M. L.; Drache, M.; Fukuda, T.; Goto, A.; Klumperman, B.; Lowe, A. B.; McLeary, J. B.; Moad, G.; Monteiro, M. J.; Sanderson, R. D.; Tonge, M. P.; Vana, P. *J. Polym. Sci. Part A Polym. Chem.* **2006**, *44*, 5809–5831.

(108) Wang, A. R.; Zhu, S. *J. Polym. Sci. Part A Polym. Chem.* **2003**, *41*, 1553–1566.

(109) Bamer-Kowollik, C.; Coote, M. L.; Davis, T. P.; Radom, L.; Vana, P. *J. Polym. Sci. Part A Polym. Chem.* **2003**, *41*, 2828–2832.

(110) Wang, A. R.; Zhu, S.; Kwak, Y.; Goto, A. .; Fukuda, T.; Monteiro, M. S. . *J. Polym. Sci. Part A Polym. Chem.* **2003**, *41*, 2833–2839.

(111) Coote, M. L.; Radom, L. *J. Am. Chem. Soc.* **2003**, *125*, 1490–1491.

(112) Hawthorne, D. G.; Moad, G.; Rizzardo, E.; Thang, S. H. *Macromolecules* **1999**, *32*, 5457–5459.

(113) Kwak, Y.; Goto, A.; Tsujii, Y.; Murata, Y.; Komatsi, K.; Fukuda, T. *Macromolecules* **2002**, *35*, 3026.

(114) Lberti, A.; Benaglia, M.; Laus, M.; Macciantelli, D.; Spamacci, K. *Macromolecules* **2003**, *36*, 736–740.

(115) Calitz, F. M.; Tonge, M. P.; Sanderson, R. D. *Macromolecules* **2003**, *36*, 5–8.

(116) Ladaviere, C.; Dorr, N.; Claverie, J. P. *Macromolecules* **2001**, *34*, 5370–5372.

(117) Bamer-Kowollik, C.; Vana, P.; Quinn, J. F.; Davis, T. P. *J. Polym. Sci. Part A Polym. Chem.* **2002**, *40*, 1058–1063.

(118) Vana, P.; Albertin, L.; Bamer, L.; Davis, T. P.; Bamer-Kowollik, C. *J. Polym. Sci.*

Part A Polym. Chem. **2002**, *40*, 4032–4037.

(119) Thomas, D. B.; Convertine, A. J.; Hester, R. D.; Lowe, A. B.; McCormick, C. L. *Macromolecules* **2004**, *37*, 1735–1741.

(120) Mayadunne, R. T. A.; Rizzardo, E.; Chiefari, J.; Kristina, J.; Moad, G.; Postma, A.; Thang, S. H. *Macromolecules* **2000**, *33*, 243–245.

(121) Francis, R.; Ajayaghosh, A. *Macromolecules* **2000**, *33*, 4699–4704.

(122) Destarac, M.; Charmot, D.; Franck, X.; Zard, S. Z. *Macromol. Rapid Commun.* **2000**, *21*, 1035–1039.

(123) Benaglia, M.; Chiefari, J.; Chong, Y. K.; Moad, G.; Rizzardo, E.; Thang, S. H. *J. Am. Chem. Soc.* **2009**, *131*, 6914–6915.

(124) Keddie, D. J.; Guerrero-Sanchez, C.; Moad, G.; Rizzardo, E.; Thang, S. H. *Macromolecules* **2011**, *44*, 6738–6745.

(125) Moad, G.; Keddie, D.; Guerrero-Sanchez, C.; Rizzardo, E.; Thang, S. H. *Macromol. Symp.* **2015**, *350*, 34–42.

(126) Skey, J.; O'Reilly, R. K. *Chem. Commun.* **2008**, *35*, 4183–4185.

(127) Wood, M. R.; Duncalf, D. J.; Rannard, S. P.; Perrier, S. *Org. Lett.* **2006**, *8*, 553–556.

(128) Coady, D. J.; Norris, B. C.; Lynch, V. M.; Bielawski, C. W. *Macromolecules* **2008**, *41*, 3775–3778.

(129) Benaglia, M.; Chiefari, J.; Chong, Y. K.; Moad, G.; Rizzardo, E.; Thang, S. H. *J. Am. Chem. Soc* **2009**, *131*, 6914–6915.

(130) Inglis, A. J.; Sinnwell, S.; Davis, T. P.; Barner-Kowoli, C.; Stenzel, M. H. *Macromolecules* **2008**, *41*, 4120–4126.

(131) Sinnwell, S.; Inglis, A. J.; Davis, T. P.; Stenzel, M. H.; Barner-Kowollik, C. *Chem. Commun.* **2008**.

(132) A. Postma, T. P. Davis, G. M. and M. S. O. *Macromolecules* **2005**, *38*, 5371–5374.

(133) Spruell, J. M.; Levy, B. A.; Sutherland, A.; Dichtel, W. R.; Cheng, J. Y.; Nelson, A.; Stoddart, F. J. *J. Polym. Sci. Part A Polym. Chem.* **2009**, *47*, 346–356.

(134) Li, M.; De, P.; Gondi, S. R.; Sumerlin, B. S. *J. Polym. Sci. Part A Polym. Chem.* **2008**, *46*, 5093–5100.

(135) Lowe, A. B.; Sumerlin, B. S.; Donovan, M. S.; McCormick, C. L. *J. Am. Chem. Soc.* **2002**, *124*, 11562–11563.

(136) Chan, J. W.; Yu, B.; Hoyle, C. E.; Lowe, A. B. *Chem. Commun.* **2008**, 4959–4961.

(137) Boyer, C.; Granville, A.; Davis, T. P.; Bulmus, V. *J. Polym. Sci. Part A Polym. Chem.* **2009**, *47*, 3773–3794.

(138) Pissuwan, D.; Boyer, C.; Gunasekaran, K.; Davis, T. P.; Bulmus, V. *Biomacromolecules* **2010**, *11*, 412–420.

(139) Moad, G.; Chong, Y. K.; Postma, A.; Rizzardo, E.; Thang, S. H. *Polymer* **2005**, *46*, 8458–8468.

(140) Chong, Y. K.; Moad, G.; Rizzardo, E.; Thang, S. H. *Macromolecules* **2007**, *40*, 4446–4455.

(141) Barner, L.; Perrier, S. In *Handbook of RAFT Polymerisation*; Barner-Kowollik, C., Ed.; Wiley-VCH, Wenheim, 2008; pp. 455–482.

(142) Perrier, S.; Takolpuckdee, P.; Mars, C. A. *Macromolecules* **2005**, *38*, 2033–2036.

(143) Schmaljohann, D. *Adv. Drug Deliv. Rev.* **2006**, *58*, 1655–1670.

(144) Smith, A. E.; Xu, X.; Mccormick, C. L. *Prog. Polym. Sci.* **2010**, *35*, 45–93.

(145) Dai, S.; Ravib, P.; Tam, K. C. *Soft Matter* **2008**, *4*, 435–449.

(146) Lokitz, B. S.; York, A. W.; Stempka, J. E.; Treat, N. D.; Li, Y.; Jarrett, W. L.; McCormick, C. L. *Macromolecules* **2007**, *40*, 6473–6480.

(147) Chong, Y. K.; Le, T. P. T.; Moad, G.; Rizzardo, E.; Thang, S. H. *Macromolecules* **1999**, *32*, 2071–2074.

(148) Wang, R.; Lowe, A. B. *J. Polym. Sci. Part A Polym. Chem.* **2007**, *45*, 2468–2483.

(149) Lowe, A. B.; Torres, M.; Wang, R. *J. Polym. Sci. Part A Polym. Chem.* **2007**, *45*, 5864–5871.

(150) Sahnoun, M.; Charreyre, M. T.; Veron, L.; Delair, T.; D'Agosto, F. *J. Polym. Sci. Part A Polym. Chem.* **2005**, *43*, 3551–3565.

(151) Yuan, J. J.; Ma, R.; Gao, Q.; Wang, Y. F.; Cheng, S. Y.; Feng, L. X. *J. Appl. Polym. Sci.* **2003**, *89*, 1017–1025.

(152) Xiong, Q. F.; Ni, P. H.; Zhang, F.; Yu, Z. Q. *Polym. Bull.* **2004**, *53*, 1–8.

(153) Mitsukami, Y.; Donovan, M. S.; Lowe, A. B.; McCormick, C. L. *Macromolecules* **2001**, *34*, 2248–2256.

(154) Morgan, S. E.; Jones, P.; Lamont, A. S.; Heidenreich, A.; McCormick, C. L. *Langmuir* **2007**, *23*, 230–240.

(155) Roy, D.; Cambre, J. N.; Sumerlin, B. S. *Prog. Polym. Sci.* **2010**, *1*, 854–859.

(156) Liu, F.; Urban, M. W. *Prog. Polym. Sci.* **2010**, *35*, 3–23.

(157) McCormick, C. L.; Kirkland, S. E.; W., Y. A. *Polym. Rev.* **2006**, *46*, 421–443.

(158) Convertine, A. J.; Ayres, N.; Scales, C. W.; Lowe, A. B.; McCormick, C. L. *Macromolecules* **2004**, *5*, 1177–1180.

(159) Li, Y.; Lokitz, B. S.; McCormick, C. L. *Angew. Chemie* **2006**, *45*, 5792–5795.

(160) Kirkland-York, S.; Hensarling, R. M.; McConaughy, S. D.; Guo, Y.; Jarrett, W. L.; McCormick, C. L. *Biomacromolecules* **2008**, *9*, 481–486.

(161) McCormick, C. L.; Sumerlin, B. S.; Lokitz, B. S.; Stempka, J. E. *Soft Matter* **2008**, *4*, 1760–1773.

(162) Cao, Y.; Zhu, X. X.; Luo, J. T.; Liu, H. Y. *Macromolecules* **2007**, *40*, 6481–6488.

(163) Xu, J.; Jiang, X. Z.; Liu, S. Y. *J. Polym. Sci. Part A Polym. Chem.* **2008**, *46*, 60–69.

(164) Ma, J.; Cheng, C.; Sun, G. R.; Wooley, K. L. *Macromolecules* **2008**, *41*, 9080–9089.

(165) Deng, J. J.; Shi, Y.; Jiang, Y. D.; Peng, Y. F.; Lu, L. C.; Cai, Y. L. *Macromolecules* **2008**, *41*, 3007–3014.

(166) Jo, Y. S.; van der Vlies, A. J.; Gantz, J.; Antonijevic, S.; Demurtas, D.; Velluto, D. *Macromolecules* **2008**, *41*, 1140–1150.

(167) Balendiran, G. K.; Dabur, R.; Fraser, D. *Cell Biochem. Funct.* **2004**, *22*, 343–352.

(168) Smith, D.; Holley, A. C.; McCormick, C. L. *Polymer* **2011**, *2*, 1428–1441.

(169) Bulmus, V.; Woodward, M.; Lin, L.; Murthy, N.; Stayton, P. S.; Hoffman, A. S. *J. Control. Release* **2003**, *93*, 105–120.

(170) El-Sayed, M. E. H.; Hoffman, A. S.; Stayton, P. S. *J. Control. Release* **2005**, *101*, 47–58.

(171) Meng, F.; Hennink, W. E.; Zhong, Z. *Biomaterials* **2009**, *30*, 2180–2198.

(172) Bulmus, V. *Polym. Chem.* **2011**, *2*, 1463–1472.

(173) Ou, M.; Wang, X.-L.; Xu, R.; Chang, C.-W.; Bull, D.; Kim, S. W. *Bioconjug. Chem.* **2008**, *19*, 626–633.

(174) Boyer, C.; Bulmus, V.; Davis, T. P.; Ladmiral, V.; Liu, J.; Perrier, S. *Chem. Rev.* **2009**, *109*, 5402–5436.

(175) Park, T. G.; Jeong, J. H.; Kim, S. W. *Adv. Drug Deliv. Rev.* **2006**, *58*, 467–486.

(176) Pack, D. W.; Hoffman, A. S.; Pun, S.; Stayton, P. S. *Nat. Rev. Drug Discov.* **2005**, *4*, 581–593.

(177) Chong, B. Y. K.; Le, T. P. T.; Moad, G.; Rizzardo, E.; Thang, S. H. *Macromolecuels* **1999**, *32*, 2071.

(178) Chernikova, E.; Terpugova, P.; Bui, C. O.; Charleux, B. *Polymer* **2003**, *44*, 4101.

(179) Moad, G.; Mayadunne, R. T. A.; Rizzardo, E.; Skidmore, M.; Thang, S. H. *Macromol. Symp.* **2003**, *192*, 1.

(180) Mayadunne, R. T. A.; Rizzardo, E.; Chiefari, J.; Krstina, J.; Moad, G.; Postma, A.; Thang, S. H. *Macromolecules* **2000**, *33*, 243.

(181) Stenzel, M. H.; Davis, T. P. *J. Polym. Sci. Part A Polym. Chem.* **2002**, *40*, 4498.

(182) Mayadunne, R. T. A.; Jeffery, J.; Moad, G.; Rizzardo, E. *Macromolecules* **2003**, *36*, 1505.

(183) Darcos, V.; Dureault, A.; Taton, D.; Gnanou, Y.; Marchand, P.; Caminade, A. M.; Majoral, J. P.; Destarac, M.; Leising, F. *Chem. Commun.* **2004**, 2110.

(184) Hao, X. J.; Nilsson, C.; Jesberger, M.; Stenzel, M. H.; Malmstrom, E.; Davis, T. P.; Ostmark, E.; Barner-Kowollik, C. *J. Polym. Sci. Part A Polym. Chem.* **2004**, *42*, 5877.

(185) You, Y. Z.; Hong, C. Y.; Pan, C. Y.; Wang, P. H. *Adv. Mater.* **2004**, *16*, 1953.

(186) Ulbrich, K.; Subr, V. *Adv. Drug Deliv. Rev.* **2010**, *62*, 150–166.

(187) Talelli, M.; Rijcken, C. J. F.; van Nostrum, C. F.; Storm, G.; Hennink, W. E. *Adv.*

Drug Deliv. Rev. **2010**, *62*, 231–239.

(188) Sheiko, S. S.; Sumerlin, B. S.; Matyjaszewski, K. *Prog. Polym. Sci.* **2008**, *33*, 759–785.

(189) Sveinbjörnsson, B. R.; Miyake, G. M.; El-Batta, A.; Grubbs, R. H. *ACS Macro Lett.* **2014**, *3*, 26–29.

(190) Zhang, M.; Mueller, A. H. E. *J. Polym. Sci. Part A Polym. Chem.* **2005**, *43*, 3461–3481.

(191) Ederle, Y.; Isel, F.; Grutke, S.; Lutz, P. *Macromol. Symp.* **1998**, *132*, 197–206.

(192) Matyjaszewski, K.; Xia, J. *Chem. Rev.* **2001**, *101*, 2921–2990.

(193) Grubbs, R. B.; Hawker, C. J.; Dao, J.; Frechet, J. M. J. *Angew. Chem. Int. Ed.* **1997**, *36*, 270–275.

(194) Venkatesh, R.; Yajjou, L.; Koning, C.; Klumperman, B. *Macromol. Chem. Phys.* **2004**, *205*, 2161–2168.

(195) Mynar, J. L.; Choi, T.-L.; Yoshida, M.; Kim, V.; Hawker, C. J.; Frechet, J. M. J. *Chem. Commun.* **2005**, *41*, 5169–5171.

(196) Helms, B.; Mynar, J. L.; Hawker, C. J.; Frechet, J. M. J. *J. Am. Chem. Soc.* **2004**, *126*, 15020–15021.

(197) Gao, H.; Matyjaszewski, K. *J. Am. Chem. Soc.* **2007**, *129*, 6633–6639.

(198) Stupp, S. I.; LeBonheur, V.; Walker, K.; Li, L. S.; Huggins, K. E.; Keser, M. *Science* **1997**, *276*, 384–389.

(199) Ruokolainen, J.; Tanner, J.; Brinke, G. ten; Ikkala, O.; Torkkeli, M.; Serimaa, R. *Macromolecules* **1995**, *28*, 7779–7784.

(200) Antonietti, M.; Conrad, J.; Thunemann, A. *Macromolecules* **1994**, *27*, 6007–6011.

(201) Seog, J.; Dean, D.; Plaas, A.; Weng-Palms, S.; Grodzinsky, A. J.; Ortiz, C. *Macromolecules* **2002**, *35*, 5601.

(202) Patton, D. L.; Advincula, R. C. *Macromolecules* **2006**, *39*, 8674–8683.

(203) Gao, H.; Matyjaszewski, K. *Macromolecules* **1999**, *32*, 2629–2637.

(204) Dziezok, P.; Sheiko, S. S.; Fischer, K.; Schmidt, M.; Moller, M. *Angew. Chem. Int. Ed.* **1997**, *36*, 2812–2815.

(205) Ito, K.; Tanaka, K.; Tanaka, H.; Imai, G.; Kawaguchi, S.; Itsuno, S. *Macromolecules* **1991**, *24*, 2348–2354.

(206) Choi, T.; Grubbs, R. H. *Angew. Chemie* **2003**, *42*, 1743–1746.

(207) Bielawski, C. W.; Grubbs, R. H. *Prog. Polym. Sci.* **2007**, *32*, 1–29.

(208) Slugovc, C.; Wappel, J.; Leitgeb, A. *Polymer* **2010**, *51*, 2927–2946.

(209) Smith, D.; Pentzer, E. B.; Nguyen, S. T. *Polym. Rev.* **2007**, *47*, 419–459.

(210) Zhang, M.; Breiner, T.; Mori, H.; Müller, A. H. E. *Polymer* **2003**, *44*, 1449–1458.

(211) Xia, Y.; Kornfield, J. A.; Grubbs, R. H. *Macromolecules* **2009**, *42*, 3761–3766.

(212) Johnson, J. A.; Lu, Y. Y.; Burts, A. O.; Xia, Y.; Durrell, A. C.; Tirrell, D. A.; Grubbs, R. H. *Macromolecules* **2010**, *43*, 10326–10335.

(213) Li, Z.; Zhang, K.; Ma, J.; Cheng, C.; Wooley, K. L. *J. Polym. Sci. Part A Polym. Chem.* **2009**, *47*, 5557–5563.

(214) Cheng, C.; Khoshdel, E.; Wooley, K. L. *Macromolecules* **2007**, *40*, 2289–2292.

(215) Gregory, A.; Stenzel, M. H. *Prog. Polym. Sci.* **2011**, *37*, 38–105.

(216) Lahasky, S. H.; Lu, L.; Huberty, W. A.; Cao, J.; Guo, L.; Garno, J. C.; Zhang, D. *Polym. Chem.* **2014**, *5*, 1418–1426.

(217) Li, Z.; Ma, J.; Cheng, C.; Zhang, K.; Wooley, K. L. *Macromolecules* **2010**, *43*,

1182–1184.

(218) Teo, Y. C.; Xia, Y. *Macromolecules* **2015**, *48*, 5656–5662.

(219) Xia, Y.; Olsen, B. D.; Kornfield, J. A.; Grubbs, R. H. *J. Am. Chem. Soc.* **2009**, *131*, 18525–18532.

(220) Sveinbjörnsson, B. R. Weitekamp, R. A.; Miyake, G. M.; Xia, Y.; Atwater, H. A.; Grubbs, R. H. *Proc. Natl. Acad. Sci.* **2012**, *109*, 14332–14336.

(221) Li, Y.; Themistou, E.; Zou, J.; Das, B. P.; Tsianou, M.; Cheng, C. *ACS Macro Lett.* **2012**, *1*, 52–56.

(222) Li, A.; Ma, J.; Sun, G.; Li, Z.; Cho, S.; Clark, C.; Wooley, K. L. *J. Polym. Sci. Part A Polym. Chem.* **2012**, *50*, 1681–1688.

(223) Jha, S.; Dutta, S.; Bowden, N. B. *Macromolecules* **2004**, *37*, 4365–4374.

(224) Fu, Q.; Ren, J. M.; Qiao, G. G. *Polym. Chem.* **2012**, *3*, 343–351.

(225) Kim, J. G.; Coates, G. W. *Macromolecules* **2012**, *45*, 7878–7883.

(226) Miyake, G. M.; Weitekamp, R. A.; Piunova, V. A.; Grubbs, R. H. *J. Am. Chem. Soc.* **2012**, *134*, 14249–14254.

(227) Zhan, Y.; Zhang, Z.; Pan, X.; Zhu, J.; Zhou, N.; Zhu, X. *J. Polym. Sci. Part A Polym. Chem.* **2013**, *51*, 1656–1663.

(228) Zhu, L.; Powell, S.; Boyes, S. G. *J. Polym. Sci. Part A Polym. Chem.* **2015**, *53*, 1010–1022.

(229) Frisch, H.; Besenius, P. *Macromol. Rapid Commun.* **2015**, *36*, 346–363.

(230) Schmaljohann, D. *Adv. Drug Deliv. Rev.* **2006**, *58*, 1655–1670.

(231) Roy, D.; Brooks, W. L.; Sumerlin, B. S. *Chem Soc Rev* **2013**, *42*, 7214–7243.

(232) Flores, J. D.; Xu, X.; Treat, N. J.; McCormick, C. L. *Macromolecules* **2009**, *42*,

4941–4945.

(233) Roy, D.; Cambre, J. N.; Sumerlin, B. S. *Prog. Polym. Sci.* **2010**, *35*, 278–301.

(234) Liu, F.; Urban, M. W. *Prog. Polym. Sci.* **2010**, *35*, 3–23.

(235) Lin, S.; Theato, P. *Macromol. Rapid Commun.* **2013**, *34*, 1118–1133.

(236) Gil, E. S.; Hudson, S. M. *Prog. Polym. Sci.* **2004**, *29*, 1173–1222.

(237) Kang, H. C.; Bae, Y. H. *Adv. Funct. Mater.* **2007**, *17*, 1263–1272.

(238) Convertine, A. J.; Benoit, D. S. W.; Duvall, C. L.; Hoffman, A. S.; Stayton, P. S. *J. Control. Release* **2009**, *133*, 221–229.

(239) Boyer, C.; Bulmus, V.; Davis, T. P.; Ladmiral, V.; Liu, J.; Perrier, S. *Chem. Rev.* **2009**, *109*, 5402–5436.

(240) Du, J.; Fan, L.; Liu, Q. *Macromolecules* **2012**, *45*, 8275–8283.

(241) Philippova, O. E.; Hourdet, D.; Audebert, R.; Khokhlov, A. R. *Macromolecules* **1997**, *30*, 8278–8285.

(242) Hofmann, V.; Przybylski, M.; Ringsdorf, H.; Ritter, H. *Makromol. Chemie* **1976**, *177*, 1791–1813.

(243) Kang, S. Il; Bae, Y. H. *J. Control. Release* **2002**, *80*, 145–155.

(244) Park, S. Y.; Bae, Y. H. *Macromol. Rapid Commun.* **1999**, *20*, 269–273.

(245) Sethuraman, V. a; Na, K.; Bae, Y. H. *Biomacromolecules* **2006**, *7*, 64–70.

(246) Matyjaszewski, K. *Macromolecules* **2012**, *45*, 4015–4039.

(247) Moad, G.; Rizzardo, E.; Thang, S. H. *Polymer* **2008**, *49*, 1079–1131.

(248) Henry, S. M.; Convertine, A. J.; Benoit, D. S. W.; Hoffman, A. S.; Stayton, P. S. *Bioconjug. Chem.* **2009**, *20*, 1122–1128.

(249) Vana, P.; Davis, T. P.; Barner-Kowollik, C. *Macromol. Theory Simulations* **2002**,

11, 823–835.

(250) Convertine, A. J.; Lokitz, B. S.; Lowe, A. B.; Scales, C. W.; Myrick, L. J.; McCormick, C. L. *Macromol. Rapid Commun.* **2005**, *26*, 791–795.

(251) Rodriguez-Emmenegger, C.; Schmidt, B. V. K. J.; Sedlakova, Z.; Šubr, V.; Alles, A. B.; Brynda, E.; Barner-Kowollik, C. *Macromol. Rapid Commun.* **2011**, *32*, 958–965.

(252) Monteiro, M. J.; de Brouwer, H. *Macromolecules* **2001**, *34*, 349–352.

(253) Barner-Kowollik, C.; Vana, P.; Quinn, J. F.; Davis, T. P. *J. Polym. Sci. Part A Polym. Chem.* **2002**, *40*, 1058–1063.

(254) Prankerd, R. J. *Profiles of Drug Substances* Brittain, H. G., Ed.; Elsevier, **2007**.

(255) Han, D.; Tong, X.; Boissière, O.; Zhao, Y. *ACS Macro Lett.* **2011**, *1*, 57–61.

(256) Han, D.; Boissière, O.; Kumar, S.; Tong, X.; Tremblay, L.; Zhao, Y. *Macromolecules* **2012**, *45*, 7440–7445.

(257) Qiu, X. P.; Winnik, F. M. *Macromol. Rapid Commun.* **2006**, *27*, 1648–1653.

(258) Spruell, J. M.; Levy, B. A.; Sutherland, A.; Dichtel, W. R.; Cheng, J. Y.; Stoddart, F.; Nelson, A. *J. Polym. Sci. Part A Polym. Chem.* **2008**, *47*, 346–356.

(259) Inglis, A. J.; Sinnwell, S.; Davis, T. P.; Barner-Kowollik, C.; Stenzel, M. H. *Macromolecules* **2008**, *41*, 4120–4126.

(260) Li, M.; De, P.; Gondi, S. R.; Sumerlin, B. S. *J. Polym. Sci. Part A Polym. Chem.* **2008**, *46*, 5093–5100.

(261) Boyer, C.; Bulmus, V.; Davis, T. P. *Macromol. Rapid Commun.* **2009**, *30*, 493–497.

(262) Boyer, C.; Granville, A.; Davis, T. P.; Bulmus, V. *J. Polym. Sci. Part A Polym.*

Chem. **2009**, *47*, 3773–3794.

(263) Tasdelen, M. A.; Kahveci, M. U.; Yagci, Y. *Prog. Polym. Sci.* **2010**, *36*, 455–567.

(264) Zhou, Y.; He, J.; Li, C.; Hong, L.; Yang, Y. *Macromolecules* **2011**, *44*, 8446–8457.

(265) Gruendling, T.; Pickford, R.; Guilhaus, M.; Barner-Kowollik, C. *J. Polym. Sci. Part A Polym. Chem.* **2008**, *46*, 7447–7461.

(266) Li, C.; He, J.; Zhou, Y.; Gu, Y.; Yang, Y. *J. Polym. Sci. Part A Polym. Chem.* **2011**, *49*, 1351–1360.

(267) Bathfield, M.; D'Agosto, F.; Spitz, R.; Ladavière, C.; Charreyre, M. T.; Delair, T. *Macromol. Rapid Commun.* **2007**, *28*, 856–862.

(268) Favier, A.; Ladavière, C.; Charreyre, M. T.; Pichot, C. *Macromolecules* **2004**, *37*, 2026–2034.

(269) Chong, B. Y. K.; Le, T. P. T.; Moad, G.; Rizzardo, E.; Thang, S. H. *Macromolecules* **1999**, *32*, 2071–2074.

(270) Pai, T. S. C.; Barner-Kowollik, C.; Davis, T. P.; Stenzel, M. H. *Polymer* **2004**, *45*, 4383–4389.

(271) Schilli, C.; Lanzendörfer, M. G.; Müller, A. H. E. *Macromolecules* **2002**, *35*, 6819–6827.

(272) Teodorescu, M.; Matyjaszewski, K. *Macromolecules* **1999**, *32*, 4826–4831.

(273) Rademacher, J. T.; Baum, M.; Pallack, M. E.; Brittain, W. J.; Simonsick, W. J. *Macromolecules* **2000**, *33*, 284–288.

(274) Alsubaie, F.; Anastasaki, A.; Wilson, P.; Haddleton, D. M. *Polym. Chem.* **2015**, *6*, 406–417.

(275) Montalbetti, C. A. G. N.; Falque, V. *Tetrahedron* **2005**, *61*, 10827–10852.

(276) Edman, P. *Acta Chem. Scand.* **1950**, *4*, 283–293.

(277) Cunningham, B. A.; Schmir, G. L. *J. Org. Chem.* **1966**, *31*, 3751–3754.

(278) Moad, G.; Solomon, D. H. *The Chemistry of Radical Polymerization*; 2nd ed.; Elsevier Ltd.: Amsterdam, **2006**.

(279) Houshyar, S.; Keddie, D. J.; Moad, G.; Mulder, R. J.; Saubern, S.; Tsanaktsidis, J. *Polym. Chem.* **2012**, *3*, 1879–1889.

(280) Vandenbergh, J.; Reekmans, G.; Adriaensens, P.; Junkers, T. *Chem. Commun.* **2013**, *49*, 10358–10360.

(281) Hong, J.; Wang, Q.; Lin, Y.; Fan, Z. *Macromolecules* **2005**, *38*, 2691–2695.

(282) Zhang, L.; Want, Q.; Lei, P.; Wang, X.; Wang, C.; Cai, L. *J. Polym. Sci. Part A Polym. Chem.* **2007**, *45*, 2617–2623.

(283) Hong, J.; Wang, Q.; Fan, Z. *Macromol. Rapid Commun.* **2006**, *27*, 57–62.

(284) Moad, G.; Rizzardo, E.; Thang, S. H. *Aust. J. Chem.* **2005**, *58*, 379–410.

(285) Hill, M. R.; Carmean, R. N.; Sumerlin, B. S. *Macromolecules* **2015**, *48*, 5459–5469.

(286) Inglis, A. J.; Sinnwell, S.; Stenzel, M. H.; Barner-Kowollik, C. *Angew. Chemie* **2009**, *48*, 2411–2414.

(287) Chan, J. W.; Yu, B.; Hoyle, C. E.; Lowe, A. B. *Polymer* **2009**, *50*, 3158–3168.

(288) Li, M.; De, P.; Gondi, S. R.; Sumerlin, B. S. *Macromol. Rapid Commun.* **2008**, *29*, 1172–1176.

(289) Moad, G.; Rizzardo, E.; Thang, S. H. *Polym. Int.* **2011**, *60*, 9–25.

(290) Willcock, H.; O'Reilly, R. K. *Polym. Chem.* **2010**, *1*, 149–157.

(291) Harvison, M. A.; Roth, P. J.; Davis, T. P.; Lowe, A. B. *Aust. J. Chem.* **2011**, *64*, 992–1006.

(292) Li, H.; Yu, B.; Matsushima, H.; Hoyle, C. E.; Lowe, A. B. *Macromolecules* **2009**, *42*, 6537–6542.

(293) Harvison, M. A.; Davis, T. P.; Lowe, A. B. *Polym. Chem.* **2011**, *2*, 1347–1354.

(294) Segui, F.; Qiu, X.-P.; Winnik, F. M. *J. Polym. Sci. Part A Polym. Chem.* **2008**, *46*, 314–326.

(295) York, A. W.; Scales, C. W.; Huang, F.; McCormick, C. L. *Biomacromolecules* **2007**, *8*, 2337–2341.

(296) Roth, P. J.; Kessler, D.; Zentel, R.; Theato, P. *Macromolecules* **2008**, *41*, 8316–8319.

(297) Boyer, C.; Bulmus, V.; Davis, T. P. *Macromol. Rapid Commun.* **2009**, *30*, 493–497.

(298) Lowe, A. B. *Polym. Chem.* **2010**, *1*, 17–36.

(299) Lowe, A. B. *Polym. Chem.* **2014**, *5*, 4820–4870.

(300) Chan, J. W.; Hoyle, C. E.; Lowe, A. B.; Bowman, M. *Macromolecules* **2010**, *43*, 6381–6388.

(301) Scales, C. W.; Convertine, A. J.; Mccormick, C. L. *Biomacromolecules* **2006**, *7*, 1389–1392.

(302) Li, M.; De, P.; Li, H.; Sumerlin, B. S. *Polym. Chem.* **2010**, *1*, 854–859.

(303) Huang, X.; Boyer, C.; Davis, T. P.; Bulmus, V. *Polym. Chem.* **2011**, *2*, 1505–1512.

(304) Delaittre, G.; Pauloehrl, T.; Bastmeyer, M.; Barner-Kowollik, C. *Macromolecules* **2012**, *45*, 1792–1802.

(305) Mather, B. D.; Viswanathan, K.; Miller, K. M.; Long, T. E. *Prog. Polym. Sci.* **2006**, *31*, 487–531.

(306) Li, G.-Z.; Randev, R. K.; Soeriyadi, A. H.; Rees, G.; Boyer, C.; Tong, Z.; Davis, T. P.; Becer, C. R.; Haddleton, D. M. *Polym. Chem.* **2010**, *1*, 1196.

(307) Gimbert, C.; Lumbierres, M.; Marchi, C.; Moreno-Mañas, M.; Sebastián, R. M.; Vallribera, A. *Tetrahedron* **2005**, *61*, 8598–8605.

(308) Methot, J. L.; Roush, W. R. *Adv. Synth. Catal.* **2004**, *346*, 1035–1050.

(309) Stewart, I. C.; Bergman, R. G.; Toste, F. D. *J. Am. Chem. Soc.* **2003**, *125*, 8696–8697.

(310) Xi, W.; Wang, C.; Kloxin, C. J.; Bowman, C. N. *ACS Macro Lett.* **2012**, *1*, 811–814.

(311) Taylor, J. E.; Bull, S. D.; Williams, J. M. J. *Chem. Soc. Rev.* **2012**, *41*, 2109–2121.

(312) Northrop, B. H.; Frayne, S. H.; Choudhary, U. U. *Polym. Chem.* **2015**, *6*, 3415–3430.

(313) Azechi, M.; Toyota, N.; Yamabuki, K.; Onimura, K.; Oishi, T. *Polym. Bull.* **2011**, *67*, 631–640.

(314) Jaacks, V.; Franzmann, G. *Die Makromol. Chemie* **1971**, *143*, 283–288.

(315) Pepper, D. C. *Polym. J.* **1980**, *12*, 629–637.

(316) Sahu, U. S.; Bhadani, S. *Makromolecular Chemie Rapid Commun.* **1982**, *3*, 103–107.

(317) Ho, H. T.; Levere, M. E.; Pascual, S.; Montembault, V.; Soutif, J.-C.; Fontaine, L. *J. Polym. Sci. Part A Polym. Chem.* **2012**, *50*, 1657–1661.

(318) Nordqvist, A.; Björkelid, C.; Andaloussi, M.; Jansson, A. M.; Mowbray, S. L.;

Karlén, A.; Larhed, M. *J. Org. Chem.* **2011**, *76*, 8986–8998.

(319) Kim, S. H.; Kim, S. H.; Kim, H. J.; Kim, J. N. *Bull. Korean Chem. Soc.* **2013**, *34*, 989–992.

(320) Humphrey, R. E.; Oleson, C. L.; Matula, G. M.; Vaught, A. C. *Microchem. J.* **1971**, *16*, 429–436.

(321) Radkiewicz, J. L.; Zipse, H.; Clarke, S.; Houk, K. N. *J. Am. Chem. Soc.* **1996**, *118*, 9148–9155.

(322) Zhang, M.; Müller, A. H. E. *J. Polym. Sci. Part A Polym. Chem.* **2005**, *43*, 3461–3481.

(323) Li, X.; Prukop, S. L.; Biswal, S. L.; Verduzco, R. *Macromolecules* **2012**, *45*, 7118–7127.

(324) Fenyves, R.; Schmutz, M.; Horner, I. J.; Bright, F. V.; Rzayev, J. *J. Am. Chem. Soc.* **2014**, *136*, 7762–7770.

(325) Huang, K.; Rzayev, J. *J. Am. Chem. Soc.* **2011**, *133*, 16726–16729.

(326) Hadjichristidis, N. P. M.; Pispas, S.; Iatrou, H. *Chem. Rev.* **2001**, *101*, 3747–3792.

(327) Kwat, H.; Burchuk, I. *J. Am. Chem. Soc.* **1952**, *74*, 3094–3097.

(328) Keller, O.; Rudinger, J. *Helv. Chim. Acta* **1975**, *58*, 532–541.

(329) Slugovc, C.; Demel, S.; Riegler, S.; Hobisch, J.; Stelzer, F. *J. Mol. Catal.* **2004**, *213*, 107–113.

(330) Abel, B. A.; McCormick, C. L. *Macromolecules* **2016**, *49*, 465–474.

(331) Smith, M. B. *March's Advanced Organic Chemistry*; 7th ed.; John Wiley & Sons, Inc.: Hoboken, **2013**.

(332) Bordwell, F. G.; Harrelson, J. A.; Lynch, T. Y. *J. Org. Chem.* **1990**, *55*, 3337–

3341.

(333) Bordwell, F. G.; Ji, G. Z. *J. Am. Chem. Soc.* **1991**, *113*, 8398–8401.

(334) Kolthoff, I. M.; Chantooni, M. K.; Bhowmik, S. *J. Am. Chem. Soc.* **1968**, *90*, 23–28.

(335) Matthews, W. S.; Bares, J. E.; Bartmess, J. E.; Bordwell, F. G.; Cornforth, F. J.; Drucker, G. E.; Margolin, Z.; McCallum, R. J.; McCollum, G. J.; Vanier, N. R. *J. Am. Chem. Soc.* **1975**, *97*, 7006–7014.